TELEPEN

MX 8201015 3

D41688/82

A STUDY OF

REACTIVE SPUTTER ETCHING BY DIRECTED ION BEAMS AND R.F. PLASMAS

A thesis submitted by

Peter James REVELL, HND, LRSC

in partial fulfilment of the requirements

for the degree of

Doctor of Philosophy

of the Council for National Academic Awards

January 1982

Sponsoring Establishment:-

Middlesex Polytechnic

Collaborating Organisation:-

Ion-Tech Ltd.

Site HE BG	MIDDLESEX POLYTECHNIC LIBRARY
Accession No.	8201015
Class No.	621.38173 REV
Special Collection ✓	REFERENCE BLDSC THESIS NO. D041689

A STUDY OF REACTIVE SPUTTER ETCHING BY

DIRECTED ION BEAMS AND R.F. PLASMAS

by Peter James Revell

ABSTRACT

This work compares the alternative methods of etching silicon semiconductor materials. Conventional methods of pattern delineation using aqueous etchants are being replaced for some applications by dry processing. The reasons for the move towards plasma and ion beam etching are examined particularly in relation to very large scale integration (VLSI) technology and the required reduction in feature size. A review of the published information on the use of reactive gas plasmas shows that this etching process is capable of producing vertical profiles without loss of pattern definition in 1μm. features.

Noble gas ion beam sputtering, another alternative dry etching process, has some advantages over plasma etching but does not compare favourably in terms of material etch-rate selectivity and profile replication.

Reactive ion beams produced by heated filament sources etch silicon compounds more rapidly than argon beams, but undesirable topographical features such as "facets" and "trenches" may be observed after beam energies greater than about 1 keV have been used.

The total beam current and current distribution have been determined for a medium sized (B93) Saddle-Field source. The etch rates of several materials were greater with a fluorocarbon beam than with an argon beam produced by this source.

Examination of profiles produced by etching silicon dioxide with beams from the B93 source injected with either CHF_3 or CF_4 showed no evidence of sputtering-induced artefacts or lateral attack due to the diffusion of chemically reactive fragments. The results of reactive ion beam etching (RIBE) with a Saddle-Field source suggest that chemical attack predominates over sputtering. A two stage mechanism is proposed in which the incident particles cause bond cleavage at the surface followed by addition and abstraction reactions, leading ultimately to the formation of volatile products.

The possible commercial applications of RIBE with Saddle-Field sources are discussed, and suggestions are advanced for further work in this area.

ACKNOWLEDGEMENTS

This work was supported during the period 1st November 1978 to 31st January 1980 by ACTP Contract 3034.

The financial support by the Science and Engineering Research Council in the form of a CASE Award and Conference expenses, is gratefully acknowledged.

The generous provision of financial support by Ion-Tech Ltd. under the terms of the CASE Award and for Conference expenses is acknowledged with gratitude.

The assistance of Dr. J. Franks and Mr. E. Mihill of Ion-Tech Ltd. is recorded with appreciation. Particular thanks go to Mr. A.C. Evans (Ion-Tech Ltd.) for practical assistance, the freedom to use experimental apparatus and for giving up so much of his time to teach me the intricacies of Saddle-Field Sources.

I consider myself fortunate in having had the opportunity to draw on the expert and enthusiastic technical support of Members of Staff of the Microelectronics Centre. My thanks go to Gary Shorthouse, John Linnell, Roger Ransom, Dave Court and Dave Hacker. No matter what pressing work he had at the time, Dick Gledhill was always willing and able to help with computing and mathematical problems. The assistance of Ian Oliver in the Library is much appreciated for his patient tracking-down of obscure literature and hours spent communicating with a computer data-base. The assistance of Mr. M. Hamer with C-V measurements made at the British Telecom Research Laboratories is gratefully acknowledged. Many fruitful discussions were held with Mr. C. Heslop, also of that Laboratory.

It is with pleasure that I acknowledge the unceasing encouragement and able supervision of Dr. George Goldspink of Middlesex Polytechnic and Dr. Ian Wilson of the University of Surrey.

I express my most profound gratitude to my Wife, Lyn. Without her I would never have started, and so much would have been missed. Without her patient understanding and constant reassurance I certainly would never have finished.

Last, but by no means least, I would like to thank Shirley Hammond for her accurate and efficient typing of this thesis.

I dedicate this work to the memory of my Sister, Helen. The willingness with which she helped others was an inspiration to all who knew her.

CONTENTS

Page

ABSTRACT (i)

ACKNOWLEDGEMENTS (ii)

LIST OF ILLUSTRATIONS (viii)

1. INTRODUCTION 1

2. REVIEW OF PREVIOUS WORK

2.1 PLASMA AND REACTIVE ION ETCHING

2.1.1 Introduction 16
2.1.2 Anisotropy 17
2.1.3 Selectivity 22
2.1.4 Etch Rates 23
2.1.5 Analytical Techniques 27
2.1.6 Safety 29

2.2 SADDLE FIELD SOURCES

2.2.1 Introduction 31
2.2.2 Early Working Models 31
2.2.3 Anodes 32
2.2.4 Cathodes 35
2.2.5 Ion Exit Aperture 37
2.2.6 Discharge Characteristics 38
2.2.7 The Neutral Component of the Beam 39

2.3 SPUTTER ETCHING WITH SADDLE FIELD SOURCES

2.3.1 Sputtering of Copper 41
2.3.2 Miscellaneous Applications 42

3. CHARACTERISATION OF THE B93 SADDLE FIELD SOURCE

3.1 INTRODUCTION 52

3.2 DESCRIPTION OF THE SOURCE

3.2.1 Construction Details 52

Page

			Page
	3.2.2	Operating Parameters	54
	3.2.3	Source Instability	55
	3.2.4	Source Heating	59
3.3	TOTAL BEAM CURRENT DETERMINATION		
	3.3.1	Experimental Objectives	61
	3.3.2	Design of the Experiment	62
	3.3.3	Experimental Method	63
	3.3.4	Results	65
	3.3.5	Errors in Beam Current Determinations	67
3.4	BEAM ENERGY DETERMINATIONS		69
3.5	BEAM CURRENT DISTRIBUTION		
	3.5.1	Sputtering of Copper with Argon	70
	3.5.2	Beam Divergence	74
	3.5.3	Beam "Current" Density	75
	3.5.4	Beamlet Etch Patterns	76
	3.5.5	Particle Extraction Efficiency	78

4. ION BEAM ETCHING WITH SADDLE FIELD SOURCES

4.1	INTRODUCTION		94
4.2	ETCHING OF SiO_2		
	4.2.1	Etching with Argon	97
	4.2.2	Etching with CF_4	102
	4.2.3	Etching with CHF_3	105
	4.2.4	Etching with other Gases	107
4.3	ETCHING OF Si		
	4.3.1	Etch Rates	107
	4.3.2	Etched Profiles	109
4.4	ETCHING OF Si_3N_4		
	4.4.1	Etch Rates	109
	4.4.2	Etched Profiles	110

Page

			Page
	4.5	ETCHING OF Al	
		4.5.1 Etch Rates	110
		4.5.2 Etched Profiles	112
	4.6	ETCHING OF W	
		4.6.1 Etch Rates	114
		4.6.2 Etched Profiles	114
	4.7	VACUUM EQUIPMENT	115
	4.8	SUMMARY	116
5.	SUB-MICRON DEVICE GEOMETRIES		
	5.1	INTRODUCTION	138
	5.2	ADVANTAGES OF REDUCING DEVICE DIMENSIONS	138
	5.3	LITHOGRAPHY	140
	5.4	LINEWIDTH CONTROL	141
	5.5	EXPERIMENTAL	142
	5.6	SUMMARY	144
6.	RADIATION DAMAGE STUDIES		
	6.1	INTRODUCTION	153
	6.2	THEORY OF THE M.O.S. CAPACITOR	153
		6.2.1 Accumulation	154
		6.2.2 Depletion	154
		6.2.3 Inversion	155
		6.2.4 Flat Band Condition	155
	6.3	THE Si-SiO_2 INTERFACE	
		6.3.1 Fixed Surface States	157
		6.3.2 Mobile Ionic Charge	158
		6.3.3 Fast Surface States	158
		6.3.4 Traps Ionised by Radiation	158
		6.3.5 Total Charge	159
	6.4	RADIATION EFFECTS	160

Page

6.5 EXPERIMENTAL

6.5.1 Preparation and Oxidation of Wafers 162

6.5.2 Ion Beam Etching of SiO_2 162

6.5.3 Metallisation and Electrode Definition 163

6.5.4 C-V Measurements 165

6.6 RESULTS

6.6.1 Control Wafers 165

6.6.2 Ion Beam Etched Wafers 169

6.6.3 Etch Rates 169

6.6.4 Modification of C-V Characteristics 170

6.7 SUMMARY OF RESULTS 173

7 MECHANISMS OF REACTIVE ION BEAM ETCHING

7.1 INTRODUCTION 178

7.2 ETCHING BY CHEMICAL REACTIONS

7.2.1 Etching of Silicon Compounds by Fluorine and Fluorinated Compounds 178

7.2.2 Etching of Aluminium and Tungsten by Fluorine and Fluorinated Compounds 184

7.2.3 Etching by Free Radicals 185

7.3 FORMATION OF REACTIVE SPECIES WITHIN THE B93

7.3.1 Dissociation of Freons and Recombination Processes 189

7.3.2 Dissociation of SF_6 and Recombination Processes 193

7.4 ETCHING BY SPUTTERING AND CHEMICAL PROCESSES

7.4.1 Energy Transfer Considerations for some Etchant-Target Combinations 195

7.4.2 Experimental Evidence of Sputtering and Chemical Etching 196

			Page
	7.4.3	Discussion	199
	7.4.4	Suggested Mechanism	201
8	CONCLUSIONS		208
9	RECOMMENDATIONS FOR FURTHER WORK		
	9.1	THE B93 SOURCE	
	9.1.1	Beam Uniformity	210
	9.1.2	Control of Gas Flow	210
	9.1.3	Carbon Particulates	211
	9.1.4	The Production of Etchant Species	211
	9.1.5	Beam Energy Determinations	212
	9.2	ETCHING UNIFORMITY	213
	9.3	ANGLE OF INCIDENCE OF THE BEAM	213
	9.4	MASS SPECTROMETRY OF REACTIVE ION BEAMS	213
	9.5	ETCH RATE SELECTIVITIES	214
	9.6	ETCHING CHARACTERISTICS OF RESIST MATERIALS	215
10	GLOSSARY		216
11	REFERENCES		222
12	PUBLICATIONS		234
	APPENDICES		
	I	PREPARATION OF SPECIMENS FOR ETCHING	3 pages
	II	EXPERIMENTAL PROCEDURE FOR ION BEAM ETCHING USING THE B93 SOURCE	2 pages
	III	ATOMIC DENSITY DATA.FORMULAE, NOMENCLATURE AND PHYSICAL DATA FOR GASEOUS ETCHANTS USED IN R.I.B.E. HAZARDS INFORMATION	2 pages
	IV	CHARACTERISTICS AND OPERATING CONDITIONS OF THE THREE SADDLE FIELD SOURCES USED IN THIS STUDY	1 page

LIST OF ILLUSTRATIONS

FIG.NO.		Page
1.1	Silicon etch depth as a function of over-etch time for various selectivities. For any etchant on SiO_2.	15
2.1	Contributions to the etch rates of Si and SiO_2 targets by ionic and free-radical components.	45
2.2	Anisotropic etching of single crystal silicon using an SF_6 plasma. (Micrograph).	46
2.3	SiO_2 etch rate dependence on RF power density.	47
2.4	Si etch rate as a function of excitation frequency.	47
2.5	SiO_2 etch rate as a function of chamber pressure.	48
2.6	Si etch rate dependence on target area.	48
2.7	SiO_2 etch rate dependence on reactor temperature.	49
2.8	Etch rate variation with chemical composition for four materials.	49
2.9	The Saddle Field Source.	50
2.10	The Charged Particle Oscillator.	51
3.1	Construction details of the B93 source.	80
3.2	Variation of Discharge Impedance with time, for B93 source starting at 20°C and injected with argon.	81
3.3	Total beam "current", I_B and removal rate of copper as a function of B93-argon discharge current (I_D).	82
3.4	Removal rate of copper as a function of bombarding particle energy for a B93 argon beam	83
3.5	Copper foil matrix used for beam current distribution measurements. (Photograph)	84
3.6	Representation of the B93 beam based upon the argon sputtering of copper.	85

FIG.NO.		Page
3.7	B93 Ar beam "current" distribution parallel and perpendicular to the Anode axes.	86
3.8	B93 argon beam divergence and sputter etch rate of copper for the component parallel to the anode axes.	87
3.9	B93 argon beam divergence and sputter etch rate of copper for the component perpendicular to the anode axes.	88
3.10	B93 beam area (determined for argon) as a function of the Cathode Aperture to Target distance.	89
3.11	B93 beam "current" density (determined for argon) as a function of discharge current.	90
3.12	(a) and (b) B93 argon beamlet etch patterns on SiO_2.	91
3.13	Etch depth variation produced by the action of one beamlet.	92
3.14	Particle extraction efficiency for constant current and constant voltage.	93
4.1	Etch rate data for the action of beams produced by the B93 source on silicon dioxide targets.	118
4.2	SiO_2 etch rate dependence on argon energy using the B93 source.	119
4.3	SiO_2 sputter yield dependence on Ar^+ energy for published data and experimental results.	120
4.4	SiO_2 sputter etch rate dependence on "current" density for a B93-Ar beam.	121
4.5	Sloping sidewalls etched into SiO_2 using a B93 argon beam.	122
4.6	Facet formation in SiO_2 caused by over-etching with an argon beam.	123
4.7	SiO_2 apparent sputter yield dependence on CF_x etchant particle energy.	124
4.8	SiO_2 apparent sputter yield dependence on CF_x etchant particle energy for B93-CHF_3 beams.	125

FIG.NO.		Page
4.9	Si Apparent Sputter Yield dependence on CF_x etchant particle energy for B93-CHF_3 beams.	126
4.10	Anisotropic etching of SiO_2 using a B93-CHF_3 beam.	127
4.11	Vertical profile etched into SiO_2 using a B93-CHF_3 beam.	128
4.12	SiO_2 apparent sputter yield dependence on etchant particle energy for B93 beams and published data for heated filament sources.	129
4.13	Silicon sputter yield dependence on particle energy (Ar).	130
4.14	Etch-rate data for the action of beams produced by the B93 source on single crystal silicon targets.	131
4.15	Etch-rate data for the action of beams produced by the B93 source on silicon nitride targets.	132
4.16	Etch-rate data for the action of beams produced by the B93 source on aluminium (film) targets.	133
4.17	Al film etch rate variation with duration of exposure to B95-Ar beams.	134
4.18	Aluminium cones produced during exposure to a B95 argon beam.	135
4.19	Aluminium ring formation produced during exposure to a B95 argon beam.	136
4.20	Etch-rate data for the action of beams produced by the B93 source on tungsten (film) targets.	137
5.1	Linewidth loss due to isotropic etching.	145
5.2	Increase of channel width due to isotropic etching.	146
5.3	Isotropic line etching. Fractional linewidth loss as a function of etched depth for various pattern widths.	147
5.4	Isotropic channel etching. Fractional channel width increase as a function of etched depth for various dimensions of resist opening.	148

FIG.NO.		Page
5.5	Dimensionally ideal case for the accurate replication of a resist pattern.	149
5.6	Vertical etched profile in SiO_2 produced with a B21-CF_4 beam (Micrograph).	150
5.7	Linewidth control achieved by etching SiO_2 with a B21-CF_4 beam (Micrograph).	151
5.8	0.5 and 1.0 μm wide channels etched into SiO_2 using a B93-CHF_3 beam.	152
6.1	The M.O.S. Capacitor: Physical and Electrical details.	174
6.2	Band structures for the M.O.S. Capacitor under various conditions of applied gate potential.	175
6.3	1 MHz C-V characteristics for B93 argon beam bombarded and control (not bombarded) M.O.S. capacitors.	176
6.4	Radiation induced surface state density as a function of total particle dose, for M.O.S. oxide films bombarded by beams from two Saddle Field sources.	177
7.1	Isotropic etching of silicon using an SF_6 plasma.	204
7.2	Etch pits in SiO_2 produced by free radical attack beneath a non-contiguous mask.	205
7.3	Theoretical maximum energy transfer to various targets, for 3 fluorocarbon ions and argon.	206
7.4	Proposed mechanism for the enhanced chemical etching of SiO_2 by CF_3.	207

1. INTRODUCTION

1.1 OBJECTIVES

The aims of this study were as follows:

(i) To compare the alternative methods of etching for semiconducting materials, with particular regard to the reduction in linewidths required for the next generation of VLSI devices.

(ii) To experimentally determine the characteristics of a beam produced by injecting argon into a medium sized Saddle Field source manufactured by Ion-Tech (UK) Ltd.

(iii) To assess the suitability of reactive ion beam etching using Saddle Field and heated filament sources as techniques for the delineation of sub-micron geometries in silicon compounds.

1.2 THE FABRICATION OF INTEGRATED CIRCUITS

Etching is a fundamental and integral part of the process for fabricating integrated circuits. The controlled and selective removal of material from the surface of a wafer leading ultimately to the production of active devices has traditionally been accomplished with aqueous etchants. The reasons for this will be discussed, and it will be shown that, in most instances, the move to etching in the gas phase is inevitable and desirable.

A typical metal-oxide-semiconductor (M.O.S.) schedule (Cannon, et. al. 1974), although rather dated by current standards - will require 38 to 45 process steps which include 1 diffusion, 2 high temperature and 4 or 5 masking stages. The remaining stages are for cleaning,

resist application and stripping, etching, examination and testing. Therefore, in such an M.O.S. process, pattern transfer steps account for approximately 30-50% of the total processing stages. "Pattern transfer step" includes:

Resist application

Pattern transfer to resist

Etching of the exposed surface

Removal of resist

The importance of the etching process and how it may affect device performance and production yield will be examined in detail.

1.3 APPLICATIONS OF ETCHING IN THE FABRICATION PROCESS

In a typical M.O.S. process, a number of different materials will be etched, as the levels of the structure are sequentially prepared. Each material must be etched through completely, despite being present in widely varying thicknesses. The rate of removal for a given substance ("etch rate") must be sufficiently rapid to avoid "bottlenecks" in the production process (a British industry criterion of 1000 Å per minute is the minimum). In addition the etchant must act selectively on the target and etch the substructure at a very much reduced rate (a British industry minimum requirement for any etchant is an etch rate selectivity of 10:1).

1.3.1 Materials to be Etched

By definition, the M.O.S. process consists of three levels:

(a) The metal layer (gate electrode, usually aluminium)

(b) The oxide or insulation layer (insulation between

source, gate and drain and barrier to dopant species introduced by diffusion or implantation, SiO_2 in this case)

(c) The semiconductor (also the substrate in this context, n-type silicon is the usual choice)

There are various permutations on this structure. For example, gold or doped polysilicon may be used as the gate electrode, silicon nitride may be employed as the dielectric and also on an overall passivating layer, and p-type silicon may be chosen as the substrate. Some data are presented on the etching of tungsten films, which are used in the fabrication of high frequency transistors. The method of formation of films used for experimental etching is given in Appendix I.

For the purposes of this work, etching has been considered at a macroscopic level (i.e. a "small" device dimension of 1 μm is equivalent to a row of 3×10^3 "average" sized atoms). The topographical characteristics of etched n-type silicon, at this level of observation, may safely be assumed as equal to those of the intrinsic material, as the dopant density (10^{15} atoms cm^{-3}) is so much lower than that of the bulk (5×10^{22} atoms cm^{-3}).

1.3.2 Pattern Definition

Solvent-based solutions of monomer sensitive to a specific region of the e.m.r. spectrum are routinely used as resist materials.

Materials other than organic polymers may be used to advantage under certain circumstances. In work to be described later (Section 7.2.3), 100 μm aluminium discs

served as ohmic contacts and etch resist during the formation of mesa diodes on silicon using an SF_6 plasma. In order to prevent facet formation on argon ion milled bubble memories with critical dimensions of 0.5 µm, a mask of low sputter-yield (Al_2O_3) was formed in-situ by the anodisation of an aluminium film (Ahn and Schwartz, 1978). The production of sub-micron etched features is described in Chapter 5.

1.3.3 Selectivity of Etching

The selectivity, or etch-rate-ratio between any pair of materials for a given etchant is defined as:

$$S = \frac{\text{Etch Rate (Target) } (\text{Å min}^{-1})}{\text{Etch Rate (Substructure) } (\text{Å min}^{-1})}$$

In a practical situation, the "dynamic" selectivity is the critical parameter. Under these circumstances, etching through the target completely reveals the substructure which proceeds to be removed at rate $E.R._{sub}$. This is a somewhat difficult condition to simulate experimentally as both target and substructure are not exposed simultaneously for the duration of etching and the respective areas vary with time. The method adopted here (as is usual in the published literature) is to report the selectivity as:

$$S = \frac{\text{Etch Rate (Target 1)}}{\text{Etch Rate (Target 2)}}$$

Targets 1 and 2 are etched separately but under identical conditions.

The ratio S is an important parameter for commercial processing where a product of consistently high quality is

required. There is no upper limit to the value obtained for S, etchants are developed with this as a criterion. For example buffered hydrofluoric acid (b.HF) etches SiO_2 at $\simeq 900$ Å min^{-1} at 18°C, but immeasurably slowly on Si. A high selectivity ratio is required as:

(a) The uniformity of etching across a wafer is rarely less than $\simeq 5\%$ total (i.e. for constant film thickness, the etch depth difference between any two points on the wafer is not less than 5%).

(b) The film thickness across a wafer is not constant, with edge to centre variations of $\pm$ 5% being not uncommon for many deposition processes.

For example, taking a 5000 Å film of SiO_2 on Si, a typical etch rate for oxide of 1000 Å min^{-1} (any etchant system), a set of selectivity curves may be produced, as shown in Fig. 1.1, which relate the overetch time to the substructure etch depth. If the SiO_2 thickness variation is $\pm$ 5%, then the film at the thinnest point will be completely etched through 0.5 minutes before that at the thickest. An "overetch" time of 0.5 minutes is, therefore required to guarantee clearing all oxide, and the resultant Si etch depth will be as shown. Correspondingly longer overetch times will produce etch depths in the substructure as indicated. Naturally, the result would be the same for non-uniformity of etching across the wafer. In the case of aqueous etchant this could be caused by an accumulation of hydrogen bubbles (aluminium etching) or localised depletion of etchant species at the target-liquid interface due to inadequate mixing. In the case

of gas-phase etching, the non-uniform distribution of ions or free radicals (or both) across the wafer would give rise to similar effects.

1.3.4 Practical Considerations

The hazards associated with the use of discharges containing halogenated compounds cannot be overemphasised. Published data on the toxic levels of compounds used in and produced during the experimental work for this study are included in Appendix III. The usual procedures apply for the safe operation of vacuum and high voltage equipment.

Contamination, especially by alkali metal ions (Na^+, K^+) in M.O.S. gate oxide and at the Si-SiO_2 interface can lead to abnormal device characteristics when present in trace quantities, especially in the presence of radiation, as described in Chapter 6. Sodium chloride occurs naturally in human skin secretions, and may, therefore, be transmitted to many wafers simply by careless handling procedures during one stage involving an aqueous etchant. Vacuum techniques for etching, however, restrict the spread of ionic contaminants, which may only occur by sputtering or diffusion mechanisms (the vapour pressure of NaCl is 1 torr at 865°C) (Handbook of Chemistry and Physics, 1963).

One other compound which must be treated as a contaminant is water vapour. The origin of water vapour in this context is from two sources:

(a) desorbed from the wall of the cylinder containing the etchant gas

(b) desorbed from vacuum chamber components

Water vapour due to (a) may be reduced or eliminated entirely by incorporating suitable cold traps and/or dessicant materials into the gas supply line. The reduction of the water vapour concentration in a vacuum system may take long periods of pumping, and baking of certain components. The system is particularly susceptible to this form of contamination when cooled target holders are fitted in the chamber, permitting rapid condensation of atmospheric water vapour when the unit is vented. Ideally venting of the chamber should be with dried gas (oxygen free nitrogen, or entry of air through a dessicant cartridge). It can be readily appreciated that water molecules may dissociate in a discharge to form:

$$H_2O \rightleftharpoons H^+ + OH^-$$
$$H_2O \xrightleftharpoons{-e} 2H^+ + O^- \quad (\text{or } O^{2-})$$

The presence of which may lead to charging at the target surface, degradation of organic resist materials and the formation of oxide films on aluminium and tungsten which sputter at lower rates than the pure metal, as shown in Chapters 3 and 4.

1.4 CRITERIA FOR ETCH PROCESSES

In order to objectively compare etching techniques, it is necessary to define the criterion by which each is assessed. The assessment will be based on theoretically optimum conditions, in the knowledge that some degree of compromise will arise in a production environment. The

sequence of presentation is not necessarily significant. A particular application may require one criterion to be set above all others; for example the introduction of electrical abnormalities into a certain M.O.S. structure may render it totally inoperative, all other standards would, therefore, become of secondary importance.

1.4.1 Selectivity (Target: Resist)

The resist may be photoresist, electron-beam resist or metal/metal oxide film. The minimum allowable selectivity will be determined by the thickness of both resist and target materials.

1.4.2 Selectivity (Target: Substructure)

This is dependent upon the degree of process control, film thickness variation and provision for end-point determination. In the absence of monitoring equipment, a selectivity of 10:1 would be considered adequate for most applications. This ratio could be reduced if such equipment was available.

1.4.3 Isotropy

Total anisotropy is normally desirable, but in some cases the formation of sloping wall profiles is advantageous.

1.4.4 Etch Rate

For use in a production environment the target should be removed at 1000 Å min^{-1} or faster (British Industry requirement, 1981) In particular, dry techniques should increase the slow aqueous etch rate of Si_3N_4.

1.4.5 Safety

The nature of liquid or gaseous starting materials

and waste products should be well characterised. All hazards should be identified and reduced to safe working levels by using fume hoods, adsorbers, scrubbers, neutralisation tanks etc.

1.4.6 Damage

Surface (etch pits, roughening of polished surface) and bulk damage (implantation of energetic etchant particles) should not be introduced as a result of the etch process.

1.4.7 Starting Materials

Resist materials and etchants should be readily available. Resists should also be compatible with other stages of the fabrication process, and be removed easily after etching of the target.

1.4.8 Resolution

The etch process should be capable of accurately reproducing the minimum feature dimensions present in the resist layer. This will be limited to a large extent by the isotropy of the etch.

1.4.9 Loading Effects

The etch rate should be independent of the target area. The target area will vary with:

(i) the nature of the pattern defined in the resist

(ii) the batch size (number of wafers)

End-point prediction may become difficult if a dependency exists.

1.4.10 Device Characteristics

The electrical characteristics of the devices should not be modified by the etching procedure. For

example, M.O.S. devices are sensitive to various types of induced charge at the Si-SiO_2 interface, leading to undesirable threshold shifts.

These criteria are compared using the published data for aqueous and plasma etching and argon ion milling in Tables 1, 2 and 3. Table 4 briefly summarises the results of experimental work conducted for this study, using the Saddle Field source for the reactive ion beam etching of certain materials.

These data show that:

The highest etch rates are usually achieved with aqueous etchants, but at the expense of undercut profiles. Aqueous etching also provides greater selectivity for most combinations of materials than the dry methods. It seems unlikely that gas phase etching will ever attain selectivities of 1000:1, but with the increasing use of instrumental techniques for end-point monitoring, rate ratios of this magnitude are probably not necessary. Increased anisotropy can be achieved with the use of reactive ion etching in a planar reactor or reactive ion beam etching with fluorinated gases injected into a Saddle Field source or a heated filament source. Argon ion milling (with heated filament sources), however, is a useful technique for pattern delineation in some metals, but undesirable sputtering-induced topographical features and low selectivity render it unsuitable in most semiconductor fabrication processes.

TABLE 1

AQUEOUS ETCHING

CRITERION	MATERIAL			
	Single Crystal Si	SiO_2	Si_3N_4	Al
1. Selectivity: Resist	Organic resists cannot be used	Adequate for etch depths to 1 μm	Organic resists cannot be used	Organic resists suitable for 1.2 μm Al thickness
2. Selectivity: Substructure	Not usually applicable	Typically 1000:1 over Si (2)	Typically 4:1 or better over silox (4)	1000:1 for SiO_2 or Si_3N_4 (5)
3. Isotropy	Formulations available for 100% anisotropy (1)	Normally isotropic (3)	Normally isotropic	Isotropic
4. Etch Rate	Anisotropic etch up to 0.8 μm/min	Thermal: 8-900 Å/min Silox: 2-4 k Å/min	Typically 100 Å/min in phosphoric acid	Typically 6 k Å/min in Isoform at 45°C
5. Major Hazards	HF, HNO_3, As, solutions	HF solutions	Phosphoric acid at 185°C	Phosphoric acid nitric acid
6. Physical Damage	Not significant Chemical polish etchants available	Smooth etched features. Bulk damage not significant	Smooth etched features	Pitting of aluminium sidewalls can occur
7. Resist Materials	Usually silox. Readily removed	Normal photo or electron beam resist	Usually Silox Readily removed	Normal photo or electron beam resist. Readily removed
8. Resolution	Limited by resolution of pattern in silox layer	Limited by resist pattern. In practice 3 μm wide lines for 1 μm deep	Limited by resolution of pattern in silox layer	Limited to ≃ 3 μm lines for 1.2 μm thick film
9. Loading Effects	Use large solution volume and controlled agitation	Large reactant volume relative to exposed area. Control agitation	Large reactant volume Agitation aided by boiling	Agitation very important
10. Device Characteristics	Dependent upon reagent purity	Very susceptible to alkaline metal ion contamination	Dependent upon reagent purity	Dependent upon reagent purity

References:
(1) Water 49.4 M%; pyrocatechol 4 M%; ethylenediamine 46.4 M%, etch under reflux (Bohg, 1971)
(2) 4 parts 40% NH_4F+1 part 42% HF, formulation of "Buffered HF"
(3) Brandes and Dudley, 1973
(4) Tombs and Sewell, 1968
(5) "Isoform" proprietary etchant (phosphoric acid, nitric acid and surfactant)

TABLE 2

PLASMA AND REACTIVE ION ETCHING

CRITERION	CHARACTERISTIC
1. Selectivity: Resist	Adequate. Oxygen and water vapour partial pressures must be maintained at very low levels
2. Selectivity: Substructure	6.8:1 for SiO_2 on Si using CHF_3(1). 3:1 for SiO_2 on Si using C_2F_6 (2) 5:1 for Si_3N_4 on SiO_2 using SiF_4+ O_2 (3) 6.25:1 for Al on SiO_2 using CCl_4+ Ar (4)
3. Isotropy	Dependent on: electrode configuration, RF power and frequency, and chamber pressure. Anisotropic etching is practicable
4. Etch Rate	For example: 4700 Å/min for CHF_3 on SiO_2 (1) 2500 Å/min for CCl_4+ Ar on Al (4) Using SF_6, up to 2 μm/min of Si achieved in this investigation
5. Major Hazards	Oxidised halocarbons (e.g. $COCl_2$, COF_2) are toxic at ppm levels (5) Corrosive hazards of e.g. SiF_4, $SiCl_4$ and other reaction products from vacuum pump exhaust
6. Physical Damage	Pitting of surface may occur (preferential etching) in localised areas with CHF_3 plasmas (6). CCl_4 etching of Al may produce corrosive residues which must be washed off (7)
7. Resist Materials	Normal electron beam and photoresists possess adequate resistance although some resists have been specially formulated (8)
8. Resolution	The ability to plasma etch 0.2 μm wide lines with no undercutting has been demonstrated. (9)
9. Loading Effects	Very significant - etch rates for particular applications must be established for pumping speed and gas flow rate variations (10)
10. Device Characteristics	Mobilisation of contaminants e.g. Na^+ at SiO_2-Si interface occurs with brief (≃ 30 sec.) exposure to plasma (11). High threshold voltage characteristics can usually be removed by annealing (12)

References: (1) Chinn, et. al. 1981
(2) Heinecke, 1976
(3) Dionex Proprietary information, Sheet 71/79
(4) Schaible, et. al. 1978
(5) See Appendix III
(6) Heslop, 1980
(7) Lee and Schwartz, 1980
(8) Photoresist type TJS-1273 produced by Ciba-Geigy Ltd
(9) Wang and Maydan, 1981
(10) Mogab, 1977
(11) McCaughan, 1980
(12) McCaughan, 1973

TABLE 3

ARGON ION BEAM MILLING

(Heated Filament Sources)

CRITERION	CHARACTERISTIC
1. Selectivity: Resist	1.4:1 for SiO_2: AZ1350 (maximum value for beam at 50° to surface) (1)
2. Selectivity: Substructure	1.07:1 for SiO_2: (100) Si (2); 1.2:1 for Al + 5% Cu on SiO_2 (3)
3. Isotropy	Beam at normal incidence produces vertical wall profiles with (a) facetted edges, and usually (b) trenches at foot of etched channel. Undercutting not present (4)
4. Etch Rates	Si = 540 Å/min (3); SiO_2 = 580 Å/min (3); Al (film) = 670 Å/min (3); Au (film) = 1040 Å/min (3) Si_3N_4 = 187-217 Å/min (5); PMMA = 400 Å/min (5)
5. Major Hazards	Hazards associated with vacuum and high voltage equipment. No toxic or corrosive gas hazards
6. Physical Damage	Not considered significant at beam energies of 500-1000 eV (penetration of ions to ≃ 10 Å) (3)
7. Resist Materials	Desirable to use metal film which has low sputter yield due to oxide film formation. Organic resists have high sputter yield (see above)
8. Resolution	Theoretical minimum considerably less than 1 μm and governed by linewidth definition in resist and process tolerance towards topographical defects
9. Loading Effects	Not applicable, chemical reactions do not occur. Collimated beam usually produces etching uniformity within ± 5% (6)
10. Device Characteristics	Mobile charge movement in M.O.S. structures caused by ionic species in beam (7). Beams normally fully neutralised in front of anode aperture. (8) Threshold shifts dependent upon beam energy and total ion dose (7).

References: (1) Lee, 1979
(2) Meusemann, 1979
(3) Bollinger and Fink, 1980
(4) Gokan and Esho, 1981
(5) Results from specimens prepared by Veeco, USA, for Middlesex Polytechnic. 75 mm beam diameter, 125 mm to target, 650 eV argon beam, 0.65 mA cm^{-2}
(6) Kaufman, 1978
(7) McCaughan, 1980
(8) Kaufman and Robinson, 1981

TABLE 4

REACTIVE ION BEAM ETCHING

WITH SADDLE FIELD SOURCES

CRITERION	CHARACTERISTIC
1. Selectivity: Resist	Resist etch-rates not determined. On basis of etched profiles, selectivity is adequate for 5000 Å deep etching of SiO_2 using CF_4 and CHF_3 beams from B93
2. Selectivity: Substructure	6:1 for SiO_2: Si using CF_4; 2:1 for Si_3N_4: SiO_2 using C_2F_6, 7:1 for Si_3N_4: Si using C_2F_6, all with B93
3. Isotropy	Vertical profiles observed in SiO_2 after etching with B93 CF_4 and CHF_3 beams. B21-SF_6 beam also produced vertical profiles in SiO_2
4. Etch Rates	Maxima: 160 Å min^{-1} for SiO_2 (CF_4, C_3F_8, SF_6); 27 Å min^{-1} for Si (all 4 Freons); 200 Å min^{-1} for Si_3N_4 (CHF_3, C_2F_6); all using B93 source, C.A.I.T. 150 mm, normal incidence, $V_A \simeq 3$ kV, I_D = 150 mA
5. Major Hazards	Toxic and corrosive waste products exhausted by pump, but flow rates lower than for plasma reactor
6. Physical Damage	Pitting of etched surface observed after using SF_6 beam. No other evidence of damage has been observed
7. Resist Materials	PMMA and Kodak 747 have been used. Resists apparently crosslink and were removed during this investigation by oxidation with an air plasma
8. Resolution	0.5 μm wide lines etched in SiO_2. Vertical profiles etched in this material indicate resolution limit set by definition of features in resist layer
9. Loading Effects	Not investigated. Etch rate limited by beam current density
10. Device Characteristics	Maximum M.O.S. capacitor flatband voltage measured was ≃6 V after 30 minute exposure to B93 Ar beam at 2.35 keV and ≃13 μA cm^{-2}

FIG.1.1 Silicon Etch Depth as a function of Over-Etch Time for various selectivities. For any etchant on SiO_2.

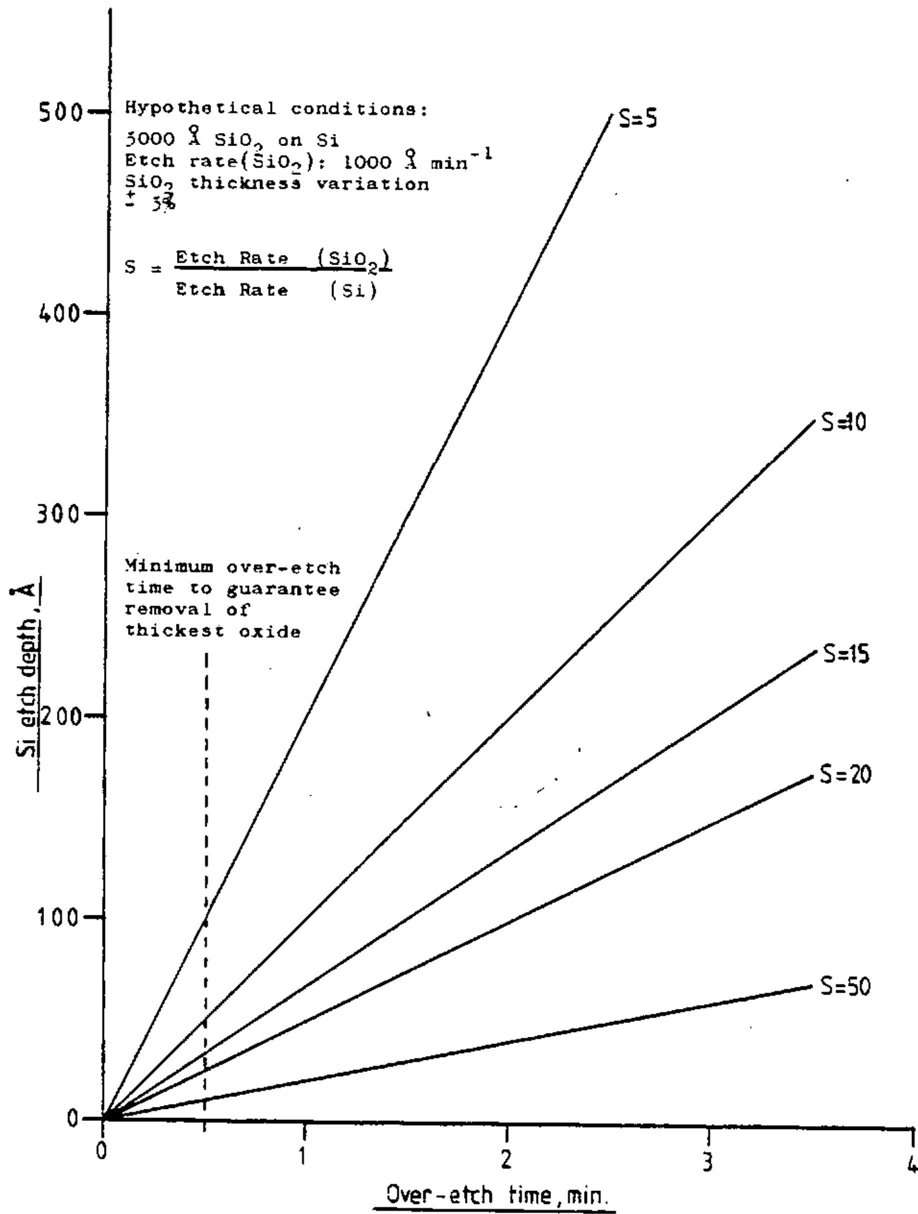

2. REVIEW OF PREVIOUS WORK

2.1 PLASMA AND REACTIVE ION ETCHING

2.1.1 Introduction

The possible uses of plasma etching as a commercial process were appreciated some time ago (Irving, et. al., 1971). The equipment described was used for detecting pin holes in insulating layers and etching deep scribe-lines as an aid to dicing wafers into individual integrated circuits. At about the same time a process was described (Irving, 1971) for the removal (or "ashing") of photoresist layers using an oxygen plasma, a procedure which is still widely used.

The commercial advantages of dry etching were identified and impetus in the research was directed at three major aspects:

(i) anisotropy

(ii) selectivity (applied to the requirements of specific processes)

(iii) wafer throughput (i.e. material etch rate)

Investigations carried out predominantly within the industry over the past ten years have been aimed at incorporating modifications to equipment and processes leading ultimately to compliance with a set of criteria (such as those described in Section 1.4) in a production environment. Consequently, designs and operating parameters have changed significantly, for example the trend towards lower pressures, internal planar electrodes and the use of chlorinated instead of fluorinated etchants.

2.1.2 Anisotropy

The degree of anisotropy produced by an etchant on a target is dependent upon

(i) the mean free path of reactive species (and hence pressure and temperature)

(ii) the nature of the etchant (i.e. atomic, free radical, ionic)

(iii) the construction of the reactor and electrode configuration

(iv) the excitation (R.F.) power and frequency.

Greater anisotropy may be obtained by increasing the etchant mean free path to a larger value than the smallest dimension in the resist layer, as shown in the literature (Jacob, 1976). This will have the effect of permitting only particles with trajectories normal, or nearly normal to the surface to enter into etching reactions. In practice, this is achievable at moderate pressures.

The mean free path of an etchant species is dependent upon the temperature, the pressure and the molecular or ionic diameter. Taking as an example the CF_3^+ ion, the diameter of which is approximately 2.8 Å (the C-F bond length is 1.41 Å) (Cotton and Wilkinson, 1967), at a pressure of 0.1 torr and temperature of 25°C, the ionic density is:

$$n' = \frac{(10^{-1}/760)(10^{-3})(6.02 \times 10^{23})}{(0.082)(298)}$$

$$= 3.24 \times 10^{15} \text{ ions cm}^{-3}$$

The ionic mean free path = $\sqrt{2}\lambda$, the molecular free path and so

$$\lambda_{ion} = (1.414) \frac{1}{4.44 \times (2.8 \times 10^{-8})^2 \times (3.24 \times 10^{15})}$$

$$= 0.126 \text{ cm}$$

which is clearly orders of magnitude greater than the minimum resist features in current use. Using the criterion of etchant mean free path alone, therefore, even pressures on the order of 0.1 torr can be used for the definition of sub-micron geometries.

The configuration of the R.F. electrodes and manner in which gas is swept over the wafers contribute to the isotropic etching which has been shown to be characteristic of barrel reactors (Bersin, 1978). Devices such as "etch tunnels" (perforated or mesh conducting screens surrounding the wafers) have been shown to improve the uniformity of etching across individual wafers (Bersin, 1976) by reducing the effect of charged species. The dominant mechanism is attack by atoms and free-radicals and as a consequence undercut profiles are usually produced (Robb, 1979). Observations that isotropy increases with increasing R.F. power density (Maddox, 1980) tend to indicate that the rate of production of uncharged species is dependent upon the ion-electron recombination rate at the mesh surface.

Planar reactors, which usually operate at lower pressures than barrel etchers, have been involved with an increasing number of applications (Heslop, 1980). Undercutting is usually significantly reduced (i.e.

anisotropy is increased), which has been shown to be predominantly due to the action of ions describing trajectories normal to the wafer surface (Poulsen, 1977). The formation of ideal mesa profiles has been demonstrated in a commercial process (Gdula, et. al., 1978). In this application, vertical edges were not required as subsequent processing produced some "mouseholing" (a void at the intersection of the etched feature and the substrate caused by poor penetration of deposited metal). Using a mixture of SF_6 and He, anisotropic plasma etching at 0.245 W cm^{-2} was used to define the features without loss of pattern definition. The vertical edges were then made slightly concave by etching at a lower power density (0.13 W cm^{-2}) in which the "chemical" etching component predominated. It would appear logical to propose that increasing power density leads to greater anisotropy because a greater proportion of the particles colliding with the target surface are ionised. The use of processes in which charged species play an active role in the etching has caused a distinction to be drawn between plasma and reactive ion etching (R.I.E.). These distinctions are somewhat arbitrary and are defined in the Glossary.

The mechanism of attack at the target is largely dependent on the species present at the wafer surface. The relative concentrations of charged and uncharged species is, in turn, a function of the chamber pressure. It has been found (Suzuki, et. al., 1978) that in a microwave discharge of CF_4, silicon is etched essentially

by ions (not specified, but presumably CF_3^+) at pressures below 1 x 10^{-3} torr. Above 1 x 10^{-2} torr the etching process is dominated by radicals and that both types of species contribute in the intermediate region (10^{-3} to 10^{-2} torr). Examination of etched profiles in Si and SiO_2 by other workers (Schwartz, et. al., 1979) showed that in a discharge of CF_4 at 20 m torr, silicon edges were straight and at about 80° to the substrate. Increasing the pressure to approximately 80 m torr produced undercut profiles typical of an isotropic process, indicative of the concentration of free radicals.

Using a discharge of chlorine (Cl_2) as an etchant for Si, an etched profile dependence on excitation frequency has been observed (Bruce, et. al., 1981). At 13.56 MHz undercutting was evident, but at 100 kHz the etched profiles were vertical. Some commercial planar reactors utilise R.F. generators towards the lower end of this range (Electrotech Plasmafab 425, 380 kHz, for example). Carbon tetrachloride (CCl_4) dissociated at a frequency of 380 kHz has been shown to produce vertical etched profiles in silicon (Gill, 1980). The profile dependence on frequency is due to the relative concentrations of the etchant species in the discharge. In a discharge of Cl_2, it has been shown (Flamm, et. al., 1981) that the concentration of Cl is nearly independent of frequency, but that the Cl^+ concentration drops very sharply above 1 MHz.

The relative concentrations of free radical and ionic species may also be altered by variation of the gas

mixture, and this subject will be discussed in more detail in Section 2.1.3. The concentration of free radicals in a discharge of CF_4 - O_2 mixture (as evidenced by the etch rate on samples protected from attack by ionic etchants) has been shown to reach a maximum at approximately 20% O_2 (Gill, 1980), which coincides with the maximum concentration of atomic fluorine, as shown in Fig. 2.1.

SF_6 (sulphur hexafluoride) plasmas were described some time ago for the etching of Si (Rai-Choudhury, 1971) and Si masked with SiO_2 (Stinson, et. al., 1976). Some experimental work has been carried out by the author using an SF_6 plasma in a planar reactor. Si has been etched for the fabrication of mesa diodes on implanted oxide layers and also for the formation of apertures for ink jet printing.

Shortage of space precludes a detailed account of that work here. Some of the results were rather inconsistent due, it is thought, to an intermittent leak of air into the plasma chamber. Anisotropic etching has been demonstrated, however, as shown in the scanning electron micrograph, Fig. 2.2. The target material was single crystal Si and the pattern was defined in Kodak 747 microneg (removed in an air plasma before examination). The wafer was bonded to the earthed electrode which was controlled at $29 \pm 1^{o}C$. The pressure was 0.15 torr, both electrodes were stainless steel, separated by 16.3 mm and the R.F. power density at 13.56 MHz was 0.93 W cm^{-2}. Another micrograph, Fig. 7.1, which is included in

Section 7.2.3 shows the isotropic etching of silicon under conditions which were ostensibly the same as those described above, but here the chemical component of etching has exceeded that due to the ionic species. This was probably due to the increased concentration of atomic fluorine caused by the admission of atmospheric oxygen. In a discharge containing SF_6 and O_2, the concentration of atomic fluorine has been shown to reach a maximum at 20% of O_2 (d'Agostino and Flamm, 1981).

2.1.3 Selectivity

The research effort applied to the formulation of gas mixtures to provide the highest possible selectivity in a particular application has been significant. Early work in this area (Heinecke, 1975) showed that the chemistry of a CF_4 discharge could be altered by the addition of hydrogen. Apart from the notable contributions made by certain workers (Flamm and co-workers, Coburn and Winters, Harshbarger and Porter) towards an understanding of the mechanisms of plasma chemistry, much of the literature describes the "cut and try" experimental approach.

Selective etchants may be grouped into three very general categories:

(i) the selectivity of a pure gas is dependent on the relative concentrations of reactive species in the discharge (CHF_3 as the parent gas, for example)

(ii) etchants in which the concentrations of some species are increased or decreased by the addition of a second gas (O_2 in CF_4, for example).

(iii) in which the selectivity of the mixture is greater than that of the individual components (C_2F_6 + Cl_2, for example)

A representative selection of data are shown in Table 5, mostly from the recent literature, which shows the increasing emphasis on chlorinated etchants. The high selectivities measured for fluorine (in atomic form and produced by the dissociation of SF_6, for example) are significant for production purposes, but the degree of isotropy may prove to be unacceptable. Variable results may be obtained, dependent upon the material used for the construction of the plasma chamber and electrodes; Stinson's results obtained using SF_6 may have been influenced by etching of the quartz vessel. High selectivities combined with increased etch rates compared to discharges of CF_4, are reported for NF_3 plasmas (Ianno, et. al.) although no observations have been described for the resultant etched profiles.

2.1.4 <u>Etch Rates</u>

The major parameters influencing material etch rate are:

(i) R.F. power density
(ii) Excitation frequency
(iii) Pressure
(iv) Etchant supply rate
(v) Target temperature
(vi) Chemical composition of the discharge

Provided the peak-to-peak voltage remains constant, increasing R.F. power density should give an approximately

TABLE 5

PUBLISHED DATA FOR PLASMA AND RIE SELECTIVITIES

Gas or Gas Mixture	Single Crystal Si: SiO_2	SiO_2: Single Crystal Si	Si_3N_4: Single Crystal Si	Poly Si: SiO_2
CF_4	1.28 (1)			
CF_4	1.9 (2)			
CF_4	1.47 (3)			
CF_4	≃10 (4)			
CF_4 + 4% O_2	-	-	-	9.8 (5)
CF_4 + 10% O_2	1.67 (1)			
CF_4 + 20% O_2	1.8 (1)			20 (14)
CHF_3		6.8 (3)		
CHF_3		>10 (6)		
C_2F_6		3 (6)		
C_3F_8		5 (4)	>15 (4)	
C_3F_8		5 (6)		
Cl_2	3.3 (7)			
CCl_4	3.31 (7)			
C_2ClF_5				3.4 (5)
C_2F_6 + Cl_2				32 (8)P
C_2F_6 + CF_3Cl				3 (8)U
F, (atoms)	42 (9)			
SiF_4 + 2% O_2	10 (10)		9 (10)	7 (10)
SiF_4 + 4% O_2	7 (10)			
SF_6	6.4 (11)			
SF_6	35 (12)			
NF_3	25 (13)			

References:

(1) Gill, 1980
(2) Schwartz et. al. 1979
(3) Chinn, et. al. 1981
(4) Heinecke, 1975
(5) Hayes & Pandhumsoporn, 1980
(6) Heinecke, 1976
(7) Schwartz & Schaible, 1980
(8) Mogab & Levinstein, 1980
(9) Flamm, 1979
(10) Boyd & Tang, 1979
(11) Stinson, et. al. 1976
(12) d'Agostino & Flamm, 1981
(13) Ianno et. al. 1981
(14) Ephrath, 1979

Notes: P: p-doped poly Si
U: undoped poly Si
Maximum selectivity values in each case

linear increase in material etch rate. This is shown to be the case for SiO_2 and Si_3N_4 (Hollahan and Bell, 1974), and is analogous to the dependence on beam current density in ion beam etching. Data presented by workers using CF_4 in the reactive ion etching of Si and SiO_2 also show an approximately linear dependence (Schwartz, et. al., 1976) as shown in Fig. 2.3. More recently, however, pronounced deviations from linearity were shown (Chinn, et. al., 1981) for Si and SiO_2 etched with CF_4. It seems likely however, that this was caused by the non-linear voltage response of the power supply.

The etch rate variation of some materials as a function of excitation frequency has been studied for chlorine plasmas and a typical curve is shown in Fig. 2.4. In this example the etch rate of Si is observed to drop rapidly when the frequency is increased above $\simeq 1$ MHz. This was shown to be due to (a) the reduced concentration of Cl^+ in the discharge and (b) the decreasing plasma impedance causing ion bombardment energies to decrease.

The effect on the SiO_2 etch rate of increasing chamber pressure, for a discharge of CF_4 is shown in Fig. 2.5. The two curves also show the difference between etching the target biased ("coupled") and floating ("decoupled"). The increasing etch rate with rising chamber pressure for the coupled samples is probably due to the increasing concentration of ionic etchant species impacting the target surface. The effect of these species decreases as the pressure is increased, due to the greater probability of collisions in the discharge.

In the case of a discharge supplied with a constant flow of parent gas, increasing the area of target material leads to a reduction in etch rate, as shown in Fig. 2.6. This "loading effect" is caused by the discharge becoming depleted of etchant species (fluorine atoms in this case). The etching mechanism is, therefore, reactant supply limited and for consistency of results it is important that this parameter is investigated for specific equipment-etchant-target combinations.

Unpredictable etch times were obtained for constant film thicknesses using early barrel reactors, and run to run variations of etch rate were significant due to the thermal characteristics of the cylinder. Data are shown in Fig. 2.7 for the SiO_2 etch rate dependence on reactor temperature, with R.F. power as parameter. The use of temperature controlled planar electrodes has reduced the influence of this variable.

The effect of varying the chemical composition of the discharge on the etch rate of four materials is shown in Fig. 2.8. The use of SiF_4 (silicon tetrafluoride) as an etchant has not been as thoroughly investigated as discharges of CF_4, and so the chemical processes are not established. The etch rate dependencies on oxygen addition are similar to those reported for CF_4/O_2 mixtures. It can be seen that the etch rate of Si_3N_4 is virtually independent of oxygen concentration in SiF_4 and that the selectivity to the other three materials is greatest at the lowest addition reported. For a production process, therefore, the only benefit to be

gained by oxygen addition would be to increase the (111) Si or poly-Si etch rate to economic levels and to still maintain selectivity over SiO_2.

Exceptionally high etch rates have been reported for the laser-induced dissociation of halogenated compounds (Steinfeld, et. al., 1980). A "true etch rate" of 12×10^6 Å min^{-1} was quoted for the removal of SiO_2 by CF_3Br dissociated using a pulsed CO_2 laser (9.23 μm). Only preliminary results have been reported for this technique and it is not certain that the beam "on time" and duration of reactive species formation are identical. In addition, only etching by CF_3 was considered, even though the action of bromine atoms would be anticipated.

2.1.5 Analytical Techniques

Methods of end point detection fall into two broad categories:

(i) Those in which the characteristics of the discharge are monitored.

(ii) Those in which the properties of the target are monitored.

During the etching of Al with CCl_4, the change in discharge impedance was shown to correlate with the Al-Cl emission at 2616 Å (Ukai and Hanazawa, 1979). Measurements of the electrode voltage showed an initial decrease, a period of constant potential while $AlCl_3$ was present in the plasma, followed by an increase to the original level when all Al had been removed.

A simple technique using measurements of pressure has been shown to be applicable to some target-etchant

combinations (Hitchman and Einchenberger, 1980). The increase in pressure detected by either Pirani or capacitance manometer gauges when a poly-Si film had been etched through was due to the increase in F atom concentration, as indicated by the increased emission at 7040 Å.

Several techniques have been reported for the in-situ monitoring of target properties. Instrumental chemical analysis, for example the emission spectroscopy of the chlorine etching of InP (indium phosphide) and Ga As (gallium arsenide) (Donnelly, et. al., 1981) has provided information on the etching process and can be used for process control by monitoring appropriate spectral lines. The use of mass spectrometry has been shown to be an invaluable technique for investigations of plasma chemistry (Flamm, 1981). The use of this technique for process control must, however, be viewed with some caution as the large volume of data produced usually requires analysis by computer, especially the assignment of specific ions to the multiplicity of m/c values usually recorded.

An in-situ optical technique using a He-Ne (helium-neon) laser has been described for the reflectivity comparison of the etching target surface with that of an unetched reference (Rodionov, et. al., 1980). The use of a strobe light to generate photocarriers in nude Si following the removal of an SiO_2 film (Geipel, 1977) was an elegant technique, but is probably excessively complex for production purposes.

2.1.6 Safety

The major hazards associated with all forms of gas phase etching are:

(i) The toxicity of the parent gas and the possible need for special handling procedures (for example the vapourisation of liquid sources). Some toxicity data are included in Appendix III.

(ii) Emission of toxic waste products from the vacuum exhaust.

(iii) The adsorption of toxic reaction products (particularly oxidised compounds such as the carbonyls) on vacuum chamber fittings and cylinders, which may be harmful by skin contact and/or inhalation.

(iv) The accumulation of corrosive and/or toxic reaction products in pump fluids. These hazards can be significant when pump oil changes are undertaken. Some details of vacuum equipment performance and analysis of pump fluids are included in Section 4.7.

(v) Explosion due to the high temperature oxidation of hydrocarbon pump fluid when exhausting pure oxygen through a rotary pump. A detailed study of this subject (Weikel and Yuen, 1972) concluded that certain fluids (for example Welch Duo-Seal and MIL-H-19457B hydraulic fluid) detonated whilst in the form of a mist or when trapped in the exhaust filter when 100% oxygen was pumped. Changing the fluid to Krytox 143AY (perfluorinated alkyl polyether manufactured by the Du Pont Company)

completely prevented the occurrence of further events.

(vi) Those associated with R.F. generators operating at up to 700 volts and 13.56 MHz; D.C. high voltage (up to 6 kV, 300 mA) supplies used with Saddle Field sources, and vacuum equipment generally.

2.2 SADDLE FIELD SOURCES

2.2.1 Introduction

Saddle Field sources possess a number of advantages over heated filament ("Kaufman") ion sources. Among these advantages are: the absence of filaments and large magnets, the requirement of only one power supply and neutralisation of the beam without additional filaments. In contrast, however, the disadvantages associated with Saddle Field sources are: lower beam "currents" are produced than with a heated filament source of comparable size and input power, the beam is always divergent and satisfactory operation is not usually possible with an anode potential of less than 800 to 1000 volts. This chapter will review the published literature on the development of sources utilising the cold cathode oscillating electron principle, with particular reference to their use as tools for the dry etching process.

2.2.2 Early Working Models

The principle of confinement of charged particles by electrostatic fields alone was demonstrated by A.H. McIlraith (McIlraith, 1966). He used a cylinder of 25 mm diameter and 102 mm long as the cathode, with twin copper wire anodes 0.318 mm diameter and 2.5 mm apart equally disposed internally on its axis (see Fig. 2.9). McIlraith was able to sustain a glow discharge of air within the source at a vacuum chamber pressure of 4×10^{-4} torr. The discharge drew 10 to 20 μA at an anode potential of 4 kV. The interdependence of source pressure and anode potential was also demonstrated, as

the discharge could not be sustained with a chamber pressure of 8 x 10^{-5} torr, even with an anode potential of 6 kV. The twin anode configuration was shown to be superior to the single anode construction produced earlier (McClure, 1963), which was not capable of sustaining a discharge at chamber pressures below 3 x 10^{-3} torr. These measurements led to the conclusion that the electron mean free path was increased approximately 40 times by incorporating a second anode. McIlraith postulated that electrons originating from certain regions of the cathode cylinder would describe stable trajectories, some of which are shown in Fig.2.10. In a later paper (McIlraith, 1972) it was shown that the mean distance travelled by an electron before capture at one of the anodes was of the order of 5 km for a stable discharge to exist within the source at a chamber pressure of 5 x 10^{-6} torr. The possible applications of this device to the thinning of specimens for electron microscopy and the etching of microelectronic circuits were also realised at this time (McIlraith, 1972). It is appropriate at this stage to consider the physical constraints on the working of these devices, and the mechanisms of operation.

2.2.3 Anodes

The earliest source reported (McIlraith, 1966), contained twin copper wires as anodes, presumably for ease of construction. Various workers appreciated that the inter-anode spacing and anode-cathode separation dimensions were critical to the performance of the source. In order to prevent distortion of the anodes due to

thermal stress, one of the first working sources to be described (Fitch, 1970) was made with two tungsten wires 0.3 mm diameter held in tension with springs. Greater stability of the anode assembly was demonstrated later (Franks, 1972a)when a source was operated with tungsten wires of 1 mm diameter. Sources of similar construction were produced by many workers, using a maximum anode wire diameter of 1.5 mm. It was observed (Fitch and Rushton, 1971) that specimens subjected to ion bombardment were also exposed to radiant heating from the anodes. These workers estimated the temperature of the wires at equilibrium to be approximately 1000°C and proposed water cooled anodes. In order to reduce the heating effects, these workers (Fitch, et al., 1974) and another, later (Ghander, 1976) replaced the tungsten wires with 3 mm diameter stainless steel tubes and circulated cold water through them, using PTFE tubing to provide the necessary isolation from earth. The stability of the source was improved, as "sooty" deposits observed on the anodes of the uncooled source were no longer apparent. Instead, the cooled anodes became covered with a "blue coating", which research into the cross-linking of pump fluids (Baker, et. al., 1971 and Holland, et. al, 1973) has indicated could be attributed to electron cross-linked polymer formation. More recent work (Fitch, et. al., 1981) has shown that the stability of one type of source used for specimen thinning is temperature dependent. Experiments by these workers showed that a pronounced reduction (2×10^9 to 10^7 ohms) in resistance of the

alumina high voltage insulator bushes occurred at an anode temperature in the region of 460°C. A discussion of the failure modes of the B93 source used in this study is included in section 3.2.3.

A "saddle field ion source", described in the literature (Franks and Ghander, 1974) was a significant departure from the design of McIlraith. This device employed a flat plate of refractory metal (probably tungsten) with a central aperture, mounted between two "shields" at cathode potential and was capable of producing two symmetrical "ion" beams. Sputtering experiments with this source will be described in section 2.3.

Many workers have studied the effect of the inter-anode separation on source characteristics. In one design (Rushton and Fitch, 1971) the performance was optimised with a separation of 6 mm. At a separation of 4 mm a discharge could not be sustained with an anode potential of 9 kV. Under these conditions of applied voltage and anode separation there is effectively no "saddle point" and the source would be expected to operate in a similar fashion to the single anode configuration. This is because the flux fields of two positively charged parallel wires produce lines of equipotential which are "dumbell" shaped (Attwood, 1967). As the potentials are brought together, the equipotential surfaces become less sharply convergent at the point midway between them and electrons undergo progressively decreasing electrostatic acceleration.

The separation between anodes cannot be considered in isolation, however. It has been shown (McIlraith, 1972) that if the cathode diameter is greater than 13 times the distance between the anode rods, stable oscillation of electrons is not possible, and no discharge will occur. Computer simulations to verify this have been carried out (Dean and Hibbins-Butler, cited by McIlraith, 1972) but the results have not been located in the published literature.

An inter-anode distance of 8 mm has been used in several source designs (Rushton, et. al., 1973 and Fitch, et. al., 1974), in these cases the cathode diameter was selected essentially on the basis of the above design criterion.

2.2.4 Cathodes

The first working oscillator to be described by McIlraith used a cylindrical copper cathode. This material was found to be unsuitable, because of

(i) poor mechanical strength, especially after heating
(ii) the rapid rate of oxidation, again especially at high temperatures
(iii) the difficulty of machining, due to its softness

Stainless steel cathodes were, as a result, used almost exclusively following this early work.

It was recognised (McIlraith, 1972) that the operation of the cold cathode source was dependent upon the emission of one or more secondary electrons at the cathode for every oscillating electron lost by capture at the anodes. Experimental evidence (Rushton and Fitch,

1971) indicated that sources constructed with a stainless steel cathode could not be operated at vacuum chamber pressures lower than 10^{-6} torr, presumably due to the excessive mean free path of the oscillating electrons. An experimental source constructed by Ion-Tech Ltd which incorporated a magnesium cathode displayed similar discharge threshold and current efficiency characteristics to a device of the same size with a stainless steel cathode (Evans, 1981). These observations were not altogether surprising as the δ_{max} values for Mg and Fe are 0.95 and 1.3 respectively at primary electron energies (E_{pmax}) of 300 and 400 eV (Handbook of Chemistry and Physics, 1972). The choice of materials for the construction of the B93 source are described in section 3.2.1.

It was found that (McIlraith, 1972) electrically conducting plates were required to enclose the ends of the cylinder, to prevent ejection of electrons. Electrons oscillating longitudinally between the cylinder end plates cause perturbations in the stable trajectories of those electrons oscillating between the cathode and the saddle-point. The minimum cylinder length which could be used without the influence of these "end effects" was found to be:

$$L = 2d + a \qquad \text{(Franks, 1972)}$$

where: d is the internal diameter of the cathode cylinder
a is the length of the ion exit aperture (see section 2.2.5)

Measurements of "witness marks" caused by sputter erosion of the cathode, enabled other workers (Rushton and Fitch, 1971) to formulate the minimum cylinder length as:

$$L = 2\left(\frac{0.75}{2} \times d\right) + a$$

The stability of these sources was found to be improved by the addition of metal cooling coils to the outside of the cylinder (Fitch, et. al., 1974 and Ghander, 1976). The first group measured the temperature of an uncooled cathode and found that it reached 170°C. Experimental work by the author with an uncooled B21 source (Revell, 1979a)has shown that this temperature is reached after about 25 minutes (argon discharge, $V_A = 6$ kV, $I_D = 2.5$ mA).

2.2.5 Ion Exit Aperture

Some of the early particle oscillators were simple "discharge tubes" and no attempt was made to extract ions from them. Observations of the discharge were made through an electrically conducting mesh covering one end of the cathode cylinder (McIlraith, 1966). By cutting a rectangular aperture (5 x 25 mm) in the cylinder such that the long sides were parallel to the plane of the twin anodes, an argon ion beam was extracted (Fitch, et. al., 1970). Current measurements made by translating a Faraday cage on the long axis of the aperture showed the beam to be well-collinated in that direction. Perpendicular to the anode axes, however, the profile was more wedge-shaped indicating significant beam divergence. At a chamber pressure of 5×10^{-4} torr, for a source

input of V_A : 6 kV and I_D : 5 mA, the maximum argon ion current density detected by the Faraday cage was 53 μA cm^{-2}.

Work with these early sources demonstrated that by variation of the shape and dimensions of the ion exit aperture,

(a) the shape and area of the beam at the target surface

and (b) the beam current profile in x and y axes could be altered.

2.2.6 Discharge Characteristics

Using a discharge of air which diffused into the source, the discharge current dependence on anode potential was measured with chamber pressure as parameter (Rushton and Fitch, 1971). Between 10^{-5} and 10^{-4} torr, large increases in anode voltage were accompanied by small increases in discharge current. At pressures greater than 2×10^{-4} torr, however, the rate of current rise with voltage became progressively steeper, reaching

$$\frac{dI_d}{dV_A} = 7.0 \text{ mA kV}^{-1} \text{ at } 8 \times 10^{-4} \text{ torr}$$

The discharge threshold, defined as the anode potential at a given chamber pressure for zero discharge current was 4.15 kV for this experiment. Measurements of discharge characteristics for a source made with anode rods and operating with argon showed consistently lower discharge thresholds and higher discharge currents, but the slopes of the curves were substantially the same as those described above.

Using a source fitted with 1.5 mm diameter anode rods, double diametrically opposed ion exit apertures and with argon supplied directly to the discharge region (as described by Franks, 1972 b), later workers (Ghander and Fitch, 1973) measured discharge characteristics significantly different to those reported before. In the chamber pressure range of 6 to 8 x 10^{-4} torr, the double beam source had a discharge threshold of 2-3 kV, approximately half that of the single aperture device. At lower chamber pressures, however, (10^{-4} to 6 x 10^{-5} torr) the discharge threshold of the double beam source was slightly higher (8.5-9.5 kV compared to 7-7.5 kV). It seems likely that the pressure inside the source was increased by the direct admission of gas more than it was decreased by incorporation of a second ion exit aperture.

2.2.7 The Neutral Component of the Beam

The neutral component of an argon beam produced by a source used for the thinning of specimens for examination using a transmission electron microscope (TEM), was estimated to be 30% (Franks and Ghander, 1974), based upon etching experiments in which electrostatic deflection was used to remove charged species. Etching experiments with an argon beam on glass targets produced smooth, polished features (Ghander and Fitch, 1974), from which these workers concluded that electrons present in the beam (as shown by Holland, 1972) prevented positive charge accumulation due to ion bombardment.

Experiments with a source using water cooled anodes and cathode (Ghander, 1976) showed that the argon beam

contained a similar neutral component to that described above, located in the centre of the beam. As with other work, electrons were detected in the beam, although no details were given on the method of distinguishing these from secondary electrons emitted from the target surface. Low energy (200 eV maximum) electrons have also been detected in high concentration (67% of the ion current) in a beam of H_2^+ and H^+ at 8 keV (Beghin, 1979).

It has been suggested (Franks, 1979) that ions recombine with secondary electrons produced by the ion bombardment of the cathode aperture. This mechanism would suggest that ion-electron recombination is more likely at the periphery of the beam, where the generation of secondary electrons is greatest. This does not explain the existence of the central neutral component observed by Ghander. Graphical data in this paper by Franks shows the dependence of neutral atom dose on anode potential (V_A). From this it appears that neutrals are formed in greater concentration at low values of V_A (which is directly proportional to the beam energy, V_B). Other work has shown (Rushton, et. al., 1973) that the beam divergence varies with chamber pressure, being greatest at high pressures (low V_A, "glow discharge" or "wide-beam mode"). It could be that the emission of secondary electrons required for the neutralisation process reaches a maximum at low energy due to the angle of incidence of ions on the edges of the cathode aperture.

Workers concerned with the production of ions for use in atomic spectroscopy (Freeman and Guern, 1978)

concluded that the beam produced by a small Saddle Field source contained a large proportion of "unionised atoms or molecules". The data presented gave the gas flow to the source as 2×10^{13} atoms sec^{-1} and the beam current equivalent to 6.3×10^{14} ions sec^{-1} (measured as ion current on a plate intercepting the beam). The electrical efficiency for Ar (beam current/discharge current x 100) was found to be 3%; no details were given of methods used to compensate for secondary electron emission due to the energetic atom bombardment of the receiver.

Several applications of neutral argon beams have been reported. The sputter cleaning of and subsequent film deposition onto insulating substrates is a useful technique which has been shown (Franks, et. al., 1979), under certain circumstances to provide increased film adhesion compared to deposition in the absence of atom bombardment. The fragmentation of temperature sensitive macromolecules by neutral (so-called "Fast Atom") argon beams has been used to advantage in the study, by mass spectrometry, of penicillins and peptides (New Scientist, 1981).

2.3 SPUTTER ETCHING WITH SADDLE FIELD SOURCES

2.3.1 Sputtering of Copper

Significant variations exist in the literature on the etch rate (hence S_m) of copper when etched by an argon beam produced by a Saddle Field source.

Figures reported for TEM specimen preparation (Franks and Ghander, 1974) were taken for a 2 mm diameter etched area. The etch rate of 18 $\mu m h^{-1}$ (3000 Å min^{-1}) is

equivalent to a sputter yield of 2.65 atoms/particle, using the b.c.d. (beam current density) of 1 mA cm^{-2} specified in the paper, although the measurement technique is not given. This value of S_m is extremely low, and would be obtained with 650 eV Ar^+ bombardment of Cu. It appears likely, therefore, that the b.c.d. has been overestimated in this case, and that a value of 0.5 mA cm^{-2} would give S_m = 5.3 atoms/particle which is in better agreement with the published sputter-yield data (Almen and Bruce, 1961) at 4.25 to 5 keV.

Similar, but more detailed work was carried out by another group (Fitch et. al., 1970) but there are apparent discrepancies. From the description in the paper it seems that the copper was etched for 60 min with a beam produced by injecting argon into the source, and that V_A was 8 kV (estimated V_B = 6.8 keV). The removal of 0.85 mg corresponds to 14.2 μg min^{-1} or 142 Å min^{-1} over a 0.9 cm^2 target area. Using the quoted b.c.d. of 0.1 mA cm^{-2}, the sputter yield is calculated to be 1.25 atoms/particle, which is equivalent to argon ion bombardment at energies of 200-300 eV. These authors also report that the sputter yield was 4 atoms/ion and that the b.c.d. was 100 μA cm^{-2}. Assuming that the weight loss figures are correct then there is a significant inconsistency between the b.c.d., the sputter yield and particle energy.

2.3.2 Miscellaneous Applications

The advantages of etching specimens for E.M. (electron microscopy) studies with an argon ion beam produced by a Saddle Field source were demonstrated

previously (Fitch and Rushton, 1971). These workers were able to observe details in the surface structure of several metals, a weld joint and an organic copolymer which was not possible using conventional (aqueous) etchants. A cold cathode source was also used for the treatment of specimens within an S.E.M. sample chamber, without removal between observations (Kynaston, 1970). By progressive etching of the specimen with an argon ion beam, successive layers of delicate plant cell structure were revealed.

Argon ion beam sputtering with a Saddle Field source is a useful technique for the controlled removal of material to form angular structures such as field-ion emission tips (Fitch, et. al., 1974) and sharp edges such as those required for small surgical scalpels (Evans, 1981).

The technique of thinning was automated with the introduction of commercially available equipment (Franks, 1974). Using such equipment, ion beam sputtering techniques for E.M. specimen preparation were shown to be relatively quick (material etch rates generally in the range 2 to 8 μm hour^{-1}) after initial thinning with abrasives and/or aqueous etchants, and improved analysis of the surface structure was demonstrated (Franks, 1977). The formation of electrically conducting coatings on specimens to be examined by S.E. microscopy has been accomplished by argon ion beam sputtering from various targets on to the sample (Franks, 1980). The grain size of films deposited in this manner is reported to be less

than the highest attainable S.E.M. resolution at present.

The incorporation of a fine beam Saddle Field source into the specimen chamber of an S.E.M. allowed another group (Lewis, et. al., 1980) to perform dynamic, in situ studies of the growth and erosion of cones on silicon due to argon ion/atom bombardment.

The foregoing literature contains very few details of beam characteristics, such as the neutral component. These workers considered the main advantages of this type of etching to be: relatively low bombardment energy, exposure to low levels of radiation (no heated filaments), processing in a "clean" environment (moderate vacuum) and equipment simplicity and reliability.

The author is not aware of any published literature (except that listed in Chapter 12) concerning the use of the B93 source with argon or fluorine-containing gases.

FIG.2.1

Contributions to the etch rates of Si and SiO_2 targets by ionic and free-radical components.

Etch-rate data: Gill, 1980
Fluorine emission data: Flamm, 1979

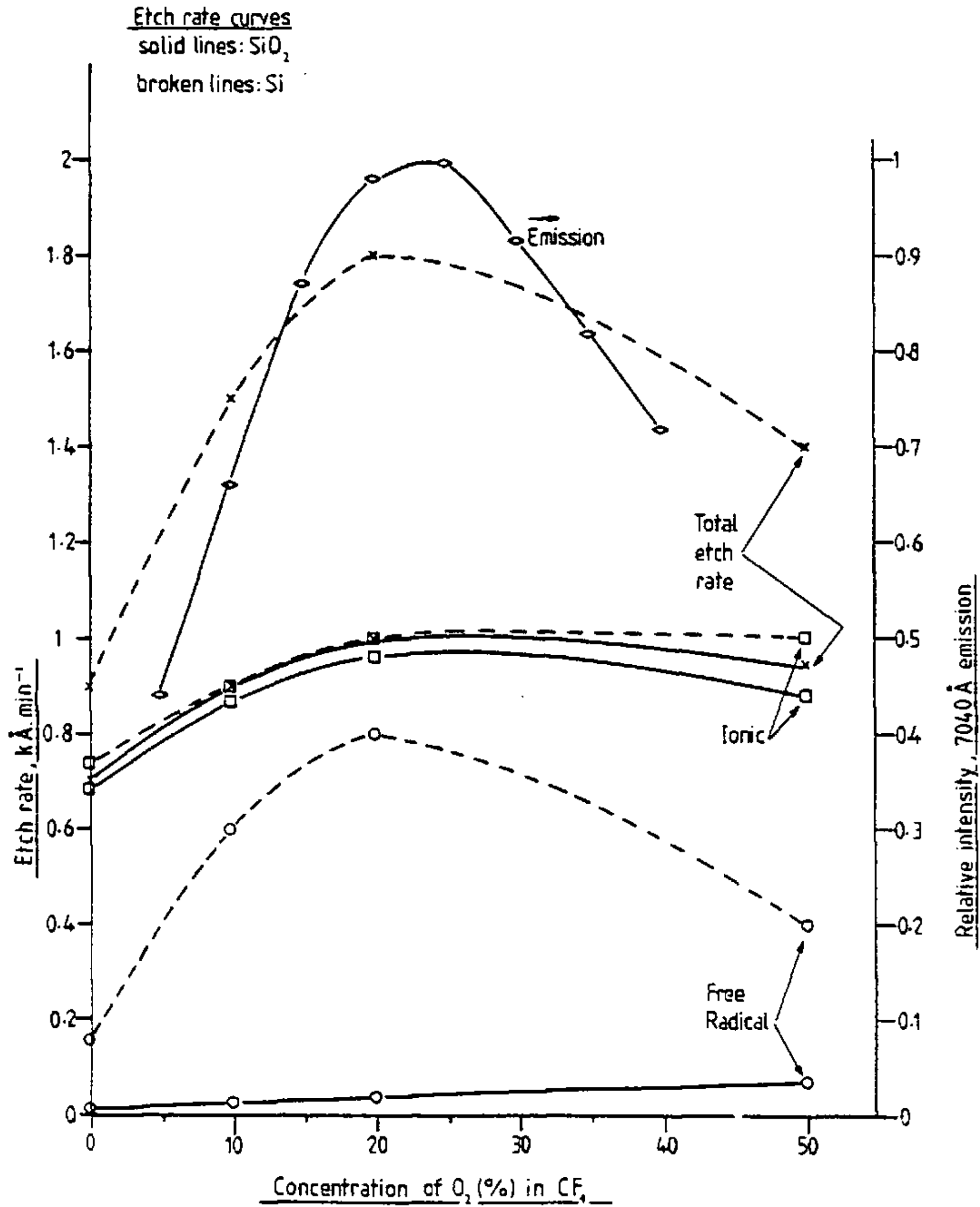

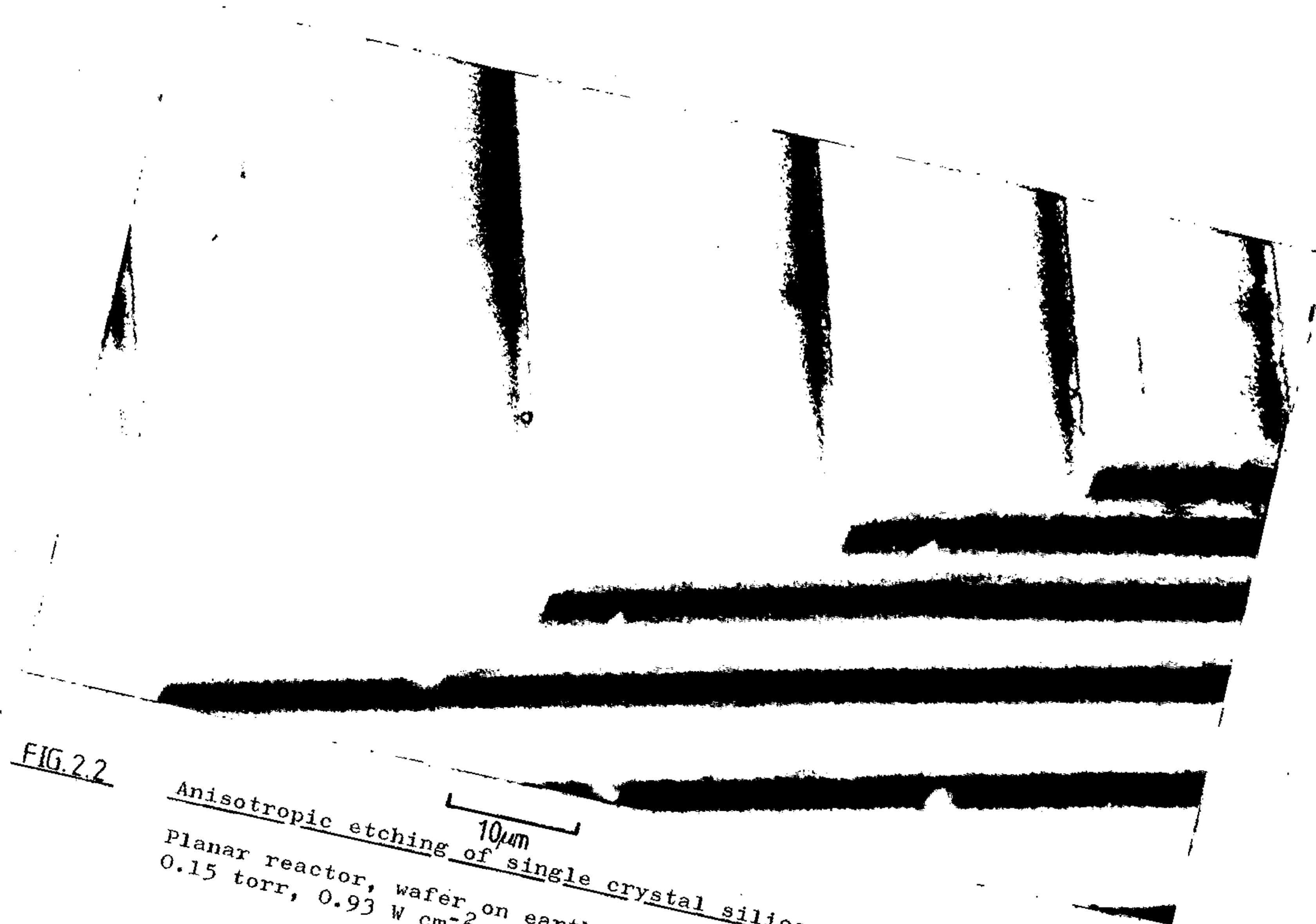

FIG.2.2 Anisotropic etching of single crystal silicon using an SF_6-plasma.

Planar reactor, wafer on earthed electrode controlled at 29 ± 1°C.
0.15 torr, 0.93 W cm^{-2}, 13.56 MHz, 2 minutes

FIG. 2.3

SiO_2 etch rate dependence on R.F. power density.

Planar reactor.
13.56 MHz, 0.05 torr
CF_4, Electrode area 613 cm^2.

After Schwartz et. al., 1976.

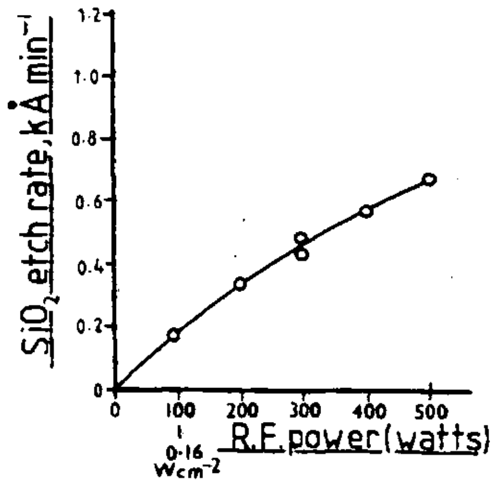

FIG. 2.4

Si etch rate as a function of excitation frequency.

Planar reactor, 0.6 W cm^{-2}, 0.3 torr, Cl_2.

After Flamm et. al., 1981(a).

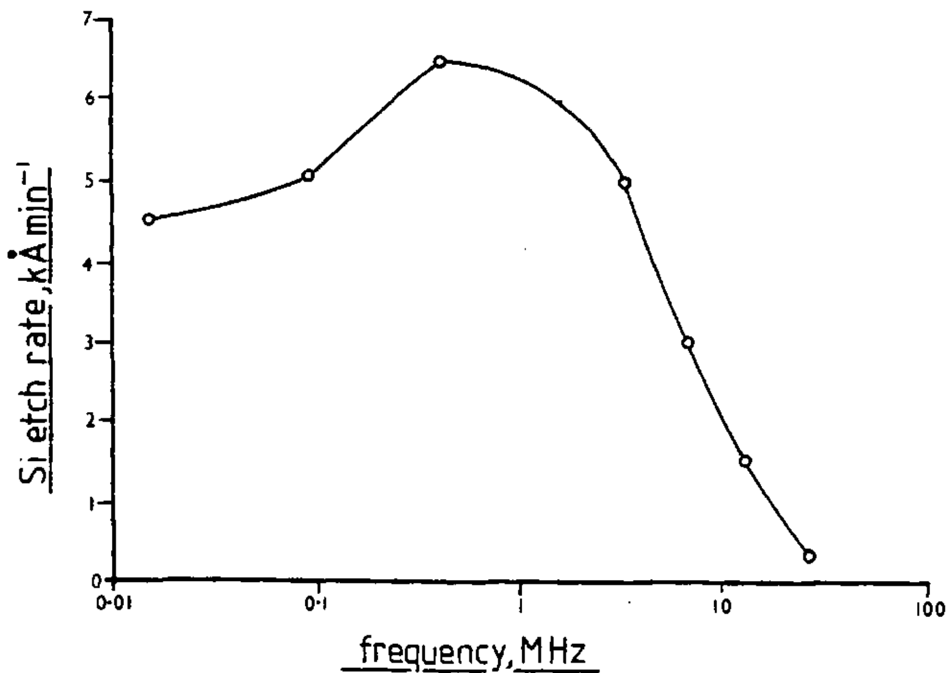

FIG. 2.5

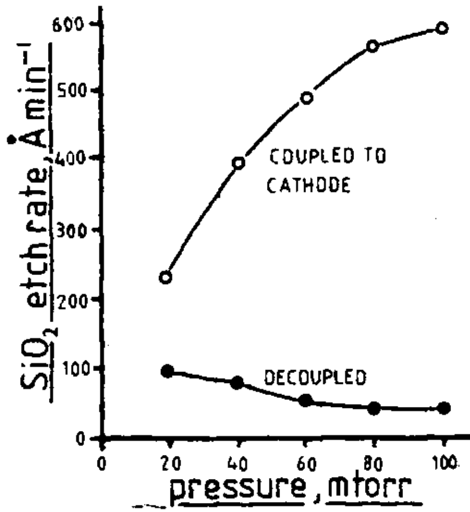

SiO_2 etch rate as a function of chamber pressure.

Planar reactor, 13.56 MHz 0.73 W cm^{-2}, CF_4, SiO_2 cathode.

After Schwartz et. al., 1979.

FIG. 2.6

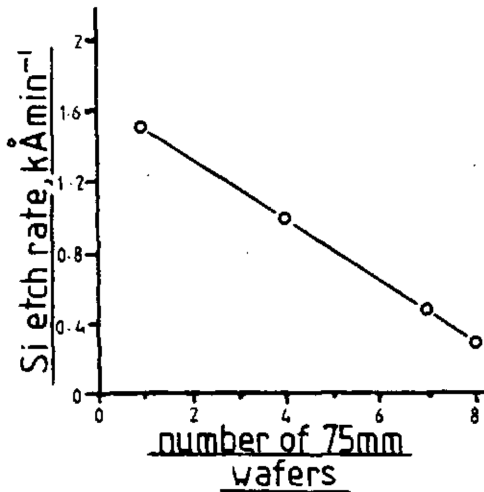

Si etch rate dependence on target area.

Barrel reactor, 50 W at 13.56 MHz, CF_4 + 4% O_2.

After Doken and Miyata, 1979.

FIG. 2.7

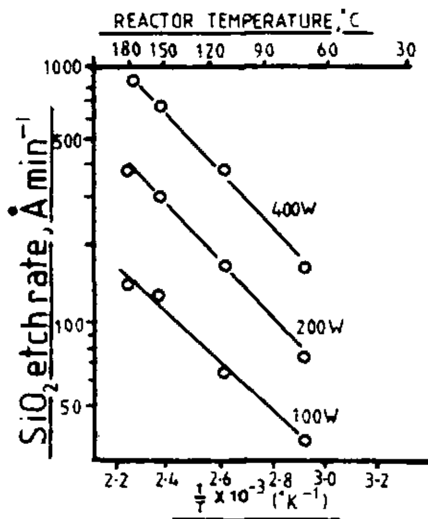

SiO_2 etch rate dependence on reactor temperature.

Barrel reactor, 1 torr, CF_4 + 5% O_2.

After Poulsen, 1977.

FIG. 2.8

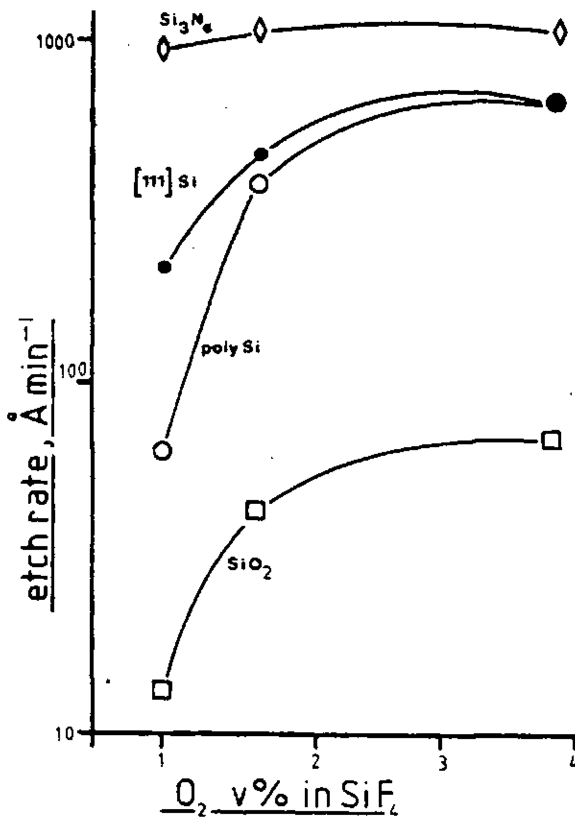

Etch rate variation with chemical composition, for four materials.

Barrel reactor, 1 torr 250 W at 13.56 MHz.

After Boyd and Tang, 1979.

FIG.2.9 The Saddle Field Source

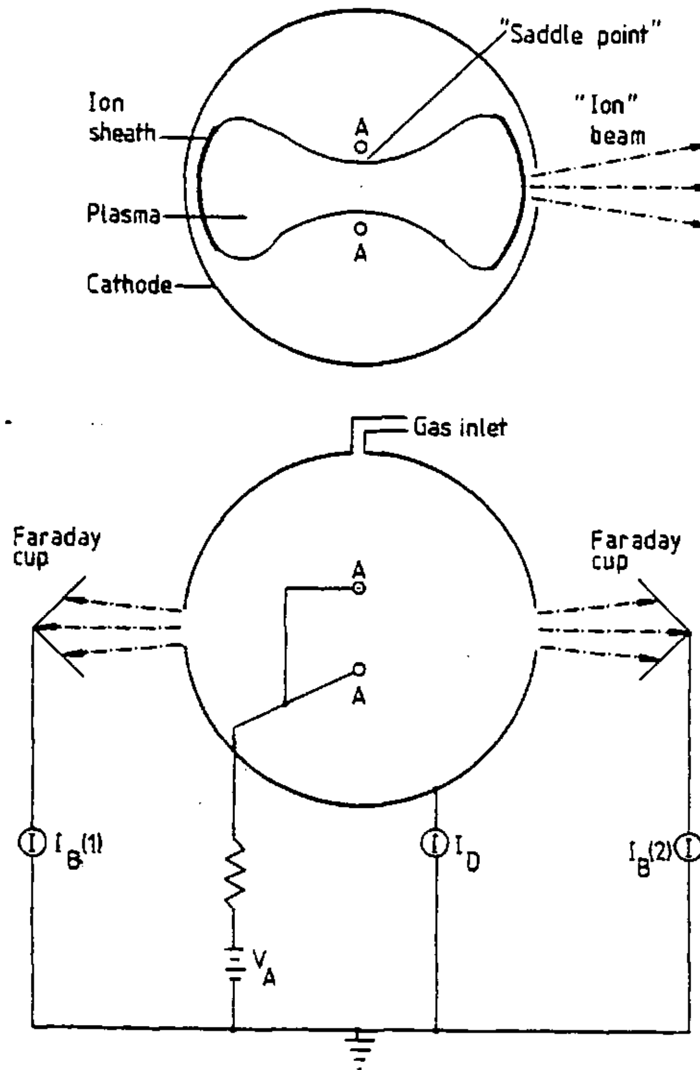

Top Sectional view of source showing the confined discharge reported by McIlraith (1966).

Bottom Electrical schematic showing the method used by Ghander and Fitch (1973) for determinations of beam current produced by a symmetrical source

FIG. 2.10 The Charged Particle Oscillator

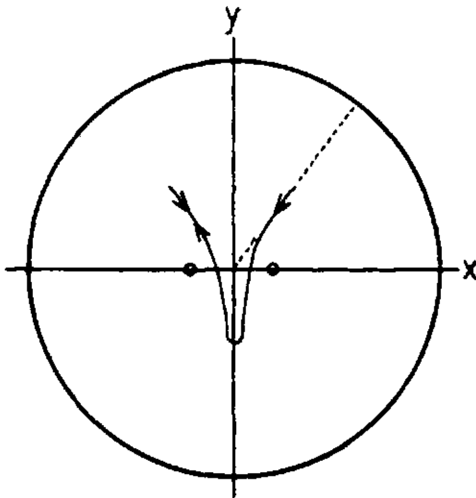

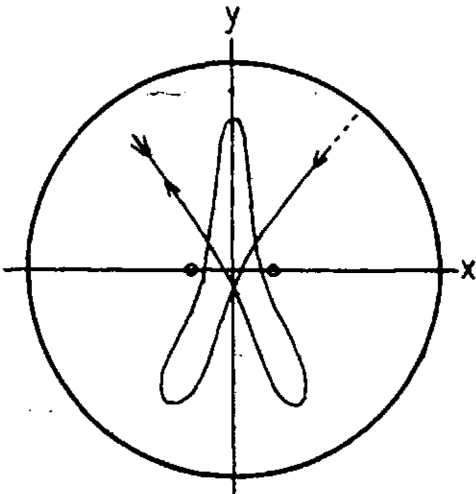

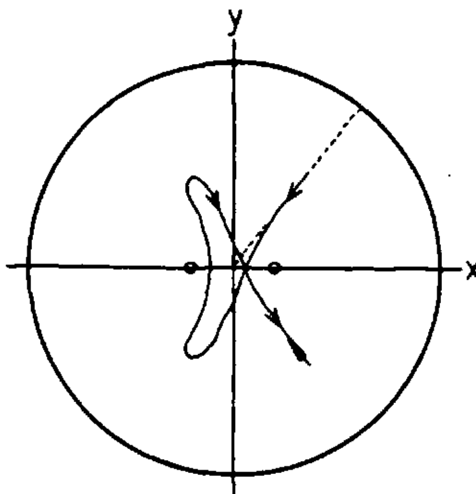

The principle by which a discharge is sustained in a Saddle-Field source. Three stable trajectories are shown for an electron attracted by a pair of equal, positively charged anodes.

After McIlraith, 1966.

3. CHARACTERISATION OF THE B93 SADDLE-FIELD SOURCE

3.1 INTRODUCTION

Three Saddle-Field sources produced by Ion-Tech Ltd have been used, the low power B21, the B93, and the largest source of this type, the B95; the characteristics are summarised in Appendix IV.

The following characteristics of the B93 source, injected with argon, have been measured and used as a basis for understanding experimental results such as etch rates, etch-depth variations across a target and radiation-induced damage in M.O.S. devices:

1. The total beam "current"
2. The beam "current" density distribution
3. The angular divergence of the beam
4. The beam energy dependence on anode potential
5. The particle extraction efficiency

3.2 DESCRIPTION OF THE SOURCE

3.2.1 Construction Details

The structure of the B93 source is shown diagrammatically in Fig. 3.1. The plasma chamber is lined with graphite, which is also the material used for the anodes. The reasons for this choice of material were:

(a) Secondary electron emission. The maximum emission yield for graphite (δ_{max}) is 1.0 at a primary electron energy ($E_{p.max}$) of 300 eV (Handbook of Chemistry and Physics, 1963). The operation of cold cathode devices is dependent upon the generation of sufficient numbers of secondary

electrons for stable plasma formation, particularly at the moment the device is energised as there is no other source (e.g. filament emission) of electrons. The choice of materials in this respect is rather limited, for example titanium (Ti) has a slightly reduced δ_{max} (0.9) at a lower $E_{p.max}$ (280 eV); silicon (Si) looks useful with a higher δ_{max} (1.1) and lower $E_{p.max}$(250 eV) but is difficult to machine. Aluminium (Al) has similar characteristics to graphite, but forms a passivating film within a few seconds of exposure to air, and this oxide has a high $E_{p.max}$(up to 1300 eV) (McDaniel, 1964).

(b) Sputter yield. It is important that positively charged, "foreign" materials are not extracted in the beam, particularly when semiconductor compounds which are sensitive to contamination are to be bombarded. The sputter yield for carbon is approximately 0.1 (atoms/ion $(1 + \delta)$ at 500 eV) (Bollinger, 1977), which is significantly lower than for most metals.

Two disadvantages of using graphite are that the thermal conductivity is low (0.012 cal cm^{-2} $cm^{o}C$) (Handbook of Chemistry and Physics, 1963) and the resistivity is excessively high (8.7×10^{-4} ohm-cm at $1000^{o}C$) (Handbook of Chemistry and Physics, 1963). The influence of both these parameters on the characteristics of the source will be discussed in Section 3.2.4.

The anode rods extend well beyond the cathode aperture region, in order to improve the beam current distribution and reduce the effect of longitudinally oscillating electrons. Cooling of the cathode aperture plate is inefficient as conduction to the water-cooled front body can only occur through the edges of the grid. Thinning of the cathode grid and end plates (A and B respectively in Fig. 3.1) by sputtering occurs, but the life expectancy of these components is many hundreds of hours under normal operating conditions. Under normal circumstances (i.e. for the work to be described here) the symmetrical rear beam is not extracted and a cathode blanking plate (also graphite) covers the aperture, although monitoring of the beam may be carried out with the installation of a suitable target to capture a proportion of the output.

The source was suspended from the top plate of the vacuum chamber by a rigid feed-through duct which carried water, gas and high voltage supplies.

3.2.2 Operating Parameters

The discharge is maintained by direct current from a current-stabilised power supply unit. The current is variable over the range 0-300 mA (I_D, discharge current).

The anode potential (V_A) may not be controlled directly, but is dependent upon the plasma impedance. The impedance of the discharge is dependent upon the gas pressure within the source. This internal pressure may be varied by control of the gas flow rate into the source, provided the pumping speed is constant. In practice,

V_A varies over the range - 800 V to 4000 V at the maximum current drawn by the discharge. 800 V is considered the lowest operating voltage for this source (with an argon discharge) and is the threshold below which ions are not extracted in significant quantities. There is a clear transition at about this energy, between the normal "oscillating" mode and the "glow discharge" mode which occurs at abnormally high source pressures (see Section 2.2.7).

3.2.3 Source Instability

The B93 source operated reliably with argon for hundreds of hours with little or no maintenance. Prolonged operation leads to instability which is observed as a low frequency oscillation between the stable "oscillating" state and the "glow" or "transition" states. The instability is due to one or more of the following:

(a) The most frequent cause is particulate carbon, sputtered from the plasma chamber or produced by the total dissociation of organic molecules becoming lodged in a region of high electric field. Regions most vulnerable to this form of tracking are the annular clearances between the anode rods and plasma chamber end plates (shown as 'C' in Fig. 3.1) and to a lesser extent the space between the anode termination plates and plasma chamber ('D' in Fig. 3.1). The resulting low impedance in parallel with the discharge causes a rapid drop in V_A (as I_D is held constant) and a reduction in beam power. In severe cases the resistive paths may be

sufficiently low to effect the operation of the overload protection circuit.

(b) Gradual deterioration of the high voltage insulator bushes (alumina) usually results in voltage oscillations or short-circuit conditions as previously described, which are exacerbated by the increasing temperature within the source. The dependence of insulator resistance on temperature has already been described. The deterioration of the insulators is also due to the accumulation of low molecular weight fragments produced by the dissociation of organic pump fluid vapour in this high field, high temperature region. As these bushes are porous, organic material diffuses into the structure, and subsequent cleaning is ineffective.

(c) Variation of beam power may also be caused by a change in the gas composition or flow rate into the source. A change in argon throughput from 0.339 torr litre sec^{-1} to 0.221 torr litre sec^{-1} (measured at the vacuum chamber baffle) will result in V_A increasing from 2 kV to 3 kV (I_D constant, 100 mA). To prevent fluctuations in flow rate due to debris accumulating in the gas control or associated pipes a stainless steel sinter of 2 μm porosity was installed immediately before the needle valve.

The length of time for stable operation decreases significantly when the source is operated with Freons.

One ultimate dissociation product of all halocarbons is carbon and, therefore, the major cause of source instability when operating with these compounds is a short-circuit due to tracking by trapped, conducting particulates. The mechanisms by which carbon is deposited, and also removed from the source is discussed in Section 7.3.1.

Apart from beam power fluctuations as a characteristic of electrical malfunction, the presence of particulate carbon within the source may be observed as small particles are ejected through the cathode apertures. This carbon is usually expelled at high velocity and is incandescent, indicating a particle temperature in the region of 1000°C.

The approximate "beam-on" time before instability is shown for 6 gases in Table 6. The times shown are accumulated over many experiments and the source was allowed to cool and was exposed to atmosphere between each run. It may be that the carbon produced by the dissociation of halocarbon molecules has a different coefficient of thermal expansion to the carbon of the anodes. The deposited film would, therefore, reach a critical thickness beyond which mechanical forces would cause flaking of the carbon away from the graphite. Thus it is not strictly valid to compare time-to-failure for Ar with times for the other gases, as most sputtering experiments with the noble gas ran for significantly longer than with the fluorinated compounds. The table

TABLE 6

Duration of Stable Operation for the

B93 with Various Gases

Parameter	Ar	CF_4	CHF_3	C_2F_6	C_3F_8	SF_6
Time Before Breakdown (min)	900	306	162	160	209	300
Number of Experiments	23 (1)	5 (2)	5 (2)	4	4 (3)	6 (4)

Notes

(1) A representative mixture of short and long runs. Shortest experiment = 23 min, longest = 100 min

(2) Incandescent particles ejected during run 5

(3) Includes 10 minutes operation with C_2F_6

(4) Breakdown not observed

includes the number of experiments performed, for the purpose of comparison. These data suggest that the maximum number of heating and cooling cycles before corrective maintenance, is 4 for the Freons tested. The accumulation of elemental sulphur on the anodes observed after using SF_6, did not seriously impair the performance of the source. Possible solutions to the problem of carbon accumulation are presented in Section 9.1.3.

Small quantities of particulate carbon may be removed in-situ by oxidation using an air discharge. This should only be viewed as a temporary solution and is not a substitute for thorough cleaning of the source components and replacement of the high voltage insulators. In addition, the graphite components of the discharge chamber will also become oxidised by this treatment, the cathode grid is particularly vulnerable in this respect.

3.2.4 Source Heating

Saddle-Field sources operate as cold cathode devices. Sources of low output power, such as the B21 rely on conduction of heat through the body and vacuum chamber fixtures for cooling. The B93 source will operate with a maximum input power of 900 W, and forced cooling of the source body by circulating mains water is necessary to remove the thermal energy generated in the plasma chamber. The anodes of this device are thermally floating and must attain equilibrium before a beam of constant energy is produced.

The "drift" of source characteristics with time, starting with the source at room temperature, is observed

as a progressive increase in anode potential (I_D, gas flow, pumping speed all constant). Fig. 3.2 shows the variation of plasma impedance with time, for an argon discharge. The curve clearly demonstrates the likely errors of etch-rate results from samples exposed to the beam for short periods (i.e. less than 30 minutes), with the source starting cold. The consistency of etch-rate data improved significantly after the installation of a beam shutter which was used to protect the targets during the initial period of beam energy drift. Based upon visual inspection, the B93 anodes are considered to equilibrate at approximately 900°C. The total impedance of the anode rods is calculated to be 7.22×10^{-3} ohms, and increasing to 7.80×10^{-3} ohms at 900°C.

The increasing plasma impedance is due to the decrease in the ion number density. This is so because the electron mean free path increases by a factor of 4 when the gas temperature is raised from 293°K to 1173°K (at this higher temperature λ_e = 114.55 cm for a hypothetical source plasma chamber pressure of 1×10^{-3} torr) - provided the pressure and atomic diameter are constant. From this it follows that the ratio

$$\frac{N_{Ar^+}}{N_{Ar^o}}$$

Where N is the number density of: ions accelerated towards the cathode and atoms injected into the source

decreases with time until thermal equilibrium has been established.

3.3 TOTAL BEAM CURRENT DETERMINATION

3.3.1 Experimental Objectives

(i) To determine the total beam current (I_B) by measurements of the etch rate of a given material.

(ii) To show the correlation between the etch rate and discharge current (I_D) and hence

$$I_B \propto I_D$$

(iii) With a knowledge of total beam area at a given distance (see Section 3.5), generate curves for the beam current density variation with cathode aperture to target (C.A.T.T.) distance, for use in other parts of this work.

At this point it is necessary to define the parameter that is to be measured. It is usual to describe beam current as the directional flow of charged species, that is, the current produced by a dose of n particles over a unit area in unit time, where the particles are either singly charged ions or electrons. It has been reported (Franks and Ghander, 1974) that some evidence has been obtained which indicates that a proportion of the beam from certain Saddle-Field sources is uncharged. Thus, the "beam current" determination is an "effective beam current" measurement, as no electrical parameters have been investigated.

The "effective beam current", I_B is defined as that dose of particles which produces an effect due to sputtering, equivalent to a flow of current caused by total ionisation (singly charged species) of the beam.

It is also necessary to define sputter yields:

$$S_{(atoms/atom)} = S_{(atoms/ion)}$$

given that the two species differ in mass only by one electron, and that the transfer of kinetic energy at the solid boundary is equal. For this to be true it is assumed that ions are accelerated to the maximum potential across the ion sheath close to the cathode aperture and that those which capture electrons subsequently suffer negligible retardation as a result of that interaction.

3.3.2 Design of the Experiment

Experimental criteria were adopted, as follows:

(i) The determination of sputter etch rate was by weight loss for known conditions of I_D, V_A, distance and time

(ii) The entire beam was incident upon the target

(iii) Sputter etching experiments were conducted with the source operating in (a) constant current and (b) constant voltage mode

(iv) The effects of contamination were minimised by: liquid nitrogen cooling of the diffusion pump baffle, clean preparation of samples and exclusion of all "foreign" materials from the area exposed to the beam

(v) The cathode grid was parallel to the target for all determinations (that is, the axis of the source normal to the plane of the target)

(vi) The target material was chosen on the basis of:

(a) availability in suitable sizes

(b) bulk, rather than film, of well-documented sputtering characteristics

(c) oxide formation at a "slow" rate, and easily removed by sputtering

(d) high sputter-yield under B93-Ar beam operating conditions

(e) sufficiently low resistivity to prevent charging by either positive ions (if present) or secondary electron emission

(f) low density and minimum sheet thickness, to minimise weighing errors

3.3.3 Experimental Method

3.3.3.1 Target Preparation

Copper (Cu) foil was selected on the basis of the listed criteria. The foil, in the form of rolled strip 38 mm wide and 0.29 mm thick was of low mass per unit area (approximately 0.226 g cm^{-2}). Three pieces of foil, each 107 mm long were used for each target. The target was assembled by clamping the foil strips at the edges using stainless steel screws set in an aluminium backing plate. The strips of foil overlapped such that the target presented to the beam consisted only of copper, the exposed area of which was 115.56 cm^2.

3.3.3.2 Target Cleaning

Each foil strip was degreased in isopropyl alcohol (ultrasonically agitated), rinsed in deionised water, etched in nitric acid to remove oxide (150 ml of 70% HNO_3 + 450 ml deionised water) for 3 minutes, rinsed

three times in deionised water, washed with isopropyl alcohol and blow-dried with warm nitrogen. Specimens were weighed immediately after cleaning.

3.3.3.3 Weighing

All targets were weighed on the same balance, of the single-beam, knife edge type. The balance vernier could be read to within an uncertainty of $\pm$ 50 µg. Errors introduced into the experiment are discussed later (see Section 3.3.5).

3.3.3.4 Target Mounting

After weighing, the three strips were positioned and clamped to the backing plate. The plate was equipped with studs which located precisely on the water-cooled platten in a fixed position beneath the B93. The cathode aperture to target distance was 73 mm throughout these experiments.

3.3.3.5 Sputter Etching

Argon was used as etchant gas for all of these experiments. After evacuation of the chamber to the usual base pressure (1.2×10^{-5} torr), the source was allowed to reach thermal equilibrium at V_A = 3 kV with the beam shutter closed (shutter positioned approximately 30 mm from the cathode aperture). Targets were exposed to the beam for the required duration by opening and closing the shutter with the beam conditions as specified. After etching, the source was de-energised and allowed to cool. Venting of the chamber was carried out by admission of oxygen-free nitrogen. The target plate was removed, strips were unclamped and re-weighed as described before.

3.3.4 Results

3.3.4.1 Sputter Yield Data

Sputter yields $[S_m/(1 + \delta \mp)]$ for Ar^+ on Cu have been obtained from the published literature (Almén and Bruce, 1961; Chopra, 1969; Eckertová, 1977; Laegreid and Wehner, 1961 and Southern, 1963). These data were plotted as a function of ion energy and the yields over the range of interest are shown in Table 7.

3.3.4.2 Treatment of Weight Loss Data

The "effective beam current" (I_B) has been determined for 5 values of discharge current (I_D), at fixed anode potential (V_A = 3 kV). The sputter etch rate dependence on particle energy will be discussed in Section 3.4. As the energy of the beam could not be measured directly, the following relationship, which was reported by Franks and Ghander (1974), has been used:

$$V_B = V_A \cdot 0.85 \quad \text{(keV)}$$

For the purposes of this work it has been assumed that the beam is monoenergetic and homogeneous.

The relationship between I_B and weight loss is found from the equation:

$$I_B = \frac{10^5 \quad W}{S_m . A . t} \quad \text{(Laegreid and Wehner, 1961)}$$

where I_B = Total beam "effective current", (A)

W = Mass of sputtered copper, (g)

S_m = Sputter yield, at given energy $[\text{atoms}/(1 + \delta \mp)]$ (see Table 7)

TABLE 7

Reported Values of the Sputter Yield

for Ar^+ on Cu

Ar^+ Energy keV	Sputter Yield, S_m, atoms/$(1 + \delta \mp)$			
	Maximum	Minimum	Mean	$\pm$ Standard Error
1.0	3.25	2.5	2.98	0.242
1.5	3.85	3.2	3.62	0.209
2.0	4.35	3.7	4.01	0.153
2.5	4.8	4.1	4.43	0.165
3.0	5.3	4.3	4.74	0.219
3.5	5.7	4.5	5.01	0.255

Data obtained by interpolation from smoothed curves derived from experimental results reported in literature cited in Section 3.3.4.1.

A = Atomic weight of copper, (63.54)

t = Duration of sputtering (sec)

S_m was taken as 4.45 for V_B = 2.55 keV.

The results are plotted in Fig.3.3 which shows both "effective total current" and rate of mass loss dependence on discharge current. These data fit the linear relationship with only small errors at I_D = 150 and 250 mA. The "current" curve indicates an apparent positive intercept on the ordinate. It is believed that this is due, not to deviation from linearity at $I_D < 50$ mA, but to a zero error on all scale readings of I_D. With the source current control set at minimum, the indicated discharge current is never less than $\simeq 25$ mA when the source is operated at $V_A \geq 800$ V.

These data will be used, in conjunction with beam area determinations, as the standards for the etching work to be described.

3.3.5 Errors in Beam Current Determinations

The known errors, some of which may be quantified, are as follows:

(a) The value chosen for S_m, the Sputter Yield. Table 7 gives the deviation from the value selected, at a given energy. Large variations in experimental determinations of S_m and deviation from sputtering theory are shown in the literature (Sigmund, 1969). The material used for this work was thought to be essentially polycrystalline as it was rolled foil. Fig.3.3 shows the effect of variations in published

values of S_m (all at 2.55 keV) on the "total effective beam current".

(b) The beam energy. This will be discussed in more detail in Section 3.4. As no beam energy data are available for this source, there is no means of quantifying the deviation (if any) from the previously described relationship between V_A and V_B. Care was taken to maintain V_A at the specified level, errors would, therefore be constant and only influence the value of S_m.

(c) Weighing errors. The maximum known error introduced into the weight determinations is $\pm$ 50 µg. The minimum measured weight loss from any one strip of foil was 1.1 mg. The maximum error in this case is

$$\frac{50 \times 10^{-6}}{1.1 \times 10^{-3}} \times 100 = \pm 4.5\%$$

This decreased to $\pm$ 0.3% at the maximum weight loss of 15.5 mg for one strip of foil.

(d) Surface contamination of the target. There was a small but detectable weight gain associated with the polymerisation of condensed organic materials on targets to be described in Section 3.5.1. This reaction only occurs at the periphery of the beam where the molecular condensation rate is equal to, or exceeds the arrival rate of bombarding particles. This source of error is most likely to be observed as a reduction in total beam area as the beam current density decreases at the edges.

(e) The angle of incidence. This will be shown later (see Section 3.5.2) to vary quite markedly across the beam area. As stated in point (a), the targets were of low crystallinity and as such would not be expected to display a significant sputter yield dependence on bombarding particle angle of incidence. To a degree, the effect of increasing S_m with deviation from normal incidence would be compensated by the reduced beam current density found when moving radially away from the centre of the beam (see Section 3.5).

3.4 BEAM ENERGY DETERMINATIONS

The etch rate dependence on particle energy has been measured using Ar bombardment of copper. The experimental procedures were identical to those described in Sections 3.3.1 to 3.3.4. The source was stabilised at I_D = 150 mA, with five values of V_A in the range 1 kV to 3 kV.

Fig.3.4 shows the removal rate of copper from the entire target plotted as a function of particle energy. This graph also shows the sputter yields published in the literature (cited in Section 3.3.4.1) plotted against Ar^+ energy. The curve of experimental results show that the removal rate increases smoothly with increasing energy. There is no evidence to suggest any deviation from the proportionality:

$$V_B = V_A . k$$

over the range of energies examined, although the value for k is assumed to be 0.85 in the absence of analysis by other techniques.

The question of absolute values for I_B and V_B are discussed in Section 9.1.5.

3.5 BEAM CURRENT DISTRIBUTION

The "current" distribution within the beam is primarily dependent upon:

(a) The anode plane to cathode aperture distance

(b) The anode rod separation

(c) The size, shape and distribution of the cathode apertures.

In addition, this characteristic is dependent upon the anode potential (i.e. the gas pressure within the plasma chamber), as already discussed (see Section 2.2.7). This effect will be investigated as part of the Proposals for Further Work (see Section 9.1.1).

Using weight loss data, the beam current distribution of the B93 source operating with argon has been obtained.

3.5.1 Sputtering of Copper with Argon

For this experiment, copper foil identical to that described in Section 3.3.3.1 was used. Using a sheet metal punch, 100 foil squares 10 mm x 10 mm were prepared. The squares were individually numbered (by scribing on the rear face), cleaned and weighed as previously described (see Sections 3.3.3.2 and 3.3.3.3). A matrix of 10 columns and 10 rows of copper pieces was prepared by mounting on an aluminium backing plate, using silver "Dag" as adhesive.

After evaporation of the solvent contained in the "Dag", residual silver particles were removed from the

exposed surface of copper using a swab soaked with acetone. The target so produced was a 10 cm x 10 cm copper sheet which was mounted beneath the B93 in the same position as for previous experiments (see Section 3.3.3.4). Due to the precision with which the squares had been cut, there was no significant exposed area of silver or aluminium between any of the individual targets.

After the usual pump-down and source equilibration procedures, the target was exposed to an argon beam of V_B=2.55 keV, I_D = 250 mA, 72 mm cathode aperture to target distance, for 100 minutes. The axis of the source was normal to the target plane, the etchant gas was filtered and the diffusion pump baffle was cooled with liquid nitrogen. Fig. 3.5 shows the target after etching.

The copper squares were removed from the backing plate after sputter etching, using acetone to re-suspend the silver. Finally, the squares were weighed and the weight loss was expressed directly as grammes cm^{-2}.

The results are shown plotted in Fig.3.6 in which lines on the X and Y axes represent columns and rows of the matrix. The Z axis is plotted directly as weight loss, the peak represents 4.6 mg cm^{-2}. The "effective beam current density" over any 1 cm^2 area of the matrix is directly proportional to the weight loss, provided:

(a) variations due to bombarding particle angle of incidence, and

(b) differences in beam energy, are small enough to be disregarded

As stated previously, (a) is expected to be very small for this target. No experimental data are available on the energy distribution, this must be analysed at a later date. Therefore, using the available data, Fig.3.6 is a representation of the B93 argon beam.

The data produced by analysis of the experimental results are summarised in Table 8. The figure of 4.8 mA for the total "current" is lower than the mean value (6.4 mA) described in Section 3.3.4.2. The reason for this is as follows: during the first few minutes of bombardment, the target appeared to darken, then the centre gradually became lighter as bright, atomically clean copper was exposed. After etching, the edges of the target appeared dark, with "streaks" clearly visible. The "streaks" coincided with the swabbing movements made to remove the excess "Dag" from the surface. In order to correct this total beam "current" it would be necessary to allow for:

(a) The time difference: $t_{total} = t_1 + t_2$

where t_1 is the time taken to remove the contamination by sputtering

t_2 is the duration of sputtering the copper target

(b) The reduced area of the beam - this effect is considerably smaller than that of (a). For the periphery of the beam, Where the "current" density is low, the ion arrival rate is similar to the condensation rate of organic contaminants (from the "Dag" and from the vacuum pumps), there was only

TABLE 8

Summarised Data for

B93 Beam "Current" Distribution

Parameter	Total Target	Mean Distribution
Weight Loss	81.4 mg	1.43 mg cm^{-2}
"Effective Current" *	4.8 mA	84.15 μA cm^{-2}
Area with Measured Weight Loss	57 cm^2	-
Area with Measured Weight Gain	30 cm^2 (4.95 mg total)	-
Area with no Measured Weight Change	13 cm^2	-

* Sputter yield (S_m) taken as 4.45 atoms/"ion" at 2.55 keV

slow sputter removal of contamination introduced by the swabbing and the copper remained coated. It is of interest to note that after bombardment, the contamination present on the targets outside of the defined beam area was tenaciously bonded and appeared to remain after ultrasonic agitation in acetone.

The distribution of "current density" within the beam is shown plotted in Fig. 3.7. This graph shows the rate of decrease of "beam current density" when moving away from the point of maximum (271 $\mu A\ cm^{-2}$).

3.5.2 Beam Divergence

At the target surface (described in Section 3.5.1), the beam area is defined by an etched region enclosed by an octagon. This geometric shape is solely due to the projection of the cathode grid matrix on to the target. The cathode grid comprises 52 holes in a symmetrical array of 8 rows, the outermost holes in this matrix form a regular octagon. The beam contains 52 "beamlets" as a consequence. The octagonal etched area at the target, however, is elongated in that plane, in the direction perpendicular to the anode axes. It is possible to characterise the beam in terms of:

(a) The component parallel to the anode rods

(b) The component perpendicular to the anode rods

(c) The beamlet matrix (this will be discussed in Section 3.5.3).

3.5.2.1 The Parallel Component

Fig. 3.8 shows a sectional,exploded view of the source and target arrangement. The weight loss

distribution is directly proportional to the particle dose. From this distribution it can be seen that a central, intense beam is superimposed on a broad element with steep leading and trailing edges. This beam profile is totally dissimilar to the collinated output of a heated filament source with extraction grids, but demonstrates the uniformity that has been obtained by designing the rods to be significantly larger than the cathode aperture. The angular divergence of the beam in this direction is 38.3 degrees, taking the point of origin as the plane which intersects both anode axes.

3.5.2.2 The Perpendicular Component

The component of the beam perpendicular to the anode rods is depicted in Fig. 3.9. In this direction, the target etch rates show that the central peak is still present, but that "beam current" decreases more slowly on moving away from the centre. In this direction, therefore, the beam divergence is greater (42.8° from the anode plane centre point), and the uniformity is reduced.

3.5.3 Beam "Current" Density

Fig. 3.7 shows that the beam "current" density varies considerably. These data were obtained for a cathode aperture to target distance of 73 mm, but most of the etching of semiconductor materials, to be described, was carried out at a C.A.T.T. separation of 150 mm. Therefore it is necessary to correlate:

(a) Total beam "current" (Fig. 3.3)

(b) Total beam area (Table 8)

(c) Variation of beam area with distance from the cathode and hence beam "current" density dependence on distance and discharge current.

Fig.3.10 gives the calculated expansion in beam area for the range of separations normally encountered (100 - 250 mm). At greater distances the "current" density is too low to be of practical use. Fig. 3.11 is the working calibration chart for experiments to be described on the etching of semiconductor materials. The error bars have been transferred from Fig. 3.3 and indicate the spread of possible values for S_m. The positive intercept on the abcissa is due to the discharge current offset zero, as described in Section 3.3.4.2.

3.5.4 Beamlet Etch Patterns

At C.A.T.T. distances of 150 mm or less, etch patterns produced by individual beamlets are often clearly visible to the unaided eye, as shown in Fig. 3.12. This effect is most pronounced close to the centre of the beam where:

(a) the "current" is greatest and hence so is the etch rate

(b) individual "beamlets" are less divergent than those at the edges of the beam

Table 9 gives brief details of measurements taken on four wafers exposed to an argon beam. These data suggest a correlation between the beamlet divergence and discharge current, possibly due to space charge limiting. The implications of this type of etching non-uniformity are important, and will be discussed in Section 9.2.

TABLE 9

"Beamlet" Etching of SiO_2 by

B93 Injected with Argon

All at: $V_A = 3$ kV

C.A.T.T. Distance = 150 mm

Source Axis Normal to Target Plane

Sample	I_D (mA)	Mean Distance Between Centres mm *	Mean Beamlet Etched Pattern Diameter, mm	Beamlet Divergence Degrees
(48AO) 1	100	12.75	10	3.3
2	150	12.9	10.5	3.4
3	200	12.12	7.6	2.5
4	250	12.5	6.75	2.2

* 38 mm diameter wafers

At lower particle energies ($<< 2.0\ kV_A$), the beamlet etch patterns are less clearly defined. Operation of the source in the "glow discharge" or "wide beam" mode at low anode potential gives rise to this characteristic of low particle extraction efficiency.

Fig.3.13 shows the variation in etch depth over a small area of sputtered SiO_2. The resolution test pattern was defined in negative photoresist and the etching conditions were as shown on the graph. As these patterns are arranged in groups, some data are missing from the area between two sets of etched profiles. The maximum variation is 2240 to 2740 Å depth along a 2.2 mm Talysurf Scan length, which corresponds to an etch rate uncertainty of $\sim \pm$ 10% (41.5 $\pm$ 4.18 Å min^{-1}).

3.5.5 Particle Extraction Efficiency

This section continues the analysis of the results described in Sections 3.3.4.2 and 3.4, sputtering of copper with argon. The terms are defined as follows:

(a) Extraction - electrostatic acceleration of a charged species (singly or multiply positively charged) across the ion sheath and out of the source through the cathode aperture.

(b) Particles - positively charged species which may be derivatives of atoms or molecules, neutralisation of the positive charge may or may not occur before impact at the target surface.

From previous sections, the definition that I_B, the "effective beam current" refers to all bombarding particles in the beam. The "effective beam power" is:

$$W_{beam} = V_B \cdot I_B \text{ (watts)}$$

The power supplied to the discharge is:

$$W_{discharge} = V_A \cdot I_D \text{ (watts)}$$

where V_A = anode potential, volts

I_D = discharge current, amp

The particle extraction efficiency (which would be electrical conversion efficiency if the beam were composed entirely of ions) is

$$\frac{W_{beam}}{W_{discharge}} \times 100 \text{ percent}$$

Reference to Fig.314 shows that the efficiency slope of

I_D = constant, is greater than that for the case

V_A = constant

Efficiency I_D constant = 2.86%

Efficiency V_A constant = 1.98%

The results appear to be consistent for the two groups as the same W_{beam} was obtained (10.56 W) in both sets of experiments (argon beam, V_A: 3 kV, I_D: 150 mA). The increase in the slope of the [I_D constant] curve is considered to be due to the increasing ionisation efficiency of electrons accelerated to greater energies in the saddle field, because of the rise in anode potential.

FIG.3.1 Construction details of the B93 source.

All dimensions in mm.
Scale 1:2

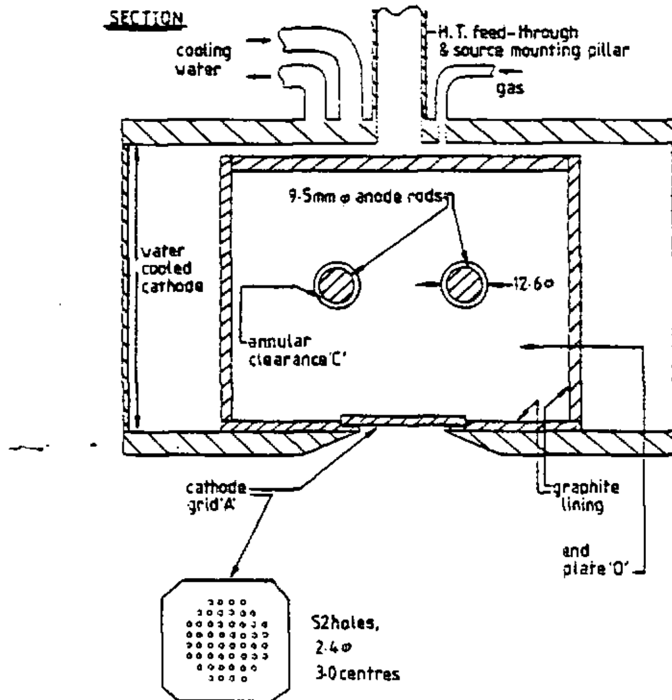

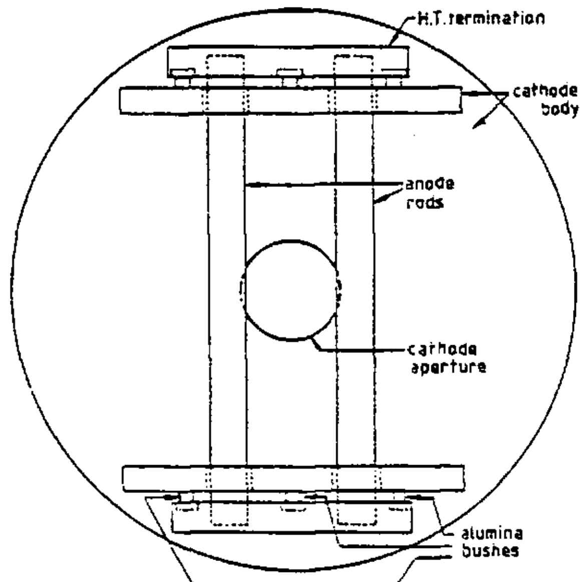

FIG. 3.2 Variation of Discharge Impedance with time, for B93 source starting at 20°C and injected with argon

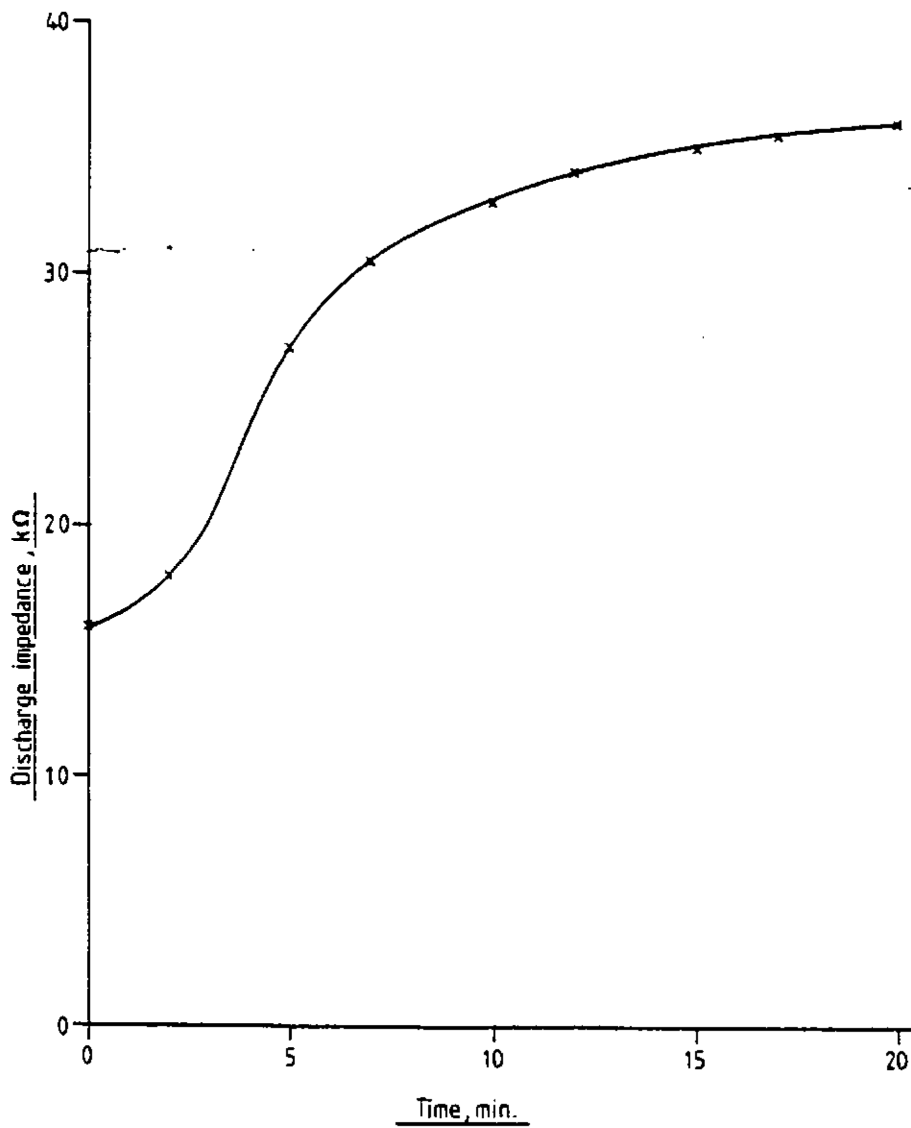

FIG.3.3 Total Beam "Current", I_B, and removal rate of copper as a function of B93-argon discharge current (I_D). For V_B = 2.55 keV

Error bars indicate the variation of published sputter-yield data

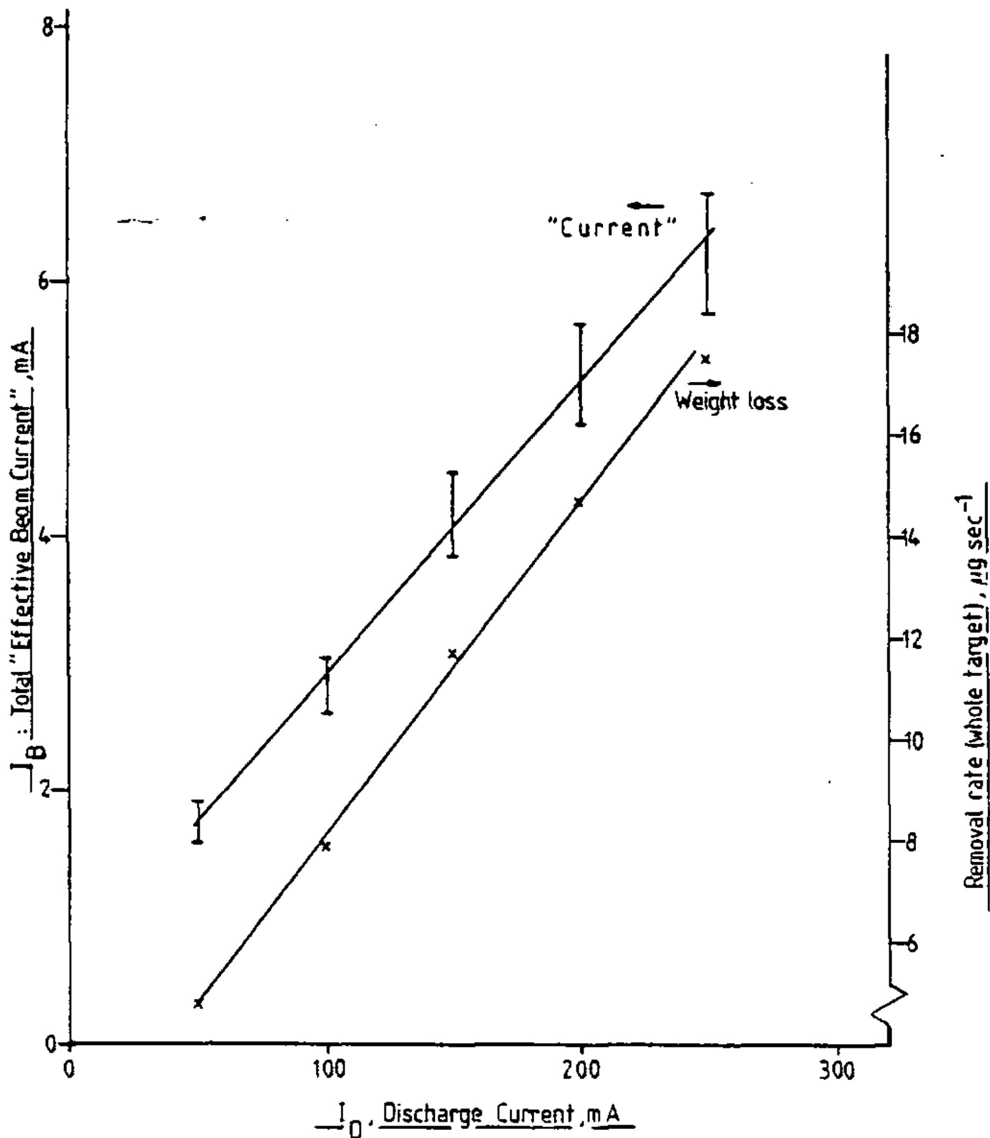

FIG.3.4 Removal rate of copper as a function of bombarding particle energy for a B93 argon beam

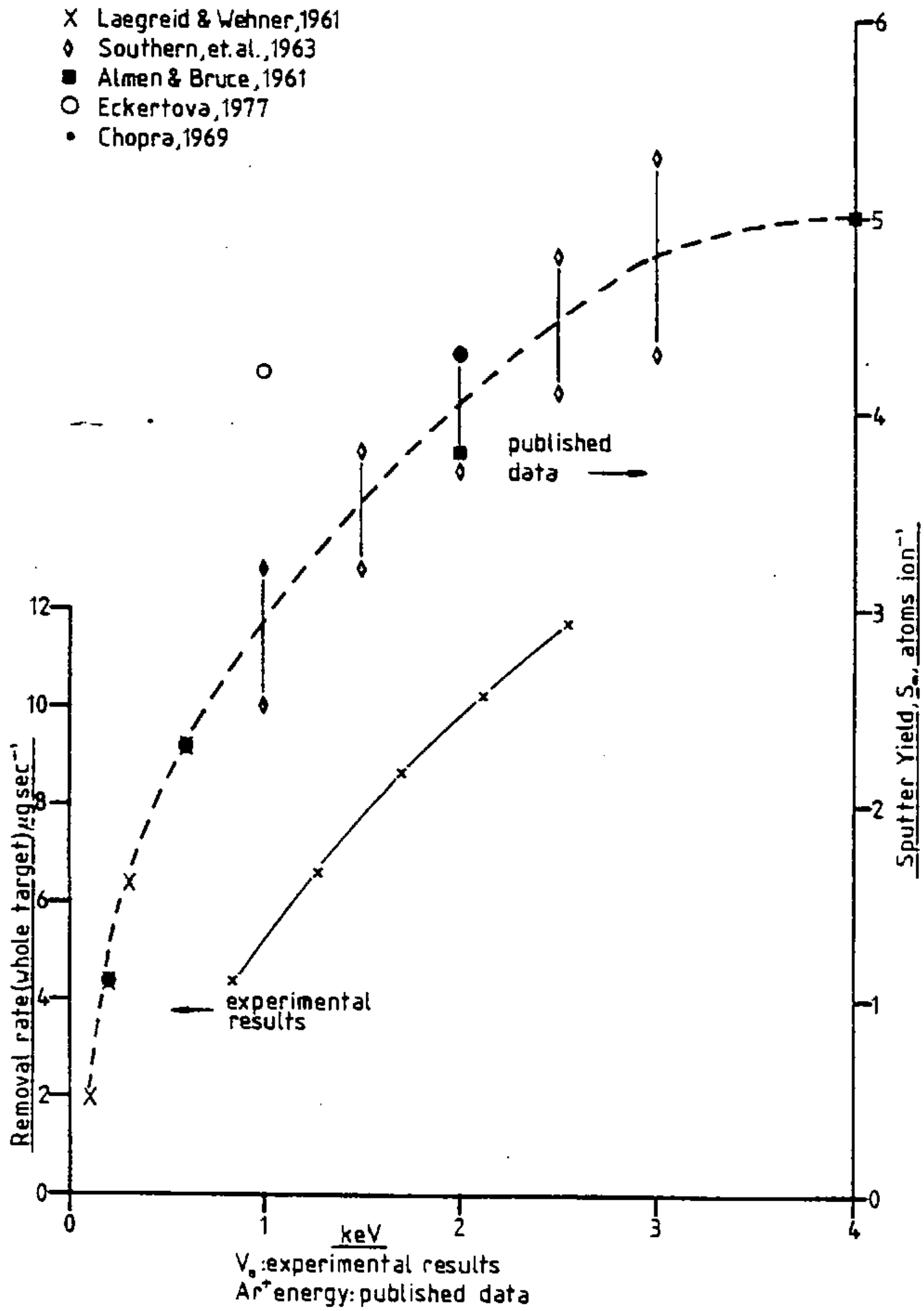

FIG.3.5 Copper foil matrix used for beam "current" distribution measurements.

Target shown after sputtering using:

B93 source injected with argon

V_B: 2.55 keV

I_D: 250 mA

C.A.T.T.: 72 mm

100 minutes

The octagonal outline of the beam can be identified from the changes in colour of the target.

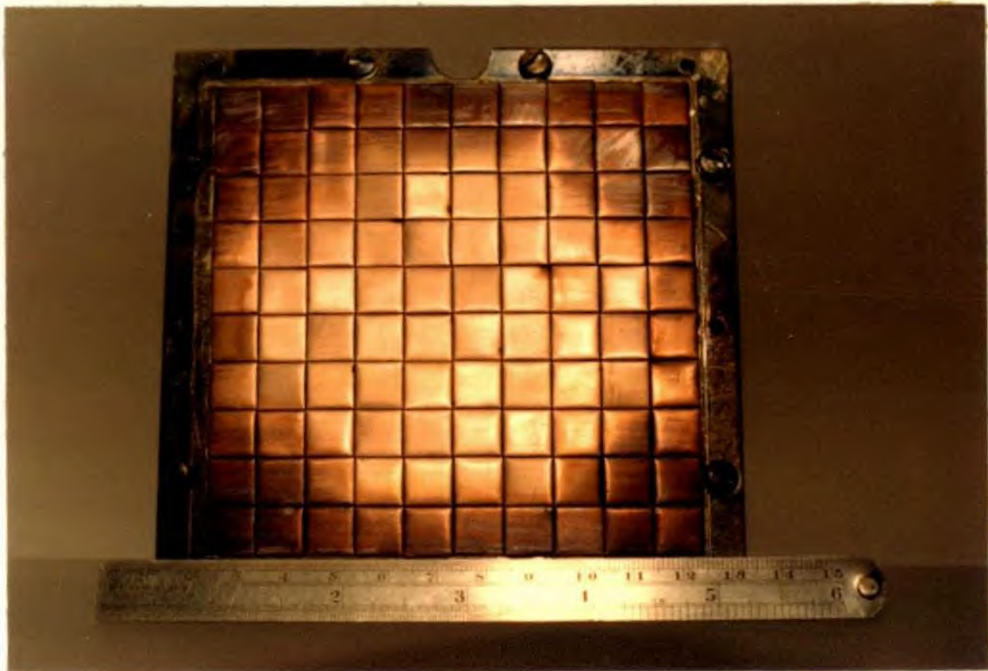

FIG. 3.6 Representation of the B93 beam based upon the argon sputtering of copper. For a matrix of 10 x 10 foil squares. V_B = 2.55 keV, I_D = 250 mA, C.A.T.T. = 72 mm, 180 min.

The Z axis is plotted as weight loss, the peak corresponds to 4.6 mg cm^{-2}

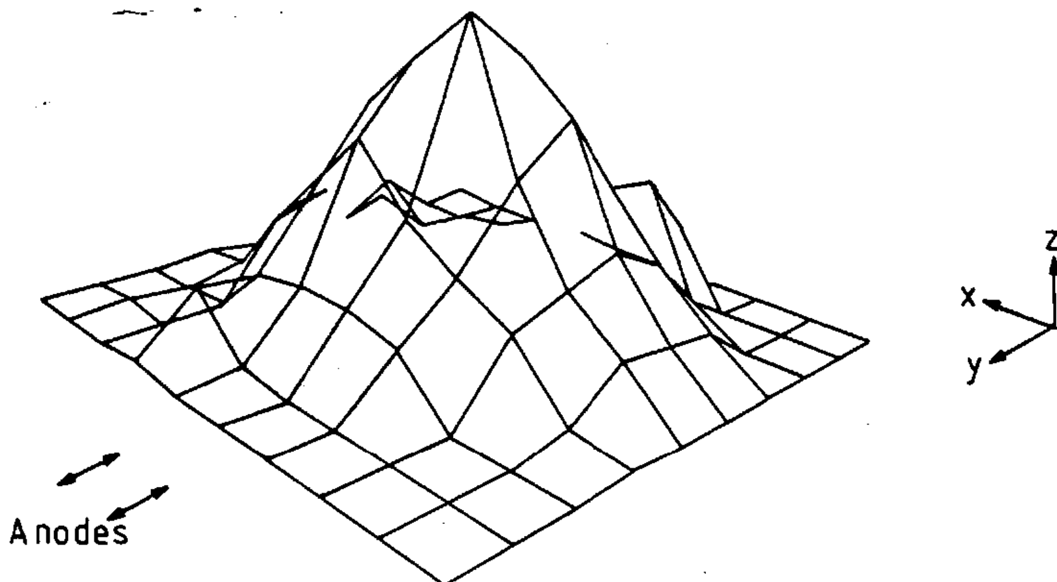

FIG.3.7

B93 Ar Beam "Current" Distribution Parallel and Perpendicular to the Anode Axes.

V_A 3kV
I_D 250mA
CATT 72mm

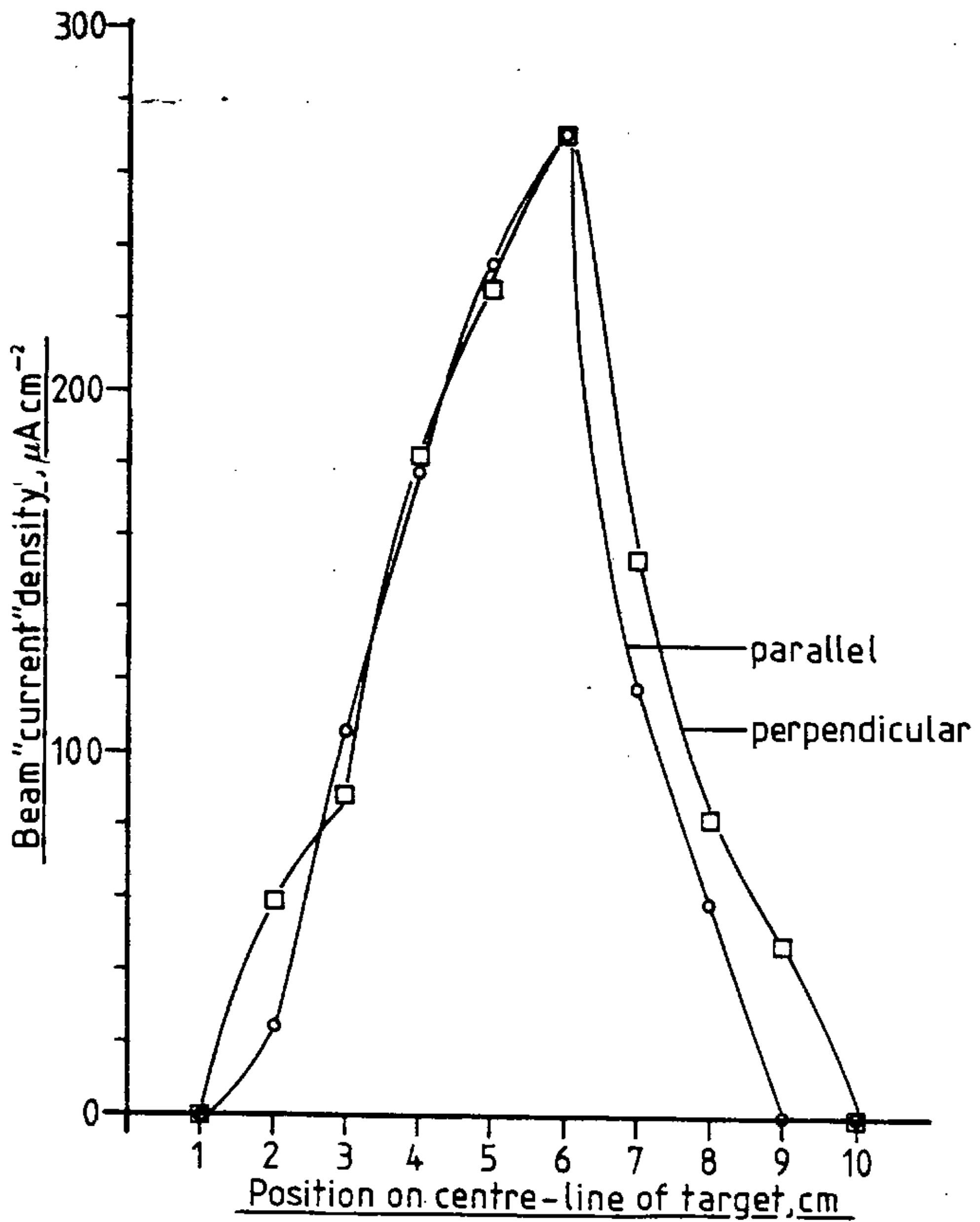

FIG. 3.8 B93 argon beam divergence and sputter etch rate of copper for the component parallel to the anode axes.

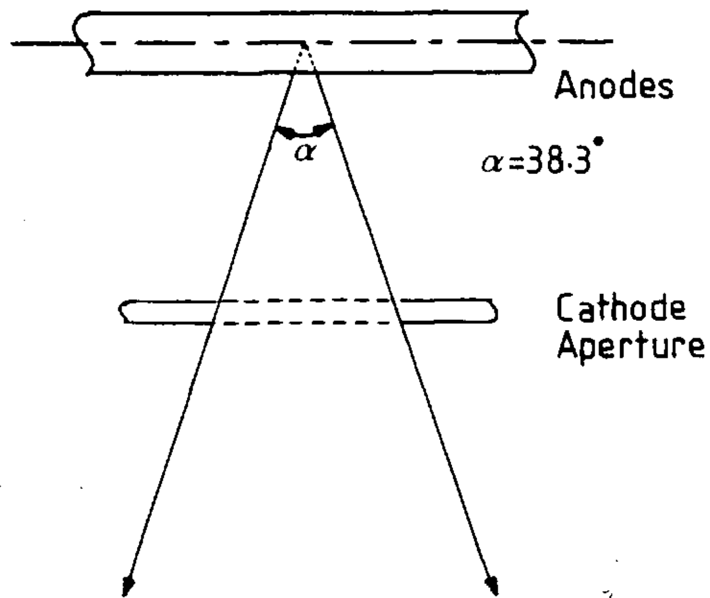

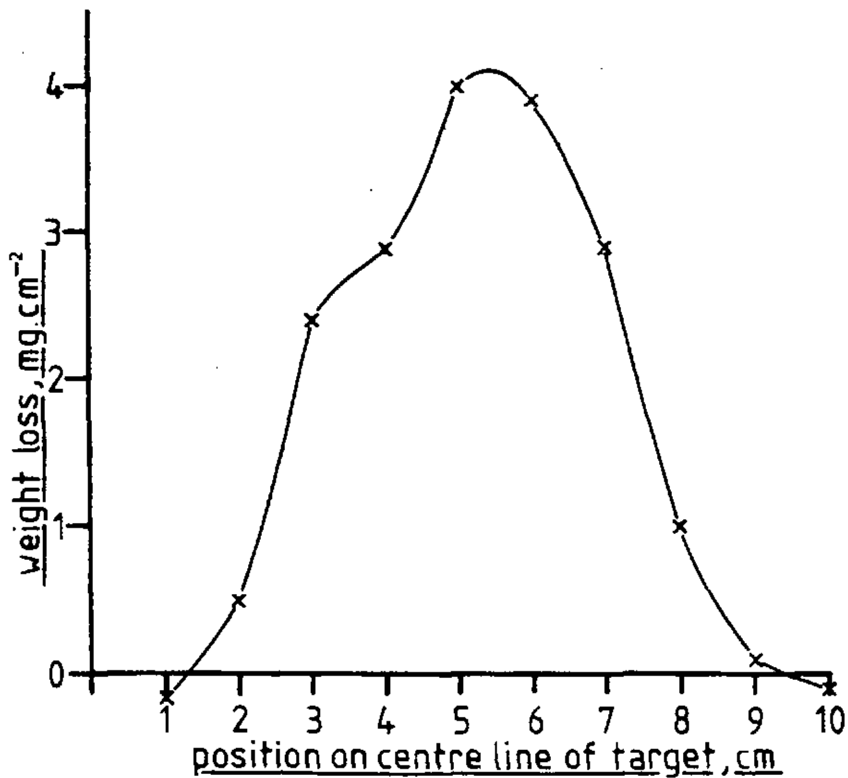

FIG.3.9 B93 argon beam divergence and sputter etch rate of copper for the component perpendicular to the anode axes.

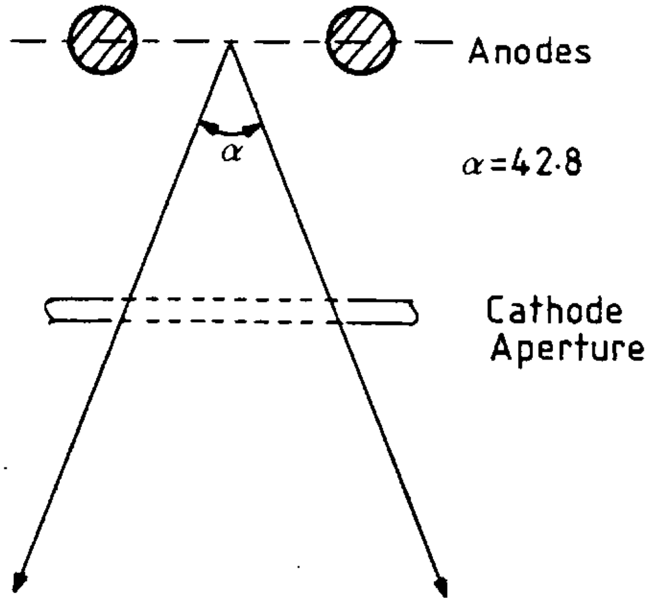

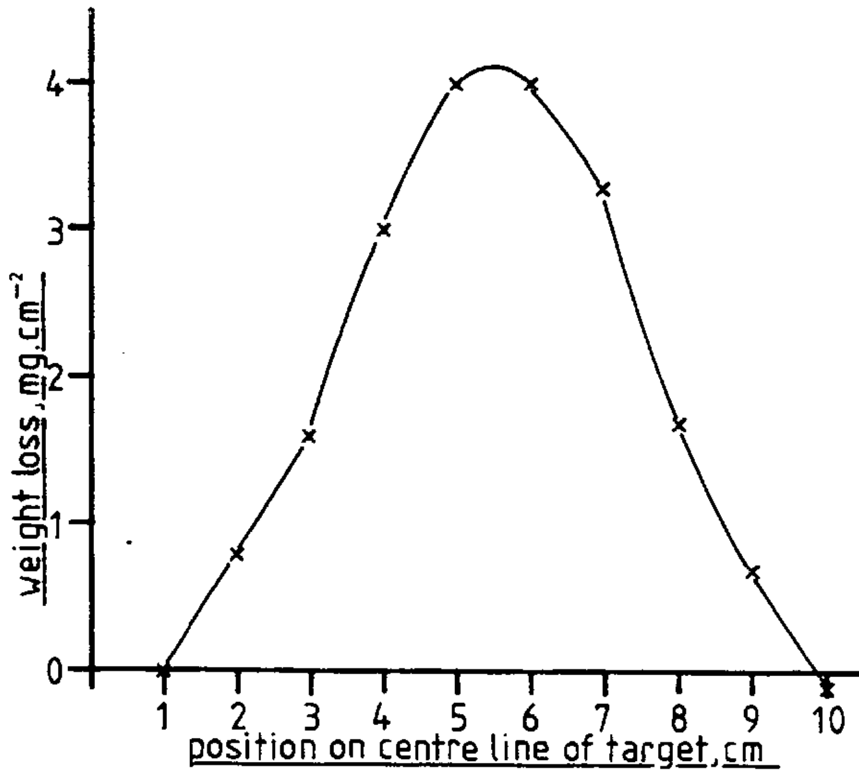

FIG. 3.10 B93 Beam Area (determined for argon) as a Function of the Cathode Aperture to Target distance

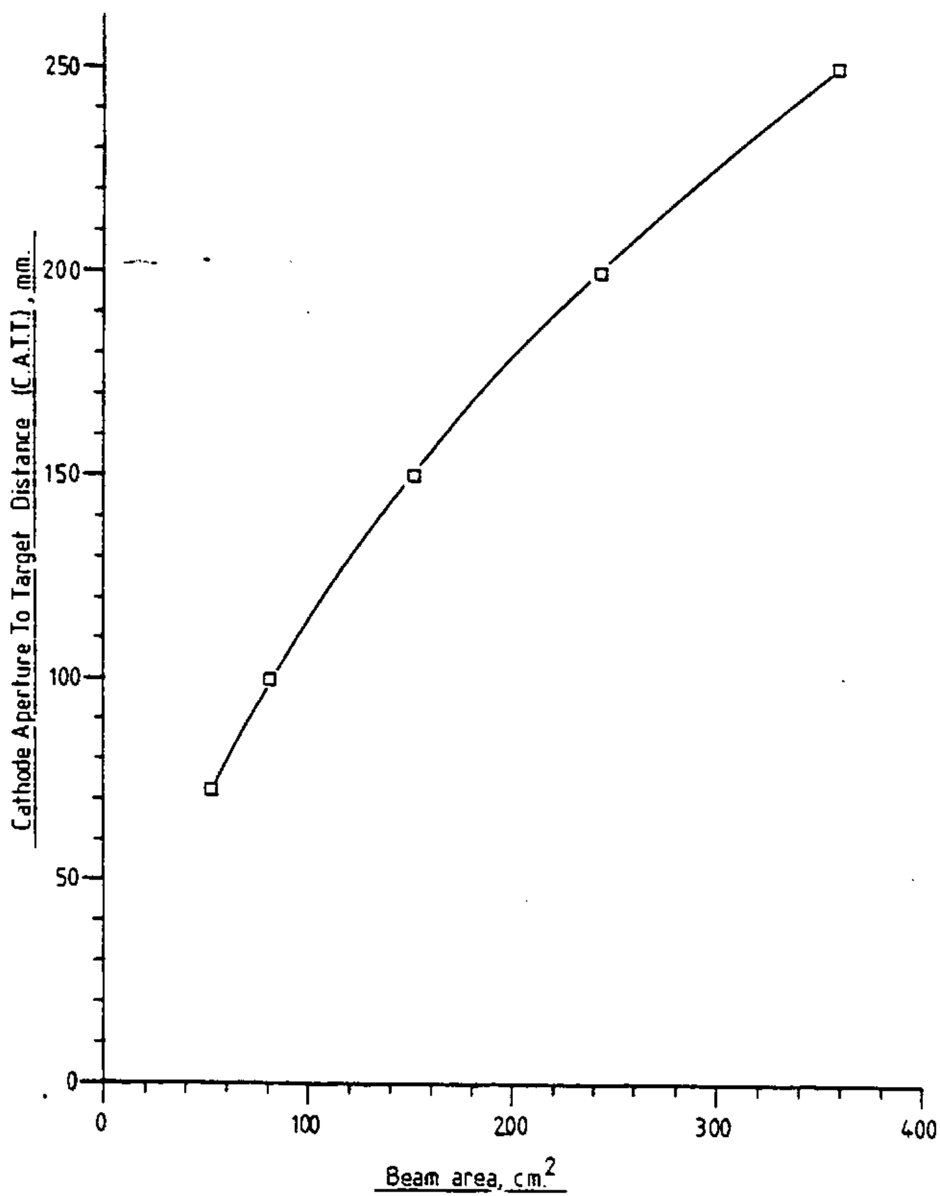

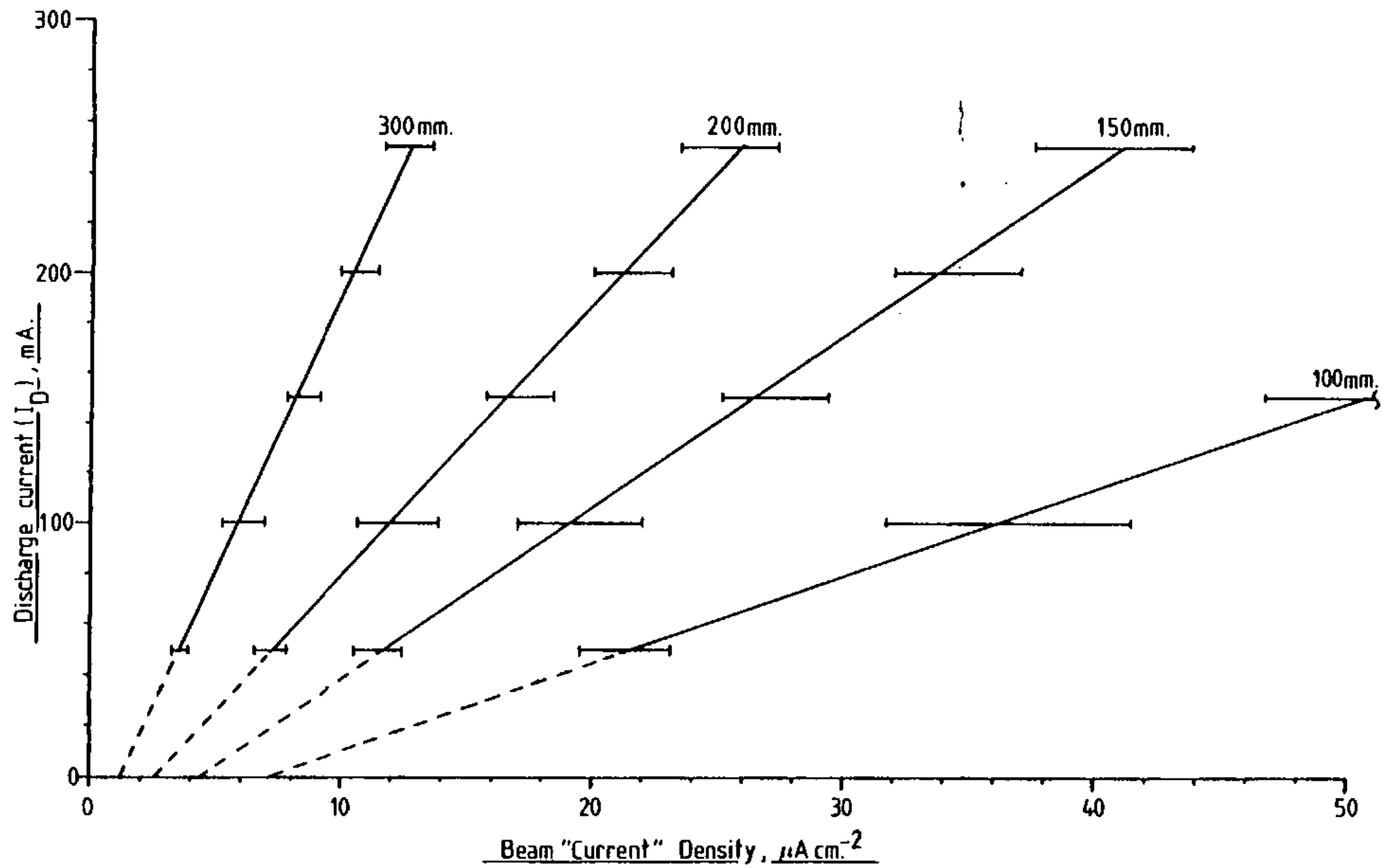

FIG. 3.11 B93 Beam "Current" Density (determined for argon) as a function of discharge current, with C.A.T.T. distance as parameter

FIG.3.12 B93 argon beamlet etch patterns on SiO_2.

C.A.T.T. 150 mm, V_B: 2.55 keV. Source axis normal to target plane.

(a) Specimen 48A02, I_B (mean value): 26 $\mu A\ cm^{-2}$

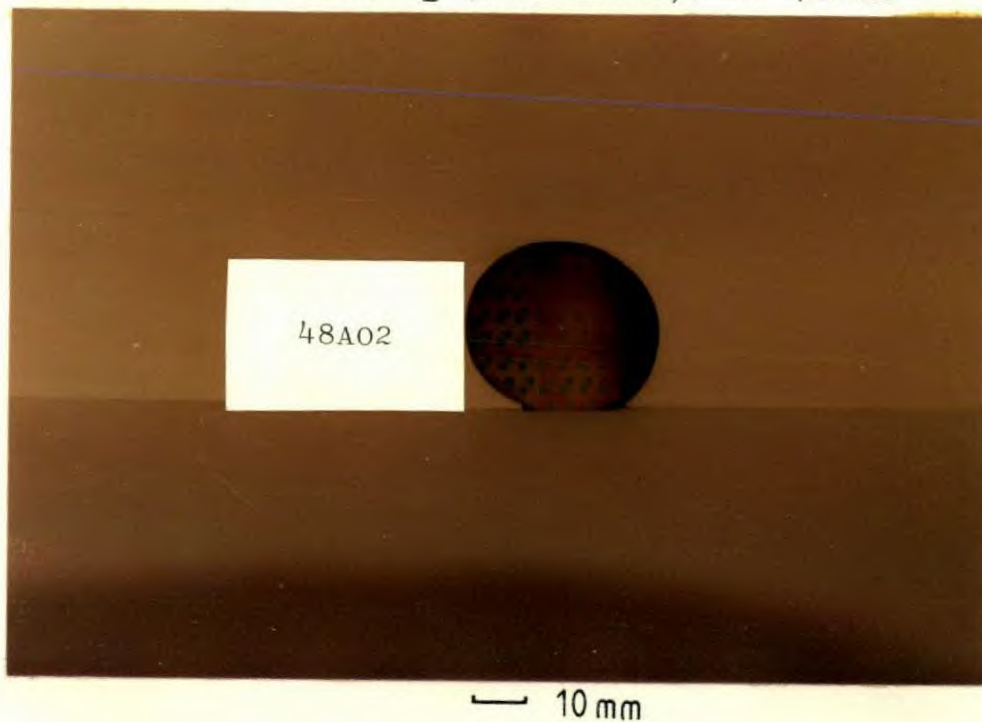

(b) Specimen 48A04, I_B (mean value): 41 $\mu A\ cm^{-2}$

FIG.3.13 Etch depth variation produced by the action of one beamlet. B93 argon beam, SiO_2 target. Wafer shown in Fig. 3.12(b)

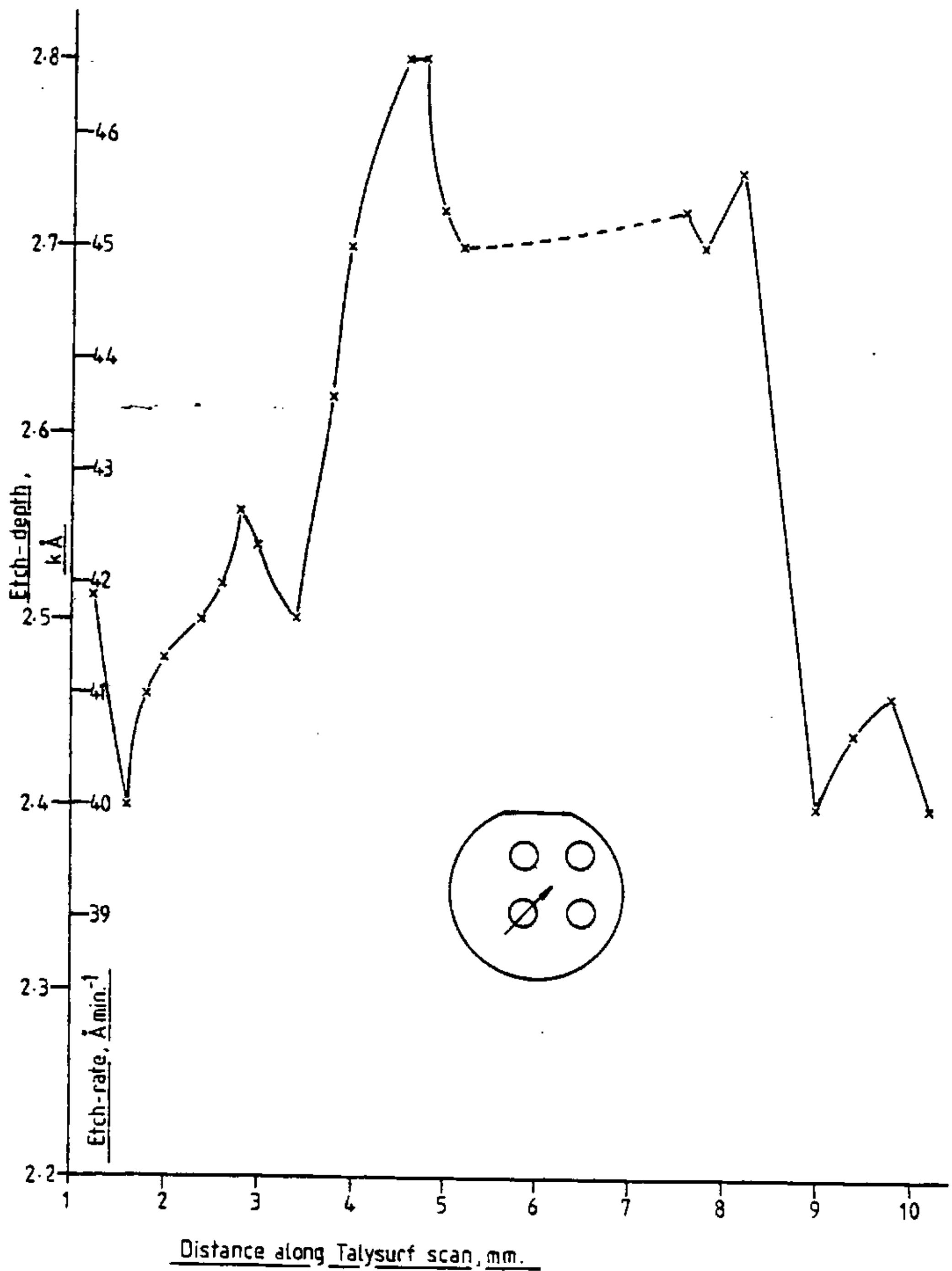

FIG. 3.14 Particle Extraction Efficiency for constant current and constant voltage. B93 source, argon beam, sputtering of copper.

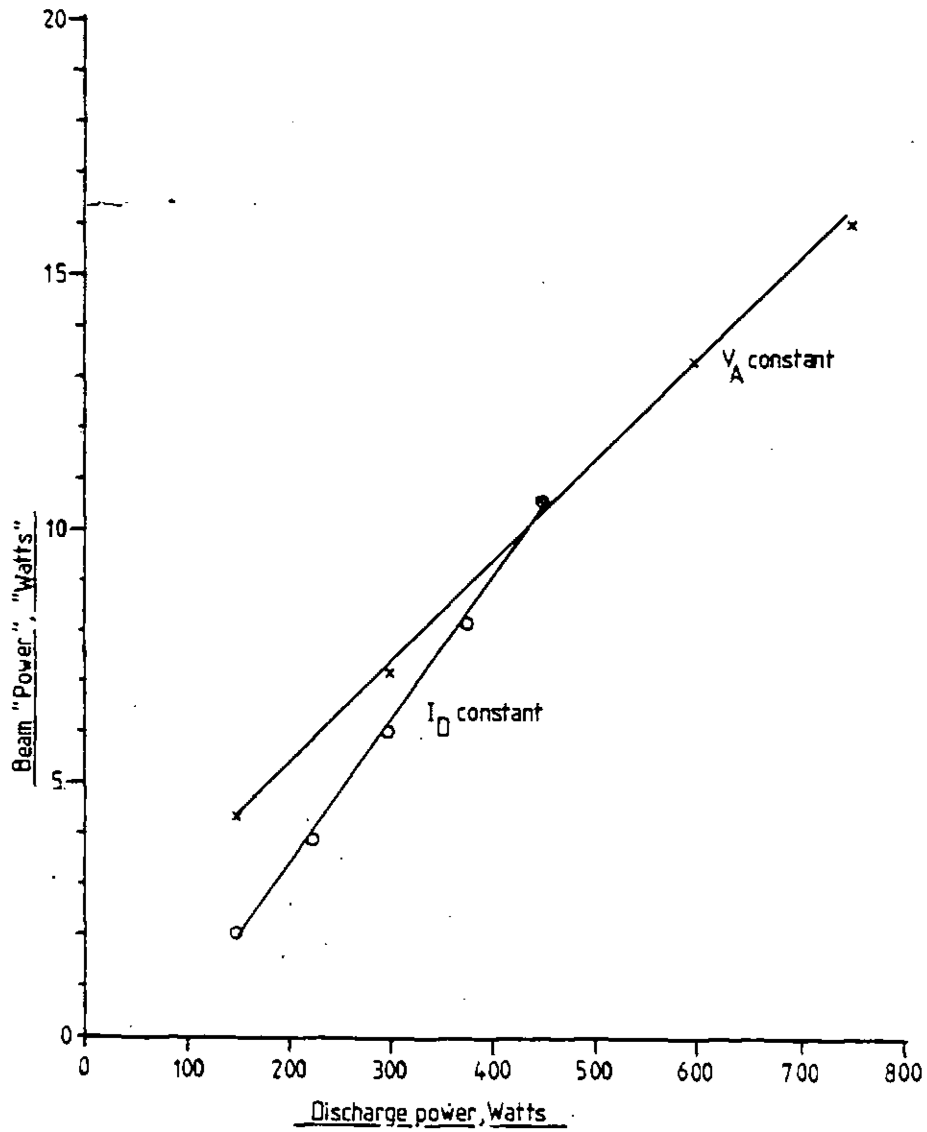

4. ION BEAM ETCHING WITH SADDLE-FIELD SOURCES

4.1 INTRODUCTION

Ion beam sputtering (or "ion milling") using noble gases such as argon is an established technique that has been applied, using various types of ion source to: shaping and polishing of glass for lenses (Townsend,1970), preparation of specimens for electron microscopy (Kynaston, 1970), fabrication of Surface Acoustic Wave (S.A.W.) devices (Bollinger, 1977), production of bubble memories (Maddox, 1980; Melliar-Smith, 1976; Texas Instruments, 1977) and in-situ SEM studies of the sputtering process (Lewis, et al., 1980).

This chapter will describe the experimental results that have been obtained for various materials by ion milling using Saddle-Field sources, such as etch rates, etch-rate ratios and etched profiles. These data will be compared with the results of reactive ion beam etching of the same materials. Most of this work has been carried out with the B93 source, which was described in detail in Chapter 3. Certain data are presented on the use of two other sources, the B21 and the B95, the characteristics of which are given in Appendix IV.

Reactive ion beam etching (R.I.B.E.) (or "reactive ion milling", R.I.M.) is a hybrid of two techniques and combines the anisotropy of sputtering with the chemical affinity of plasma/reactive ion etching. For the satisfactory definition of sub-micron etched lines vertical profiles are required and so the etchant species should be directed normally to the target and with the

minimum of kinetic energy to reduce sputtering effects and damage to the material. It is important that the etchant species possess chemical affinity for the target, ideally not for the resist and substructure and do not diffuse and cause lateral etching. In addition, the products of the reaction must be sufficiently volatile at $\simeq 10^{o}C$ (the usual temperature of a water-cooled wafer holder) to be removed in the pump exhaust.

As with plasma and reactive ion etching, the reactive species usually chosen is a halocarbon or halogen-containing fragment, produced by the dissociation of a normally stable, parent halocarbon (or other source of halogens). The work to be described has been with four fluorocarbons of the "Freon" family and sulphur hexafluoride. Brief details of these compounds are included in Appendix III.

The use of chlorine and chlorocarbons has recently been described by workers investigating the reactive ion etching of silicon and III-V compounds (Smolinsky, et. al., 1981; Donnelly and Flamm, 1981). Chlorinated compounds have not been used as etchants in this study. As the B93 source is constructed mainly of aluminium, and the plasma chamber is lined with graphite, exposure to a discharge containing chlorine is expected to lead to degradation of the source components.

A number of papers have been published in the literature on the use of heated filament sources for argon ion milling and reactive ion beam etching. The author is not aware of any published information, except that listed

in Chapter 12, on the use of Saddle-Field sources with reactive gases. Comparisons will be made, where possible, between the experimental work carried out by the author and published data for heated filament sources.

Etching of Polymeric Resist Materials

The etching characteristics of resist (U.V. and electron-beam crosslinking materials) have not been investigated for the following reasons:

(a) This programme was concerned with the mechanisms of etching at the target surface (resist materials are specifically excluded as targets in this context). Masks of photoresist and electron-beam resist have been used solely to transfer a pattern for the purposes of investigating the etching process. The characteristics of resist films are, therefore, of secondary importance, and reference will be made to this aspect in Section 9.6.

(b) The measurement of resist film thickness could not be readily undertaken. Contact methods (Rank-Taylor-Hobson Talysurf IV instrument) proved to be too severe, producing scoring of the film even after application of a sputtered gold film.

4.2 ETCHING OF SiO_2

The silicon dioxide used in this work was exclusively of the form produced by the high temperature ($\simeq 1000^{\circ}C$) oxidation of semiconductor quality polished silicon (for process schedule see Appendix I). This material is required as an integral part of the M.O.S. fabrication process, which is described elsewhere in this

thesis (see Chapters 5 and 6). It is of fundamental importance that the criteria outlined in Section 1.4 should be followed in the case of SiO_2 etching if the required reduction in device geometries is to become a reality.

The etching of SiO_2 by ion milling is well documented in the literature and typical data are given in Table 10. This information may be compared with the etching characteristics of the beams produced by Saddle Field sources. As SiO_2 is etched more rapidly than Si by fluorocarbon particle beams, this is a useful diagnostic technique for the evaluation of wall profiles and assessment of the etching process. Summarised data for the etching of SiO_2 with beams produced by injecting various gases into the B93 source, are shown in Fig. 4.1.

4.2.1 Etching with Argon

4.2.1.1 Etch Rate Dependence on Particle Energy

The SiO_2 etch rate dependence on argon particle energy is shown in Fig. 4.2 for measurement made at four points on each of four wafers. Position B consistently etches faster than the points closer to the periphery of the wafer, due to the increased current density on the beam axis. The drop in etch rate at Position B, 2.55 keV beam energy is greater than expected, but can be explained in terms of errors introduced by not taking "Talysurf" measurements at identical points on each wafer. Similarly, positioning errors are probably responsible for the abnormally low etch rate at V_B = 1.28 keV on Position D.

TABLE 10

Published Etch-Rate Data for the

Ar^+ Milling of Si and SiO_2

Material	Etch Rate Å min^{-1} *	B.C.D.** mA cm^{-2}	Ion Energy eV	Reference
SiO_2	120	0.32	300	(1)
	100	?	500	(2)
	55	0.4	500	(3)
	280	1.0	500	(4)
	399	1.0	500	(5)
	180	0.5	600	(6)
	255	0.6	1000	(7)
	450	0.8	1000	(8)
	417	0.85	1000	(9)
	420	1.0	1000	(10)
Si	215	1.0	500	(4)
	488	1.0	500	(5)
	165	0.5	600	(6)
	230	0.4	1000	(11)
	265	0.6	1000	(7)
	420	0.8	1000	(8)
	333	0.85	1000	(9)
	360	1.0	1000	(10)

* Beam at normal incidence. ** Beam Current Density

References

(1) Lee, 1979
(2) Horiike, et. al., 1979
(3) Matsui, et. al., 1980
(4) Gloersen, 1976
(5) Harper, et. al., 1981
(6) Mader and Hoepfner, 1976
(7) Cantagrel and Marchal, 1973
(8) Meusemann, 1979
(9) Spencer and Schmidt, 1971
(10) Bollinger, 1977
(11) Hosaka, et. al., 1981

4.2.1.2 Sputter Yield Determinations

Etch rate data are not very meaningful unless all the relevant etching parameters are quoted. Comparisons of results published by several workers using identical equipment are often not possible as beam energy and current density are at variance. Table 10 illustrates this point by showing a representative selection of etch rate data from literature published over an eight-year period. All of the results were obtained from the etching of single crystal Si and thermal SiO_2 by argon ion beams at normal incidence, produced by heated filament ("Kaufman") sources.

The measured sputter yield for argon bombardment is denoted by S_m. In the case of fluorinated etchants, the measured or "apparent" yield is:

$S_A = S_m + S_c$ where S_c is the yield due to chemical reaction

The true and apparent sputter yields for all materials have been determined using the relationship:

$$R(\theta) = 9.6 \times 10^{25}\, I\, \frac{S(\theta)}{n} \cos(\theta)$$ (Bollinger and Fink, 1980)

where $R(\theta)$ = removal rate, Å min^{-1}

I = beam current, mA cm^{-2}

$S(\theta)$ = Sputter yield, atoms or molecules ion^{-1} ($particle^{-1}$)

θ = angle of incidence of the beam ($\cos\theta = 1$ for normal incidence)

n = atomic or molecular density of the target (cm^{-3}) (see Appendix III for values used)

$$n = \frac{\text{Number of atoms or molecules mole}^{-1}}{\text{Molecular Weight/Density}} \quad cm^{-3}$$

which is the practical method for the treatment of etch-rate data. By rearranging and ensuring that:

(a) the beam energy is constant between experiments

and(b) only data are taken from the sample exposed to that part of the beam at normal incidence (close to the centre of the B93 beam) then:

$$S_m = \frac{Rn}{I \times 9.6 \times 10^{25}} \quad \text{atoms or molecules/particle}$$

which may be used to give the true or apparent sputter yield for individual etch-rate results. Alternatively, the following has been used where several data points were available (at constant particle energy), by plotting R against I, the sputter yield is found from:

$$S_m = \frac{\text{Slope} \times n}{9.6 \times 10^{25}} \quad \text{atoms or molecules/particle}$$

Fig. 4.3 shows the sputter yield dependence on ion energy for the published data presented in Table 10. Apart from the curious position of point (3), all of these data show the general trend of increasing S_m with ion energy. Only data taken from the etching of SiO_2 by B93 argon beam at V_B values less than 1 keV can be compared directly with the published "ion beam" data, but the agreement here is good. Also shown for comparison are five data points for the Ar^+ sputtering of fused quartz (Davidse and Maissel, 1967). The variation of sputter yield data for the B93 beam etched specimens is rather large. The most accurate data, at 2.55 keV were taken

from the graph of R against I shown in Fig. 4.4 for five separate experiments. The variation of the slope was from 1300 to 1460 (Å min^{-1}) (mA $cm^{-2})^{-1}$. The weight loss dependence of copper targets on particle energy (Fig. 3.4) shows a smooth increase, in accord with the published data. It seems likely, therefore, that the shallow slope of the B93 curve is mainly due to errors in etch depth measurements at predetermined points on the four wafers. The B93 beam results are also displaced towards higher energy (comparing sputter yields) which is in agreement with the findings of Davidse and Maissel. The absolute values of sputter yield appear to be consistent with those given in the literature, which tends to confirm the estimations of beam "current" by the sputtering of copper.

4.2.1.3 Etched Profiles

From S.E.M. studies of etched bars defined in photoresist using a grating pattern, the wall angle is estimated to be approximately 60" to the substrate, as shown in Fig. 4.5. The angle of maximum etch rate, which leads to facets of corresponding wall angle, is given by some workers (Lee, 1979) and (Bollinger and Fink, 1980) as 45-50°, and by others (Mader and Hoepfner, 1976) as 60°, for beams produced by heated filament sources. Continued milling causes thinning of the resist, transfer of the angled wall to the target bulk and loss of linewidth control. Ultimately, as shown in Fig. 4.6 the sidewall slopes join at the centre of the bar. In this micrograph the facet angle is at about 30° to the substrate, significantly lower than that seen in Fig. 4.5. It is

likely that this deviation was caused by the two different C.A.T.T. distances used, and hence the variation in angle of incidence of the beam. Craters are also evident in this micrograph where, it is thought, localised heating of the resist has caused blisters to form and burst, leaving the SiO_2 unprotected.

After etching SiO_2 masked with a pattern in polymethyl-methacrylate (PMMA), using an argon beam from a B21 source, redeposited debris has been observed, and is described in Chapter 5. Redeposited particulate debris of this nature has not been observed on samples exposed to a B93 argon beam.

4.2.2 Etching with CF_4

4.2.2.1 Etch Rate Dependence on Particle Energy

The apparent sputter yields obtained by two groups using heated filament sources are shown in Fig. 4.7, along with the experimental data for this study. The single data point due to the Japanese study (Matsui, et. al., 1980) is again conspicuously low, suggesting a possible error in beam current determination or etch depth measurement. The data points shown for B93 etching are derived from a graph of R against I at constant energy. The apparent sputter yield dependence on particle energy has not been investigated for B93-CF_4 beams.

The work reported by Harper, et. al. was expressed as atoms/ion and for consistency here has been scaled to give SiO_2 molecules/ion. No data are given by Harper for ion energies in excess of 1.5 keV, which is greater than the normal operating maximum for that type of source. If

the same rate of increase with energy were to be maintained, the apparent sputter yield would be approximately 1.23 at 2.55 keV, which is only about 10% greater than the maximum value determined at that energy for the B93-CF_4 etching of SiO_2. The results of Harper et. al. show that when etching was performed with a single grid heated filament source the sputter yield was significantly lower (1.3 compared to 2 at 200 eV), data were not presented for energies in excess of 250 eV. These authors attribute this to an accumulation of polymeric material on the target and source anode, which depletes the beam of etchant species. It is not possible to compare the characteristics of the two sources directly as the B93 will not produce particles of less than about 800 eV (V_B). Polymer deposits have not been observed inside the B93 source or on targets when CF_4 has been injected and when V_B = 2.55 keV. The reported formation of polymers at low energy is indicative of a free radical mechanism (which would account for the formation of polymers on the hot anode surface of the heated filament source), possibly based on the difluoro-methyl diradical, $\ddot{C}F_2$.

The apparent sputter yields determined for SiO_2 etched by B93-CF_4 beam appear to be either shifted towards higher energy or a lower value of S_A. For these results to agree with those for the heated filament source, the relationship between V_A and V_B would have to be: $V_B = 0.4.V_A$. Alternatively, the value of S_A is artificially low because of the use of invalid beam "current" data. The beam

"current" density for a CF_4 beam has not been measured directly, any suggestion of a deviation from the value obtained for Ar would, therefore, be speculative. For agreement between values of S_A for the two sources, the B93 data would have to be increased to a mean of 1.25 molecules/particle. This would indicate a "true" beam "current" density of 0.022 mA cm^{-2}, which is about 30% lower than the value obtained for an argon beam at the same discharge current (I_D).

4.2.2.2 Etched Profiles

A micrograph of a vertical wall profile etched into SiO_2 using a "B21 CF_4 beam" is shown in Chapter 5 as evidence of the satisfactory nature of this technique for etching sub micron geometries.

Using a beam produced by injecting CF_4 into the B93 source, etched profiles in SiO_2 have been observed to be vertical and free of trenches, polymer formation and the deposition of particulates. These observations suggest that sputtering mechanisms played a minor role in the etching experiments.

Near-vertical profiles shown in the literature (Harper, et. al., 1981) were produced at very low beam energies (200 eV) in order to avoid sputtering-induced artefacts, but the polymer residues visible on the SiO_2 are clearly undesirable.

The indications are, therefore, that similar mechanisms are involved for etching with beams produced by the two types of source. Uncertainties regarding the B93 beam energy and current when using gases other than

Ar have yet to be resolved.

4.2.3 Etching with CHF_3

4.2.3.1 Etch Rate Dependence on Particle Energy

The variation of apparent sputter yield of SiO_2 with etchant particle energy is shown in Fig. 4.8. Also included on the graph is one data point from the published literature (Meusemann, 1979) in which a heated filament source was used. As with the other etch rate determinations, large variations have occurred on the depth measurements; the error bars indicate the maximum spread of results (as etch depth) at five positions on each wafer. The etch depths for the sample treated at V_B : 0.85 keV were all in the region of 90 Å and, hence close to the limit of detection for the Talysurf instrument.

The pronounced energy threshold is an effect that has not been observed elsewhere in this study. Data are not available for the etch rate dependence of SiO_2 on etchant energy for other gases, except argon. The experimental procedures did not differ from those adopted for other sample etchings, and there is no reason to doubt the validity of these data.

It is useful to compare these results with those shown in Fig. 4.7. The etch rate dependence on energy for CF_4 suggested that the data were displaced towards higher energy, the same argument could apply to the CHF_3 data. This would suggest that fewer etchant particles were extracted at 0.85 keV than was the case for Ar^+ at the same energy. This view tends to be contradicated,

however, by the data of Fig. 4.9 which shows a smooth apparent sputter yield dependence on etchant energy. The presence of the one data point from the literature on the curve between 0.85 and 1.55 keV may be coincidental. It seems likely, therefore that energetic particle activation of the SiO_2 surface occurs in a manner similar to that described previously (Coburn et. al., 1977), leading to enhanced chemical etching.

Fig. 4.8 indicates, therefore, that an apparent sputter yield dependence on etchant energy exists below 1.5 keV, but that the presence of such a dependence at higher energies is debatable and should be clarified with further investigation.

4.2.3.2 Etched Profiles

Samples of SiO_2 etched with a beam produced by injecting CHF_3 into the B93 source have consistently exhibited vertical profiles. Figure 4.10 is a scanning electron micrograph of a pattern defined in Kodak 747 resist. The bars and troughs of approximately equal mark-space ratio have been accurately reproduced without apparent linewidth loss. There is no evidence of undercutting or sputtering-induced effects. Observations of the S.E. micrograph in Fig. 4.11 may be described similarly. For this specimen the pattern was defined by optical lithography in Kodak 747 resist using a commercially available mask (M.I.T.E.). The rather large particles are thought to have been introduced following etching and are not present as a result of that process.

4.2.4 Etching with Other Gases

Etch rates have been determined for the action of beams produced by injecting the B93 source with three other gases: C_2F_6, C_3F_8 and SF_6. The summarised etch rate data are shown in Fig. 4.1. On the basis of the limited experimental work that has been carried out, there are no strong indications of significant differences in etch rate caused by the five reactive gases. Due to the discharge potential variations described in Section 3.2.4. not all of the samples were exposed to beams of constant energy and hence certain inaccuracies are inherent in these results.

The apparent sputter yield data are summarised in Fig. 4.12 and are compared with literature values obtained from work with heated filament sources injected with the same gases. The values determined by experiment all fall within the range 0.8-1.4. The reason for the apparently low published values is not clear, although it could be that low etch rates resulted from an accumulation of polymeric material on the source filament or target.

Of these three gases, only SF_6 has been used to define a pattern in SiO_2. Etching with a beam produced by the B21 source generated vertical wall profiles with no measurable loss of linewidth, but the horizontal etched features were observed to be pitted (Revell 1980).

4.3 ETCHING OF Si

4.3.1 Etch Rates

Fewer experimental results have been obtained for the etching of this material than was the case for SiO_2

because of the low etch rate.

Fig. 4.13 shows the sputter yield dependence on Ar energy for published data on heated filament sources and B93 beam etched specimens. The B93 data were taken from a curve of etch rate against beam current density, plotted for the results of six separate experiments. The points fall on a smooth curve over the range 0.5 to 2.55 keV, and the B93 experimental results appear to be consistent in this respect.

The etch rates for Si targets exposed to six etchant beams are shown in Fig. 4.14. It can be seen that the four Freons produced similar etch rates in this material. The "enhancement" of etching is approximately 2:1 over that obtained with an argon beam. SF_6, however, etched Si approximately 4 times faster than Ar, which is probably attributable to the action of atomic fluorine. Data to be presented later (Section 7.2.1), however, will show that attack by this etchant is probably not the major mechanism.

The apparent sputter yield dependence on etchant energy for Si is shown in Fig. 4.9 for a B93-CHF_3 beam. As with the etching of SiO_2 (Fig. 4.8), an exceptionally low yield is observed at 0.85 keV. In Fig. 4.9, however, the dependence is more progressive and is characteristic of a sputter-yield curve as seen in the work described previously for Ar beams. The mechanisms to be described later indicate that an accumulation of carbon on the target surface can occur if the bombarding species is CF_x and oxygen is not present in sufficient quantity for

the formation of CO or CO_2. The data of Fig. 4.9 tend to indicate, therefore, that sputtering mechanisms occur with this etchant-target combination.

4.3.2 Etched Profiles

For the detailed examination of profiles, etch depths of at least 3000 Å are required. As the etch rate of Si is so low, long periods of exposure to the beam are required, leading to complications with source instability and varying beam energy.

The hypothesis that atomic fluorine is produced when the B93 is injected with SF_6 could only be tested by examination of etched patterns, or by instrumental chemical analysis. However, there was no evidence of attack by diffusing species when a B93 SF_6 beam was used to etch Si which was masked with stainless steel.

Shallow etched profiles (1000-2000 Å) produced in Si with B93 CF_4 and CHF_3 beams were well defined with no observed artefacts due to sputtering or free radical etching. Further experiments, aimed at producing much deeper etched structures, are required to evaluate the etch rate dependence on beam angle of incidence and facet angle.

4.4 ETCHING OF Si_3N_4

4.4.1 Etch Rates

The experimental data obtained for the etching of Si_3N_4 by six B93 etchant beams are shown in Fig. 4.15. In all cases, significant (greater than 7:1) increases in etch rate have been determined compared to the rate produced by Ar sputtering. The fact that C_2F_6 etched

Si_3N_4 at twice the rate of CF_4 could be explained in terms of the increased production of etchant species, but the same ratio was not determined for the etching of SiO_2. The wide variations in CHF_3 etch rate on different samples using the same etching conditions suggest varying specimen characteristics. Variations in processing conditions could have been responsible for the formation of films of different density and elemental composition, either of which could have caused the observed effects. It is not possible to compare this work with published information as there is a scarcity of data in this area.

4.4.2 Etched Profiles

Films no greater than 2000 Å thick were deposited on Si. Consequently, a detailed evaluation of the etched profiles has not been possible. Etching with CF_4, however, (B93 source, 3 kV_A, 150 mA I_D, C.A.T.T. 150 mm) has shown that accurate pattern replication and control of linewidth can be achieved (Revell and Evans, 1982).

4.5 ETCHING OF Al

4.5.1 Etch Rates

For the efficient sputter etching of aluminium films, the native oxide must first be removed and the oxygen concentration in the vacuum chamber must be sufficiently low to preclude the reformation of that layer. Work with argon ion beams produced by heated filament sources has indicated that by increasing the oxygen partial pressure from 3.5×10^{-6} torr to 3×10^{-5} torr the etch rate decreased from $\simeq 200$ Å min^{-1} to $\simeq 10$ Å min^{-1} (Mader and Hoepfner, 1976).

The etch rates of Al films exposed to beams produced by the B93 source injected with five different gases are shown in Fig. 4.16. These data are difficult to analyse because of the unknown thickness and sputter yield of the oxide film. Of particular interest here are the increased etch rates when fluorinated species bombarded the targets. The similar removal rates determined for the action of the three Freons suggests that the effect is caused by the same fluorocarbon species. It may be that removal of the metal is due to the sputtering of a fluorinated compound of aluminium. Alternatively the metal oxide may be removed by the oxidation of the fluorocarbon which left the metal film unprotected, and hence more susceptible to sputtering.

For the case of SF_6, the etch rate is approximately twice that determined for the fluorocarbons. The chemistry of etching reactions using SF_6 are not as well characterised as those for the fluorocarbons and so the processes are somewhat speculative. The action of the lower sulphur fluorides (SF_4, SF_5) on the oxide film to form volatile oxyfluorides cannot be ruled out, however. This could lead to enhanced removal of the metal by sputtering mechanisms.

For the experimental result of sputtering with argon, a sputter-yield of 0.085 is indicated. This is very much lower than the value of 0.35 quoted in the literature by one group of workers (Maniv and Westwood, 1980) who used argon ions of 1 keV, but only marginally lower than that reported by others (Davidse and Maissel,

1967): 0.12 at 2 keV.

Additional experiments which were conducted with the B95 source (the characteristics of which are summarised in Appendix IV) showed that run-to-run and day-to-day variations of etch rate occurred. Fig. 4.17 shows the results of these experiments which clearly fall into two groups: "high" etch rate ($\simeq 27$ Å min^{-1}) and "low" etch rate ($\simeq 7$ Å min^{-1}). The beam current density of this source has not been established, and in view of the wide variation in published values of sputter yield for aluminium and aluminium oxide, no attempt has been made to further analyse these data. It is considered that these results are symptomatic of unreliable vacuum conditions. This could have been due to the residual oxygen in the chamber, or to water vapour which condensed on the stainless steel vessel walls when the door was opened.

4.5.2 Etched Profiles

A detailed examination of etched profiles in aluminium films has not been possible, except in isolated cases, because of: (a) the shallow etch depth resulting from the low etch rate of the material, and (b) the presence of topographical features such as "cones" and "rings".

Early work in this study using the B21 source showed that cone formation was dependent upon the temperature of the aluminium film. Film temperatures were not measured, but thermal transfer from the bombarded layer through the substrate using "heat-sink

grease" to a water cooled platten, was shown to be necessary for the prevention of cone growth (Revell, 1979b). Analysis by E.D.A.X. (Energy Dispersive Analysis by X-rays) confirmed that the particles were aluminium. It was concluded that the growth of these features was essentially by surface diffusion. A study of cone growth on argon beam bombarded surfaces (Robinson, 1979) showed that the critical temperature below which these structures did not form was approximately $400^{\circ}C$ for Al. An example of aluminium cone formation is shown in Fig. 4.18. In this micrograph it can be clearly seen that the concentration of cones is very much greater on areas coated with photoresist than those consisting of bare aluminium. This is thought to be due to the higher surface temperature of the resist film and the availability of sites for nucleation.

The presence of aluminium rings, as shown in Fig. 4.19, has also been frequently observed on samples that were exposed to B93 and B95 argon beams. This micrograph clearly shows that ring formation has only occurred on areas not protected with resist. The micrograph is included here only to illustrate the phenomenon, the mechanism by which these structures are formed is uncertain. One suggestion is that the ring represents a low energy state for the accretion of particles. It is also possible that secondary electron emission from the bare aluminium causes charging of the surface, which because of the electrical isolation cannot dissipate. Quite how this could lead to

aggregates in the form of rings is unclear at the present time. An investigation of this phenomenon might be a fruitful area for further study.

4.6 ETCHING OF W

4.6.1 Etch Rates

Tungsten (W) films, prepared by the method described in Appendix I have been etched with noble gas and reactive particle beams from the B93 source. These data are presented in Fig. 4.20. The three Freons produced etch rates in this material that were between two and three times lower than those for an argon beam. On the basis of kinetic energy transferred to the target, the CF_3 ion (proposed as the predominant species when the B93 source is injected with a Freon) would be expected to be more effective than Ar^+ (as shown in Fig. 7.3). The experimental results, however, suggest that elemental tungsten was removed at a slow rate by sputtering when CF_x species bombarded the metal surface. This could be attributable to the formation of a passivating film of tungsten fluoride with a low sputter yield, or the dissociation of CF_x to form a carbon film.

The etch rate for the action of a B93-SF_6 beam on W was determined to be similar to that for an argon beam. It seems likely that a combination of processes occurs: sputtering due to bombardment by CF_x species (formed by the process described in Section 7.3.2) and attack by fluorine free radicals which diffuse from the source.

4.6.2 Etched Profiles

As the film thickness of this material was on the

order of 2000 Å, a detailed evaluation of etched profiles has not been possible. A step etched into W using a B93-SF_6 beam was examined using the S.E.M. and the observations were of a clean profile free of redeposition and trenching. The edge appeared to be vertical, but further work with an increased thickness of metal should be carried out to confirm this.

Debris in the form of particulates and spikes have been observed using the S.E.M. on a W film etched with a B93-C_3F_8 beam. These artefacts are similar to those which were observed on aluminium films following argon bombardment. The chemical composition of these particles has not been established.

4.7 VACUUM EQUIPMENT

The condition of the vacuum pumps used in this study has been monitored by:

(i) measuring the time taken for the pumps to reduce the chamber to a predetermined pressure, and

(ii) comparing the results of infra-red spectroscopic analysis on virgin oils and those periodically sampled from the rotary and diffusion pumps.

Pump-down times were influenced by factors such as the sample change-over time (duration for the chamber open to atmosphere and relative humidity). The chamber roughing cycle, from atmospheric pressure to 0.05 torr lasted between 2.75 and 3.1 minutes. The time taken to reduce the chamber pressure from atmospheric to 1×10^{-4} torr (ionisation gauge determination) was usually no greater than 3.5 minutes using automatic valve operation.

Longer pumping times were only measured after experiments with exceptionally high gas loads (for example, using the B93 source with 1 kV applied at the anodes). A short period of operation with the rotary pump on full gas ballast corrected this. No deterioration in the performance of the pumps has been detected after $\simeq 200$ hours of operation with B93-Freon beams.

An infra-red spectrophotometric examination over the wavenumber range 4000 to 200 cm^{-1} (2.5 to 50 μm) was carried out on unused Invoil 30 and Duo Seal oils and on the same type of fluid withdrawn from the diffusion and rotary pumps after exposure to B93-Freon and SF_6 beams for approximately 25 hours. No evidence was obtained for the presence of fluorinated compounds in any of the "exposed" samples. The infra-red spectra were compared over the range 1400-1000 cm^{-1} which is the region assigned to the C-F stretching absorption. The absence of new absorption maxima in this region indicated that the concentration of compounds containing this bond structure was below the limit of detection for the instrument used (1 or 2% by volume).

4.8 SUMMARY

Using fluorinated beams from the B93 source the etch rates of Si, SiO_2 and Si_3N_4 are greater than those obtained by sputtering with argon under the same conditions of beam "current" and energy. Chemical reactions are important for the removal of these target materials with fluorinated etchant species. These results are generally consistent with the findings of

workers using heated filament sources injected with similar compounds (Mayer, et. al., 1981). Using the conditions that have been described, the etch rates of silicon compounds were significantly lower than would be required in a commercial fabrication process. Etched profiles, particularly in CF_4 and CHF_3-beam etched SiO_2 have been observed to be vertical and free of sputtering-induced artefacts.

The etching of aluminium films proceeds at greater rates with fluorinated beams than with argon. The inconsistent etch rate data obtained when argon beams were used indicate that variations occurred in the oxygen partial pressure and/or water vapour concentration in the vacuum chamber. The production of topographical defects (cones, rings) on etched aluminium films is associated with inadequate cooling of the target.

FIG.4.1 Etch-rate data for the action of beams produced by the B93 source on silicon dioxide targets.

Source axis normal to target plane, C.A.T.T. 150 mm. Targets cooled, static. Mean beam "current" density(determined for Ar): 27 $\mu A\ cm^{-2}$. Beam energy (V_B, keV) shown in parentheses.

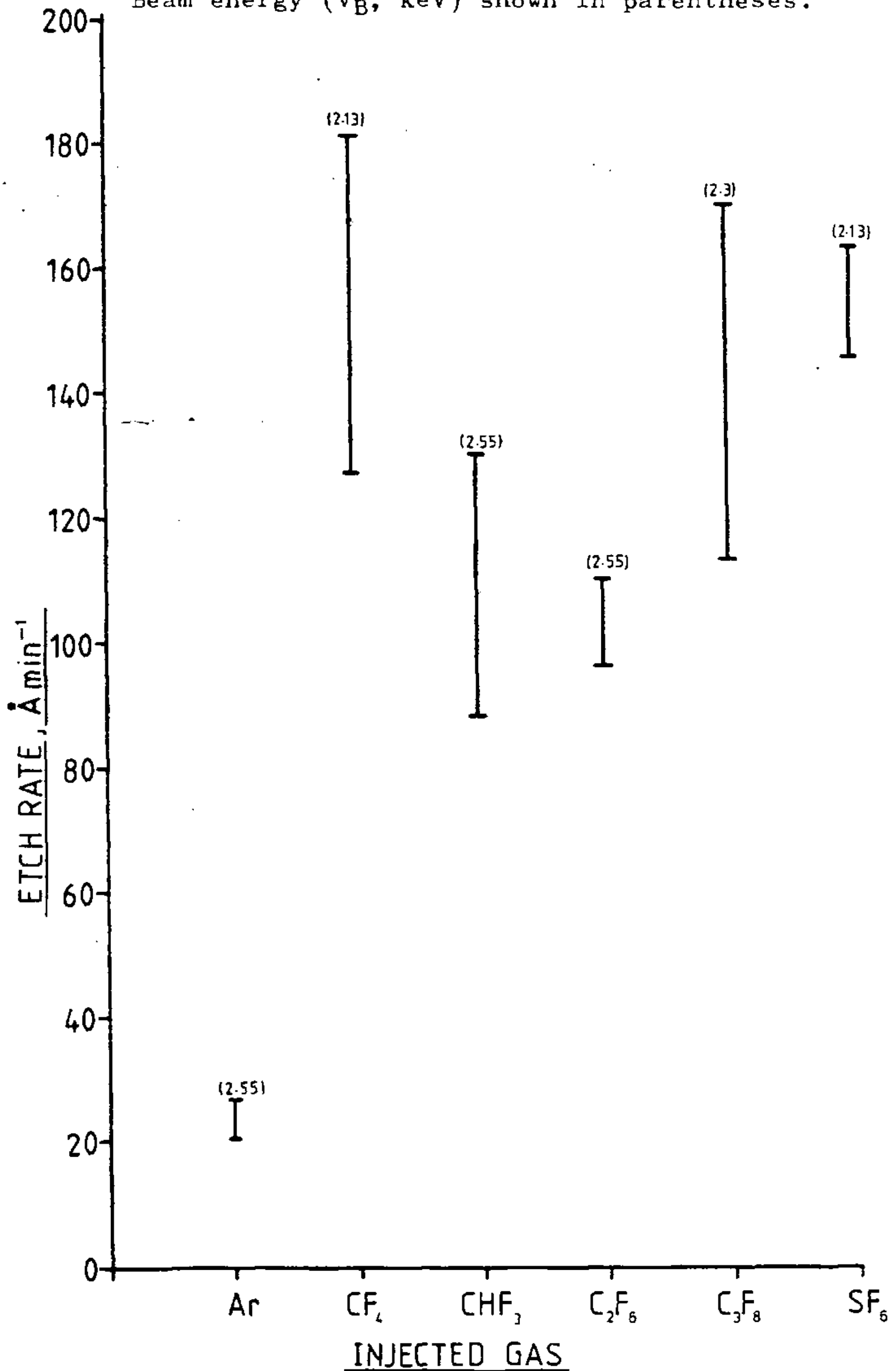

FIG.4.2 SiO$_2$ etch-rate dependence on argon energy using the B93 source.

Variation of etch-rate at four positions on wafers normal to the axis of the B93 source. C.A.T.T.: 150 mm, mean beam "current" density: 34 μA cm^{-2}. Water cooled, static targets.

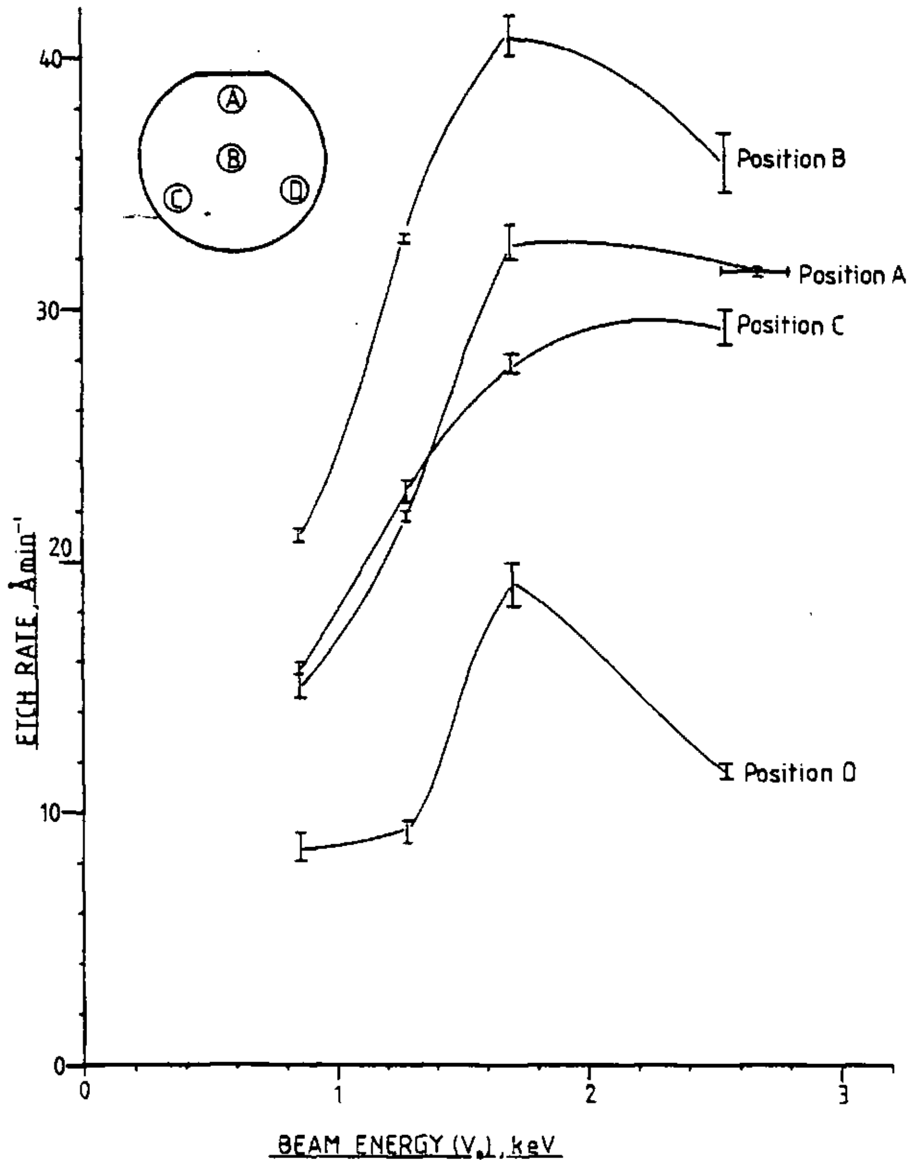

FIG.4.3 SiO_2 sputter yield dependence on Ar^+ energy for published data and experimental results.

Data points for heated filament sources refer to Table 10.

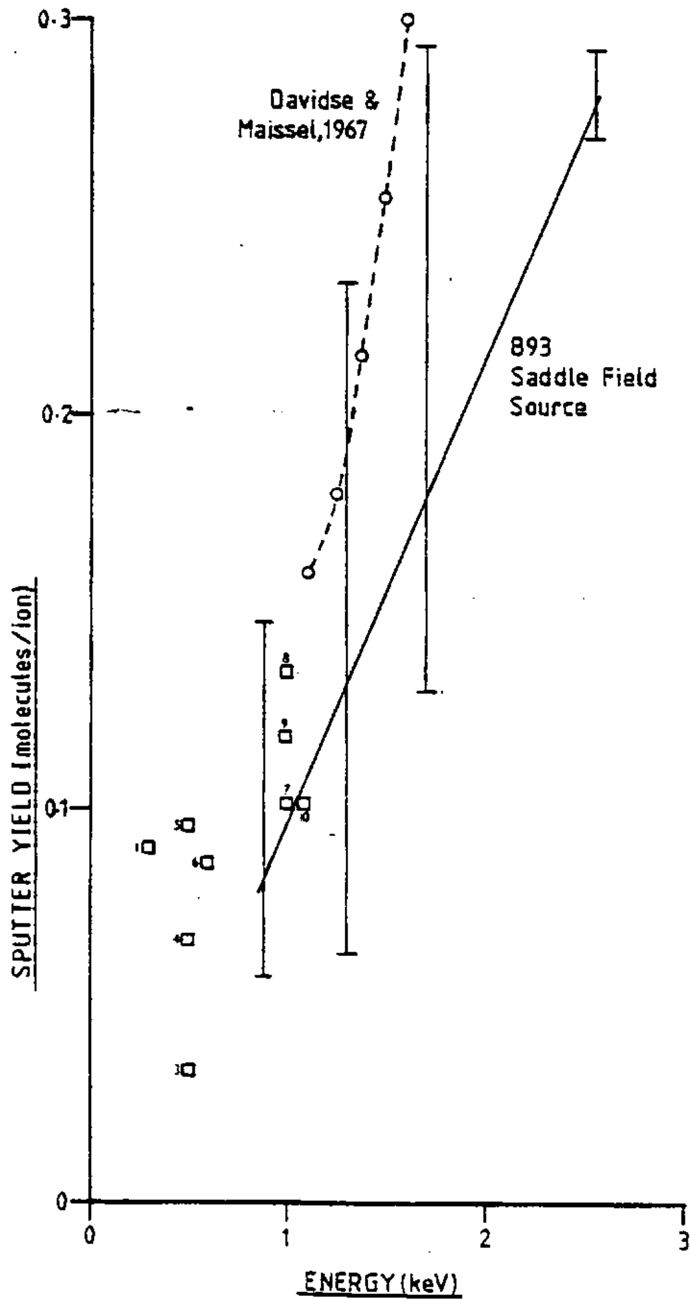

FIG.4.4 SiO_2 Sputter Etch Rate Dependence on "Current" Density for a B93-Ar Beam.

V_B: 2.55 keV, C.A.T.T.: 150 mm, normal incidence.

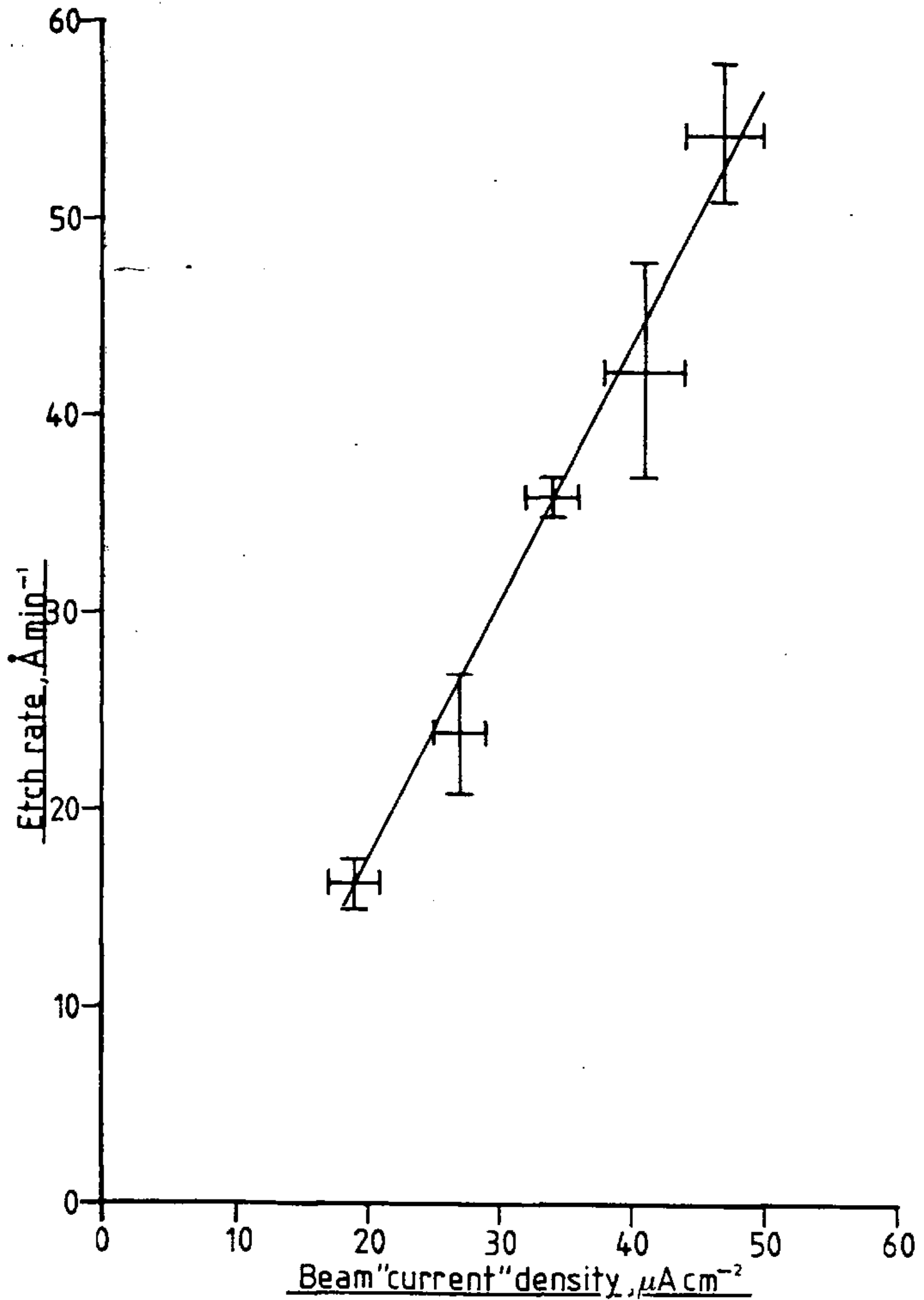

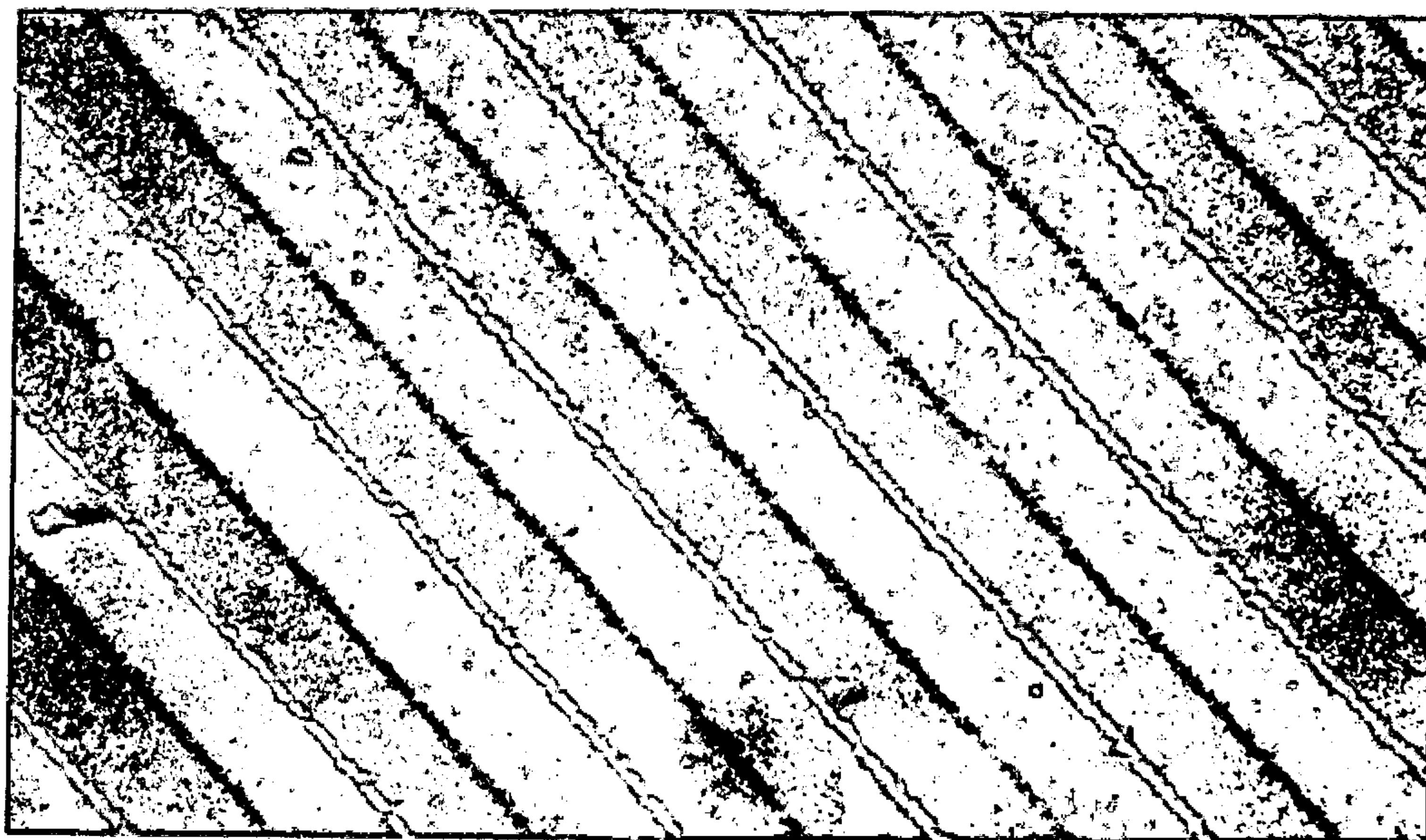

10μm

FIG.4.5 Sloping sidewalls etched into SiO_2 using a B93 argon beam
V_B : 2.55 keV, I_B : 34 μA cm^{-2}, C.A.T.T. : 150 mm, 20 minutes

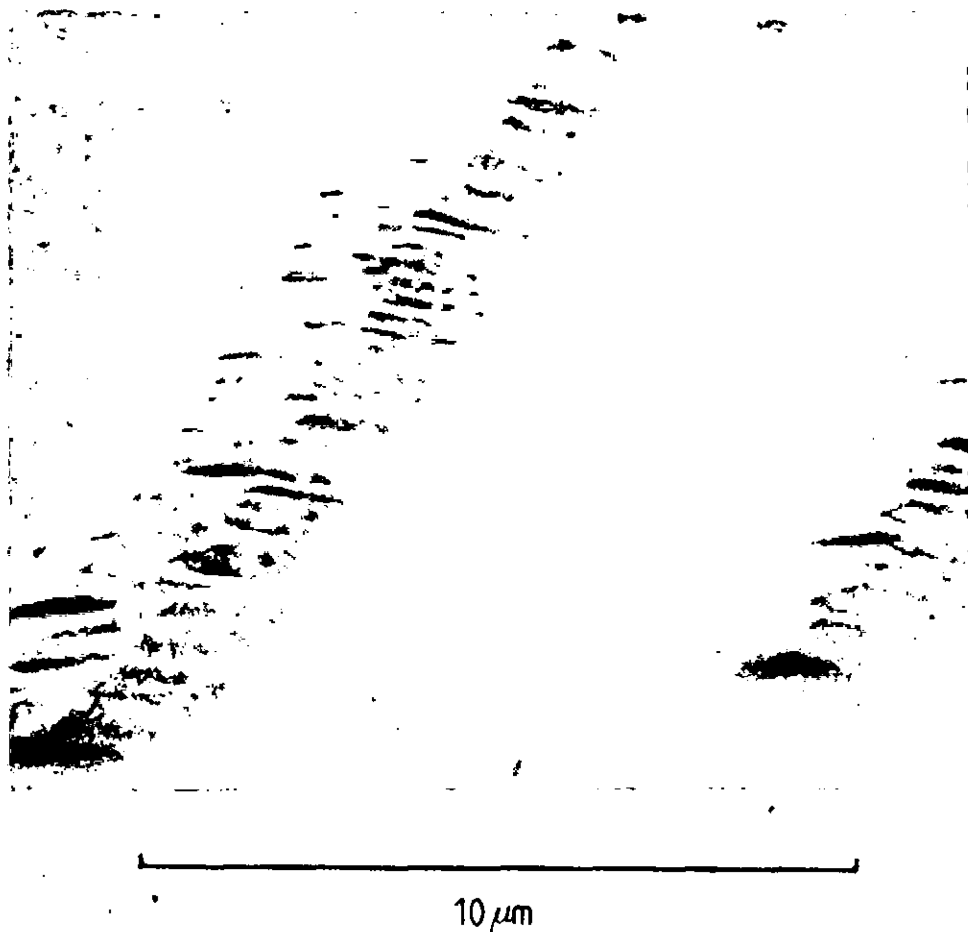

FIG.4.6 Facet formation in SiO_2 caused by over-etching with an argon beam.

B94 source, V_B : 2.55 keV, I_D : 150 mA, C.A.T.T. : 251 mm, 500 minutes

FIG.4.7 SiO_2 apparent sputter yield dependence on CF_x etchant particle energy.

For beams produced by injecting CF_4 into heated filament sources (published data) and experimental results using the B93 source.

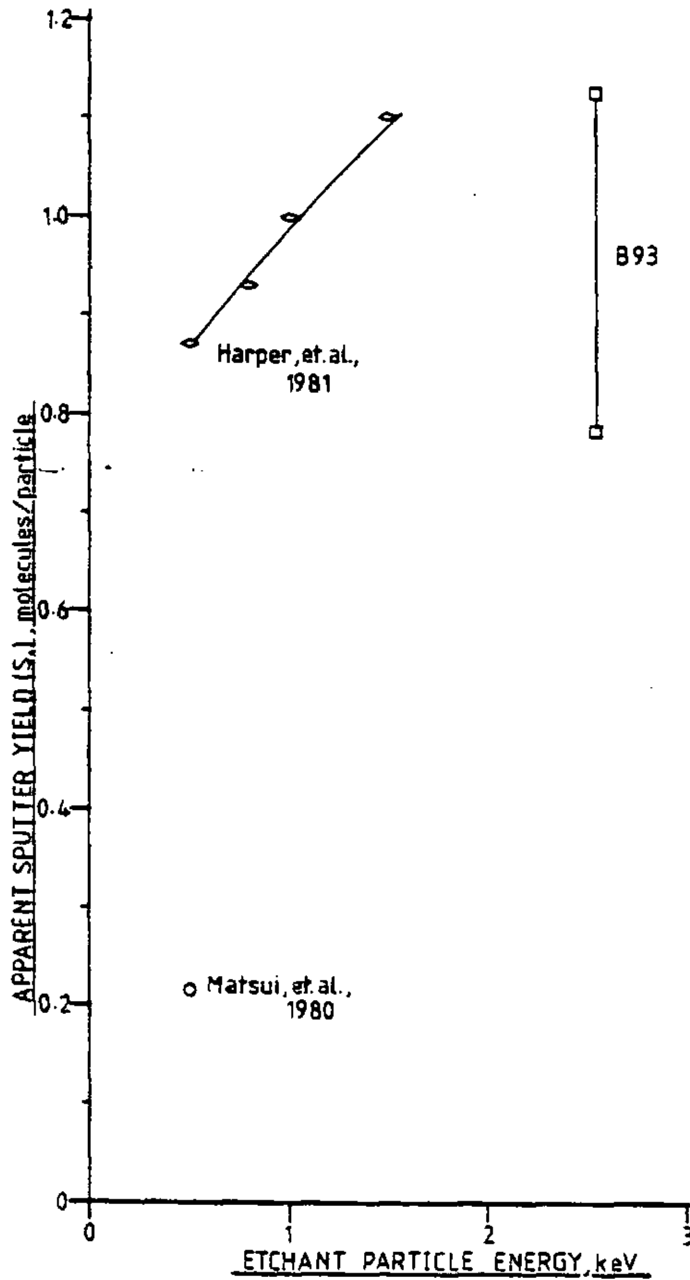

FIG.4.8 SiO_2 apparent sputter yield dependence on CF_x etchant particle energy for B93-CHF_3 beams.

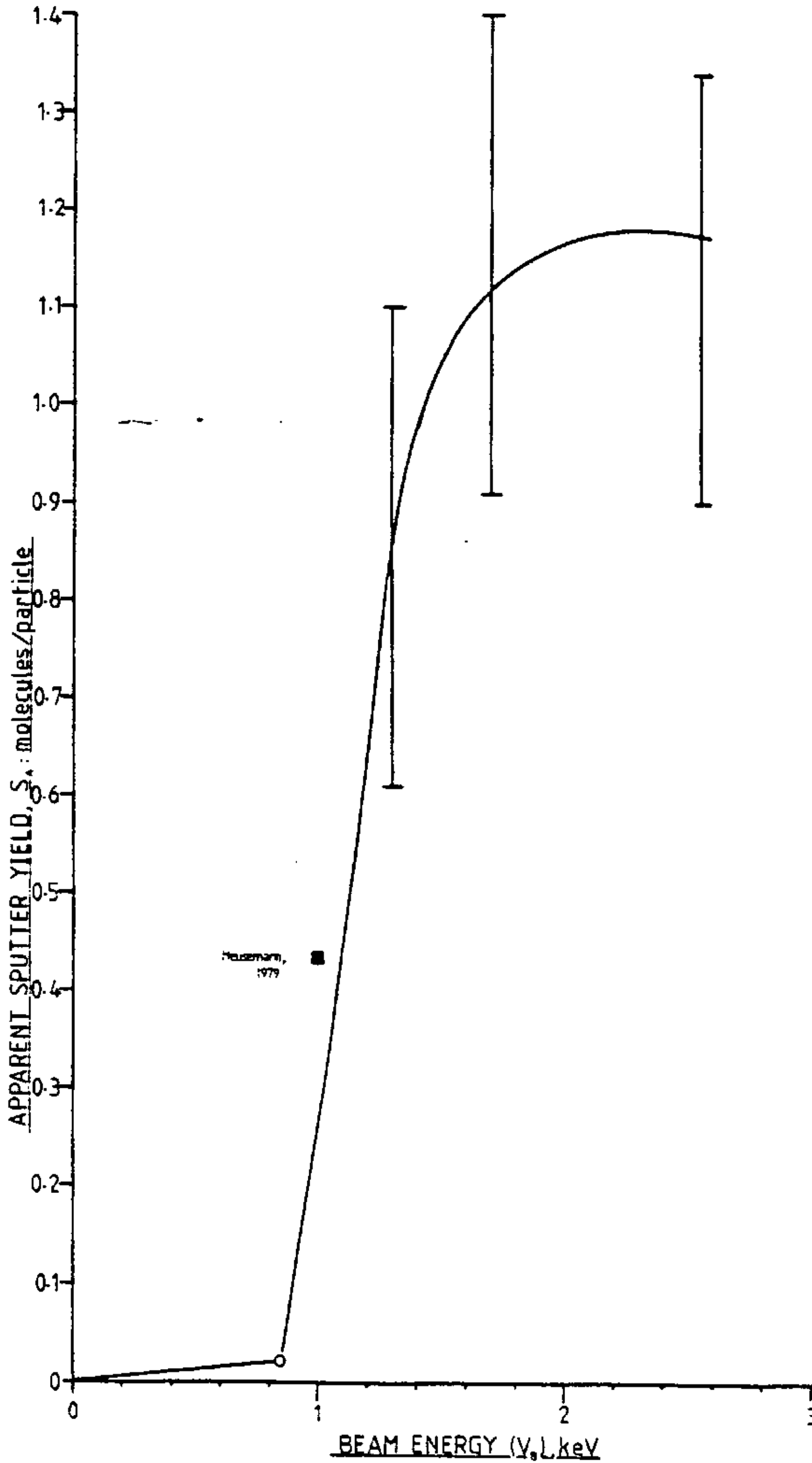

FIG.4.9 Si Apparent Sputter Yield Dependence on CF_x etchant particle energy for B93-CHF_3 beams.

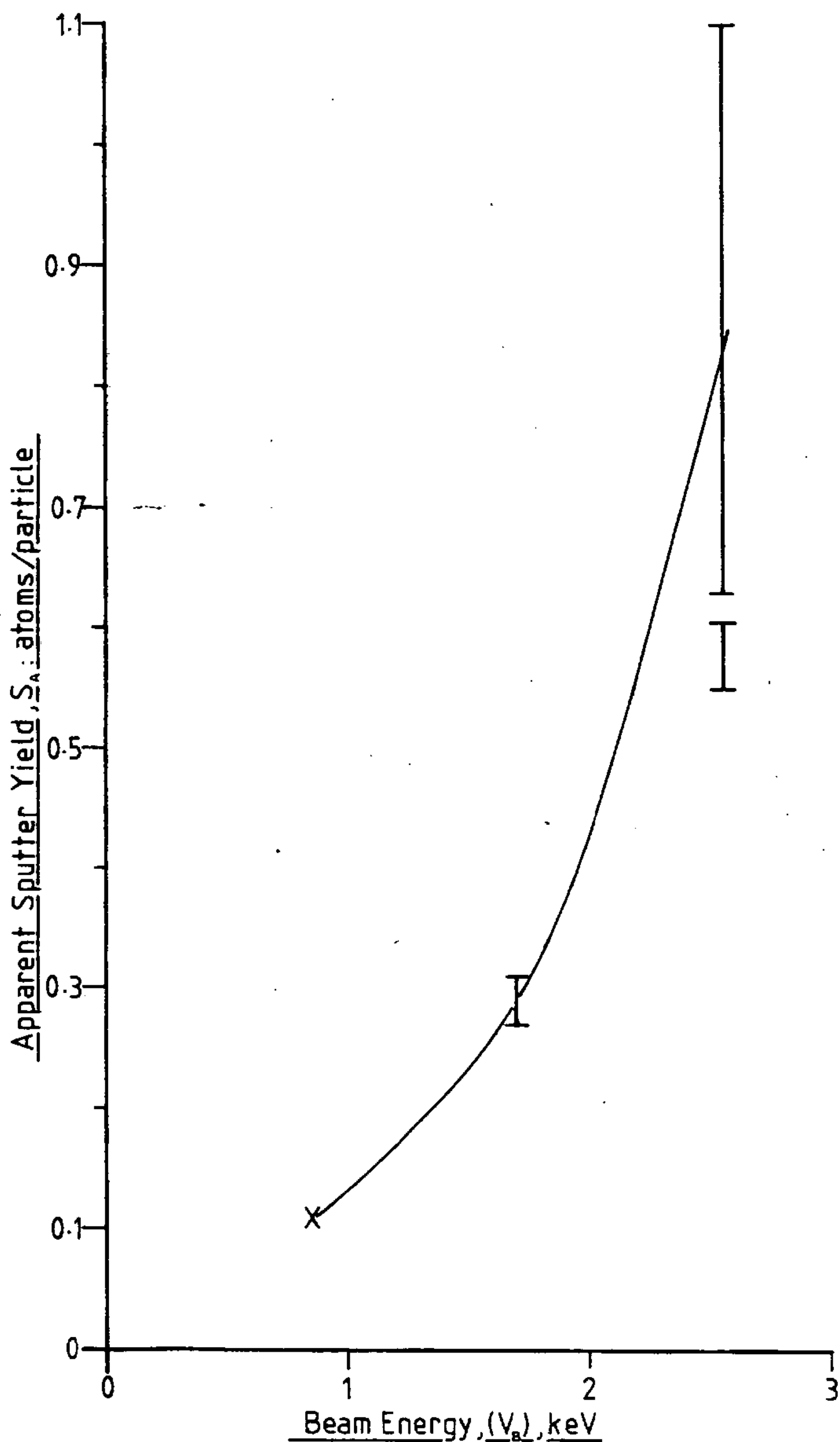

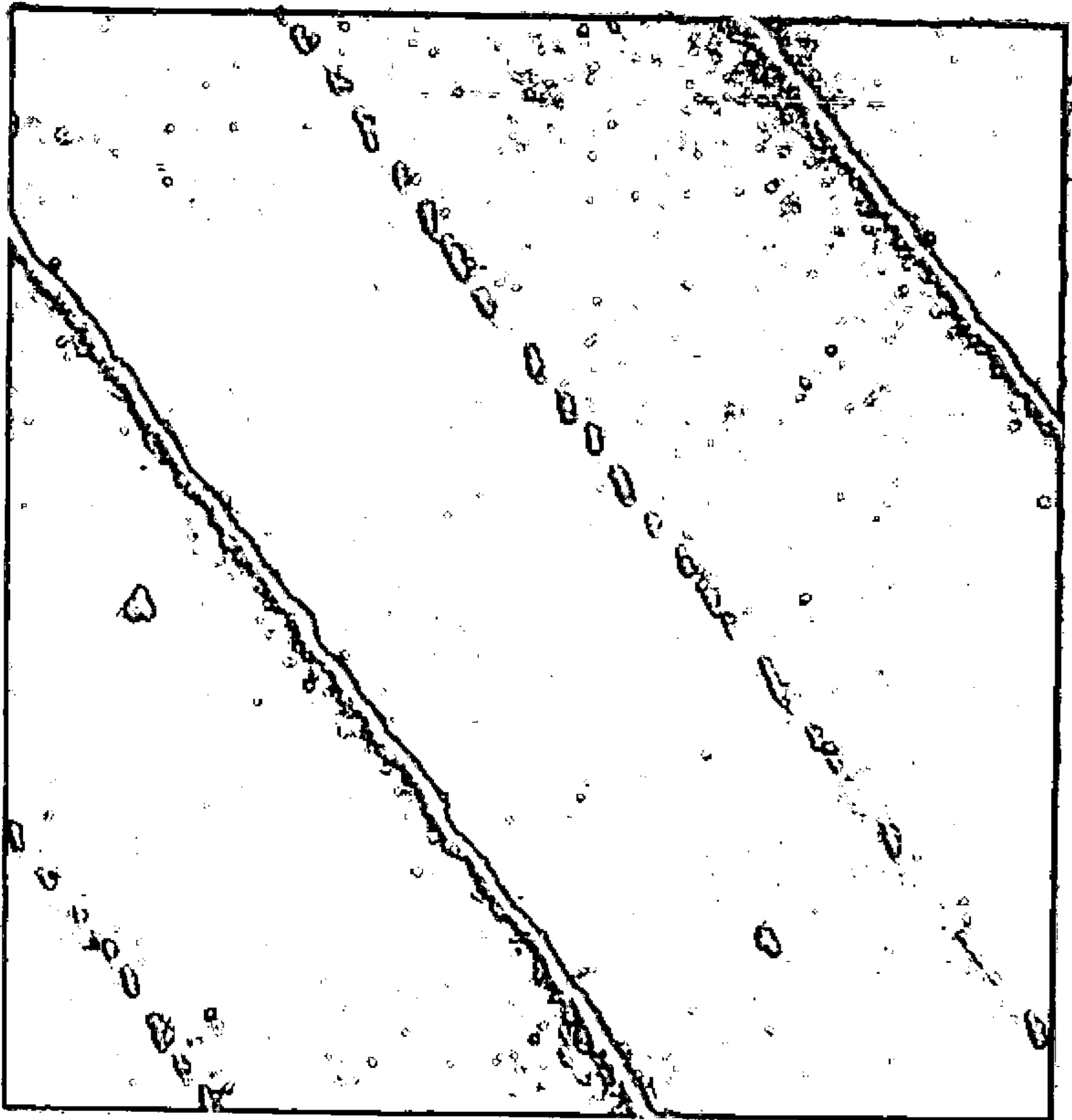

FIG.4.10 Anisotropic etching of SiO_2 using a B93-CHF_3 beam.

Pattern defined in Kodak 747 resist (negative), removed after etching.

Static, cooled target, on and normal to source axis.
V_B: 2.55 keV, I_B: 34 μA cm^{-2}, C.A.T.T.: 150 mm, 20 minutes.

FIG.4.11 Vertical profile etched into SiO_2 using a B93-CHF_3 beam.

MITE Resolution test pattern defined in Kodak 747 (negative) resist, removed after etching.

Static, cooled target, on and normal to source axis.
V_B: 2.55 keV, I_B: 41 μA cm^{-2}, C.A.T.T.: 150 mm, 25 minutes.

FIG.4.12 SiO_2 Apparent Sputter Yield Dependence on Etchant Particle Energy for B93 beams and Published Data for Heated Filament Sources.

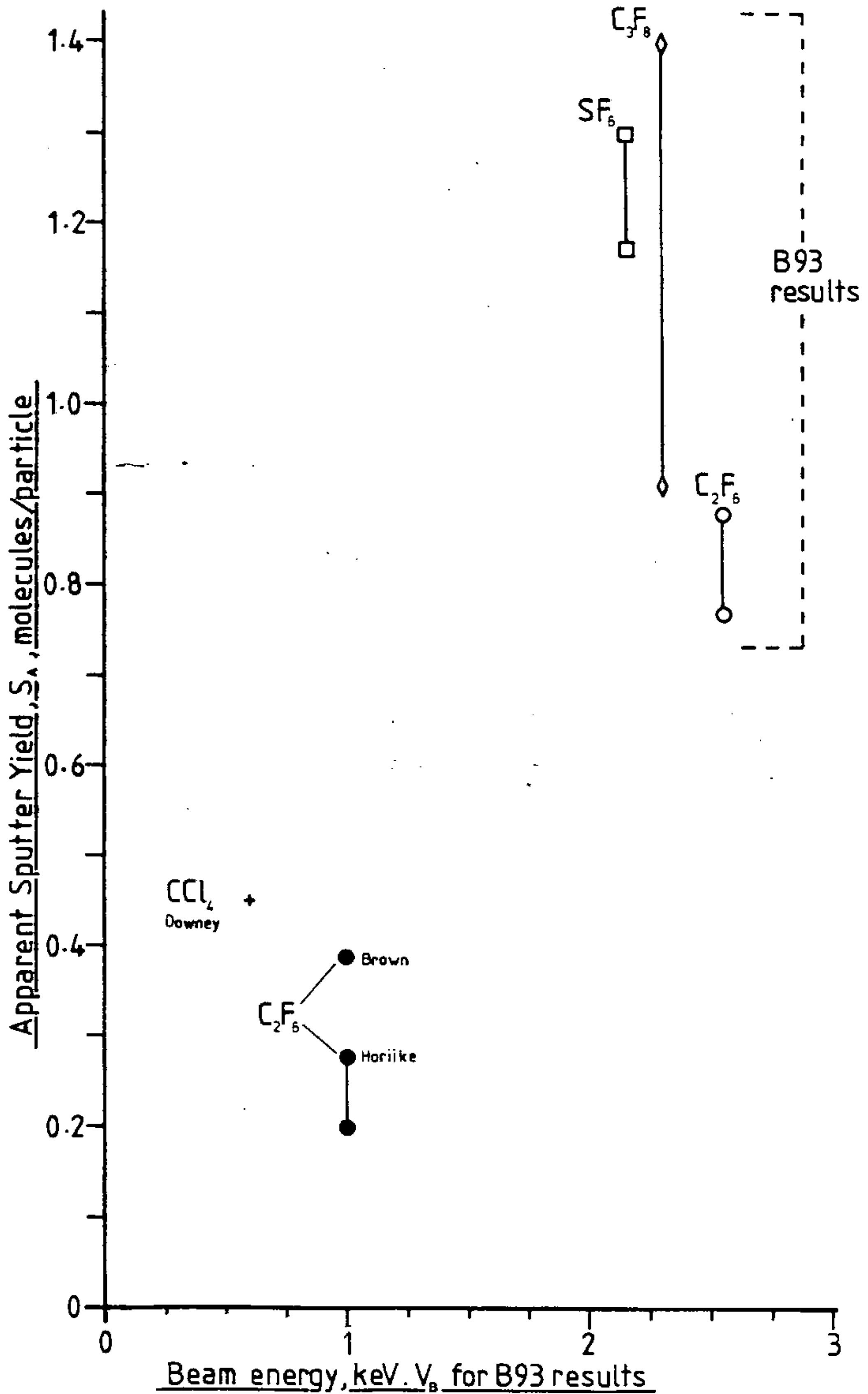

FIG.4.13 Silicon sputter yield dependence on particle energy.

For argon beams produced by heated filament sources and the B93 Saddle Field source. Data points are for the references in Table 10.

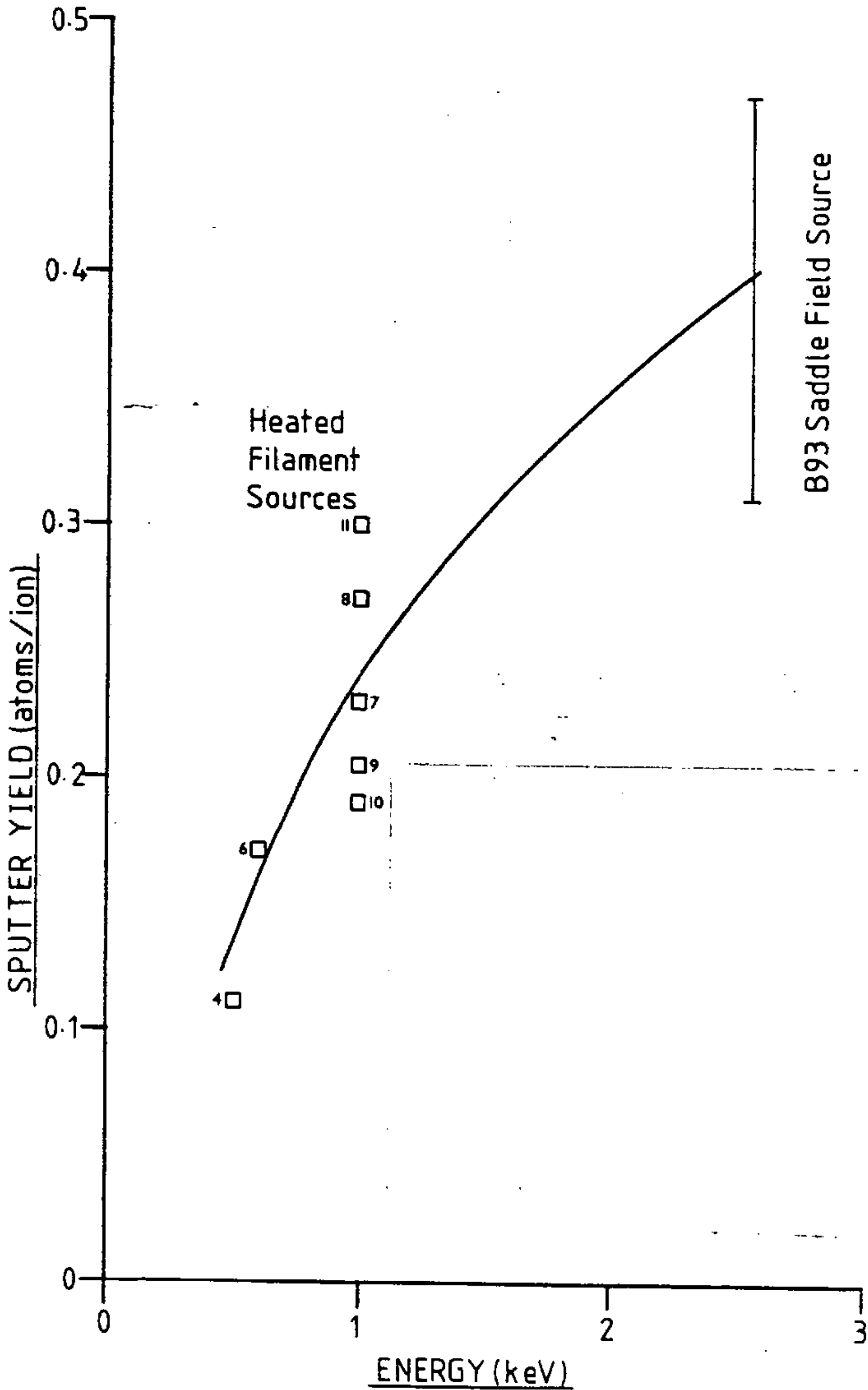

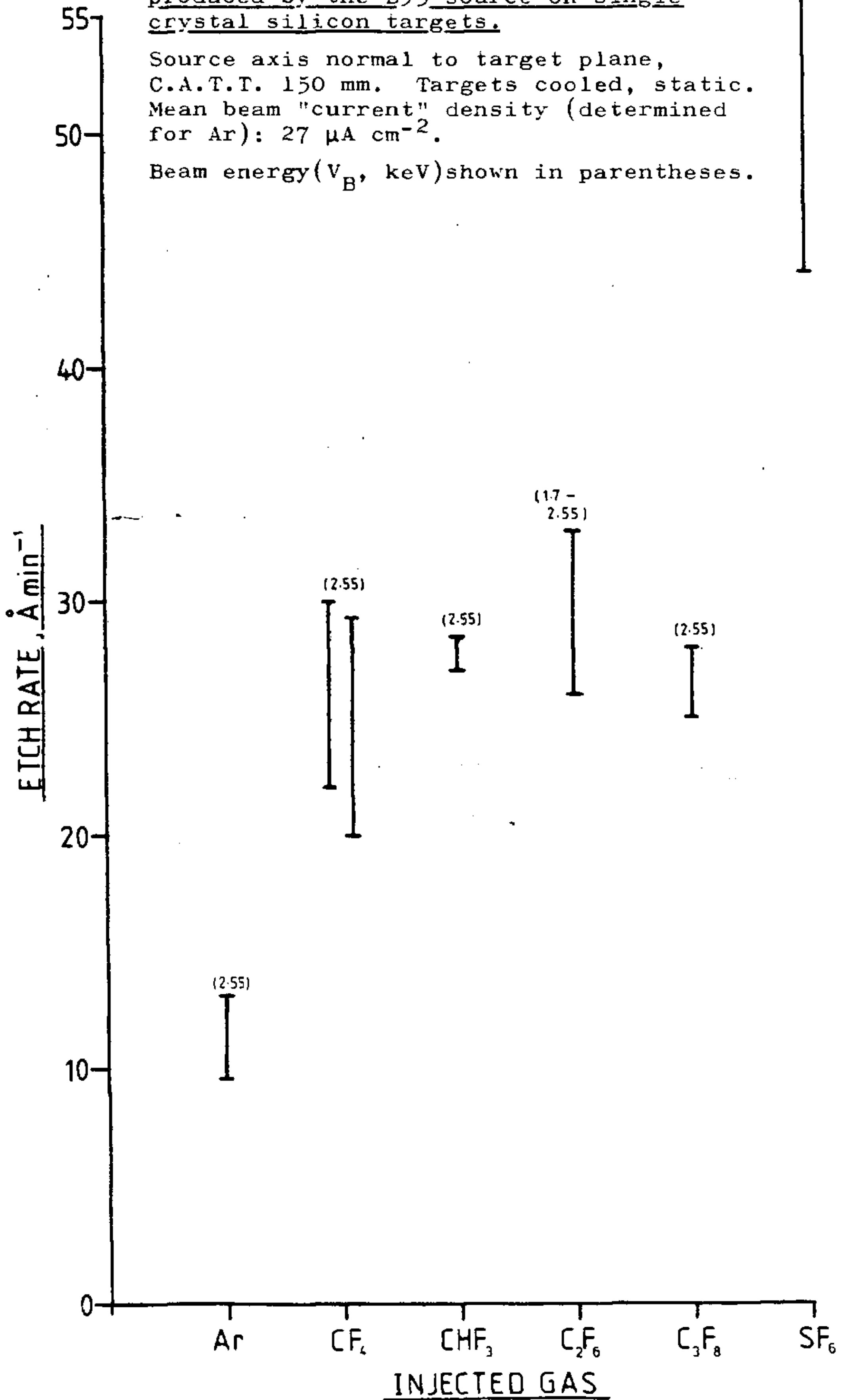

FIG. 4.14 Etch-rate data for the action of beams produced by the B93 source on single crystal silicon targets.

Source axis normal to target plane, C.A.T.T. 150 mm. Targets cooled, static. Mean beam "current" density (determined for Ar): 27 $\mu A\ cm^{-2}$.

Beam energy (V_B, keV) shown in parentheses.

FIG.4.15 Etch-rate data for the action of beams produced by the B93 source on silicon nitride targets. Source axis normal to target plane, C.A.T.T. 150 mm. Targets cooled, static. Mean beam "current" density (determined for Ar): 27 $\mu A\ cm^{-2}$. Beam energy (V_B, keV) shown in parentheses.

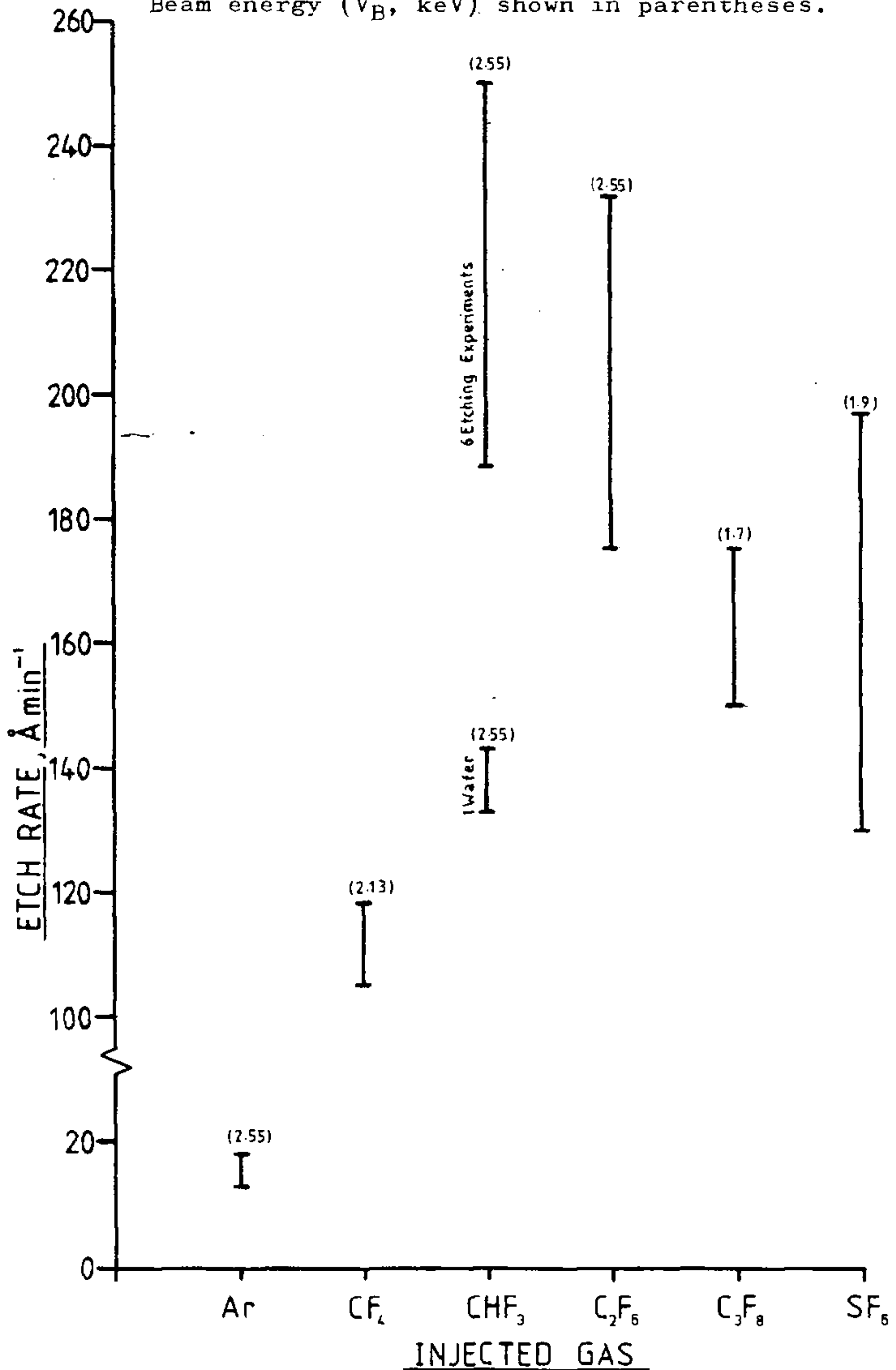

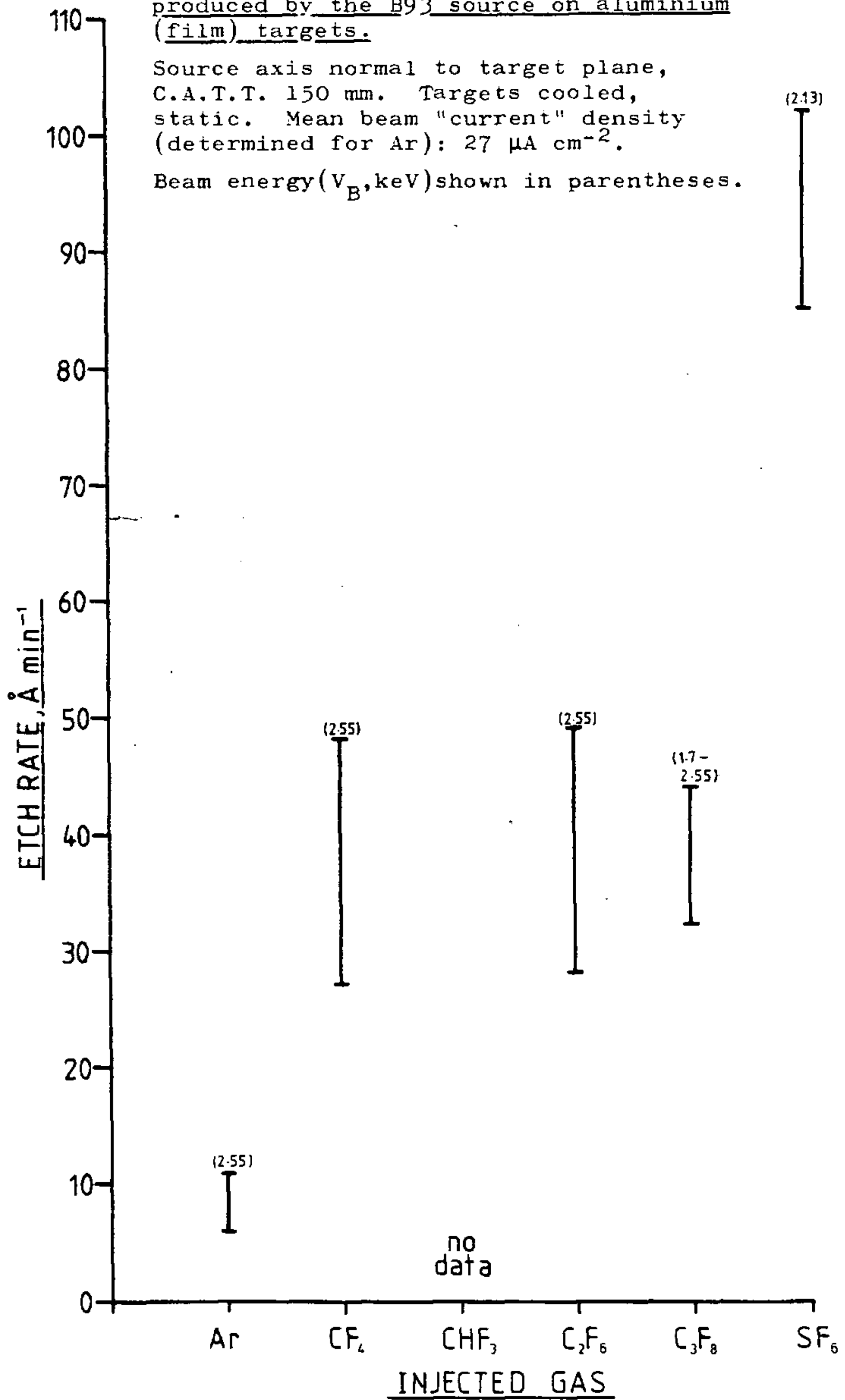
FIG.4.16
Etch-rate data for the action of beams produced by the B93 source on aluminium (film) targets.
Source axis normal to target plane, C.A.T.T. 150 mm. Targets cooled, static. Mean beam "current" density (determined for Ar): 27 µA cm⁻².
Beam energy(V_B,keV)shown in parentheses.
ETCH RATE, Å min⁻¹
110
100
90
80
70
60
50
40
30
20
10
0
(2.13)
(2.55)
(2.55)
(1.7 - 2.55)
(2.55)
no data
Ar
CF4
CHF3
C2F6
C3F8
SF6
INJECTED GAS

FIG.4.17 Al Film Etch Rate Variation with Duration of Exposure to B95-Ar beams.

V_A: 3 kV, I_D: 300 mA, C.A.T.T.: 250 mm
Chronological sequence given by A, B, C, for each day.

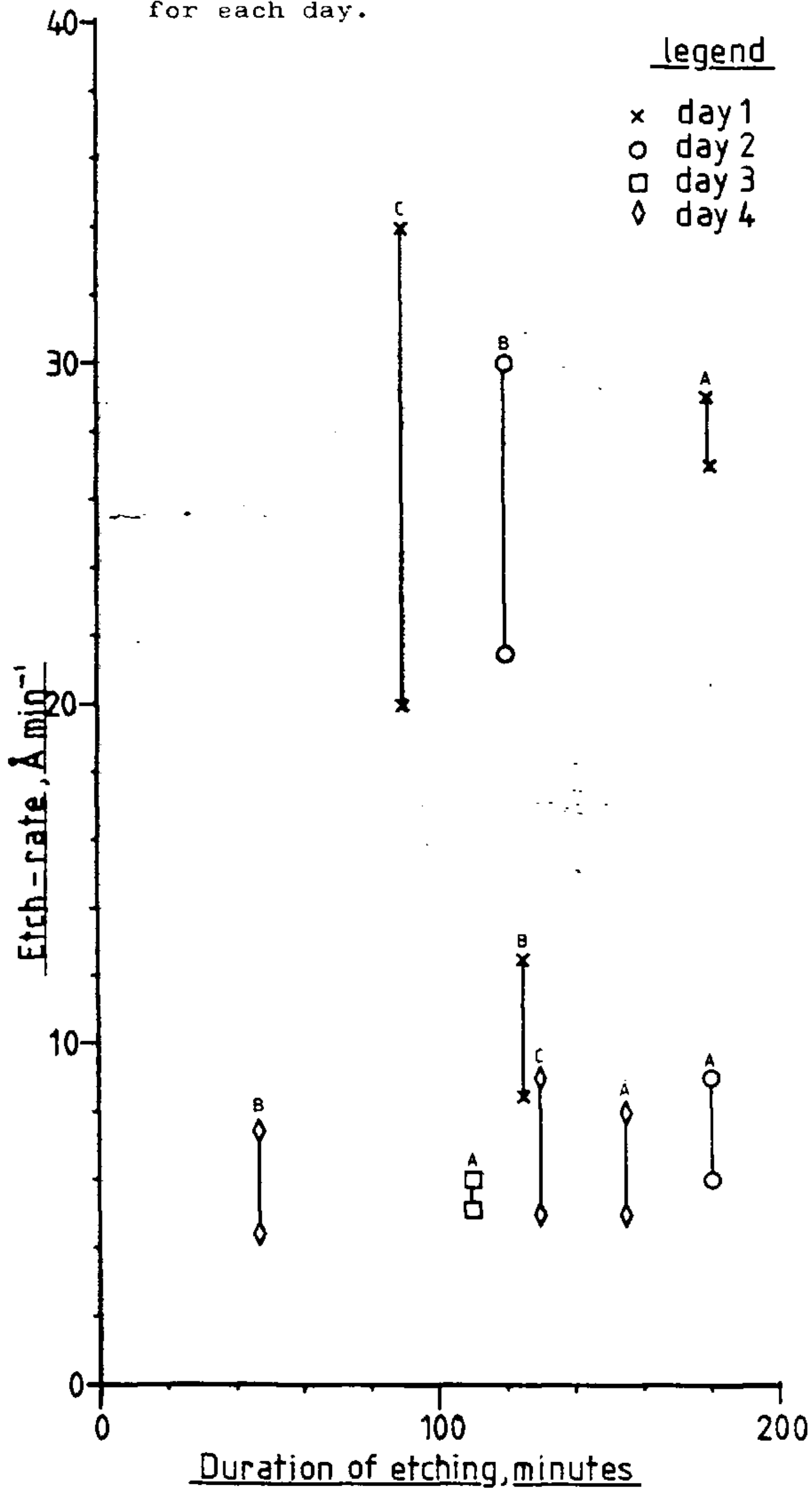

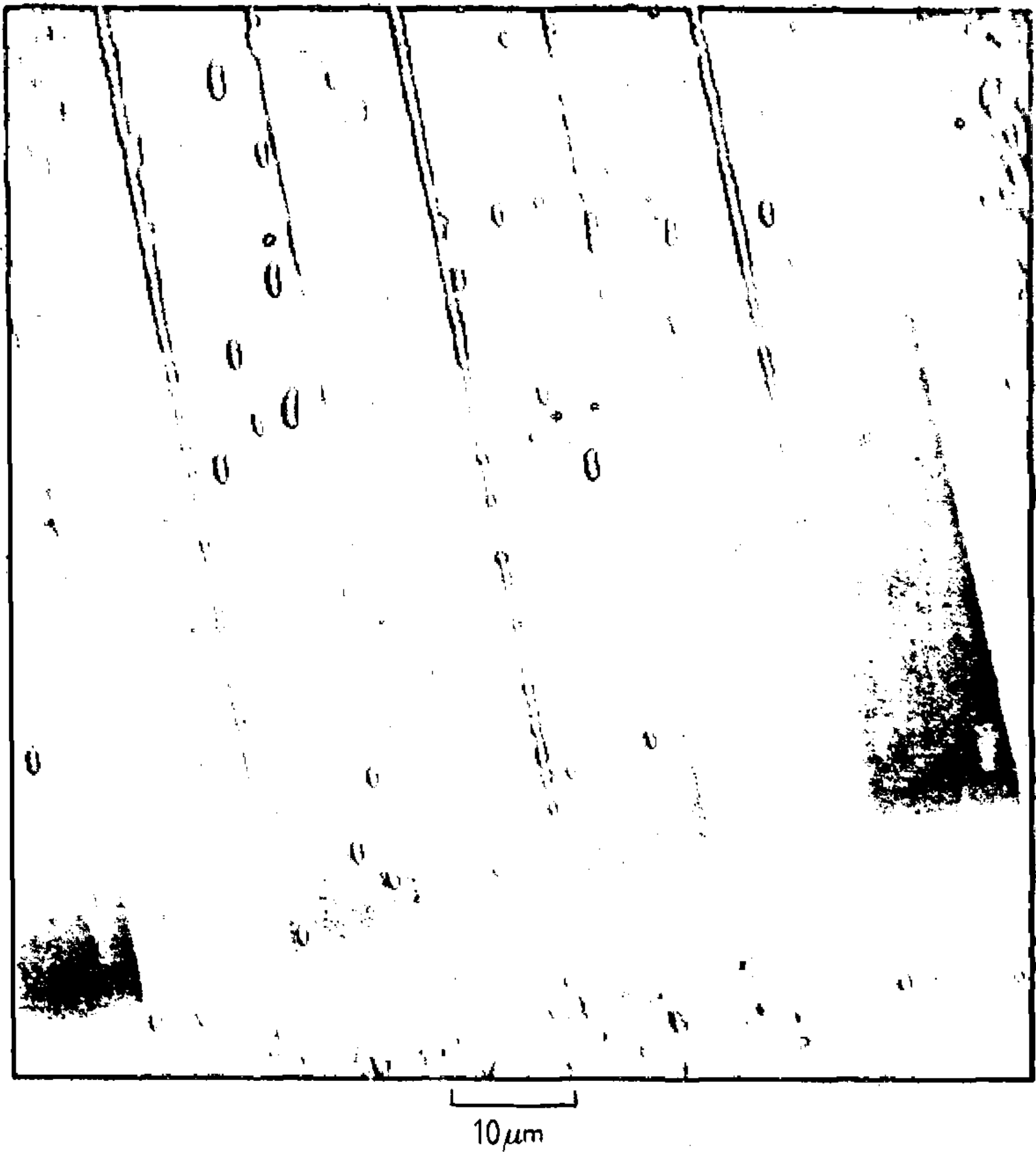

FIG.4.18 Aluminium cones produced during exposure to a B95 argon beam.

MITE resolution test pattern defined in Kodak 747 (negative) resist, not removed.

V_A: 3 kV, I_D: 300 mA, C.A.T.T.: 250 mm, 120 minutes, uncooled planetary target holder.

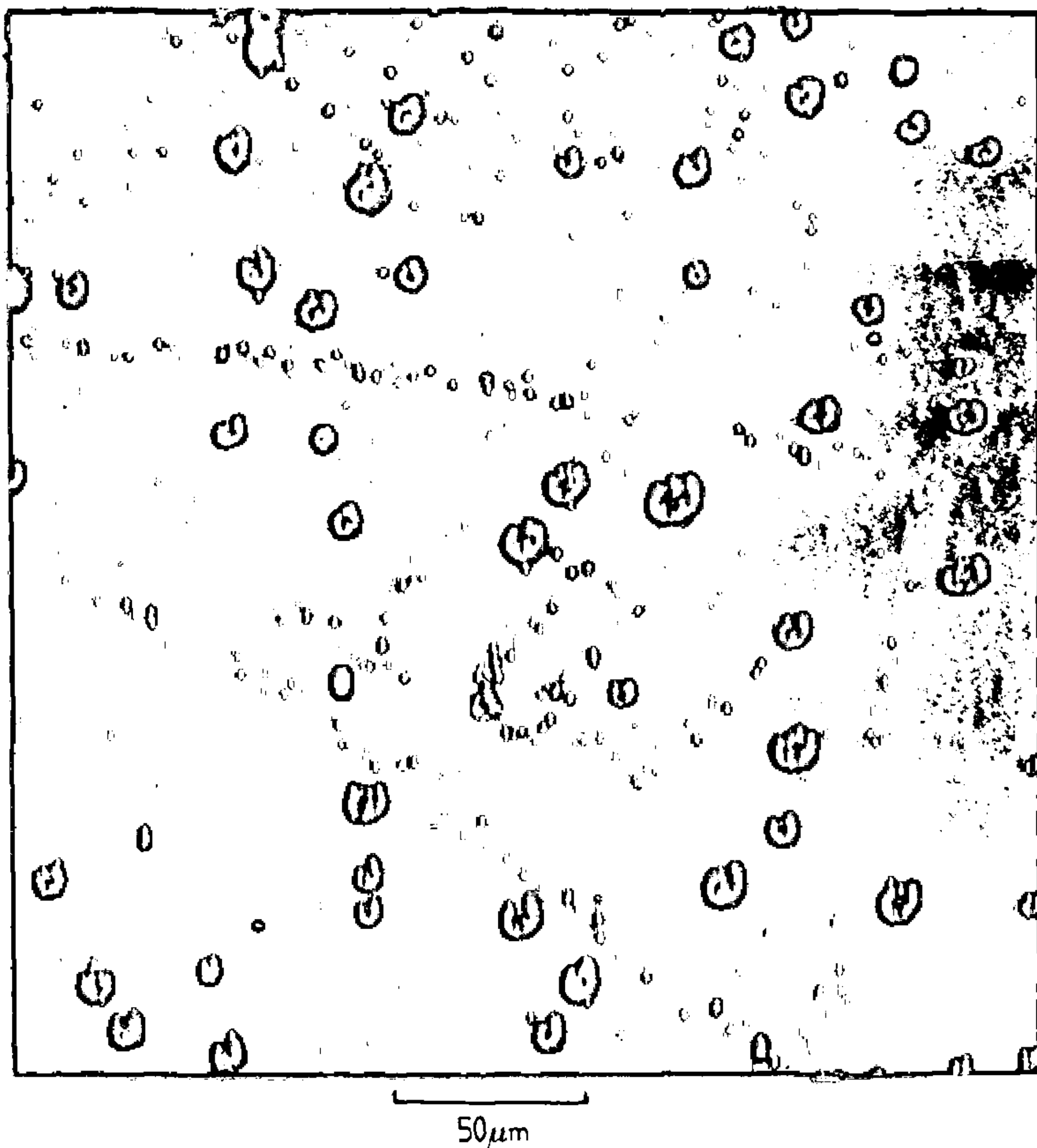

FIG.4.19 Aluminium ring formation produced during exposure to a B95 argon beam.

MITE resolution test pattern defined in Kodak 747 (negative) resist, not removed.

V_A: 3 kV, I_D: 300 mA, C.A.T.T.: 250 mm, 90 minutes, uncooled planetary target holder.

FIG.4.20 Etch-rate data for the action of beams produced by the B93 source on tungsten (film) targets.

Source axis normal to target plane, C.A.T.T. 150 mm. Targets cooled, static. Mean beam "current" density(determined for Ar): 27 μA cm^{-2}. Beam energy(V_B, keV)shown in parentheses.

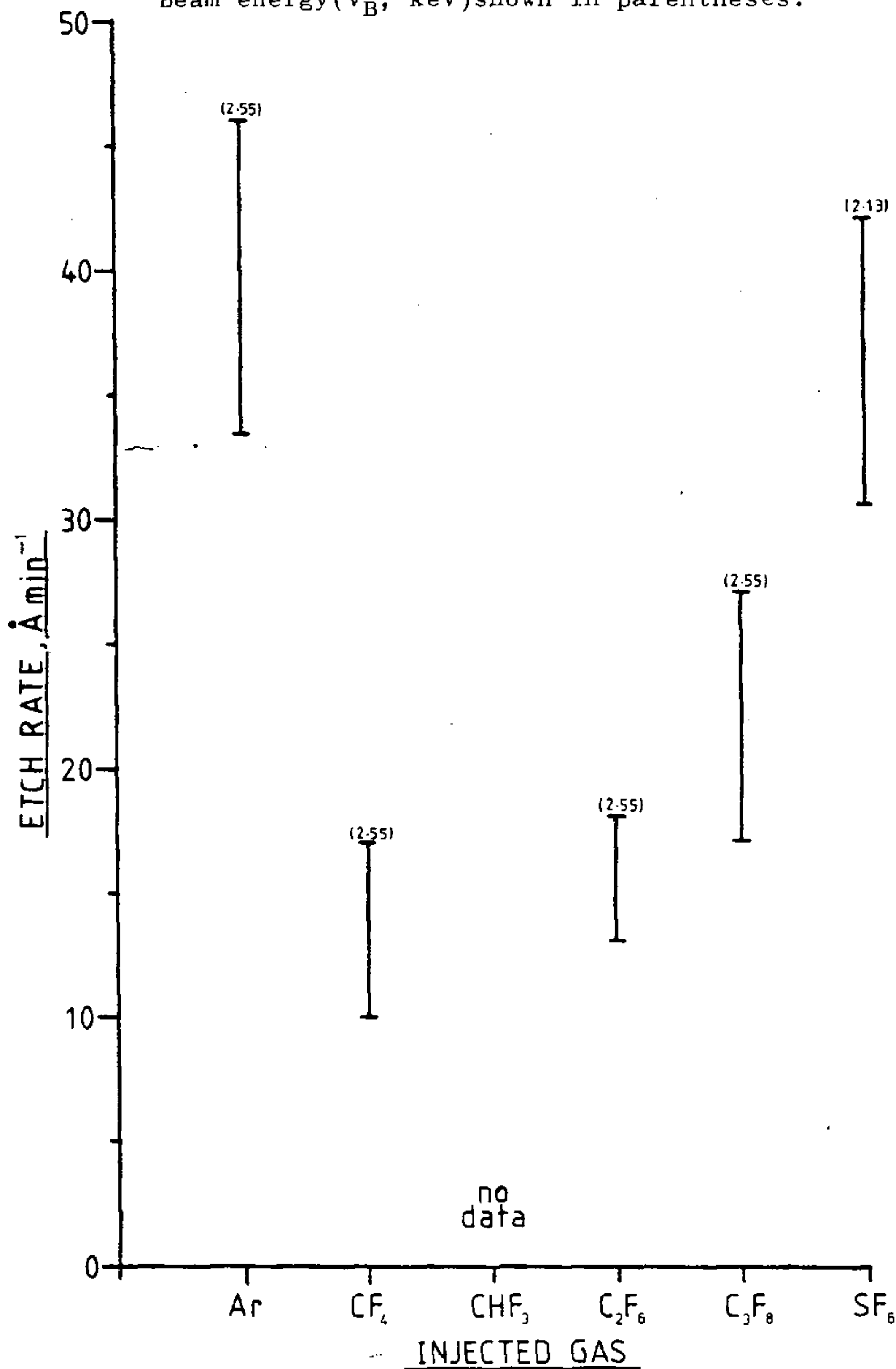

5. SUB-MICRON DEVICE GEOMETRIES

5.1 INTRODUCTION

The trend towards smaller device dimensions was recognised some time ago and embodied in "Moore's Law" (Moore, 1975) which predicts certain technological advances in the microelectronics industry based on previous performance. If the slope of the curve remains constant (this has been the case between 1968 and 1980), reductions in feature size from 5 μm to 0.5 μm will be accomplished by 1989 for experimental processing (stringent design and fabrication) and by 2010 for industrial production (Coker, 1980). In practical terms, one goal of the American VHSIC (Very High Speed Integrated Circuit) programme is for the experimental production of devices with 0.5 μm minimum features by 1985 (Weisberg, 1978). By this date, the typical area of one gate is predicted to be 129 μm^2 (Douglas, 1981).

5.2 ADVANTAGES OF REDUCING DEVICE DIMENSIONS

The continuing reduction of device linewidths is important for several reasons:

(i) Increasing the packing density and degree of circuit complexity per unit area. This is partly due to "fashion" - consumer demands for increasing miniaturisation and partly to the increasing capabilities of the more complex circuits.

(ii) Reducing the current consumption and voltage requirements of individual transistors.

(iii) Improvements in speed of response, by reducing the clock period (i.e. the time between charging and

discharging of the device capacitance).

For a ten-fold reduction of all dimensions, it has been shown that (Mead and Conway, 1980):

(a) the number of transistors will be increased by two orders of magnitude for the same surface area

(b) the voltage will be reduced by a factor of 10

(c) the total power supplied to a unit area will remain constant

One disadvantage is, however, that the current supplied for a unit surface area increases by an order of magnitude. This may impose limitations on the size and shape of metal tracks on the I.C. for distributing the current.

Volume-production of some devices which incorporate 1 μm minimum features have been available for some time (Hunter, et. al., 1978). These insulated-gate field effect transistor programmable logic arrays (IGFET-PLA) were fabricated using electron beam lithography and CF_4-O_2 R.I.E. to achieve control over linewidths and to provide highly discriminatory etching of polysilicon (20:1 against SiO_2) described elsewhere in the literature (Ephrath, 1979). High density memory circuits, for example a 16 k Static CMOS-RAM (Random Access Memory) have also been reported with minimum features of 2 μm (Iizuka, et. al., 1980), again using R.I.E. as an integral part of the process.

It would appear that most production facilities have not incorporated device geometries at the sub-micron level. In discussions the author has had with personnel from

industry, the current minimum feature sizes employed in routine fabrication are: 3 μm (UK) and 2 μm (USA).

5.3 LITHOGRAPHY

The etching process is only capable of transferring patterns defined in a resist on the target surface. The lithographic processes by which these patterns are transferred to the resist are becoming increasingly sophisticated as linewidths are reduced.

The resolution of optical lithography, by which pattern transfer to photoresist is accomplished with a glass mask and a U.V. source is limited by mechanical alignment, incorrect registration of the mask and wafer, and the wavelength of the light. "State of the art" optical exposure systems currently producing volume-quantities of devices are defining minimum features of 2 μm (Cobilt, 1981). The use of shorter wavelengths (deep U.V., 2000-2500 Å) and alternative methods of printing on the wafer will probably extend this limit to about 1 μm (Coker, 1980). The definition of features smaller than this will require the use of x-ray or electron beam techniques.

One of the major restrictions on the use of electron beam direct-write systems has been the low wafer throughput. Equipment which has recently been described, however, can expose up to 20, 3 inch wafers per hour at 1 μm feature sizes (Moore, et. al., 1981). To deal with VLSI requirements well into the foreseeable future it may be that electron-beam projection equipment such as that recently described (Ward, 1981) with an ultimate

resolution of 0.2 μm and a throughput potential of up to 25 wafers per hour will be used.

5.4 LINEWIDTH CONTROL

In addition to the design criteria dictated by specified device performance, electronic engineers responsible for a typical wet etch process are usually required to incorporate "over etch factors" (compensation for lateral etching). For a wet etch stage, in which the removal of material is purely isotropic (neglecting some specially formulated reagents for the preferential etching of certain crystal planes), the resulting width of channel or line is dependent on the etch depth, as shown in Fig. 5.1 and Fig. 5.2. Calculated values for the ratio of etched width to opening width (i.e. the width defined in the resist) are shown plotted against etch depth for lines and channels, for the purely isotropic condition, in Fig. 5.3 and Fig. 5.4 respectively. Referring to Fig. 5.3 and taking a practical example of a 5 μm wide line defined in resist, removal of a 1.0 μm thick layer (of SiO_2, for example) will result in a minimum width of the apex of 3.0 μm. If this proportional reduction in linewidth were to be considered acceptable, the maximum depth of etching for 1 μm wide lines would be 0.2 μm and for 0.5 μm wide lines this would be reduced to 0.1 μm. For devices made on this basis with a linear reduction of $^1/10$ on all dimensions, the SiO_2 film would be 0.1 μm thick and the resulting linewidth would be 0.3 μm at the apex.

Considering the effect of isotropic etching on channel width, reference to Fig. 5.4 shows that etching of a 1.0 μm thick (e.g. SiO_2) film with an initial resist opening width of 5 μm will result in a maximum etched width of 7 μm. A resist opening of 0.5 μm would expand to 0.7 μm if the underlying film were to be etched to a depth of 0.1 μm.

Design rule tolerances assume a greater proportion of the finished feature size as linewidths are scaled down. Ideally, all etched features should be of the same dimensions as shown on the design and layout artwork, as depicted in Fig. 5.5. Disregarding the question of pattern transfer to the resist layer, which has been discussed separately, linewidth modification may occur at the etching stage as a result of

(i) Resist pattern deformation (shrinkage, loss of adhesion, distortion)

(ii) Isotropic etching

The suitability of an etching process for defining linewidths of 1 μm and less has been assessed in this study according to the dimensional stability of the resist and the resulting etched profile.

5.5 EXPERIMENTAL

High resolution test patterns, with minimum linewidths of 0.5 μm were defined in PMMA (polymethylmethacrylate) resist on SiO_2 using electron-beam direct-writing at the Science and Engineering Research Council's Rutherford Laboratory electron beam facility, for the use of the author.

As the wafers supplied to Rutherford Laboratory were of non-standard size, they could not be correctly clamped and registered on the wafer holder, as a result the pattern definition was imperfect and considerable variation in resist exposure occurred.

Profiles etched into SiO_2 using these patterns as resist against a "B21 CF_4 beam" have been shown in the literature (Goldspink and Revell, 1980). At positions on the pattern where the resist was thickest, vertical profiles were observed. At positions where the resist tapered due to electron beam dose variation, the etched profile sloped similarly, as the PMMA was preferentially removed from the thinner areas. The existence of a small quantity of redeposited debris, presumably SiO_2, was only observed on the unetched pattern adjacent to the 0.5 and 1.0 µm wide troughs. This effect, which has not been observed on any other sample etched with a "B21 CF_4 beam" may have been caused by sputtering with a trace of residual argon in the gas supply. Evidence of the artefact-free vertical wall profile in SiO_2 after etching with a "B21 CF_4 beam" is seen in Fig. 5.6 Fig. 5.7 shows a larger portion of the same sample, indicating that accurate pattern replication from the resist layer has occurred without measurable linewidth loss.

The B93 source, injected with CHF_3, has been used to transfer the electron-beam generated pattern into SiO_2, as shown in Fig. 5.8. This scanning electron micrograph is not sufficiently clear to permit a detailed evaluation of the etched profiles, but the dimensions of the etched

troughs are the same as those in the unetched resist layer of another specimen. The "ragged" appearance of the bars between the 1 μm troughs has been faithfully reproduced from the PMMA, and is due to the scanning spot of the electron beam lithography unit.

5.6 SUMMARY

Etched profiles defined in Si and SiO_2 using beams produced by injecting CF_4 or CHF_3 into the B21 and B93 sources have been shown to accurately reproduce the resist pattern. For the delineation of sub-micron features, pattern transfer into the resist layer is probably the most critical stage in the lithographic process. Provided near-vertical resist features of thickness adequate for the proposed etch depth are used, R.I.B.E. with a Saddle Field source is capable of accurate pattern transfer of dimensions less than one micron.

FIG.5.1 Linewidth loss due to isotropic etching

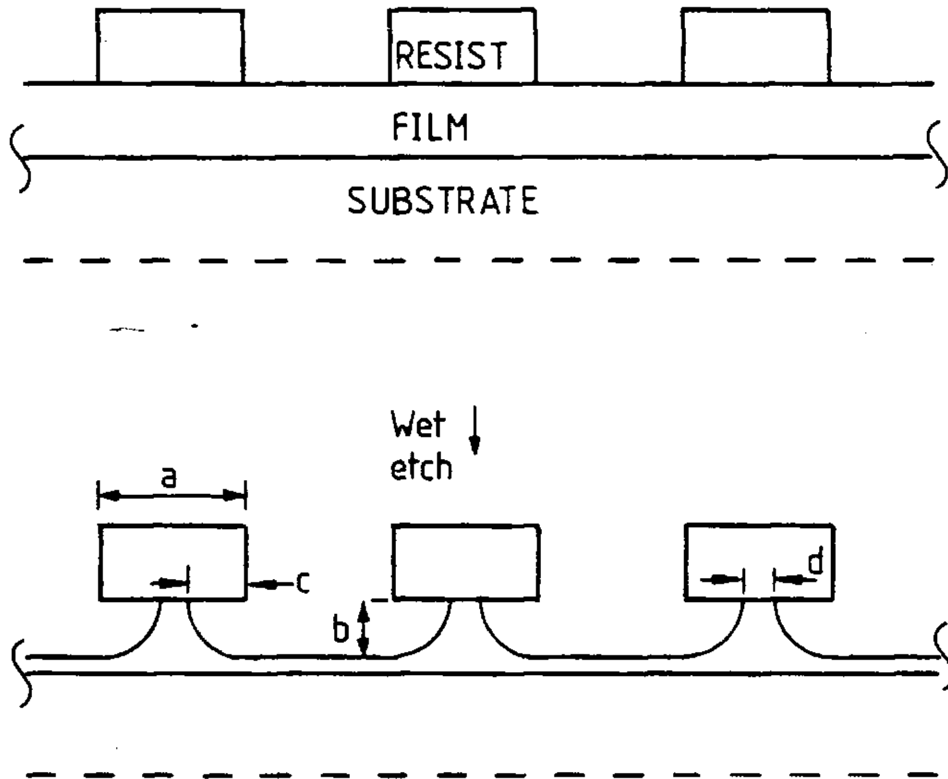

Assuming: No erosion, shrinkage or reduced adhesion of resist.

For clarity some target material is shown remaining after etching.

Relationship between mask width and etched line width:

For mask width a

Undercut c = etch depth b

Resultant line width at apex, $d = a - 2c$

$= a - 2b$

FIG.5.2 Increase of channel width due to isotropic etching

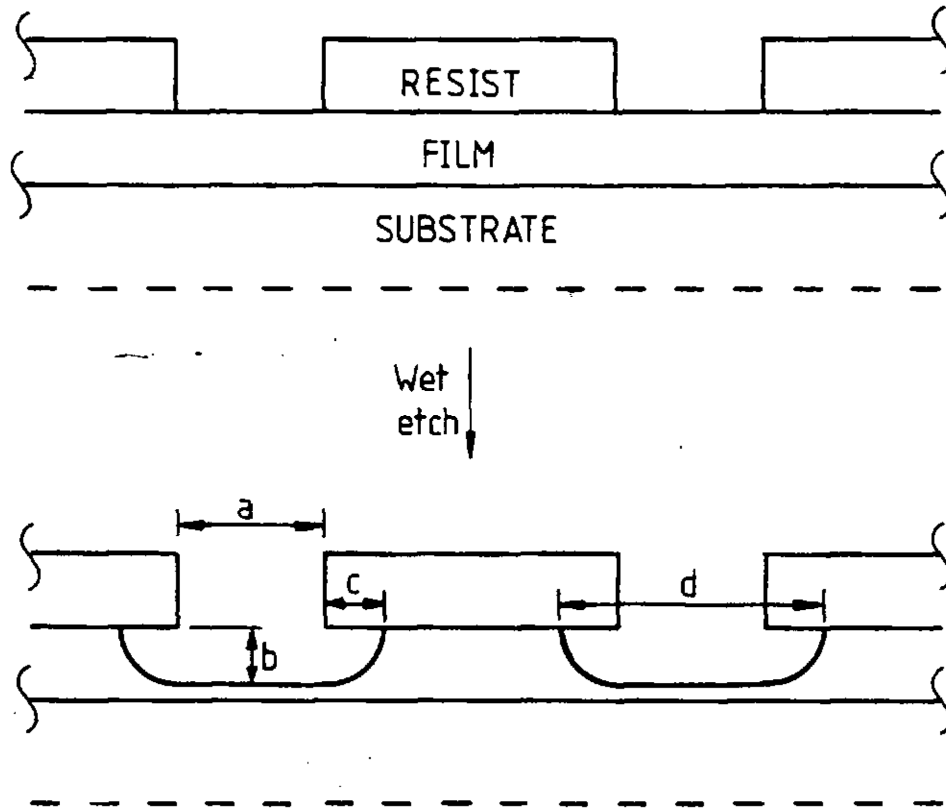

Assumptions as for Fig. 5.1.

For clarity some target material is shown remaining after etching.

Relationship between exposed areas and etched channel width:

For channel width a

Undercut c = etch depth b

Resultant channel width at apex, $d = a + 2c$

$= a + 2b$

Profile curvature given by radius c at point of intersection of resist with original surface.

FIG.5.3

Isotropic Line Etching.
Fractional line-width loss as a function of etched depth for various resist pattern widths

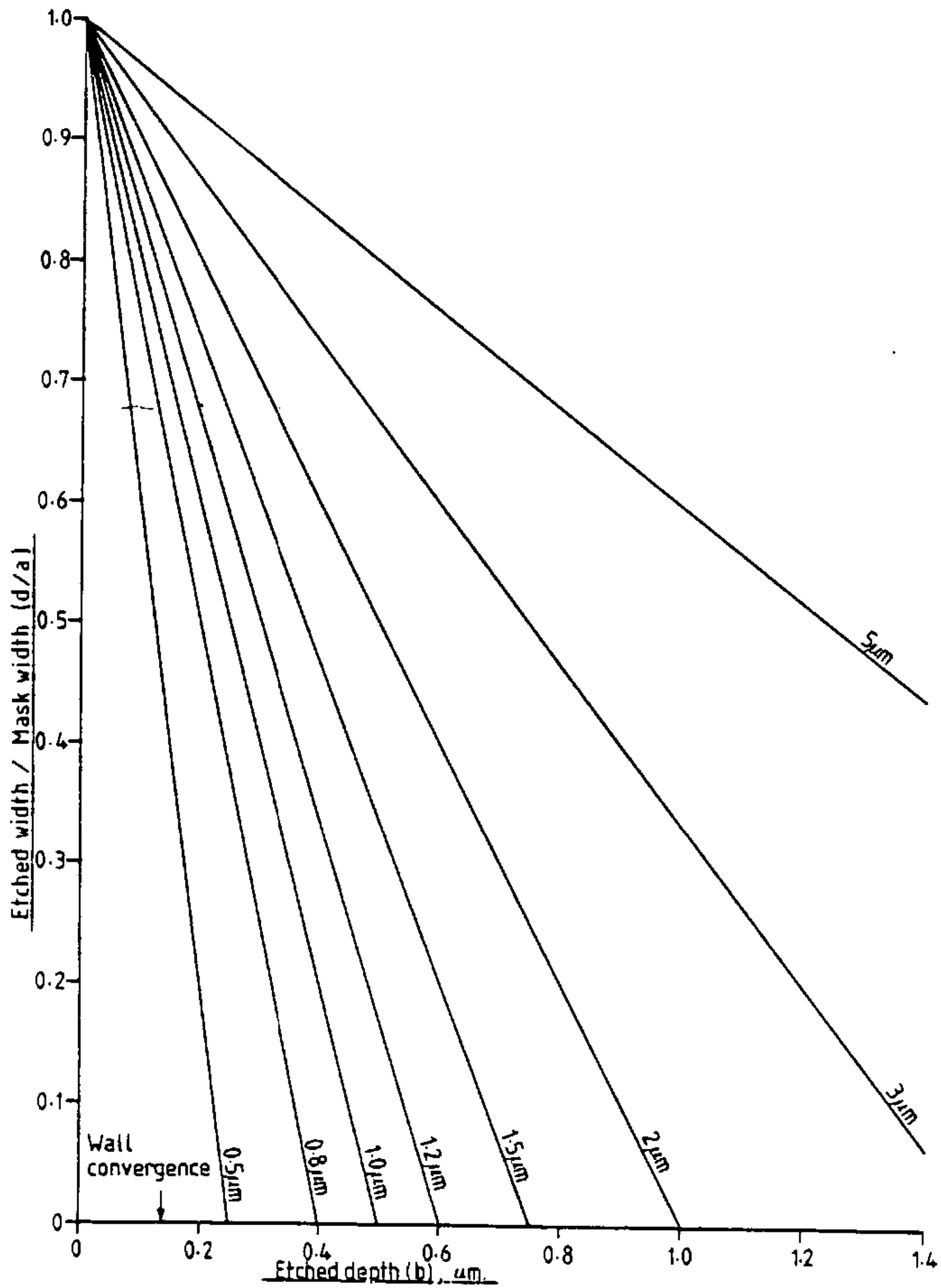

FIG.5.4 Isotropic Channel Etching. Fractional channel-width increase as a function of etched depth for various dimensions of resist opening

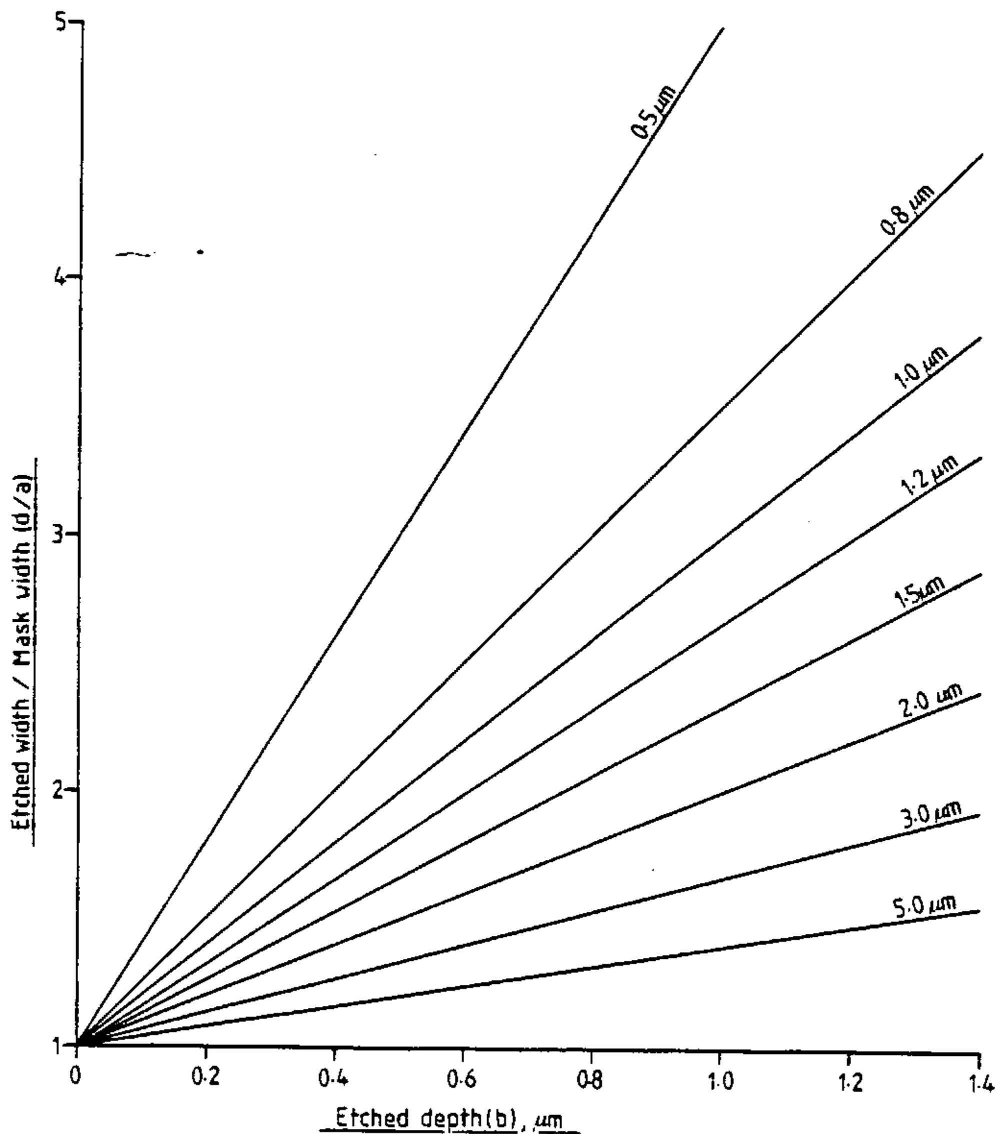

FIG.5.5 Dimensionally ideal case for the accurate replication of a resist pattern.

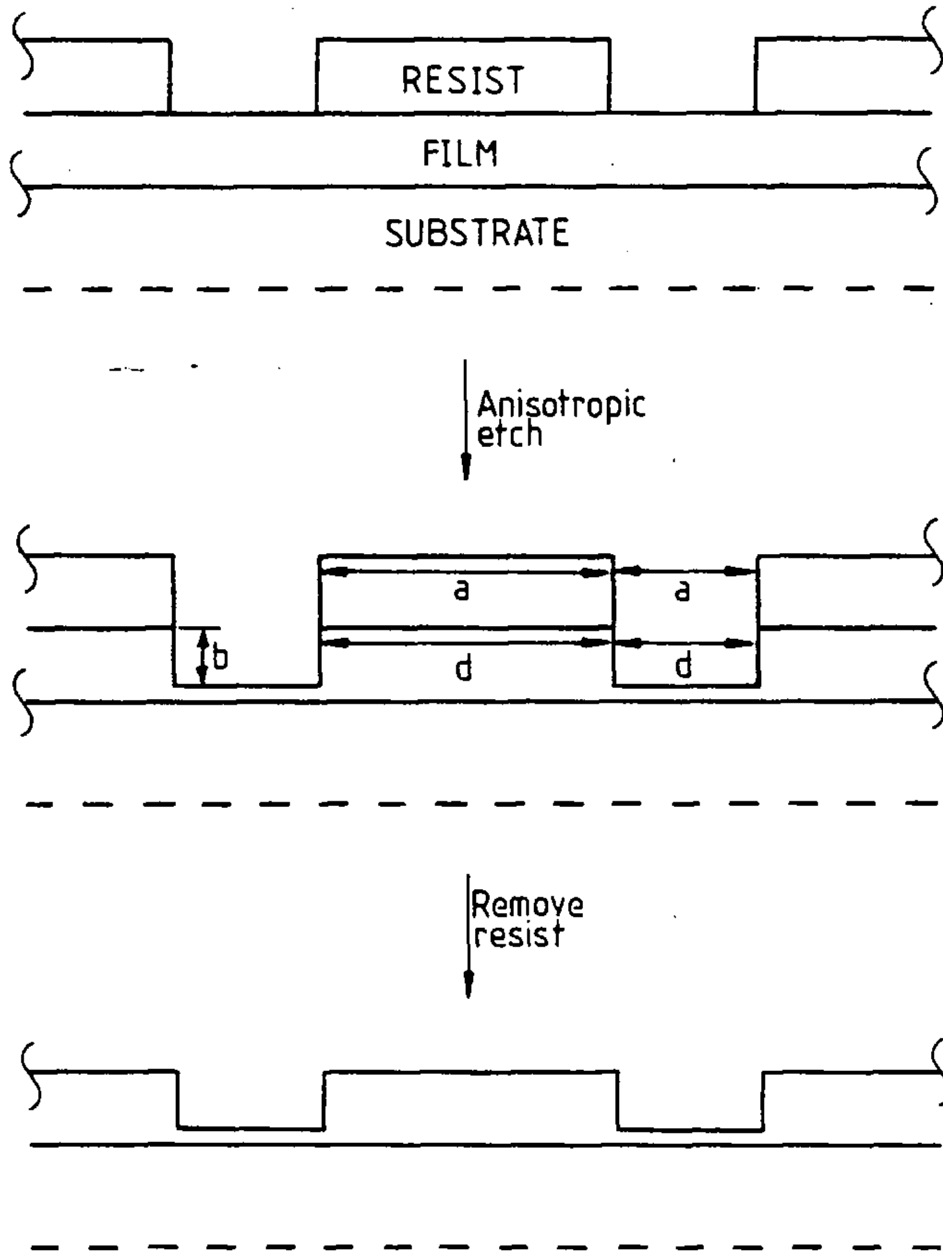

Assumes that the resist dimensions are unchanged as a consequence of the etching proceedure. Residual film is shown for clarity.

Line or channel width d = resist or opening width a

FIG.5.6 Vertical etched profile in SiO_2 produced with a B21-CF_4 beam.

Target on and normal to source axis, cooled, static.
Photoresist removed after etching.
V_A: .5 kV, I_D: 2 mA, C.A.T.T.: 75 mm, 300 minutes.

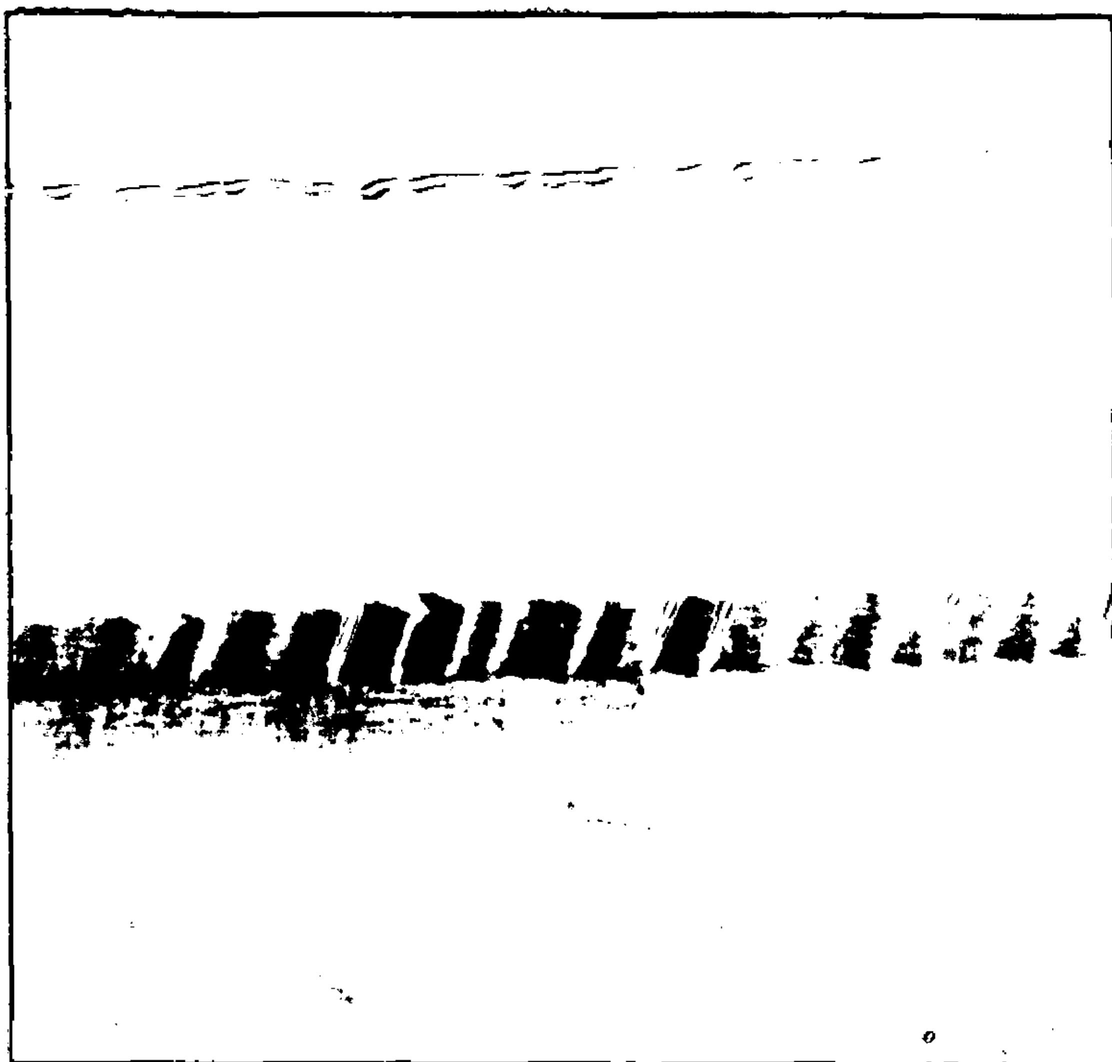

1μm

FIG.5.7 Linewidth control achieved by etching SiO_2 with a B21-CF_4 beam.

Another view of the specimen shown in Fig. 5.6, etching conditions as described before.

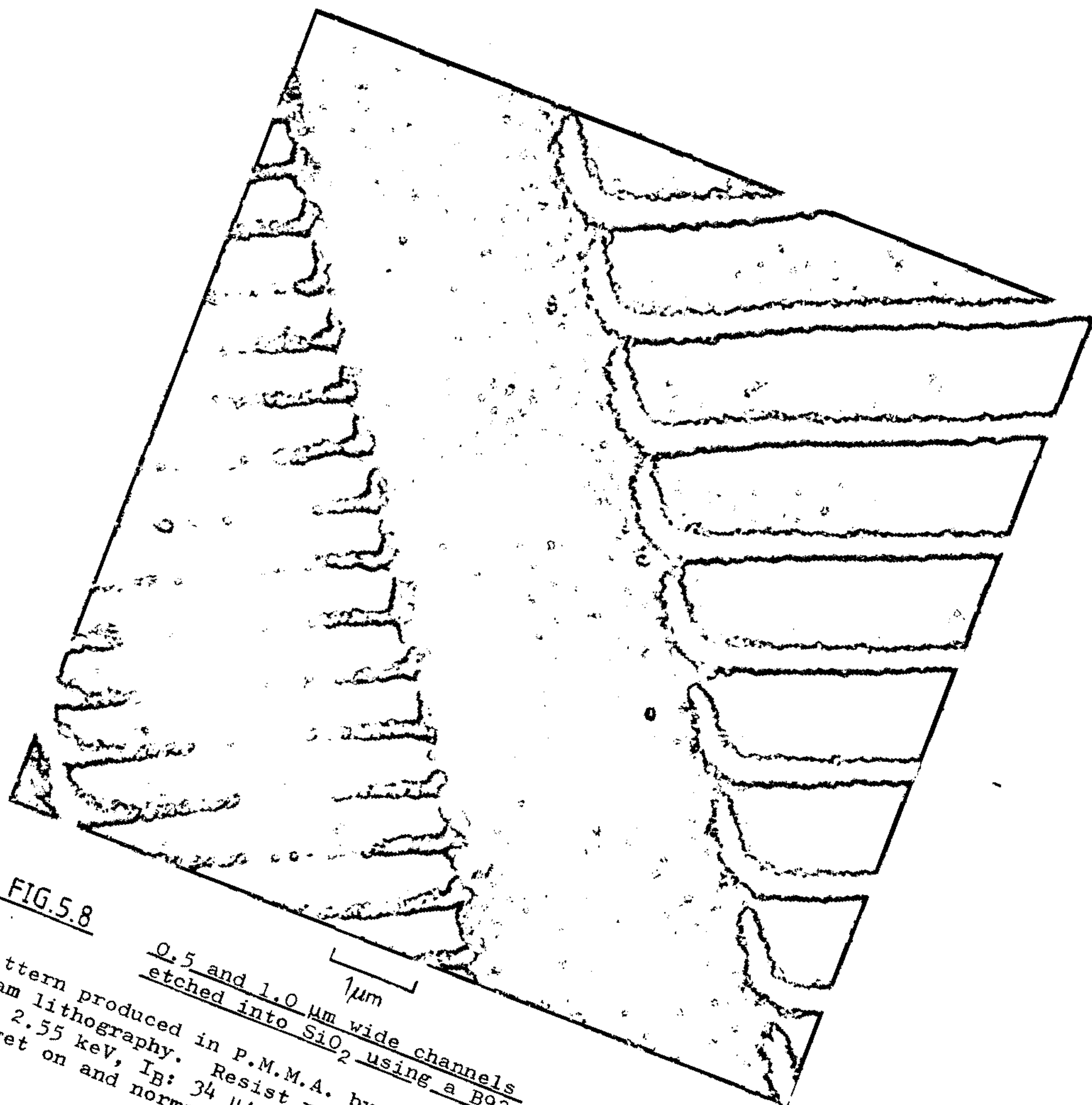

FIG.5.8

0.5 and 1.0 µm wide channels etched into SiO_2 using a B93-CHF_3 beam.

Pattern produced in P.M.M.A. by direct-write electron beam lithography. Resist removed after etching.
V_B: 2.55 keV, I_B: 34 µA cm^{-2}, C.A.T.T.: 150 mm.
Target on and normal to source axis, cooled, static.

6.0 RADIATION DAMAGE STUDIES

6.1 Introduction

The objectives of this study were as follows:

(a) To evaluate the change in electrical characteristics of M.O.S. capacitors after etching with ion beams produced by two Saddle-Field Sources.

(b) Using the known characteristics of MOSFET devices, to investigate the characteristics of the ion beam.

Using the procedures described in Section 6.5 M.O.S. capacitors have been fabricated. Measurements of the C-V characteristics (using apparatus described in Section 6.5.4) of these devices have provided information on:

(a) the etching characteristics of beams produced by two sources (B21 and B92)

(b) the effects of energetic particle bombardment on the electrical characteristics of the devices.

(c) the relative abundance of ions and neutral species in the beams produced by the two sources.

6.2 Theory of the M.O.S. Capacitor

The construction of a typical M.O.S. capacitor is shown diagrammatically in Fig.6.1. The silicon substrate doping may be p or n-type, but the latter was used exclusively in this work. The thickness of the oxide film, typically in the range 100 to 2000 Å (Zaininger & Heiman, 1970a), is usually steam grown to provide a convenient value of capacitance for the metal contact area to be deposited, according to the relationship:

$$C = \frac{Q}{V} = \frac{A\varepsilon_0}{d} \qquad (1)$$

where: C is the capacitance in farads

A is the metal electrode area, cm^2

d is the oxide thickness, cm

ε_o is the relative permittivity of the oxide, taken as $8.86 \times 10^{-14} F\ cm^{-1}$

Islands of SiO_2 may be etched down to the substrate, as shown in Fig. 6.1. The gate electrode (usually aluminium) is deposited on to the oxide and then etched to leave pads of known area. Ohmic contact to the substrate is accomplished with silver dag, a probe or a vacuum chuck, and must be carried out immediately after removal of oxide from the affected area using buffered HF.

Fig.6.1 shows the band structure for a capacitor at room temperature, with no applied bias voltage ($V_G = 0$). The Si conductor band is represented by E_C, and it can be seen that the Fermi level (E_F) is at a constant height through the three materials. There are four important and distinct conditions for the capacitor, depending upon the polarity and magnitude of the bias voltage. Figure 6.2 shows the band structure for these conditions, which are:

6.2.1 Accumulation $V_G > 0$

Majority carriers (electrons in the case of n-type Si) are attracted to, and accumulate at the Si-SiO_2 interface. The surface potential, V_S is greater than zero, and describes the degree of bending of the semiconductor conduction band at the surface of the Si.

6.2.2 Depletion $V_G < 0$ (small negative bias)

Electrons are repelled, the resultant space-charge region is occupied by uncompensated ionised donors.

In this condition $V_S < 0$.

6.2.3 Inversion $V_G << 0$

Minority carriers (holes in the case of n-type Si) are attracted to the $Si-SiO_2$ interface.

$$V_S = V_{i.d} + V_h$$

$V_{i.d}$ = charge due to ionised donors

V_h = charge due to accumulated holes

6.2.4 Flat Band Condition $V_S = 0$

When there is no bending of the conduction band, the flat-band voltage (V_{FB}) is defined as being equal to the gate bias (V_G). The capacitance at this point is defined as the Flat Band Capacitance, C_{FB}. The magnitude of V_{FB} is dependent upon the difference in work function (Φ) between the metal contact and the semiconductor, and on the charge due to surface states, Q_{SS}:

$$\frac{Q}{q} ss = (-V_{FB} + \Phi_{MS}) \frac{C_{ox}}{q} \qquad (2)$$

where q = the electronic charge, 1.6×10^{-19} coulomb

C_{ox} = oxide capacitance at accumulation, farads

The value of Φ_{MS} may be found from:

$$\Phi_{MS} = \Phi_{M-OX} - \Phi_{S-OX} - \frac{Eg}{2q} - \Phi_F \qquad (3)$$

where Φ_{M-OX} the metal-oxide work function, 4.3 V for Al on SiO_2

Φ_{S-OX} the silicon-oxide work function, 4.35 V

$\frac{Eg}{q}$ the silicon band-gap voltage, 1.12 V

Φ_F the Fermi level (or background potential),

-0.33 V for n-type Si at a donor concentration of 10^{15} atoms cm^{-3}

Φ_{MS} is negative for n and p-type Si and is logarithmically dependent on the doping density (Burger and Donovan, 1967).

$$\Phi_{MS} = 0.062 \log N_D - 1.228 \quad (4)$$

where N_D is the donor density in n-type Si.

C-V curves produced by evaluation of theoretical data have been published (Goetzberger, 1966). These graphs were plotted after setting Φ_{MS} and Q_{SS} to zero, thus simulating the ideal M.O.S. capacitor.

In this work the value for C_{FB} is taken as

$$C_{FB} = 0.95 \, C_{ox} \quad (5)$$

where $C_{ox} = C_{max}$, and is derived from the plot of C against V for each device. The flat band voltage for n-type Si is, therefore:

$$V_{FB} = V_{(C_{FB})} \quad (6)$$

as reported (Zaininger and Heiman,1970b and Cullen, 1978).

This method of evaluating the results of C-V curves has been reported (Zaininger and Heiman, 1970,b;Deal, 1974) to be in good agreement with analysis performed by numerical techniques, and is used extensively to provide comparative data on large numbers of specimens (Hosaka, et al., 1981; Burggraaf, 1980).

One critical characteristic of all M.O.S. devices is the turn-on, or threshold voltage (V_{TH}), the point at which the surface resistivity equals the bulk

resistivity when the device is in the inversion mode. Later sections will describe the various charges responsible for modification of the threshold voltage. V_{FB} is, therefore, a convenient estimation of device quality and is related to V_{TH} by:

$$V_{TH} = V_{FB} + 2\Phi_F - \frac{Q_B}{C_{ox}} \qquad (7)$$

where Q_B = the bulk charge, 1.4×10^{-8} coulomb cm^{-2} for $N_D = 10^{15}$ donors cm^{-3}

Threshold voltages may be positive or negative, a high value would be in the region of 3 to 4 volts, whilst 1 to 2 volts is considered low (Cannon, et.al.1974).

6.3 The Si-SiO_2 Interface

Semiconductor grade silicon is now manufactured with an acceptably low intrinsic impurity concentration (impurity concentration $\ll$ 1 in 10^8 atoms) (Hall, 1978), known doping level and controlled dopant profile. The formation of a silicon dioxide layer on the substrate silicon is an essential stage in M.O.S. fabrication and the characteristics of the interface between the two materials significantly influences the device performance. The interface characteristics are dependent upon four types of charge associated with the oxidised silicon structure (Deal, 1974), these are:

6.3.1 Q_{ss}: Fixed Surface State or Fixed Charge

This is always positive, located within $\simeq 200$Å of the interface it confers n-type behaviour on the oxide. This charge cannot be removed, does not migrate with applied field and its magnitude is dependent upon the method of oxidation and annealing. Q_{ss} varies with

crystal orientation, being greatest with [111] > [110] > [100] (Grove, 1967). The value for $\frac{Q_{ss}}{q}$ usually lies in the range 1 to 10 x 10^{11} cm^{-2} (i.e. Q_{ss} = 1.6 x 10^{-8} to 1.6 x 10^{-7} coulomb cm^{-2})

6.3.2 Q_o: Mobile Ionic Charge

The charge due to positive ion contaminants introduced into the oxide during processing; sodium (Na^+) and potassium (K^+) are the most common. Mobility of these ions increases with increasing temperature and applied field. Methods adopted to reduce the contamination include: replacement of quartz furnace liners with those made of alumina, the addition of HCl to water bubblers and reduction in operator handling. Phosphosilicate glass acts as a getter for these ions at $\simeq 900^oC$.

6.3.3 N_{st}: Fast Surface States

Similar in some respects to Q_{ss}, to which it is proportional initially. The magnitude of this charge is dependent on crystal orientation, annealing in hydrogen above $\simeq 300^oC$ reduces the charge density. Changes in the silicon surface potential causes variation in N_{st} as holes or electrons become trapped at various energy levels.

6.3.4 N_{ot}: Traps Ionised by Radiation

Ionising radiation (i.e. x-rays, electrons, neutrons) causes trapping of holes associated with N_{ot} and also N_{st}. The measured charge is dependent upon the field across the oxide during radiation, the particle energy, its ionisation potential and the total dose received. Annealing at 350-450^oC in an inert ambient is reported (McCaughan and Kushner, 1974) to

significantly reduce, or even eliminate N_{ot} and N_{st}.

6.3.5 Total Charge

It is not necessary to consider the effects of all four charges in the experimental work to be described. The fixed charge, Q_{ss} is present as a result of crystal orientation and oxidation conditions; provided these remain constant for any experiment and a statistically meaningful number of control samples are included, specimens within the group may be quantitatively compared. Q_{SS}, or the density of states $\frac{Q_{ss}}{q}$ has been evaluated from the expression quoted previously (2). The presence of charge due to mobile contaminant (Q_o) is determined by processing stages before and during the oxidation of the silicon surface. In addition, contaminant species such as Na^+ present at the air -SiO_2 interface will give rise to charge Q_o upon bombardment by energetic particles (charged and uncharged), as described in the literature (Kushner, et. al. 1974). It will be shown later that an analysis of the ionic density results provides information on the nature of the bombarding species. The density of charges Q_o due to process-induced contamination may be eliminated with the use of data from control specimens, provided all samples have been treated identically. The inadvertent addition of Na^+ for example, to the SiO_2 surface, may be a significant source of errors in an experiment consisting of a small number of wafers. The assumption has been made that specimens subjected to etching by an ion beam were not exposed to mobile contaminants at a concentration likely to place undue bias on the results. This assumption is shown to be

substantiated (see section 6.6.4). A detailed analysis of the data (see section 6.6.4) shows that the effects caused by such contamination can be separated from the variable under investigation.

6.4 Radiation Effects

Considerable data are available in the published literature quantifying the degradation of the SiO_2:Si interface as a function of radiation species, energy and dose. The parameters which have a bearing on this study are shown in Table 11. The main points which emerge are:

(i) The electrical characteristics of the SiO_2:Si interface are modified by exposure to radiation over a wide range of energies (U.V. photon energy to 20 keV electrons and x-rays at 1.2×10^7 eV)

(ii) Incident radiation degrades the interface by modification of material properties (SiO_2, Si or the interface) - producing dielectric breakdown and an increase in charged states (interface states, for example)

(iii) Degradation caused by a modification of the device characteristics incorporated as a result of the processing. In particular, the mobilisation of ionic contaminant (for example Na^+) incorporated in the oxide or at the SiO_2:Si interface.

TABLE 11

RADIATION DAMAGE IN M.O.S. DEVICES, CAUSES AND EFFECTS

Nature of Radiation	Energy Range (eV)	Charge or Damage Produced	Effect of Annealing
Positive Ions			
Ar^+ (1)	50 - 1400	Dielectric breakdown at dose $\geq 10^{14}$ ions cm^{-2}	No improvement
I.P. $\geq$ 11 eV (2)	50 - 2000 Energy dependent	Mobilisation of Na^+ - diffusion through SiO_2	900°C inert ambient, significant improvement
Induced	U.V. Photons ($\simeq$8 eV)	Interface states produced by ion-surface collision.	Removed at $\simeq$400°C
Ar^+, N_2^+	50 - 2000	Increase in fixed charge. Poor interface degraded.	No data available
Ar^+ (3)	$\geq$150 eV	Implantation - diffusion of trapped gas-metal lifts	Heat treat bare oxide, improvement at $\simeq$400°C
Atoms			
N_2^o, Ar^o (4)	200 - 2000 Small energy dependence	Interface states. Small increase in fixed charge. Significantly lower charge density than with ion of same energy at same dose	Complete removal in inert ambient, 400°C, 30 min
X-Rays (2)	$\simeq 1.2 \times 10^7$	Similar degradation to that observed with atoms	500° removes most damage
Photons (4)	$\geq$8.8, mainly U.V. wavelengths	Interface degradation Transport of holes across SiO_2 film	500° removes most charge
Electrons (2)	100 - 5000	Increase in fixed charge and interface states. Dielectric degradation.	500° removes most charge Partial recovery.
	5000 - 20,000	Interface charge and interface state increase.	Improvement after anneal at 400°C
	20,000	Na^+ mobilisation	Improvement at $\simeq$900°C
Negative Ions	Little experimental data available	Suggested (2) that dielectric breakdown (as for electrons) will occur, and increase in interface states as for positive ions and atoms. No mobilisation of Na^+ in SiO_2	Predicted that most damage should be removable at 500°C (2)
O^- (5)			
Pulsed Laser (6)	CO_2 laser, 9.23 μm 0.4 J/pulse (45 nsec) [middle infra-red region $\simeq$ 0.134 eV]	Claimed as radiation-damage free process No data on charges produced. Energy level should be low enough to avoid damage in majority of structures	No data available Annealing may not be necessary

References:

(1) McCaughan & Murphy (1973)
(2) McCaughan & Kushner (1974)
(3) Koch, et. al. (1974)
(4) McCaughan, et. al. (1980)
(5) Hughes & Baxter (1972)
(6) Steinfeld, et. al. (1980)

6.5 Experimental

Three experiments were carried out, of which complete data from one will be presented.

6.5.1 Preparation and Oxidation of Wafers

20, 50 mm diameter "Topsil" silicon wafers were used. The crystal orientation was [111], thickness 318 ± 25 μm and the resistivity was 9-15 Ωcm, n-type ($N_D = 5 \times 10^{14}$ cm^{-3}). The wafers were cleaned and oxidised according to the current M.O.S. fabrication schedule (see Appendix I). The set was divided into 5 groups of 4 wafers as follows:

A: Etching of oxide with B21 argon beam

B: Etching of oxide with B21 CF_4 beam

C: Etching of oxide with B92 argon beam, 20 minutes

D: Etching of oxide with B92 argon beam, 30 minutes

E: Control group, oxide not etched

6.5.2 Ion Beam Etching of SiO_2

The thickness of oxide grown on these wafers was estimated to be approximately 1000 Å. The gate electrode pattern consisted of an array of squares covering the range 1.6 to 6.9×10^{-3} cm^2, and so to produce capacitors within the range of the capacitance bridge the etching stage was adjusted to remove no more than $\simeq 500$ Å of oxide.

Etching Using the B21 Source

The B21 source was positioned with its axis perpendicular to the target plane. Wafers were etched whilst stationary and bonded to a water cooled platten with thermally conductive grease. The vacuum system was pumped to a base pressure of 2×10^{-5} torr before each

experiment, the chevron baffle was maintained at liquid nitrogen temperature ($77^{o}K$) throughout. Venting to atmospheric pressure was accomplished between runs by backfilling with oxygen-free nitrogen. The etchant gases were passed through molecular sieve (dessicated at $200^{o}C$ for 6 hours with flowing nitrogen) followed by a 2 µm sinter-filter to remove gross particulates.

Etching Using the B92 Source

The B92 was mounted, as was the B21, with its axis normal to the target plane. One set of four wafers was etched simultaneously, in good thermal contact with the target holder, which was rotating at 4 r.p.m. The vacuum system was pumped to a base pressure of 2×10^{-5} torr before each experiment and the chevron baffle was cooled with running mains water ($\simeq 283^{o}K$). The chamber was vented using atmospheric air. The etchant gas was supplied to the source without filtration.

The experimental conditions for all ion beam etching experiments are summarised in Table 12.

6.5.3 Metallisation and Electrode Definition

All 20 wafers were coated with high purity aluminium to a thickness of approximately 1 µm in a commercial M.O.S. processing facility.

Kodak Microneg 747 (negative working) photoresist was spun on to each wafer and baked as described in Appendix I. Using the mask previously described (section 6.5.2) the photoresist was exposed on a mask aligner. After development and baking the aluminium film was etched in "Isoform" at $45^{o}C$, with constant gentle agitation. Photoresist was removed from

TABLE 12

EXPERIMENTAL CONDITIONS

ION BEAM ETCHING OF OXIDE FILMS FOR M.O.S. CAPACITORS

Group	Wafer Numbers	Ion Source	Etchant Gas	Cathode Aperture to Target Distance mm	Anode Potential V_A kV	Discharge Current I_D mA	Duration of Etching min	Chamber Pressure with Source Operating torr
A	1,2,3,4	B21	Ar	75	6	2.5	20	5×10^{-4}
B	5,6	B21	CF_4*	75	5	3	20	1×10^{-5}
	7,8	B21	CF_4*	75	5	3	5	1×10^{-5}
C	9,10,11,12	B92	Ar	253	3	150	20	4×10^{-4}
D	13,14,15,16	B92	Ar	253	3	150	30	4×10^{-4}
E	17,18,19,20	CONTROL GROUP, NOT ETCHED						

* Etch rate data (Table 14) indicate a gradual blending of CF_4 + Ar

all wafers using "J100" stripper, followed by acetone quenching and rinsing in deionised water.

6.5.4 C-V Measurements

The rear surface of each wafer was swabbed with buffered HF and thoroughly rinsed immediately prior to electrical testing. Ohmic contact to the substrate was effected by means of a vacuum chuck.

Capacitance-voltage (C-V) characteristics were measured at five points on each wafer (centre, N, S, E, W), under dark conditions. Apparatus similar to that used for these measurements has been described in the literature (Burggraaf, 1980). The measurement frequency was 1.0 MHz, the capacitance values were displayed on a Boonton Bridge and simultaneously recorded as a function of the D.C. bias using an arbitrary scale on the Y-axis of an X-Y recorder. The d.c. bias was controlled by a ramp generator over the range + 9 V to - 9 V (maximum field strength $\pm 9 \times 10^5$ V cm^{-1} for 1000 Å thick film). Two curves are shown, superimposed, in Fig. 6.3, in which a control wafer (unetched, not bombarded) is compared with wafer 16 which was subjected to a total dose of 1.4×10^{17} Ar $(\overset{+}{o})$ cm^{-2}.

6.6 RESULTS

The experimental results are shown in Tables 13 and 14. Wafer 2 was broken during metallisation, hence no data are available. To obtain these data the following procedure was adopted:

6.6.1 Control Wafers

$$V_{FC} = V_{FB} - \Phi_{MS} \quad (8)$$

TABLE 13

EXPERIMENTAL RESULTS

ION BEAM ETCHING OF SiO_2 FOR M.O.S. CAPACITORS

Wafer Number	Etch Rate Å min^{-1}		Particle Energy V_B keV (1)	Mean beam "current" density μA cm^{-2}	Mean total dose (Ar or CF_x) (5) cm^{-2}
	min.	max.			
1 2 3 4	- 3.35 1.35 3.45	- 16.6 13.7 14.85	- 5.1(Ar) 5.1 5.1	15.6 (2)	1.12×10^{17}
5 6	2.4 5	16.25 18.25	4.25(CF_4) 4.25	15.6 (2)	1.12×10^{17}
7 8	8.2 8.8	26.6 32	4.25(CF_4) 4.25	15.6 (2)	2.8×10^{16}
9 10 (3) 11 12	6.95 6.95 4.9 7.45	(21.55) 11.35 12.65 11.6	2.55 2.55 2.55 2.55	13 (4)	9.4×10^{16}
13 14 (3) 15 16	12.8 12.8 13.3 13.3	13.8 13.8 14.5 14.8	2.55 2.55 2.55 2.55	13 (4)	1.4×10^{17}
17 18 19 20	Mean oxide thickness (from C_{ox} measurements) = 1033 Å				

Notes

(1) Calculated as $V_B = 0.85\ V_A$. Assumes beam is isoenergetic.

(2) Beam "current" density values (for Ar) quoted by Ion-Tech Ltd (see Appendix IV).

(3) For comparison of etch rates for wafers 9-12 and 13-16, see text.

(4) Beam "current" density values based on data reported in Section 3.3. The B92 source produces a beam very similar to that of the B93.

(5) 1 μA cm^{-2} = 6×10^{12} cm^{-2} sec^{-1} particles.

TABLE 14

EXPERIMENTAL RESULTS

MODIFICATION OF FLATBAND CHARACTERISTIC, M.O.S. CAPACITORS

Wafer	Particle Energy (V_B)	Total Particle Dose	V_{FB} (negative) volts			Initial Density of States at Mid-Gap N_{SS} (control) $cm^{-2}eV \times 10^{11}$		Total Density of States at Mid-Gap $N_{SS}(tot)$ $cm^{-2}eV \times 10^{11}$		Radiation-induced Density of States at Mid-Gap, $N_{SS}(RI)$ $cm^{-2}eV \times 10^{11}$	
	keV	cm^{-2}	min.	max.	mean	min.	max.	min.	max.	min.	max.
1	—	—	—	—	—	—	—	—	—	—	—
2	5.1	1.12×10^{17}	0.8	1.1	0.98	2.57*		1.08	2.41	All ≈ N_{SS} (control)	
3	5.1		0.58	1.2	0.96			0.56	2.5		
4	5.1		0.84	1.16	1.01			1.16	1.72		
5	4.25	1.12×10^{17}	0.34	1.3	0.88	2.57		0.05	2.61	Max 0.88	
6	4.25		1.38	1.9	1.59			3.3	3.45	Min 0.04	
7	4.25	2.8×10^{16}	0.8	1.6	1.14	2.57		1.04	3.08	Max 0.51	
8	4.25		0.5	1.4	0.99			0.39	2.68	Min 0.11	
9	2.55	9.4×10^{16}	2.26	2.56	2.39	2.57		4.68	8.03	2.11	5.46
10	2.55		1.9	1.96	1.92			3.96	4.24	1.39	1.67
11	2.55		1.26	1.68	1.53			2.6	3.54	0.03	0.97
12	2.55		1.3	1.58	1.47			2.64	3.39	0.07	0.82
13	2.55	1.4×10^{17}	4.18	4.5	4.37	2.57		12.9	14.6	10.33	12.03
14	2.55		4.8	6.08	5.57			-	19.2	-	16.63
15	2.55		3.14	3.74	3.43			9.9	12.4	7.33	9.83
16	2.55		5.56	6.3	6.01			17.9	21.6	15.3	19.03
17	-	-	1.4	2.44	1.97	2.35	4.52	Mean 2.57		-	-
18	-	-	1.4	1.8	1.64	2.26	3.09			-	-
19	-	-	1.0	1.0	1.0	1.46	1.46			-	-
20	-	-	1.4	2.06	1.67	2.18	3.25			-	-

* Mean value for control samples $= 2.57 \times 10^{11}$ cm^{-2}

where V_{FC} = potential due to fixed charge (see below)

V_{FB} = potential at flat band capacitance

Φ_{MS} = metal-semiconductor work function

where from equation 4:

$$\Phi_{MS} = 0.062 \log 5 \times 10^{14} - 1.228 \qquad (9)$$

$$= -0.317 \text{ V}$$

The fixed charge is made up of:

Q_{ss}: fixed surface state charge

Q_{st}: fast surface state charge

Q_o : mobile ion charge

By defining Q_i as the initial charge on the control wafers as a result of crystal orientation, oxidation and other fabrication stages, then

$$Q_i = Q_{ss} + Q_{st} + Q_o$$

and so,

$$Q_i = \frac{C_{ox}}{A} \cdot V_{FC}$$

where Q_i is in coulombs

$\frac{C_{ox}}{A}$ is the capacitance at accumulation in units of F cm^{-2}

V_{FC} is the potential, from (8), (volts).

From this, the density of interface or surface states at mid-gap is found from:

$$N_{ss} = \frac{Q_i}{q}$$

where N_{ss} is in units of states cm^{-2} eV *

q is the electronic charge

Table 14 shows that the initial density of states (N_{ss}) varies over the range 1.46 to 4.52 x 10^{11} cm^{-2} eV. To evaluate the radiation induced charge density, the

mean value is used, 2.57 x 10^{11} cm^2 eV.

6.6.2 Ion Beam Etched Wafers

The measured flat band voltage consists of the fixed charge (V_{FC}) and the potential due to the radiation induced charge (V_{RI})

$$V_{RI} + V_{FC} = V_{FB} - \Phi_{MS}$$

V_{RI} is the potential due to:

Q_{RI} : the total radiation induced charge

Q_{ot} : traps ionised by radiation

Q_{st2}: increased surface state charge

Q_{02} : increased mobile ion charge

and so,

$$Q_{RI} = Q_{ot} + Q_{st2} + Q_{02}$$

from which:

$$Q_{RI} = \frac{C_{ox}}{A} \cdot \left[(V_{FB} - \Phi_{MS}) - V_{FC}\right]$$

The number density of radiation-induced states is best found from

$$N_{ss}\,(RI) = N_{ss}(\text{total}) - N_{ss}(\text{control})$$

and these data are listed in Table 14.

6.6.3 Etch Rates

The oxide film thickness was calculated from the measured value of C_{ox}, according to equation (1),

The etch rate data for samples 2-8, shown in Table 13 suggest that the B21 source was not operating on Ar (wafers 2-4), and then CF_4 (wafers 5-8), and it appears that the gas supply through the dessicant cartridge had not been adequately purged. The

progressive increase in etch rate between wafers 5 to 8 suggests the gradual blending of the two gases (CF_4 concentration increasing). The large variation in etch rates, especially across wafers 2-4 is to be expected with the limited beam area produced by the B21 source mounted close to the wafer.

The maximum etch rate result for wafer 9 appears to be spurious and has been disregarded in calculations of beam current density etc. The variation in etch rates across wafers 9-12 is much greater than that measured across wafers 13-16. This is attributed to the thermal stability of the B92 source (see section 3.2.4) as follows. Wafers 9-12 were etched first (as described in section 6.5.2) with the source cold at start-up. No shutter was available so the wafers were exposed to a beam that increased in energy over the first 10 minutes or so of the run, although some control was exercised by the adjustment of the plasma chamber gas pressure. Under these conditions, the current distribution within the beam would have been less uniform (Evans, 1981) than with the source operating at thermal equilibrium. The second batch to be etched, wafers 13-18, show a greater degree of etch depth uniformity, suggesting that the source was operating in a stable condition.

6.6.4 Modification of C-V Characteristics

Reference to Table 14 shows that, for samples irradiated by B21 beam, the total surface state density (N_{ss} is consistently lower than for the unirradiated, control wafers ($0.05 - 3.45 \times 10^{11}$ compared to $1.46 - 4.52 \times 10^{11}$ cm^{-2} eV). The consistency of the B21 beam

etched results indicate that any contamination which may have been introduced during bombardment was reasonably constant and of insignificant concentration. It is not possible to be certain in proposing mechanisms to explain some of these experimental results in view of the small sample size and limited number of variables investigated. The reduction calculated for the density of surface states (wafers 2, 3, 4) could be due to:

(i) The annealing effect of joule heating by the beam. For this to have occurred, the temperature at the $Si-SiO_2$ interface must have increased to about 400^oC (the temperature reported to be required for removing damage due to Ar^o bombardment, McCaughan et. al., 1980). The etching of Al films previously described (Section 4.5.2) has suggested that the surface temperature of these targets probably exceeded 400^oC when exposed to a B95-Ar beam.

(ii) The effect of water vapour (in the vacuum chamber) or water chemisorbed in the SiO_2. Energetic particle bombardment of water molecules could produce atomic hydrogen, which has been shown to be effective, both in the form of implanted H_2^+ and as annealing ambient, in the trapping of interface states (Belson and Wilson, 1979).

The results of the other B21-beam etched samples show no dependence on particle dose, again indicating that mechanisms as described above could be responsible. The effect of bombarding with CF_x species (wafers 7 and 8) has not produced any increase in $N_{ss}(RI)$ above the level

determined for an argon beam.

The increase in density of states for the two groups of B92-Ar beam bombarded wafers indicates a dose dependence similar to that shown for the published work of McCaughan et. al., (1980). These results cannot be compared directly, however, as the bombarding species were different. Comparing the results of B92-Ar beam bombarded specimens with those obtained using a 500 eV Ar^+ beam (McCaughan and Murphy, 1973), N_{ss} (RI) has been found to be 10 times lower for a total dose which was greater by a factor of 10^3, suggesting that a significant proportion of the total dose was not charged.

As further substantiation for the hypothesis that a large proportion of uncharged particles were present in both B21 and B93 Ar beams, no evidence has been found for dielectric breakdown in any of the 15 treated wafers. This is indicated by the shape of the C-V curve for one capacitor on wafer 16 (see Fig. 6.3), which shows no abnormality up to full bias voltage (+ 1.5×10^6 V cm^{-1} for the most heavily etched oxide). Published results indicate that for non-annealed samples, a dose of 10^{15} Ar^+ cm^{-2} (50-2800 eV range) caused dielectric breakdown at 2×10^6 V cm^{-1} in 90% of the samples tested (McCaughan and Murphy, 1973).

In the absence of bias-temperature stress (B.T.) and temperature-voltage-ramp (T-V-R) results, it is not possible to identify the individual charges contributing to the total Q_{RI}. Similarly, the effect of annealing on the bombarded specimens has not been studied.

6.7 Summary of Results

Using the high-frequency capacitance-voltage measurement technique, the combined surface-interface state density (N_{ss}) has been determined for control and irradiated SiO_2 films on n-type Si.

Wafers etched with the beam produced by the B21 source injected with argon or a mixture of argon and CF_4 showed two effects: no increase in N_{ss} above the control level and a marginal increase which was not dependent upon particle dose. Joule heating of the oxide film or trapping by hydrogen, produced by the dissociation of water molecules may have been responsible for the reduction in charged states.

Wafers exposed to an argon beam produced by the B92 source displayed an increase in N_{ss} which appears to correlate with increasing total dose. The dose dependence and absolute values of N_{ss}, when compared with the published literature strongly suggest a high degree of beam neutrality.

The C-V measurements also show that none of the bombarded oxide films suffered dielectric breakdown at fields of 9×10^5 V cm^{-1} and greater which again indicates that any charged component, if present, must be a small proportion of the total beam.

FIG.6.1 The M.O.S. Capacitor: Physical and Electrical Details.

SECTION

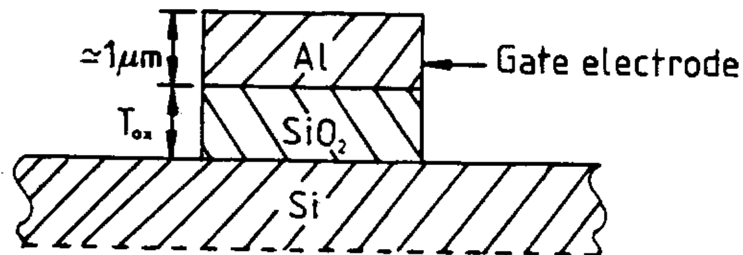

ELECTRICAL DETAIL

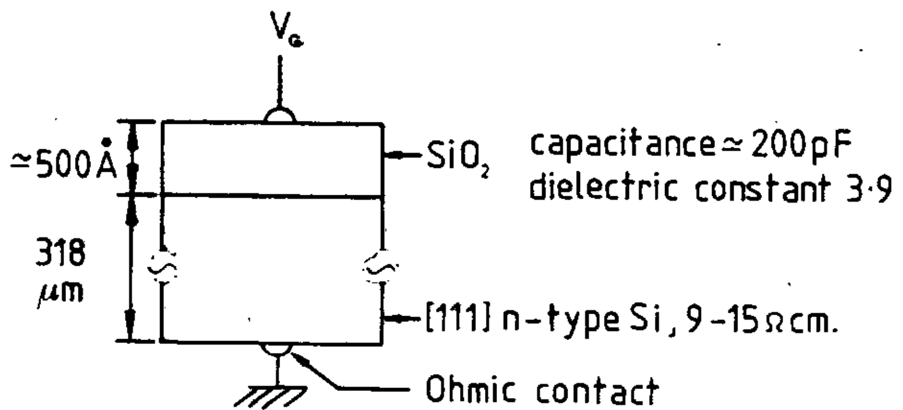

BAND STRUCTURE FOR $V_G = 0$

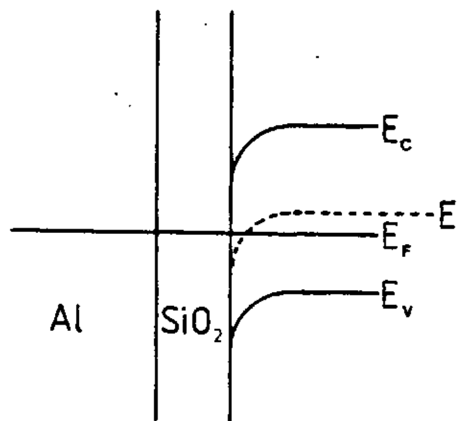

FIG.6.2 Band Structures for the M.O.S. Capacitor under various conditions of applied gate potential.

ACCUMULATION

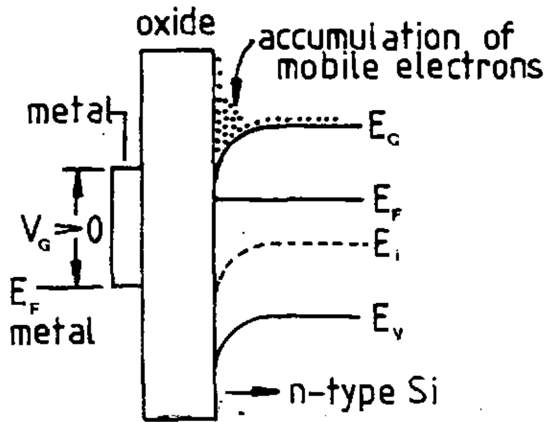

E_c : Conduction band
E_F : Fermi level
E_i : Intrinsic Fermi level
E_v : Valence band
V_G : Gate potential
V_s : Surface potential

DEPLETION

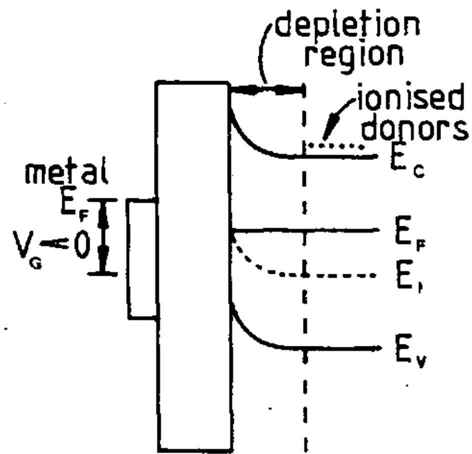

INVERSION

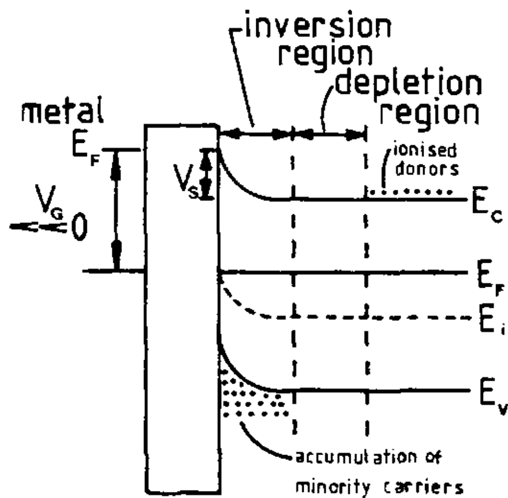

FLATBAND

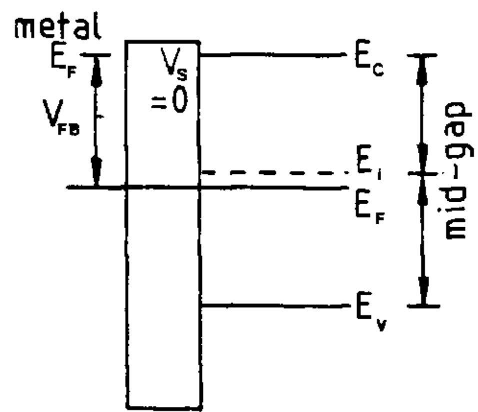

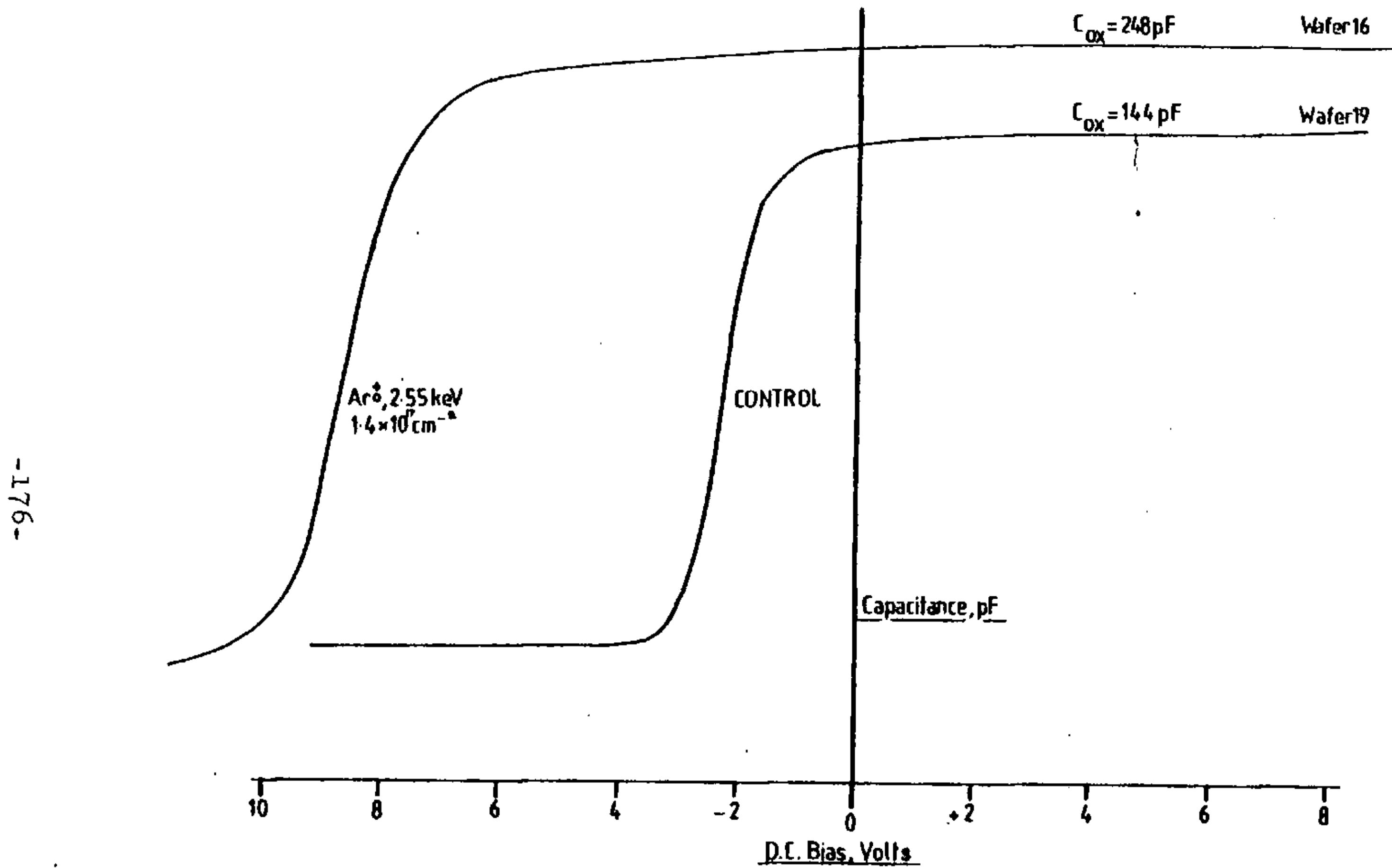

FIG. 6.3 1 MHz C-V characteristics for B93 argon beam bombarded and control (not bombarded) M.O.S. capacitors.

FIG.6.4 Radiation induced surface state density as a function of total particle dose, for M.O.S. oxide films bombarded by beams from two Saddle Field sources.

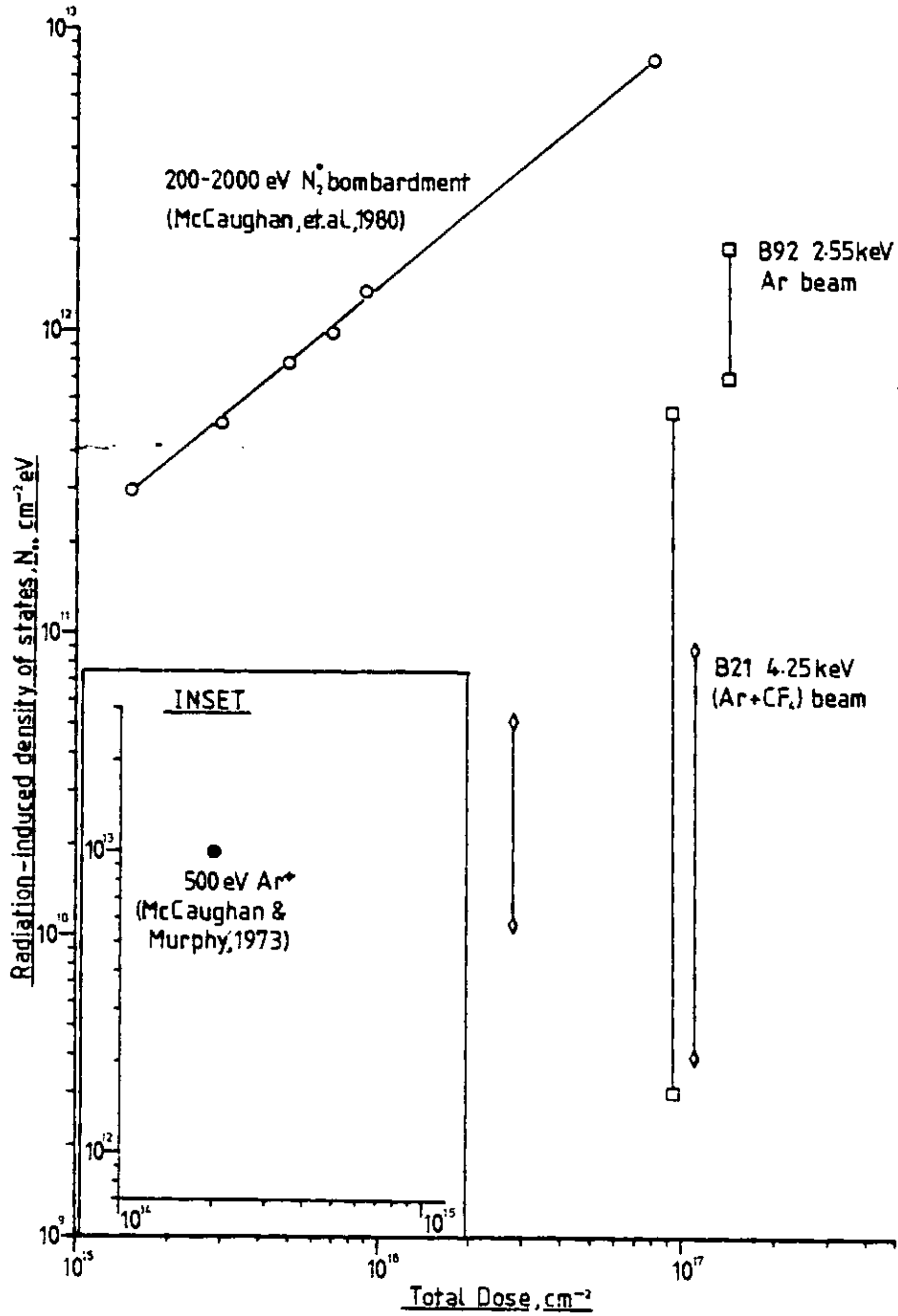

7.0 MECHANISMS OF REACTIVE ION BEAM ETCHING

7.1 INTRODUCTION

Work described in Chapter 4 has shown that, for most materials, the etch rate is increased by substituting a gas containing fluorine in place of argon.

Sputtering with argon is a purely physical process, but to understand the mechanisms of etching by a reactive ion beam it is necessary to consider energy transfer and chemical affinity.

In the case of ion milling it is necessary to understand the formation and characteristics of charged, massive particles and their effect at the target surface. The dissociation of fluorocarbons and SF_6, however, produces a wide range of fragments containing ionic, free radical and atomic species, many with the capacity to enter into sputtering and/or chemical reactions.

7.2 ETCHING BY CHEMICAL REACTIONS

7.2.1 Etching of Silicon Compounds by Fluorine and Fluorinated Compounds

The scission and formation of chemical bonds are low energy processes, requiring the transfer of usually no more than $\simeq 5$ eV.

Detailed work on the chemistry of plasma etching (Flamm, et. al., 1981,b) has shown that the etch rate of Si by F atoms is dependent on the concentration of etchant species (n_F) and the temperature (T) according to the relationship:

$$R_{Si} = 2.91 \pm 0.2 \times 10^{-12} n_F T^{\frac{1}{2}} \exp(-E/kT); \text{ Å min}^{-1} \quad (1)$$

The activation energy (E) was found by these workers to be 0.108 $\pm$ 0.005 eV. The rate-limiting step is the formation of Si-F bonds at the surface:

$$Si + 2F \rightarrow SiF_2 \qquad (2)$$

which may be removed from the site of the reaction as a volatile product, or become fully fluorinated:

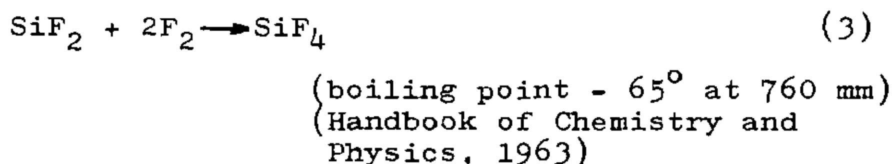

$$SiF_2 + 2F_2 \rightarrow SiF_4 \qquad (3)$$

(boiling point - 65° at 760 mm)
(Handbook of Chemistry and Physics, 1963)

where this volatile compound of Si(SiF_4) is most usually observed by mass spectrometry studies (Vasile, 1980).

The etch rate of Si by F atoms is approximately 41 times greater than that of SiO_2 at $20^{o}C$ (Flamm, et. al., 1981,b). This selectivity is ascribed to the comparable reactivities of oxygen and fluorine towards Si. For the etching of SiO_2 by fluorine atoms, the volatile end product is again SiF_4:

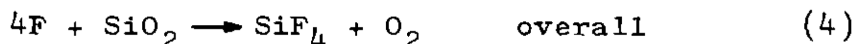

$$4F + SiO_2 \rightarrow SiF_4 + O_2 \quad \text{overall} \qquad (4)$$

Free molecular oxygen has been detected by mass spectrometry (Vasile, 1980) and has been shown to combine with carbon atoms from the dissociation of pump fluids or CF_x (see 7.3.1) in the presence of a source of excitation (such as electron bombardment) (Thomas, 1974):

$$C + O \rightarrow CO \qquad (5)$$

and ultimately to:

$$CO + O \rightarrow CO_2 \qquad (6)$$

The reaction of fluorine atoms with Si_3N_4 would be expected to follow a similar addition - abstraction sequence as in (4), but with less energy required

initially for the cleavage of the Si-N bond:

$$12F + Si_3N_4 \longrightarrow 3SiF_4 + 2N_2 \qquad (7)$$

with the likely removal of nitrogen in atomic or molecular form (Kumar, et. al., 1976). These reactions demonstrate that it is possible for volatile end products to be formed during the attack of fluorine atoms on silicon compounds.

The presence of fluorocarbons (CF_x) leads to the formation of several possible by-products during the etching of silicon compounds. The following are suggested by the author as possible reactions for the principle species identified (Coburn, et. al., 1977) in a CF_4 discharge, namely CF_3^+, CF_2^+ and CF^+ (C^+, CF_2^{++}, CF_3^{++} and F^+ were also detected). These reactions only describe the possible chemical reactions without consideration of possible charge on the species initially.

The etching of silicon inevitably leads to the presence of atomic carbon in varying quantities:

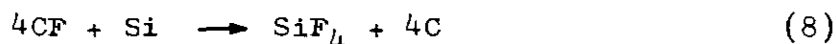

$$4CF + Si \longrightarrow SiF_4 + 4C \qquad (8)$$

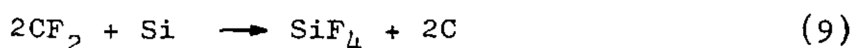

$$2CF_2 + Si \longrightarrow SiF_4 + 2C \qquad (9)$$

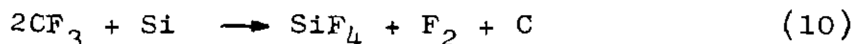

$$2CF_3 + Si \longrightarrow SiF_4 + F_2 + C \qquad (10)$$

The presence of atomic oxygen, liberated from the SiO_2 lattice, however, leads to the formation of a greater proportion of volatile products:

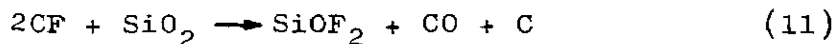

$$2CF + SiO_2 \longrightarrow SiOF_2 + CO + C \qquad (11)$$

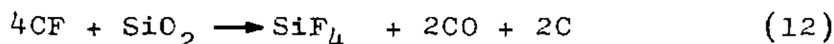

$$4CF + SiO_2 \longrightarrow SiF_4 + 2CO + 2C \qquad (12)$$

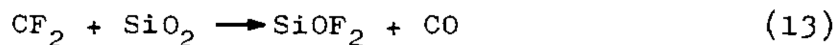

$$CF_2 + SiO_2 \longrightarrow SiOF_2 + CO \qquad (13)$$

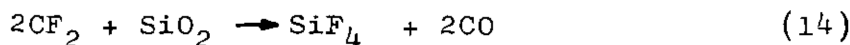

$$2CF_2 + SiO_2 \longrightarrow SiF_4 + 2CO \qquad (14)$$

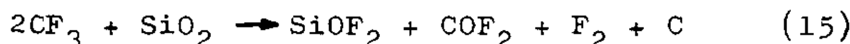

$$2CF_3 + SiO_2 \longrightarrow SiOF_2 + COF_2 + F_2 + C \qquad (15)$$

$$2CF_3 + SiO_2 \longrightarrow SiF_4 + COF_2 + CO \qquad (16)$$

$$2CF_3 + SiO_2 \longrightarrow SiF_4 + F_2 + 2CO \qquad (17)$$

The etching of Si_3N_4 is probably analogous to that of SiO_2, with the evolution of nitrogen and deposition of carbon:

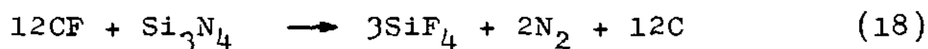

$$12CF + Si_3N_4 \longrightarrow 3SiF_4 + 2N_2 + 12C \qquad (18)$$

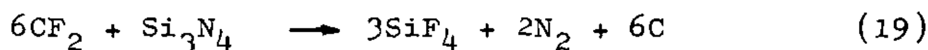

$$6CF_2 + Si_3N_4 \longrightarrow 3SiF_4 + 2N_2 + 6C \qquad (19)$$

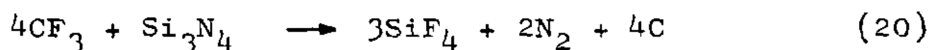

$$4CF_3 + Si_3N_4 \longrightarrow 3SiF_4 + 2N_2 + 4C \qquad (20)$$

It is possible that recombination of nitrogen and carbon occurs, complexes such as $CF_4-\dot{C}N^+$ have been detected by mass spectrometry (Coburn and Kay, 1979). The formation of cyanogen ($(CN)_2$, boiling point -21° at 760 mm, Handbook of Chemistry and Physics, 1963) is an endothermic process, requiring 71 k cal $mole^{-1}$* (Cotton and Wilkinson, 1967), which is easily available under the conditions present during bombardment by particles extracted from the B93 source.

The following reactions are proposed:

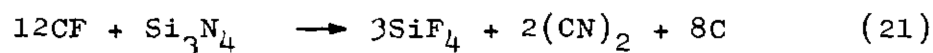

$$12CF + Si_3N_4 \longrightarrow 3SiF_4 + 2(CN)_2 + 8C \qquad (21)$$

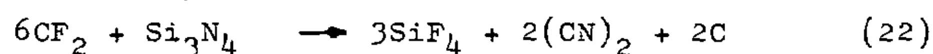

$$6CF_2 + Si_3N_4 \longrightarrow 3SiF_4 + 2(CN)_2 + 2C \qquad (22)$$

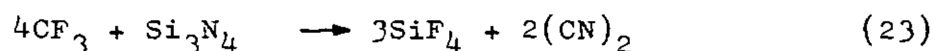

$$4CF_3 + Si_3N_4 \longrightarrow 3SiF_4 + 2(CN)_2 \qquad (23)$$

Previous work (Coburn and Kay, 1979) has shown that, in the plasma etching of silicon compounds, the reactions that lead to the presence of atomic carbon proceed at a slower rate than those in which all products are volatile. Reactions (8) to (23) show that the expected relative etch rates would be as follows, the reaction number is shown in parentheses:

*1 eV = 23.06 k cal $mole^{-1}$

	CF_3	CF_2	CF
$SiO_2 > Si$	(16 or 17,10)	(13 or 14,9)	-
$Si_3N_4 > Si$	(23,10)	-	-
$Si_3N_4 > SiO_2$	(23,15)	-	-
$SiO_2 > Si_3N_4$	(16 or 17,20)	(13 or 14,19 or 22)	-
$Si > SiO_2$	-	-	-
$Si > Si_3N_4$	-	-	-

These hierarchies only distinguish between reactions forming atomic carbon and those that do not. There are also various possibilities where the quantity of carbon is different in two reactions involving the same CF_x species.

Table 15 shows the experimental etch rate ratios for various combinations of materials and parent gases. SiO_2 is seen to consistently etch faster than Si, which indicates attack by either CF_2 or CF_3. Si_3N_4 consistently etches at a greater rate than Si which suggests CF_3 is the active species. With the exception of CF_4, all of the parent gases produced Si_3N_4 etch rates greater than those of SiO_2, again suggesting attack by CF_3. The relative etch rate hierarchy previously shown indicates that Si_3N_4 may etch faster or slower than SiO_2, depending on the nature of the products. It seems probable that CF_3 is the etchant responsible when the parent gas is a Freon. When the parent gas is SF_6, however, the question becomes rather more difficult as a variety of species may have been extracted from the source (see Section 7.3.2). Silicon has been shown to etch 70 times faster than SiO_2 in a plasma of pure SF_6 (d'Agostino and Flamm, 1981),

TABLE 15

Experimental Etch Rate Ratios for

Selected Combinations of Materials

$$\text{Expressed as } \frac{\text{Etch Rate, Target 1 (Å min}^{-1}\text{)}}{\text{Etch Rate, Target 2 (Å min}^{-1}\text{)}}$$

Combination of Materials	Ar	CF_4	CHF_3	C_2F_6	C_3F_8	SF_6
SiO_2:Si	2.1-2.2 (1)	6-6.35 (2)	3.3-4.6 (2)	3.3-3.7 (1)&(2)	4.5-6.1 (1)	2.86-3.3
Si_3N_4:SiO_2	0.62-0.67 (1)	0.65-0.83 (2)	1.1-1.5 (1)	1.82-2.11 (1)	1.03-1.33 (2)	0.9-1.21 (2)
Si_3N_4:Si	1.4 (1)	3.9-5.25 (2)	4.9-5.02 (1)	6.7-7.03 (1)	6-6.25 (2)	2.95-3.46 (2)

Conditions:

B93 source, on and normal to axis, C.A.T.T. 150 mm, beam "current" density (for Ar) 26 μA cm^{-2}, V_B = 2.55 keV (1)

V_B = 2.12 keV (2)

from which the major etchant species was concluded to be atomic fluorine. The data in Table 15 indicates that this is not the case when SF_6 is injected into the B93, thus suggesting that dissociation recombination reactions involving the carbon of the plasma chamber components lead to the extraction of CF_3^+ species as is the case with Freons (Section 7.3.2 gives more details).

7.2.2 Etching of Aluminium and Tungsten by Fluorine and Fluorinated Compounds

The only known fluoride of aluminium which occurs at ambient temperature in unco-ordinated form is AlF_3, melting point 1290°C (Cotton and Wilkinson, 1967). Chemical reactions leading to the formation of this compound are, therefore, unsuitable for etching purposes due to the high temperature required for vapourisation. As all films of aluminium become passivated by the formation of Al_2O_3, the first stage in the etching process must be removal of that layer. It seems likely that replacement of oxygen by fluorine can occur, with the formation of AlF_3:

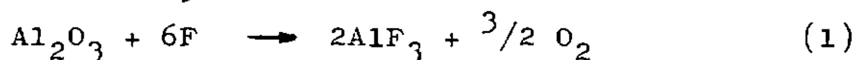

$$Al_2O_3 + 6F \longrightarrow 2AlF_3 + {}^3/2\ O_2 \qquad (1)$$

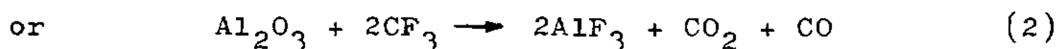

or

$$Al_2O_3 + 2CF_3 \longrightarrow 2AlF_3 + CO_2 + CO \qquad (2)$$

Sputter-yield data for AlF_3 have not been seen in the literature, the removal of this compound by physical processes alone is, therefore, speculative. There is no evidence for the existence of aluminium oxyfluorides, which might offer a convenient route to direct volatilisation. Similar reactions on deoxidised films would be expected to produce the same involatile

aluminium compound:

$$Al + 3F \longrightarrow AlF_3 \qquad (3)$$

with the possible formation of carbon films when CF_3 is the active species

$$Al + CF_3 \longrightarrow AlF_3 + C \qquad (4)$$

In contrast, however, tungsten is known to form one volatile fluoride (WF_6, boiling point 17°C, Cotton and Wilkinson, 1967). The formation of WF_6 may follow removal of surface oxide, WO_2,by liberation of WOF_4 which sublimes

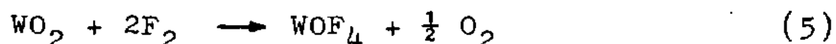

$$WO_2 + 2F_2 \longrightarrow WOF_4 + \tfrac{1}{2} O_2 \qquad (5)$$

and, assuming the absence of oxygen for further oxidation of the clean tungsten surface:

$$W + 6F \longrightarrow WF_6 \qquad (6)$$

or alternatively by CF_3:

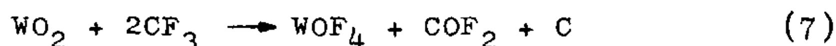

$$WO_2 + 2CF_3 \longrightarrow WOF_4 + COF_2 + C \qquad (7)$$

which suggests that further etching may be retarded as a carbon film is formed, which is also likely in the reaction following removal of the oxide:

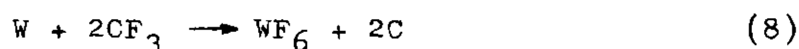

$$W + 2CF_3 \longrightarrow WF_6 + 2C \qquad (8)$$

7.2.3 Etching by Free Radicals

The term "free radical" is formally defined in the Glossary. There appears to be a degree of ambiguity in some of the literature regarding the use of this term. In the reactions of interest (i.e. the production of volatile compounds of silicon by the reaction of fluorine on Si, SiO_2 or Si_3N_4) there is no distinction between the end result of etching by fluorine free radicals and that due to fluorine atoms. The essential difference between

fluorine atoms and fluorine free radicals in this application is the activation energy with respect to a specific target material. In practice, the term free radical is often used to describe the isotropic nature of the etchant. From this is derived the distinction "Ion Associated Etching" (anisotropic, due to charged species directed electrostatically) compared with "Free Radical Etching" (isotropic, mobility of species by diffusion) (Gill, 1980; Doken and Miyata, 1979).

The free radicals of interest to this work are formed by the homolytic fission of a covalent bond. The bonding electrons are, therefore, shared equally between the two products of the dissociated parent. There is no net transfer of electrons and the products are electrically neutral, as shown with CF_4 as an example:

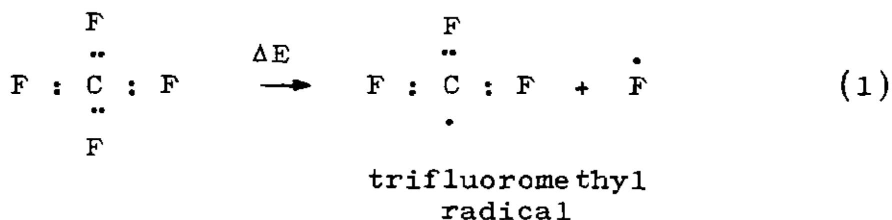

(1)

where ΔE indicates energy gain.

The lone electron attached to the carbon atom is denoted by $\dot{C}F_3$ in subsequent reaction mechanisms, the same notation is used for the fluorine radical, $\dot{F}$. In the representation shown in (1) it can be seen that the carbon atom retains three covalent bonds and, therefore, one electron in the 2p shell remains unpaired. The 2p shell in the fluorine atom requires the addition of only 1 electron for completion (hence the electron affinity of 3.45 eV) and hence the unpairing of one electron is

accomplished with the scission of the C-F bond. This is analogous to the U.V. dissociation of molecular fluorine:

$$F_2 \xrightarrow{h\nu} \dot{F} + \dot{F} \qquad (2)$$

The question of etching by CF_x fragments (where x = 1, 2 or 3) is rather complex as ionic and free radical forms probably exist. It would appear that the overall reaction of a free radical moving by diffusion alone:

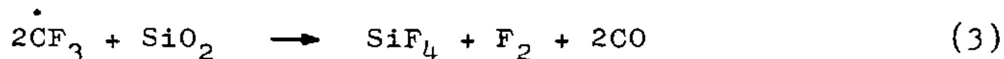

$$2\dot{C}F_3 + SiO_2 \longrightarrow SiF_4 + F_2 + 2CO \qquad (3)$$

could give the same end products as impact by an ion (or ion neutralised by collision with an electron):

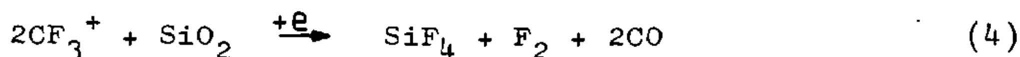

$$2CF_3^{+} + SiO_2 \xrightarrow{+e} SiF_4 + F_2 + 2CO \qquad (4)$$

although the etched profiles would be totally different.

The radicals of interest here are short-lived (half-life, $t_{\frac{1}{2}} = 10 \times 10^{-6}$ sec) (McTaggart, 1967) and decay to the ground state by: addition reactions to suitable materials, such as silicon,

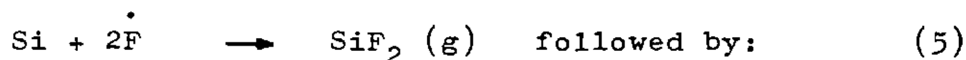

$$Si + 2\dot{F} \longrightarrow SiF_2 \text{ (g)} \quad \text{followed by:} \qquad (5)$$

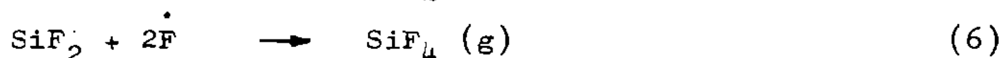

$$SiF_2 + 2\dot{F} \longrightarrow SiF_4 \text{ (g)} \qquad (6)$$

recombination at the vessel wall:

$$\dot{F} + \dot{F} \longrightarrow F_2 \qquad (7)$$

or by direct additon to a radical scavenger such as oxygen trapped in the source graphite linings or at the vacuum chamber wall:

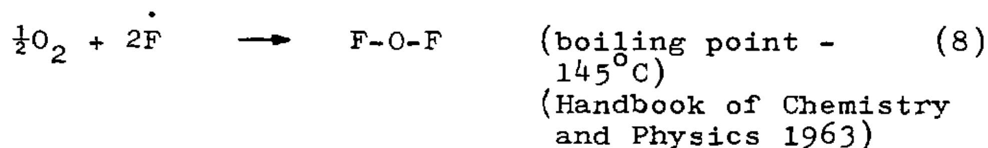

$$\tfrac{1}{2}O_2 + 2\dot{F} \longrightarrow F\text{-}O\text{-}F \qquad (8)$$

(boiling point - 145°C) (Handbook of Chemistry and Physics 1963)

As the distribution of free radicals (such as $\dot{C}F_3$, $\dot{F}$) and atoms (e.g. F^o) is by diffusion, etching reactions in which these species play a major role are

characterised by "undercut" profiles. Evidence of this is seen in Fig. 7.1 where, during the fabrication of Mesa diodes the silicon has been etched isotropically beneath the aluminium electrode disc, by fluorine from an SF_6 plasma (0.15 torr, ground electrode temperature $40^{o}C$ initially, not controlled, power density 0.99 W cm^{-2}, 13.56 MH_z, etch rate 2.2 μm min^{-1}).

It is considered possible that a charged particle (say CF_3^+), extracted from the B93 by acceleration across the ion sheath is neutralised by the capture of a secondary electron:

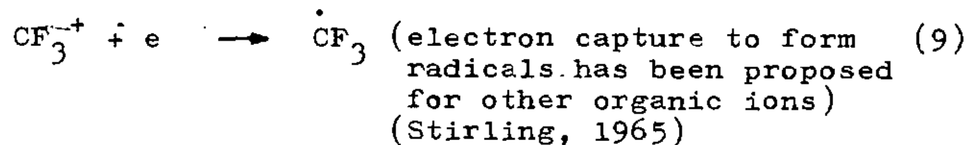

$$CF_3^+ + e \longrightarrow \dot{C}F_3 \quad \text{(electron capture to form radicals has been proposed for other organic ions) (Stirling, 1965)} \qquad (9)$$

and continues as a free radical with negligible change in direction or momentum. The time of flight across the field-free region between the cathode and target is given by:

$$t = \frac{d}{\sqrt{2E/m}} \qquad (10)$$

where t is in sec

d is 0.15 m (normal C.A.T.T. distance)

E is the ion energy x 1.602×10^{-19} Joules

m is the ion mass x 1.67×10^{-27} kg

For CF_3^+: acceleration by $V_A = 0.6$ kV, $t = 4 \times 10^{-6}$ sec, and for $V_A = 3.0$ kV, $t = 1.8 \times 10^{-6}$ sec. As these times are at the longest one half of one half-life, a significant proportion of free radicals could, if produced by this process, arrive at the target surface.

7.3 FORMATION OF REACTIVE SPECIES WITHIN THE B93

7.3.1 Dissociation of Freons and Recombination Processes

There are probably two distinct mechanisms by which fluorocarbon fragments are produced within the B93 and are subsequently extracted in charged form:

(i) electron impact dissociation

(ii) thermal dissociation

At the instant of energisation with the source at 20°C, the characteristics are not stable, and dissociation of a fluorocarbon molecule such as CF_4 may be primarily by electron impact leading to the rupture of one or more C-F bonds:

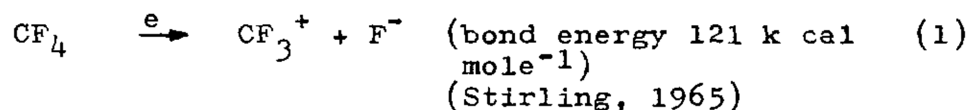

$$CF_4 \xrightarrow{e} CF_3^+ + F^- \quad \text{(bond energy 121 k cal mole}^{-1}\text{) (Stirling, 1965)} \qquad (1)$$

When the anodes have achieved thermal equilibrium at about 900°C, however, the increased collision rate for CF_4 molecules which diffuse into this high temperature region is likely to lead to total dissociation, probably stepwise:

$$CF_4 \xrightarrow{\Delta H} \dot{C}F_3 + \dot{F} \qquad (2)$$

$$\dot{C}F_3 \xrightarrow{\Delta H} \dot{C}F_2 + \dot{F} \qquad (3)$$

$$\dot{C}F_2 \xrightarrow{\Delta H} \dot{C}F + \dot{F} \qquad (4)$$

$$\dot{C}F \xrightarrow{\Delta H} \dot{C} + \dot{F} \qquad (5)$$

For which the mean bond energy is $\simeq 116$ k cal mole^{-1} (Finar, 1967). At this temperature it has been shown that the most likely dissociation mechanism is the homolytic fission of each bond (Cadogan, 1973) leading to free radicals as shown.

As the gas is injected into the source approximately 35 mm from the anodes (see Fig.3.1), and where a high density of oscillating electrons exists, mechanism (1) is likely to predominate.

From reactions (2) - (5), the overall thermal dissociation process is described by:

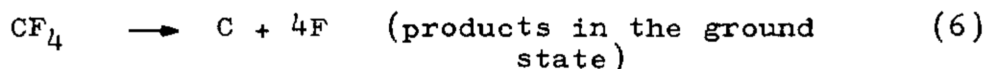

$$CF_4 \longrightarrow C + 4F \quad \text{(products in the ground state)} \qquad (6)$$

from which atomic carbon may coalesce into particles and condense on cooler areas of the plasma chamber and ends of the anode rods, or may undergo reaction with the atomic fluorine:

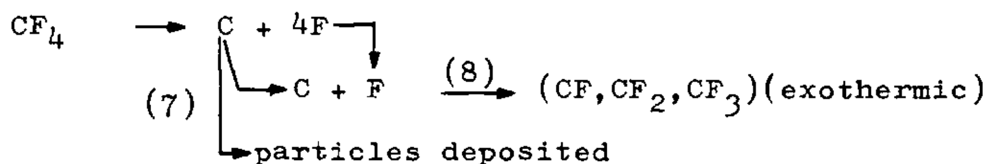

The observation that particulate carbon of low density is formed within the source suggests that reaction (7) occurs to some degree. Sputtering is thought not to be responsible for these carbon deposits. Carbon sputtered from the anodes and graphite liners of the plasma chamber and redeposited within the source following operation with argon is of such greater density and cohesion than the "fluffy" deposits observed after operation with fluorocarbons.

The removal of carbon (reaction (7)) leads to fluorine enrichment. Atomic fluorine may react at the hot graphite anodes:

$$F + C \xrightarrow{\Delta H} CF^+ + e \qquad (9)$$

or may capture an electron in the exoergic process:

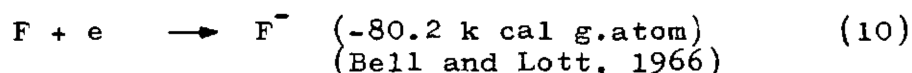

$$F + e \longrightarrow F^- \quad \begin{matrix}(-80.2 \text{ k cal g.atom}) \\ (\text{Bell and Lott, 1966})\end{matrix} \qquad (10)$$

followed by reaction at the anodes:

$$F^- + C \longrightarrow CF^+ + 2e \qquad (11)$$

$$2F^- + C \longrightarrow CF_2^+ + 3e \qquad (12)$$

$$3F^- + C \longrightarrow CF_3^+ + 4e \qquad (13)$$

These products are in equilibrium with those shown in reactions (2) - (5) due to thermal dissociation. In other words, the dissociation-recombination reactions occur simultaneously and escape from the cycle is only possible for charged species that are accelerated out of the source before dissociation occurs.

The existence of polymer deposits within the source has not been observed although the etch rate data indicate the presence of CF_x species, one typical reaction of which is (for $\ddot{C}F_2$ diradical):

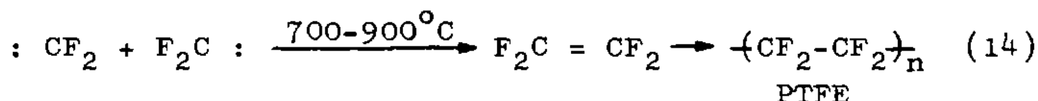

$$:CF_2 + F_2C: \xrightarrow{700\text{-}900^\circ C} F_2C = CF_2 \longrightarrow \underset{\text{PTFE}}{(CF_2\text{-}CF_2)_n} \qquad (14)$$

used in the industrial production of polytetrafluorethylene (Roberts and Caserio, 1965).

The reasons for the apparent absence of this reaction are thought to be:

(i) The pressure within the source is too low for significant numbers of collisions leading to chain propagation.

(ii) The presence of the considerable electrostatic field which tends to produce ionic, rather than free radical species.

(iii) The loss of free radicals by recombination (for

example at the walls of the plasma chamber) and inhibition of the chain sequence.

Hexafluoroethane (C_2F_6, Freon 116) may be expected to fragment initially at the weak C-C bond, when close to the hot anode rods:

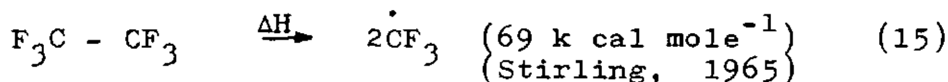

$$F_3C - CF_3 \xrightarrow{\Delta H} 2\dot{C}F_3 \quad \begin{Bmatrix} 69 \text{ k cal mole}^{-1} \\ \text{Stirling, } 1965 \end{Bmatrix} \qquad (15)$$

from which total dissociation can occur according to reactions (3) - (5). These reactions lead to the deposition of carbon and attack of fluorine at the hot graphite surface. Electron impact at the parent molecule may, however, lead to ionic fragments which are extracted from the source:

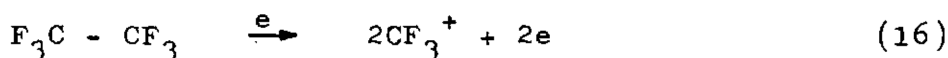

$$F_3C - CF_3 \xrightarrow{e} 2CF_3^+ + 2e \qquad (16)$$

Similarly, with trifluoromethyl radicals, although with a lower energy requirement:

$$\dot{C}F_3 \longrightarrow CF_3^+ + e \qquad (17)$$

The characteristics of octafluoropropane (C_3F_8, Freon 218) are not well documented in the literature. In consideration of the mass of the terminal fluorine atoms and their electronegativity (4.10, Allred-Rochow) (Cotton and Wilkinson, 1967) a localisation of charge would be expected towards the CF_3 groups which would also impart a bending moment. Fission of the carbon-carbon bonds by electron impact or thermally induced vibration would lead to:

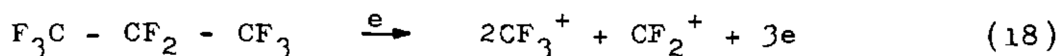

$$F_3C - CF_2 - CF_3 \xrightarrow{e} 2CF_3^+ + CF_2^+ + 3e \qquad (18)$$

or

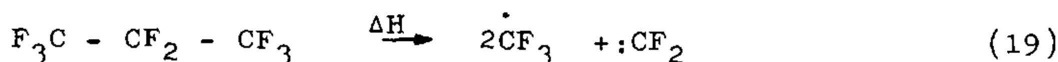

$$F_3C - CF_2 - CF_3 \xrightarrow{\Delta H} 2\dot{C}F_3 + :CF_2 \qquad (19)$$

Ionic species would probably be extracted at the cathode aperture. $\dot{C}F_3$ radicals could be retained inside the source plasma chamber and dissociated or ionised (reactions (3) - (5) or (17)). Possible reactions of the diradical would be fluorination:

$$:CF_2 + F \rightarrow \dot{C}F_3 \qquad (20)$$

direct combination with another diradical:

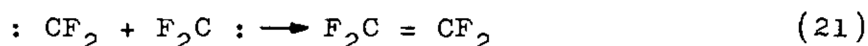

$$:CF_2 + F_2C: \rightarrow F_2C = CF_2 \qquad (21)$$

or dissociation at the anodes (reactions (4) and (5)).

Trifluoromethane (CHF_3, Freon 23) is a somewhat special case with the substitution of one hydrogen atom for one fluorine atom, and the consequent high strength (134 k cal $mole^{-1}$) (Stirling, 1965) of the H-F bond. Thermal dissociation would probably proceed as follows:

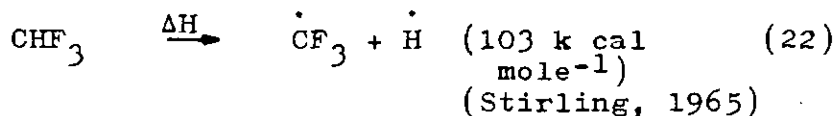

$$CHF_3 \xrightarrow{\Delta H} \dot{C}F_3 + \dot{H} \quad (103 \text{ k cal mole}^{-1}) \text{ (Stirling, 1965)} \qquad (22)$$

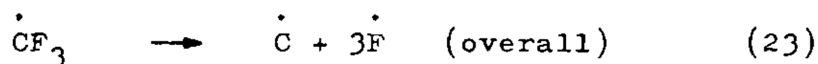

$$\dot{C}F_3 \rightarrow \dot{C} + 3\dot{F} \quad \text{(overall)} \qquad (23)$$

followed by

$$\dot{H} + \dot{F} \rightarrow HF \qquad (24)$$

Electron impact to produce ionic species would lead to two charged particles extracted from the source:

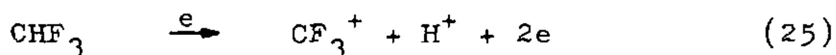

$$CHF_3 \xrightarrow{e} CF_3^+ + H^+ + 2e \qquad (25)$$

In view of the fact that lateral etching of SiO_2 is not observed after exposure to a "CHF_3 beam", reactions leading to the generation of HF (24) are considered to be of minor importance.

7.3.2 Dissociation of SF_6 and Recombination Processes

The observation that a substance with the appearance of elemental sulphur is formed as a low density, pale

yellow coloured deposit on the anodes of the B93 suggests that total dissociation of SF_6 does occur. The overall dissociation reaction would be:

$$SF_6 \xrightarrow{\Delta H} S + 6\dot{F} \qquad (1)$$

The following mechanism has been proposed (Brasted, 1966) for the electron-impact dissociation of SF_6:

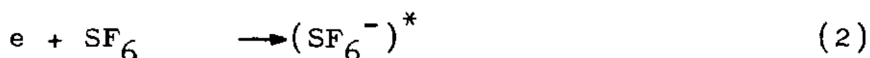

$$e + SF_6 \longrightarrow (SF_6^-)^* \qquad (2)$$

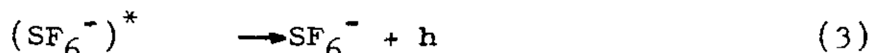

$$(SF_6^-)^* \longrightarrow SF_6^- + h \qquad (3)$$

$$\longrightarrow SF_5^- + F \qquad (4)$$

$$\longrightarrow \dot{S}F_5 + F^- \qquad (5)$$

$$\longrightarrow \dot{S}F_5 + \dot{F} + e \qquad (6)$$

It has been found (d'Agostino and Flamm, 1981) that fluorine is the principle etchant responsible for attack on Si in an SF_6 plasma. As SF_x^- species are unlikely to be extracted from the discharge within the B93 source, attack of fluorine radicals (from (1), above) at the hot anodes probably leads to the formation of fluorocarbon radicals and ions, for example:

$$3\dot{F} + C \longrightarrow \dot{C}F_3 \qquad (7)$$

$$3\dot{F} + C \longrightarrow CF_3^+ + e \qquad (8)$$

The addition reactions are in equilibrium with those leading to dissociation, as shown before (Section 7.3.1). There are indications that free fluorine leaves the source by diffusion, for example the sub-mask erosion of SiO_2, see Fig. 7.2.

The sub-mask erosion on an aluminium film exposed to an "SF_6 beam" also indicates attack by free radical species, but the chemistry of this reaction is not understood at the present time. Further work would be

needed before a satisfactory mechanism could be proposed.

7.4 ETCHING BY SPUTTERING AND CHEMICAL PROCESSES

7.4.1 Energy Transfer Considerations for some Etchant-Target Combinations

The rate of material removal due to sputtering is dependent on the energy, collision cross-section and mass of the bombarding particle and the atomic mass of the target, for a given angle of incidence. Sputter yields for combinations of etchant species and target have not been calculated due to the paucity of data on cross-sections at these "low" energies. The cross-sections of CF, CF_2 and CF_3 would be expected to differ significantly due to the size and the electronegativity of the fluorine atoms.

Using the following relationship, it is possible to compare the energy transferred by various ionic species in head on collisions with the typical target materials:

$$E_{transferred} = E_1 \frac{4m_1 m_2}{(m_1 + m_2)^2} \qquad \text{(Holland, 1972)}$$

where E_1 is the energy of the bombarding particle

m_1 and m_2 are the masses of the particle and target respectively.

Assuming that the ionic species CF^+, CF_2^+ and CF_3^+ may be extracted from the source, and are incident at the target surface as rigid spheres, the relationship for the transfer of energy with target mass is shown in Fig.7.3 It is clear from these curves that the maximum energy is

transferred as the mass of the particle (m_1) approaches the value of the target mass (m_2).

It can be seen that the transfer of energy due to impact by CF_3^+ is marginally greater than that due to Ar^+ when SiO_2 is the target. The situation is reversed with Si targets, however, and impact by Ar^+ is more effective than by CF_3^+. The mass of Si_3N_4 is such that none of these particles efficiently transfer energy by head on collision, but CF_3^+ is significantly more efficient than Ar^+.

7.4.2 Experimental Evidence of Sputtering and Chemical Etching

Characteristic features may be etched into the target as a result of sputtering, for example:

(i) The formation of "facets" and wall angles between 40 - 60° from the plane of the substrate, caused by the material etch rate dependence on the angle of incidence of the beam. This has been extensively described in the literature (for example: Spencer and Schmidt, 1971) and has been the subject of computer modelling (Neureuther, et. al., 1979).

(ii) Channel or trench formation due to secondary or reflected ion sputtering at the base of a resist pattern or other surface feature (Wilson, 1973).

Other topographical features may also be observed, such as redeposition which has been shown (Gokan and Esho, 1981) to be most significant at ion beam incidence angles of less than 40°. Redeposition may take the form

of a coating on the resist walls which is left as a raised "fence" around the feature in relief after etching (Gloersen, 1976).

Etching by chemical processes due to free radicals and atoms without momentum directed at the target, is characterised by lateral etching, penetration between target and non-contiguous masks and sloping profiles. Preferential etching at localised sites may cause "etch pits".

Table 16 summarises the topographical features observed by the author in S.E.M. studies on five materials etched by beams produced by injecting the B93 with various gases.

The data contained in this table must be examined with caution, however. In cases where the mask was stainless steel (S.S.) the experiments were carried out for the purpose of obtaining "absolute" etch rate data. It is clear from the results that some of the topographical features have arisen directly as a result of the mask shape and material. For example, on samples of Si_3N_4 etched with a beam produced by injecting CF_4 into the source, secondary sputtering and redeposition were observed on S.S. masked specimens, but not on those with a photoresist pattern. This phenomenon is further exemplified, as shown in Fig. 7.2. SF_6 was injected into the B93 source, which was operated at $V_A = 2$ to 2.5 kV, mean beam "current" density (for Ar): 26 $\mu A\ cm^{-2}$ (see Appendix II for experimental procedures). This Scanning Electron Micrograph clearly shows erosion of the target

TABLE 16

Topographical Features Observed After Reactive Ion Beam Etching of Various Materials

Material		CF_4		CHF_3	C_2F_6	C_3F_8	SF_6
Si	Profile	W.V.		W.V.(80°)	W.V.	No Data	W.S. 60°
	Features	None		None	R.E.	R	T,R
	V_B (keV)	2.55		2.55	2.12	2.55	2.12
	Mask	S.S.		P.R.	S.S.	S.S.	S.S.
SiO_2	Profile	W.V.	W.S. 30°	W.V.	W.V.	No Data	W.S. 30°*
	Features	None	None	None	T,R	No Data	E
	V_B (keV)	2.35	2.12	2.55	2.55	-	2.12
	Mask	P.R.	S.S.	P.R.	S.S.	-	S.S.
Si_3N_4	Profile	W.S. 60°	W.S. 60°	No Data	No Data	No Data	No Data
	Features	None	T,R	None	None	None	None
	V_B (keV)	2.55	2.12	2.55	2.55	2.12	1.9
	Mask	P/R	S.S.	P.R.	S.S.	S.S.	S.S.
Al (Al_2O_3)	Profile	Too Many Particles for Analysis		No Data	No Data	No Data	W.S. 60°
	Features			No Data	R	T	E
	V_B (keV)	2.55		-	2.55	2.12	2.12
	Mask	S.S. and P.R.		-	S.S.	S.S.	S.S.
W (WO_2)	Profile	No Data		No Data	No Data	W.S. 60°	W.V.
	Features	R		-	E or R	R	None
	V_B (keV)	2.55		-	2.55	2.55	2.12
	Mask	S.S.		-	S.S.	S.S.	S.S.

Notes * See Fig. 7.2

Profile
- W.V. : Wall profile approximately vertical
- W.S. : Wall profile at stated angle to substrate

Features
- T : Trench at foot of etched profile
- R : Redeposition at mask edge
- E : Erosion beneath mask (For S.S. mask only)

Mask
- S.S. : Masked with stainless steel (see Appendix II)
- P.R. : Masked with polymeric resist (see Appendix I)

Samples etched static on water-cooled table, on and normal to axis of B93, C.A.T.T. 150 mm.
Mean beam "current" density 26 μA cm^{-2}

Beam Energy
- V_B = 2.55 keV (V_A = 3 kV)
- V_B = 2.12 keV (V_A = 2.5 kV)

beneath the(non-contiguous)mask, which was probably caused by the action of fluorine atoms or free radicals which were trapped in the intervening space. "Etch pits" are also visible, a frequent feature when SF_6 is the parent gas. The pits are thought to be due to selective attack at regions of discontinuity in the SiO_2 surface structure. Using a B21 source injected with SF_6, the etching of patterns defined in photoresist produced vertical wall profiles without evidence of undercutting, although roughening of the horizontal etched surface was still evident.

7.4.3 Discussion

From an examination of the information obtained by experiment and from the literature, it is possible to compare the arguments for and against the two mechanisms by which material is removed using R.I.B.E. techniques. Only the etching of photoresist patterned targets will be discussed.

The etch rate dependence on particle energy, as shown in Section 4.3 is indicative of a sputtering mechanism. This could be as a result of the reduced chemical affinity following carbon deposition as shown by reaction (10), Section 7.2.1. However, the etched profiles of Si, SiO_2 and Si_3N_4 exposed to a "CHF_3 beam" show no evidence of facets, trench formation or redeposition. Similarly with a "CF_4 beam", Si and SiO_2 are observed to have near-vertical profiles, and freedom from features associated with sputtering. Si_3N_4 etched with a "CF_4 beam" has a shallower etched profile ($\simeq 60^o$) which may suggest an angular dependence on etch rate, but there are no other features to substantiate this.

The absence of redeposited material may indicate chemical reaction leading to volatile products, or may simply be a result of etching with the beam at normal incidence (the presence of debris on SiO_2 exposed to an argon beam was only observed on a small number of specimens). The etch rate increase for all materials above the level measured with argon, is strongly suggestive of chemical reactivity; however, the freedom from "undercutting" on "CF_4 and CHF_3 beam" etched samples indicates that the diffusion of free radical and/or atomic species at the target surface is not a significant mechanism.

This leads to the conclusion that a hybrid process is involved. There are several possible mechanisms which satisfy these results, to varying degrees.

(i) Sputtering enhanced by chemical reaction involving bond formation without dissociation of the reactive species.

(ii) A combined sputtering-chemical reaction in which bond formation is preceeded by dissociation of the reactive species to smaller fragments.

(iii) Enhanced chemical etching produced by lattice damage induced by the energetic particle bombardment. A similar mechanism was proposed (Gibbons, et. al., 1969) to explain selective etching of Ar^+ and Ne^+ bombarded silicon. In this work, the etchants were aqueous, and the etch depth (and hence etch selectivity) was linearly dependent on the ion energy up to 65 keV.

These results, when interpolated to $\simeq 5$ keV show that enhanced etching occurred in the range 50 - 100 Å below the surface for Ar^+ doses of 5×10^{15} cm^{-2}.

The proposal in (ii) would probably lead to a degree of lateral etching by fragments produced by dissociation. There is no etch rate or topographical evidence to suggest that fluorine (in atomic or free radical form) is available at the target surface when Freons are the parent gases. For the mechanism in (i) to occur, there would surely be evidence of enhanced sputtering ("trenches") and wall profiles less than 90°, although the doubtful criterion of redeposition could be explained with or without chemical attack. On the basis of the evidence available at present, the most likely explanation seems to be that of (iii), a more detailed account of which follows.

7.4.4 Suggested Mechanism

On the basis of chemical reactivity towards Si and the two silicon compounds investigated, CF_3 has been suggested as the most likely etchant produced by the dissociation of Freons in the B93. It is assumed that the particle is extracted from the source as CF_3^+, which arrives at the target at a velocity determined by the extraction potential. Electron capture by the particle, if it occurs, is expected to affect the resulting charge on the target, but not the topography or volatile compounds produced by the etching process.

Fig.7.4 shows the suggested mechanism for the enhanced chemical etching of SiO_2 by CF_3. After the approach and impact of the particle (steps 1 and 2), lattice damage (step 3) will extend into the surface to a distance determined by the energy of the projectile. At the maximum energy used in this study (V_B = 2.55 keV) the projected range (Rp) is probably less than 50 Å (for 10 keV As^+ (atomic weight 74.9) in Si, Rp = 97 $\pm$ 36 Å (Gibbons, et. al., 1975)). As the energy of the particle is increased, the damage becomes more extensive and extends further below the surface, thus leading to more rapid chemical attack as shown in the following suggested mechanism.

Co-ordination (step 4) to form an activated intermediate would be expected due to the electron deficiency at the carbon atom and the region of high electron density between silicon atoms. Due to the electron affinity of the fluorine atoms, the formation of the carbon-oxygen bond would follow (step 5) with the consequent rupture of Si - O bonds. Lattice damage producing broken Si - O bonds would enable direct co-ordination of CF_3 at this stage. In step 6 the central silicon atom becomes electron deficient as the distribution of negative charge moves towards the fluorine atoms. An active complex is formed between two (electrophilic) fluorine atoms and the central silicon atom and simultaneously the second bond in C = O is created. Further fluorination of SiF_2 is possible or it

may be removed, along with COF_2 as volatile end products (steps 7 and 8).

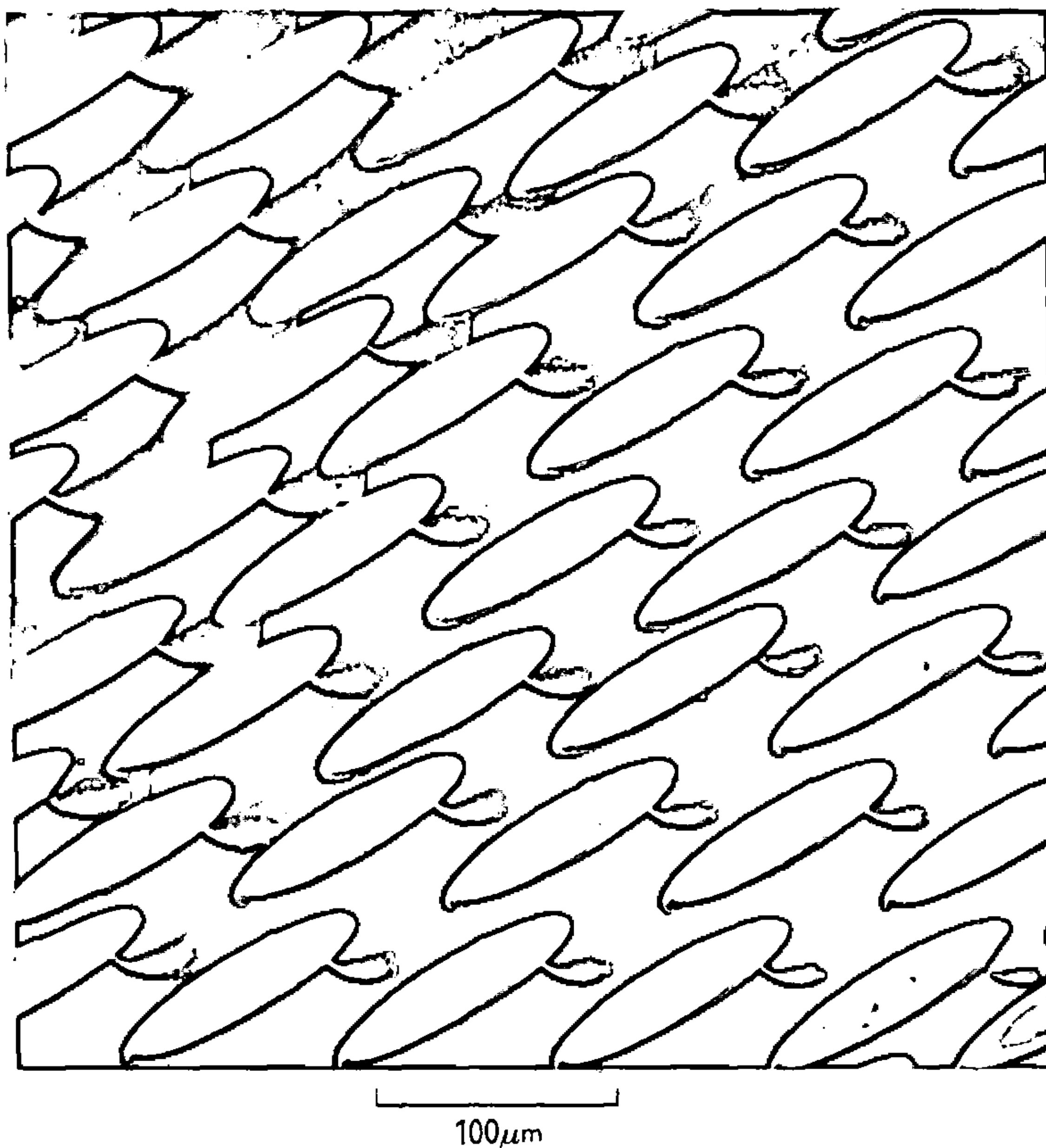

FIG.7.1 Isotropic etching of silicon using an SF_6 plasma.

Mesa diodes fabricated on oxygen-implanted silicon. Discs are aluminium electrodes which also served as etch resist.

Etched in a planar reactor using a discharge of SF_6. 0.15 torr, 0.99 W cm^{-2}, 13.56 MHz. Wafer on earthed electrode, without temperature control.

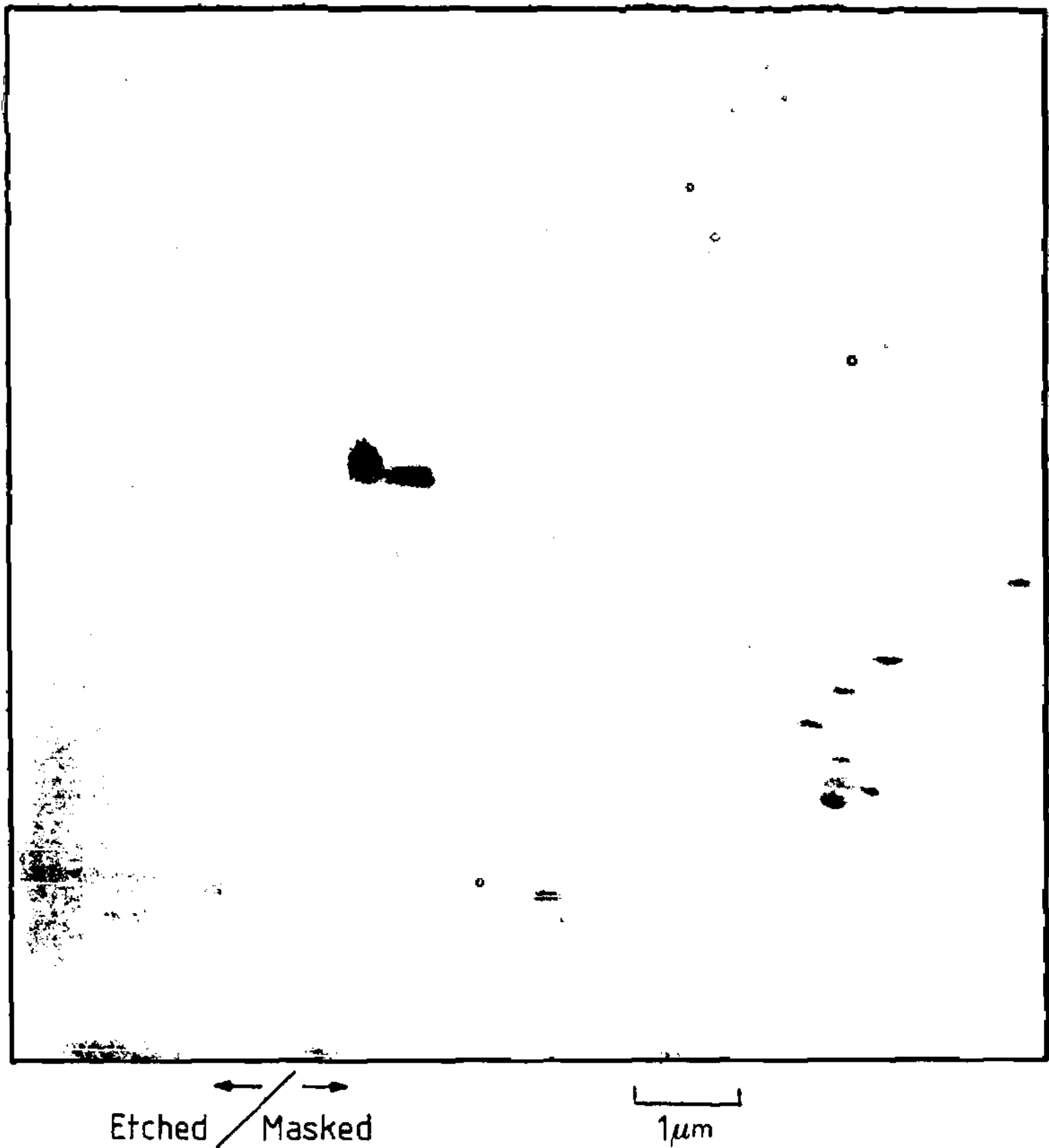

FIG.7.2 Etch pits in SiO_2 produced by free radical attack beneath a non-contiguous mask.

B93 source injected with SF_6, stainless steel mask. V_B: 1.7-2.13 keV, I_B: 26 $\mu A\ cm^{-2}$. Target on and normal to source axis, cooled, static.

FIG.7.3 **Theoretical Maximum Energy Transfer to Various Targets, for 3 Fluorocarbon Ions and Argon. For B93 Beam Energy of 2.55 keV**

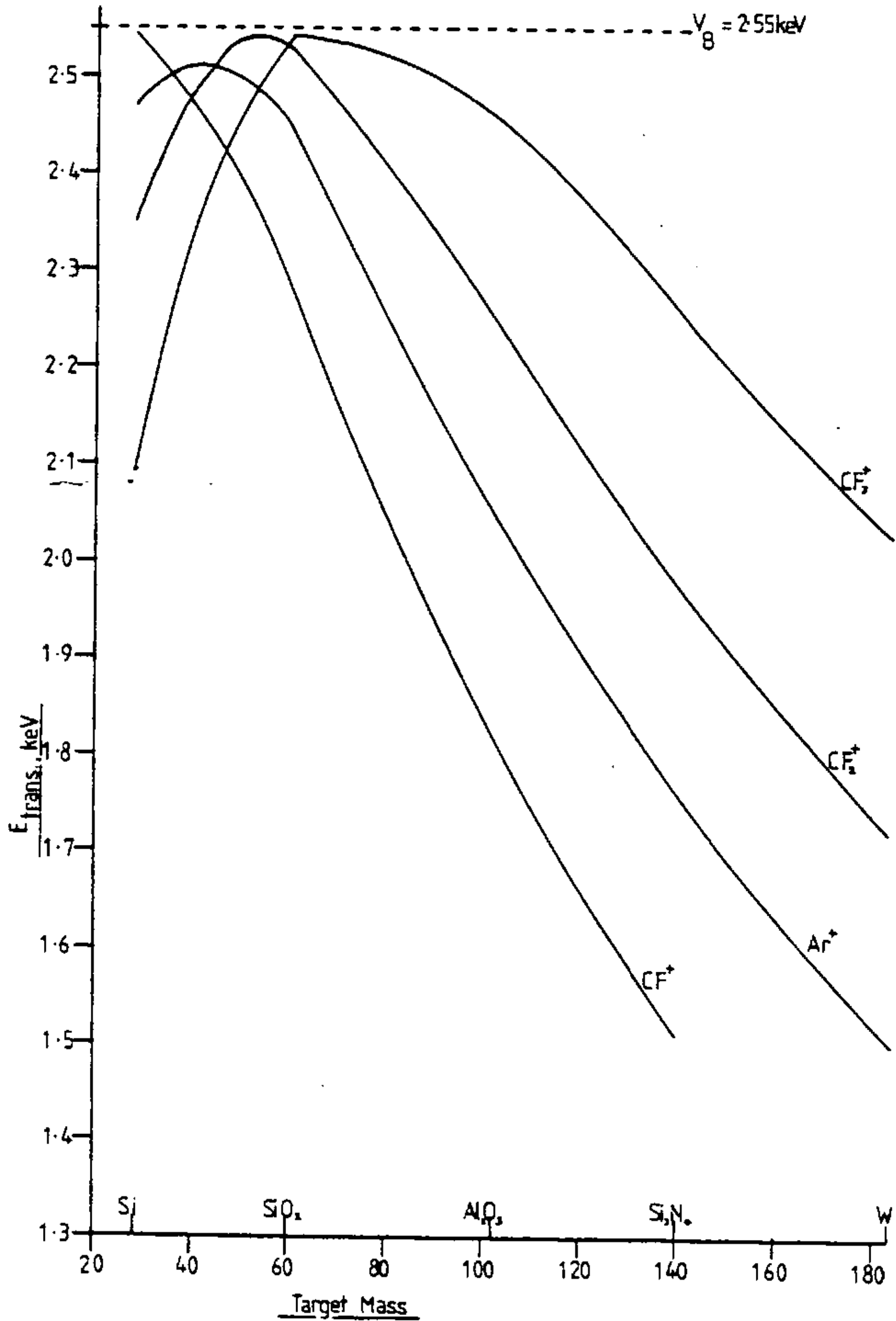

FIG.7.4

Proposed Mechanism for the Enhanced Chemical Etching of SiO_2 by CF_3.

1 Approach of etchant particle

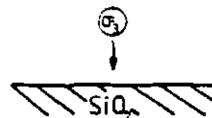

2 Impact

Secondary electron emission

3 Lattice damage

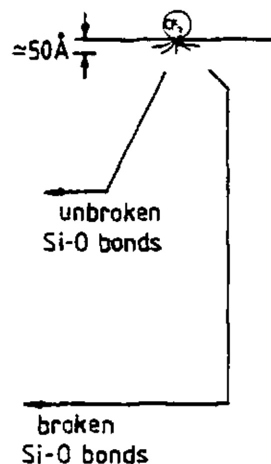

4 Formation of an active complex

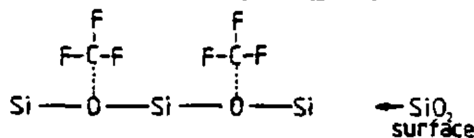

5 Rupture of Si-O bonds

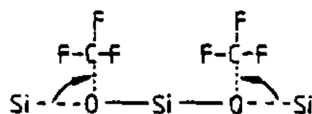

6 Formation of C=O, and F-Si activation

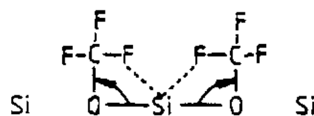

7 Production of COF_2 and SiF_2 (volatile)

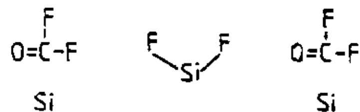

8 Further reaction to SiF_4 and CO

8. CONCLUSIONS

The etching of sub-micron features in certain silicon compounds can be carried out at commercially acceptable rates using a plasma discharge of halogenated species in a planar reactor. The selectivities attainable using this technique are generally lower than those obtained with aqueous etchants.

An argon beam produced by the B93 source was found to be significantly divergent with a non-uniform current density distribution. M.O.S. capacitors fabricated using this beam suffered less degradation than those produced by an argon ion beam of lower energy and with a total particle dose four orders of magnitude greater.

Apparent sputter yield data for B93 fluorocarbon beam etching are comparable to those reported for similar work using heated filament sources. Saddle Field sources with similar beam current densities to these heated filament devices should, therefore, be capable of etching at comparable rates. Chemical reactions play a major role in the etching of silicon compounds by fluorinated species in the B93 beam.

Sub-micron features free of undercutting, facets, trenches and redeposition have been accurately transferred from the resist layer into silicon dioxide using a fluorinated beam produced by both B21 and B93 Saddle Field sources. The maximum etch rates obtained with the B93 are four to seven times lower (for silicon dioxide and silicon nitride) than those required for commercial processing. Mechanical movement, such as a planetary system, is

required to improve the uniformity of etching across individual wafers.

9. RECOMMENDATIONS FOR FURTHER WORK

9.1 THE B93 SOURCE

9.1.1 Beam Uniformity

The argon beam "current" profile has been shown in Section 3.5 to be non-uniform with an intense central area. Work is planned for a detailed analysis of the beam profile by etching a glass plate with a matrix of aluminium discs serving as masks. Talysurf measurements of step heights after removal of the aluminium will give a more detailed picture of the beam. The Talysurf will be interfaced with the Data Acquisition System as the quantity of data will be difficult to manipulate manually. It is proposed that these experiments will be conducted using several values of V_A, in order to investigate the beam divergence and uniformity dependencies.

Following this analysis, the cathode aperture could be redesigned. It is possible that an improvement in uniformity would arise from providing more widely spaced, smaller perforations at the centre of the graphite grid.

9.1.2 Control of Gas Flow

The time taken for the source to stabilise following energisation at room temperature can be a significant proportion of the duration of etching, as shown in Section 3.2.4. This period cannot be usefully employed as the characteristics of the beam are not constant. It is proposed that gas flow to the source is regulated by a mass flow controller. The anode voltage would be constantly sensed and the signal applied to the controller, which would adjust the flow to maintain the correct plasma

chamber pressure. In the case of a transient electrical disturbance (caused by, for example carbon particles on an insulator bush) the gas flow could be automatically reduced in order to increase V_A. The source could, with this type of control, operate unattended for extended periods.

9.1.3 Carbon Particulates

Operation of the source with fluorocarbons leads to an accumulation of particulate carbon on the plasma chamber liners and anode rods (see Section 3.2.3). Thermal cycling is thought to be responsible for the detachment of these deposits, which lead to electrical malfunction of the source. With the source in its present form and with single gases it is doubtful if there are any means of preventing this accumulation. The heating excursions of the plasma chamber components can, however, be reduced. The relatively high etch rates of SiO_2 and Si_3N_4 would permit a batch of wafers to be processed reasonably quickly (precise times cannot be calculated at present because of the dependence on other equipment-related parameters such as the required uniformity of etching and hence C.A.T.T.).

It would appear to be feasible to incorporate a load-lock system into the vacuum chamber and to operate the source continuously. A beam shutter, preferably actuated electro-mechanically would also be necessary for the protection of wafers during the source warm-up cycle.

9.1.4 The Production of Etchant Species

This proposal requires the use of a mass flow

controller, as already described. In this case the controller would be used primarily to measure the rate of gas flow to the source, rather than to regulate it. With a knowledge of the number of fluorocarbon molecules entering the source and the known quantity of target material removed, the beam characteristics could be investigated. This would reduce some of the uncertainty caused by the use of argon beam "current" data in experimental work with other gases. A quantitative estimation of the dissociation and etching reactions could also be attempted with this information.

9.1.5 Beam Energy Determinations

Ideally, three parameters should be measured for B93 argon and fluorocarbon beams:

(i) The maximum beam energy (V_B), as confirmation that

$$V_B = 0.85\ V_A$$

(ii) The range of particle energies present in the beam

(iii) The proportion of the beam attributed to each energy and its location.

If it is assumed that the beam "current" determinations are sufficiently accurate, the beam energy characteristics may be obtained indirectly by measuring beam power. A scanning calorimetric technique such as that described for ion implanter characterisation (Hemment, 1978) could be used for the three measurements. A similar design for the equipment could be used as the B93 beam area at a C.A.T.T. distance of 70 mm is similar to the dimensions of the implanter beam. The anticipated maximum power of $\simeq$700 mW at the centre of the beam is

significantly higher than that measured by Hemment and the profile is considerably less uniform.

9.2 ETCHING UNIFORMITY

The large variations in etch depth on targets exposed to the B93 beam are highly undesirable. It is apparent that some degree of movement of the wafer will be required to reduce these variations to acceptable levels. Rotary motion may be adequate provided the centre of the wafer is not concentric with the source axis. The most satisfactory solution is probably a planetary motion; plans are in hand for the construction of a water cooled target holder of this type.

Solutions to this problem should be considered in conjunction with those of improving beam current uniformity, and not in isolation.

9.3 ANGLE OF INCIDENCE OF THE BEAM

Both from an academic and a practical point of view, the etching characteristics of some targets with different beam angles should be investigated.

If the conclusions are correct that the etching mechanism by fluorinated beams is essentially chemical, then the etch rate dependence on beam angle should be minor or non-existent.

Structures with sloping features, such as holographic gratings, could be fabricated using reactive beams at various angles of incidence.

9.4 MASS SPECTROMETRY OF REACTIVE ION BEAMS

The use of this technique is anticipated to be of value in: (a) confirming that certain fluorocarbon

species exist in the beam and that the proposed reactions with silicon compounds do occur, and (b) the continuing study of RIBE using other halogenated compounds and different targets. Data from the considerable quantity of published literature on the mass spectrometry of halocarbon discharges will be used initially to establish the necessary sampling techniques.

9.5 ETCH RATE SELECTIVITIES

The experimental results indicate that relatively little control can be exercised over the type of species which can be extracted from the B93 source when injected with fluorinated gases. The addition of oxygen or hydrogen to fluorocarbons before injection into the B93 would probably not significantly alter the measured SiO_2: Si selectivities as the extracted species is probably CF_3^+. It is possible that this approach would lead to an increase in isotropy, caused by the diffusion of atomic fluorine.

The best approach is considered to be the use of different halogens, mixed before injection into the source, for example CF_4 and CCl_4. The concentrations of each compound could be adjusted individually to provide a wide range of etching conditions, from CF_3^+ rich to CCl_3^+ rich. Alternative methods would involve the use of gases of mixed halogens, such as halocarbon-13 ($CClF_3$) or halocarbon-13 B1 ($CBrF_3$), but it would be more difficult to predict results as mass-spectrometry data are scarce for the dissociation of such complex molecules.

9.6 ETCHING CHARACTERISTICS OF RESIST MATERIALS

Experimental work carried out for this study has indicated that the photoresist and electron-beam resists used possessed adequate adhesion and freedom from erosion. For the continuing study of sub-micron pattern definition, more emphasis will be placed on electron-beam resists. It will become important to investigate:

(i) resist edge profiles produced by electron beam lithography

(ii) resist edge profiles following curing treatments and the effect of beam heating

(iii) resist removal rates, which are particularly important during the etching of materials with low etch-rates (e.g. Si, Al)

(iv) the rate of removal of crosslinked resist in an oxygen plasma or other oxidising environment. For the measurement of resist thickness, non-contact methods such as ellipsometry, will probably be required.

10. GLOSSARY

Alignment

The precise location of one pattern (in mask or electron beam pattern generator) on a pattern previously etched into the wafer surface such that the two levels coincide along x and y axes. Misalignment is the second largest cause of reduced active device yield after particulate contamination.

Anisotrop(ic) (y)

Having physical properties that depend on direction. Hence anisotropic etchant: etching proceeds exclusively in the direction of particle flow (ion/particle beam) or direction of certain crystal planes (e.g. "V" groove etchant for silicon).

Barrel Etcher (Reactor)

Horizontal cylindrical or "barrel" shaped vacuum chamber in which wafers are etched by a reactive gas (halogenated) which is dissociated by electrical energy of radio frequency, usually by capacitive coupling through external electrodes.

Binding Energy (E_b, Units eV)

The energy which must be supplied to a molecule or polyatomic entity to dissociate it completely into atoms, each in its ground state.

C.A.T.T. (mm)

Dimension used in all etching work with Saddle Field Sources. Cathode Aperture To Target distance; 150 mm was the normal dimension when using the B93 source.

Downstream Etcher (Reactor)

Another term for a barrel etcher in which etchant species are swept over the wafers. The objects of the etching process are, therefore, downstream of the point at which dissociation occurs.

End Point (Determination, Detection, Monitoring)

Procedure or instrumental method for deciding the moment at which the target material has been removed by etching, thus preventing excessive damage to the lower layers. Of particular advantage in cases where the etch-rate selectivity is low.

Etch-Rate Ratio (Dimensionless)

The rate (e.g. Å min^{-1}) at which one material is etched divided by the rate at which another material is removed, using identical etchants and conditions. See Selectivity.

Facet

Sputter etched profile of less than 90° to the substrate. Formed as a result of the material etch rate dependence on angle of incidence of the bombarding particles.

Free Radical

Atomic species and complexes of abnormal valency which possess additive properties but do not carry an electrical charge and are not free ions.

Freon (Trade Mark)

A group of compounds that are chemically unreactive under normal conditions of temperature and pressure and are generally of low toxicity. All contain one or more halogen atoms (F, Cl, Br) per molecule and one or more carbon atoms, hydrogen may also be included. For basic data on four Freons see Appendix III.

Heated Filament Source

A device producing a beam of ions, working on the principle of dissociation of gas molecules by electrons thermally emitted from one or more filaments (the four tungsten filaments in a 6" "Veeco" Microetch source draw 50 amps). Commercially available equipment of this type was originally developed for space vehicle propulsion.

I_B

Beam "Current".

The "current" due to the beam from a Saddle Field Source (units: mA or μA). Not necessarily ion current.

I_D

Discharge Current.

The current drawn by the discharge in a Saddle Field Source (units: mA D.C.).

Ion Beam

The directional flow of charged particles.

Ion Beam Sputtering (Sputter Etching)

Another term for Ion Milling.

Ion Milling

Removal of material by sputtering using noble gas ions, usually in the form of a beam.

Ion Source

See Heated Filament Source.

Isotrop(ic) (y)

Having the same physical properties in all directions. Hence isotropic etchant: etching at the same rate in all directions.

Kaufman Source

For description see Heated Filament Source. Credit given to Prof. H.R. Kaufman for work done on developing ion sources for propulsion purposes ("ion thrusters").

Lithography

The process of pattern transfer:

(a) by exposure of sensitive polymeric material to radiation from (usually) electron beam or U.V. source

(b) by etching of the pattern into the surface not protected by resist.

Parallel Plate Etcher (Reactor)

See Planar Etcher.

Particle Beam

Directional flow of atoms or radicals without electrical charge.

Planar Etcher (Reactor)

Gas phase etching apparatus in which the discharge is confined between two horizontal electrode discs separated by a distance (usually between 10 and 40 mm) appropriate to the impedance-matching requirements of the R.F. supply. Wafers to be etched are placed on the lower electrode which may be cooled. The R.F. energy may be applied to the electrode on which the wafers rest, or on the upper disc, the second is always earthed.

Radical

See Free Radical.

Reactive Ion Beam Etching (R.I.B.E.)

Removal of material using a beam of chemically reactive species directed at the target surface. The beam may or may not contain ions at the moment of impact at the solid surface. "Kaufman" sources are usually equipped with a heated filament immersed in the beam to provide a copious supply of electrons for neutralising the ion charge. Material removal may be by chemical or sputtering processes or a combination of both.

Reactive Ion Etching (R.I.E.)

Plasma etching at chamber pressures in the range 0.01 to 0.14 torr. This is usually done in a planar reactor, anisotropy is improved by attaching the wafers to the earthed electrode. The principle mechanism of material removal is by chemical reaction with ionic species produced by the dissociation of (usually) a parent halocarbon.

Reactive Ion Milling

Another term for reactive ion beam etching.

Reactive Sputter Etching

A hybrid technique for material removal by sputtering and chemical reaction (see R.I.B.E.).

Redeposition

Aggregation of sputtered atoms into particulate debris. The debris may collect on pattern sidewalls to form a "fence" which remains after resist removal, or may settle as amorphous lumps.

Saddle Field Source

A cold cathode source producing a beam of ions and/or energetic atoms. The discharge within the source is sustained by electrons describing oscillatory trajectories between the cathodes and the "saddle point" centrally between the anodes.

Selectivity

The preferential etch rate of one material compared to that of another, for a given etchant. There are two definitions:

(i) Dynamic selectivity: the etch rate ratio of two materials on the same wafer; one is the first

target, the second is subsequently exposed and becomes a target after a given time.

(ii) Passive selectivity: the etch rate ratio for two materials obtained by separately etching one target followed by another under identical conditions.

Sputtering, Sputter-Etching

The physical removal of atoms from the surface of a material by bombardment with particles of high mass and energy. Argon is frequently used on account of its mass (atomic weight 40), energies above $\simeq 200$ eV are typical.

Substrate

In this work the substrate was silicon. Describes the support medium for the film being etched, and may or may not contribute to the electrical characteristics (e.g. S.O.S. devices use a sapphire wafer as substrate purely as mechanical support of high resistivity).

Target

Material that is the object of the etching process. Resist is nearly always a "target" as it is exposed to etchant simultaneously with the underlying film or bulk material.

Threshold Limit Value (T.L.V.)

There are three values:

The time weighted average (TWA), the short term exposure limit (STEL) and the ceiling (C), of which the first is most usually referred to: The average concentration for a normal 8 hour workday or 40 hour workweek, to which all workers may be repeatedly exposed, day after day, without adverse effect. As defined in 1978 by the American Conference of Governmental Industrial Hygienists.

Trench

Undesirable topographical feature that may be produced during sputtering. Ions reflected from the side of a raised feature (e.g. resist pattern) may sputter material away to form a "groove" or "trench" at the foot of that feature.

V_A

Anode potential (units: kV) - Saddle Field Source only.

$\underline{V}_B$

Beam energy (units: keV) - assumed that the beam from the Saddle Field Source is essentially monoenergetic.

VLSI

Very Large Scale Integration, in which the density of components exceeds 10^4 gates per chip. The area occupied by each gate is being constantly reduced, a U.S.A. 1981 production value is approximately 510 μm^2 per gate on a chip size of 7.6 x 7.6 mm (Douglas, 1981).

Work Function

Energy which must be supplied to free electrons possessing energy E, to enable them to escape from the material (usually metal).

Yield (Production Yield)

The proportion, usually expressed as a percentage, of fully functioning integrated circuits compared to the total produced from 1 wafer.

11. REFERENCES

1. Ahn, K.Y. and Schwartz, G.C. (1978) "Fabrication of mask for dry etching of microcircuits" I.B.M. Tech. Discl. Bull., 21, 4, 1713.

2. Almen, O. and Bruce, G. (1961) "Collection and sputtering experiments with noble gas ions" Nucl. Instr. Meth., 11, 257.

3. Attwood, S.S. "Electric and magnetic fields", Dover, New York, 1967, pp 49.

4. Baker, M.A., et. al. (1971) "The use of perfluoroalkyl polyether fluids in vacuum pumps" Vacuum, 21, 10, 479.

5. Beghin, C. (1979) "Plasma physics investigations on the first Spacelab payload" E.S.A. Jnl. 3, 2, 123.

6. Bell, C.F. and Lott, K.A.K. (1966) "Modern approach to inorganic chemistry" Butterworths.

7. Belson, J. and Wilson, I.H. (1979) "Hydrogen and Deuterium Ion Bombardment Effects in SiO_2 films" I.E.E.E. Trans. Nucl. Sci., NS-26, 6, 4819.

8. Bersin, R.L. (1976) "A survey of plasma etching processes" Sol. St. Technol., May 1976, 31.

9. Bersin, R.L. (1978) "Chemically selective, anisotropic plasma etching" Sol. St. Technol., April 1978, 117.

10. Bohg, A. (1971) "Ethylene diamine-pyrocatechol-water mixture shows etching anomaly in boron-doped silicon" J. Electrochem. Soc; Electrochem. Technol., 118, 2, 401.

11. Bollinger, L.D. (1977) "Ion milling for semiconductor production processes" Sol. St. Technol., November 1977, 66.

12. Bollinger, L.D. and Fink, R. (1980) "A new production technique: Ion Milling" Sol. St Technol., November 1980, 79.

13. Boyd, H. and Tang, M.S. (1979) "Applications for silicon tetrafluoride in plasma etching" Sol. St. Technol., April 1979, 133.

14. Brandes, R.G. and Dudley, R.H. (1973) "Wall profiles produced during photoresist masked isotropic etching" J. Electrochem. Soc., Sol. St. Sci. Technol., 120, 1, 140.

15. Brown, D.M. et. al. (1980) "Reactive ion beam etching of SiO_2 and polycrystalline silicon" Appl. Phys. Lett. 37, 2, 159.

16. Bruce, R.H. et. al. (1981) "Frequency effects in chlorine plasma etching" Proc. October 1981 Meeting of the Electrochemical Society.

17. Burger, R.M. and Donovan, R.P. (1967) (Editors) "Fundamentals of silicon integrated device technology" Prentice-Hall.

18. Burggraaf, P.S. (1980) "C-V plotting, C-T measuring and dopant profiling: applications and equipment" Semiconductor International, October 1980, 29.

19. Cadogan, J.I. (1973) "Principles of free radical chemistry" Chemical Society Monograph for Teachers, Number 24.

20. Cannon, D.L. et. al. (1974 "MOS Integrated Circuits: Course Lesson Summary" Texas Instruments Inc.

21. Cantagrel, M. and Marchal, M. (1973) "Argon ion etching in a reactive gas" J. Mater. Sci., 8, 1711.

22. Chinn, J.D. et. al. (1981) "Reactive ion etching for submicron structures" IEEE 16th Symposium on Electron, Ion and Photon beam technology, Dallas, May 1981.

23. Chopra, K.L. (1969) "Thin film phenomena" McGraw-Hill.

24. Cobilt, (1981) Specified performance for Autolign CA3400 Projection Mask Aligner, data sheet 2032/681/3K.

25. Coburn, J.W. et. al. (1977) "Ion-surface interactions in plasma etching" J. Appl. Phys., 48, 8, 3532.

26. Coburn, J.W. and Kay, E. (1979) "Some chemical aspects of the fluorocarbon etching of silicon and its compounds" Sol. St. Technol., April 1979, 117.

27. Coker, C. (1980) "Lithography and pattern scaling for VLSI" Proc. Internepcon 1980, 320.

28. Cotton, F.A. and Wilkinson, G. (1967) "Advanced inorganic chemistry" Interscience.

29. Cullen, G.W. (1978) "Automatic measurement techniques" Chapter 6 of "Heteroepitaxial semiconductors for electronic devices" Springer-Verlag, New York.

30. d'Agostino, R. and Flamm, D.L. (1981) "Plasma etching of Si and SiO_2 in SF_6-O_2 mixtures" J. Appl. Phys. 52, 1, 162.

31. Davidse, P.D. and Maissel, L.I. (1967) "Equivalent D.C. sputtering yields of insulators" J. Vac. Sci. and Technol., 4, 1, 33.

32. Deal, B.E. (1974) "The current understanding of charges in the thermally oxidised silicon structure" J. Electrochem. Soc., Reviews and News, 121, 6, 198C.

33. Dean, P. and Hibbins-Butler, D.C.; cited by McIlraith (1972), not located in the published literature.

34. Dionex (1979) "Plasma etching silicon nitride" Dionex Corporation Technical Data, sheet 71/79.

35. Doken, M. and Miyata, I. (1979) "Etching uniformities of silicon in CF_4 + 4% O_2 plasma" J. Electrochem. Soc., Sol. St. Sci. and Technol., 126, 12, 2235.

36. Donnelly, V.M. and Flamm, D.L. (1981) "Anisotropic etching in chlorine-containing plasmas" Sol. St. Technol., April 1981, 161.

37. Donnelly, V.M. et. al. (1981) "Studies of plasma etching of III-V compounds, using in-situ optical diagnostic techniques" Proc. October 1981 Meeting of the Electrochemical Society.

38. Douglas, E.C. (1981) "Advanced process technology for VLSI circuits" Sol. St. Technol., May 1981, 65.

39. Downey, D.F. et. al. (1981) "Introduction to reactive ion beam etching" Sol. St. Technol., February 1981, 121.

40. Eckertová, L. (1977) "Physics of thin films" Plenum.

41. Electrotech Ltd., Abercarn, Gwent, NP1, 5AR.

42. Ephrath, L.M. (1979) "Two step dry process for delineating micron and submicron dimension polysilicon gates" I.B.M. Tech. Discl. Bull., 21, 10, 4236.

43. Evans, A.C. (1981) personal communication.

44. Finar, I.L. (1967) "Organic Chemistry" Volume I, Longmans.

45. Fitch, R.K. et. al. (1970) "A new type of ion source" J. Phys. D: Appl. Phys., 3, 1399.

46. Fitch, R.K. and Rushton, G.J. (1971) "Low pressure ion source" J. Vac. Sci. Technol., 9, 1, 379.

47. Fitch, R.K. et. al. (1974) "Design and operating characteristics of a low pressure ion source" Jap. J. Appl. Phys., Suppl. 2, Pt. 1, 411.

48. Fitch, R.K. et. al. (1981) "Temperature limitation of a Saddle-Field ion source" Vacuum, 31, 19.

49. Flamm, D.L. (1979) "Measurements and mechanisms of etchant production during the plasma oxidation of CF_4 and C_2F_6" Sol. St. Technol., April 1979, 109.

50. Flamm, D.L. (1981) "Downstream Mass Spectrometry" UTI Jnl., 3, 3, 1.

51. Flamm, D.L. et. al. (1980) "Etching and film formation in CF_3Br plasmas: some qualitative observations and their general implications" J. Vac. Sci. and Technol., 17, 6, 1341.

52. Flamm, D.L. et. al. (1981,a) "Frequency and ion effects in chlorine plasma etching" Proc. 5th International Symposium on Plasma Chemistry, Edinburgh, August 1981.

53. Flamm, D.L. et. al. (1981,b) "The reaction of fluorine atoms with silicon" J. Appl. Phys. 52, 5, 3633.

54. Franks, J. (1972,a) "The twin anode ion source" Proc. 2nd International Conference on Ion Sources, Vienna.

55. Franks, J. (1972,b) British Patent 54627/72.

56. Franks, J. (1974) British Patent 30249/74.

57. Franks, J. (1977) "Ion techniques to prepare specimens for electron microscopy" Inst. Phys. Conf. Ser. No. 36, Ch. 1, 57.

58. Franks, J. (1979) "Properties and applications of Saddle-Field ion sources" J. Vac. Sci. Technol., 16, 2, 181.

59. Franks, J. (1980) "Ion beam deposition of coatings for high resolution SEM" Proc. Micro '80, Proceedings of the Royal Microscopical Society, 15, 5.

60. Franks, J. and Ghander, A.M. (1974) "A Saddle-Field ion source of spherical configuration for etching and thinning applications" Vacuum, 24, 10, 489.

61. Franks, J. et. al. (1979) "Ion enhanced film bonding" Thin Solid Films, 60, 231.

62. Freeman, G.H.C. and Guern, Y. (1978) "The behaviour of the Saddle-Field ion source with different gases and its possible use as a source of ions for atomic spectroscopy" National Physical Laboratory Report QU49.

63. FREON: Trade mark of the DuPont Company.

64. Gdula, R.A. et. al. (1978) "Method of controlling RIE mesa edge profiles to eliminate mouseholing" I.B.M. Tech. Discl. Bull. 21, 6, 2327.

65. Geipel, H.J. (1977) "End point detection for reactive ion etching" I.B.M. Tech. Discl. Bull., 20, 2, 541.

66. Ghander, A.M. (1976) "A powerful oscillating electron electrostatic ion source" Atomkernenergie, 28, 3, 158.

67. Ghander, A.M. and Fitch, R.K. (1973) "A double beam ion source" Vacuum, 23, 8, 269.

68. Ghander, A.M. and Fitch, R.K. (1974) "An improved form of the oscillating electron electrostatic ion source for ion etching" Vacuum, 24, 10, 483.

69. Gibbons, J.F. et. al. (1969) "Ion-bombardment-enhanced etching of silicon" Appl. Phys. Lett. 15, 4, 117.

70. Gibbons, J.F. et. al. (1975) "Projected range statistics for semiconductor and related materials" Dowder, Hutchinson and Ross.

71. Gill, M.D. (1980) "A simple technique for monitoring undercutting in plasma etching" Sol. St. Electronics, 23, 995.

72. Gloersen, Per G. (1976) "Masking for ion beam etching" Sol. St. Technol., 19, 4, 68.

73. Goetzberger, A. (1966) "Ideal MOS curves for silicon" Bell Sys. Tech. J., September 1966, 1097.

74. Gokan, H. and Esho, S. (1981) "Pattern fabrication by oblique incidence ion beam etching" J. Vac. Sci. and Technol., 18, 1, 23.

75. Goldspink, G.F. and Revell, P.J. (1980) "The use of Saddle-Field ion sources for etching semiconductor materials" Microelectronics Jnl. 11, 6, 13.

76. Grove, A.S. (1967) "Physics and Technology of semiconductor devices" J. Wiley and Sons.

77. Hall, H.E. (1978) "Solid State Physics" John Wiley and Sons, England.

78. Handbook of Chemistry and Physics (1963), 44th Edition, C.D. Hodgman (Editor) Chemical Rubber Publishing Company.

79. Harper, J.M.E. et. al. (1981) "Low energy ion beam etching" J. Electrochem. Soc., 128, 5, 1077.

80. Hayes, J. and Pandhumsoporn, T. (1980) "Planar plasma etching of polycrystalline silicon" Sol. St. Technol., November 1980, 71.

81. Health and Safety Executive (1981), Guidance Notes EH/15/80, H.M.S.O.

82. Heinecke, R.A.H. (1975) "Control of relative etch rates of SiO_2 and Si in plasma etching" Sol. St. Elect. 18, 1146.

83. Heinecke, R.A.H. (1976) "Plasma reactor design for the selective etching of SiO_2 on Si", Sol. St. Elect. 19, 1040.

84. Hemment, P.L.F. (1978) "Calorimetric measurements of the neutral beam present in a 500 keV ion implanter" Inst. Phys. Conf. Ser. Number 38, pp 117-124.

85. Heslop, C.J. (1980,a) "Reactive plasma processing in I.C. manufacture", Electronic Production, February 1980, 44.

86. Heslop, C.J. (1980,b) "Plasma etching" Proc. Internepcon, October 1980, 310.

87. Hitchman, M.L. and Eichenberger, V. (1980) "A simple method of end point determination for plasma etching" J. Vac. Sci. Technol., 17, 6, 1378.

88. Hollahan, J.R. and Bell, A.T. (Eds) (1974) "Techniques and applications of plasma chemistry" Wiley and Sons, New York.

89. Holland, L. (1972) "Ion impact sputtering for etching and micro machining" Electron. Comp. 13, 10, 493.

90. Holland, L. et. al. (1973) "A simple pumping combination to reduce organic contamination in an electron microscope" Jap. J. Appl. Phys., 12, 9, 1468.

91. Horiike, Y. et. al. (1979) "Si and SiO_2 etching characteristics by fluorocarbon ion beam" Japan. J. Adv. Phys. 18, 12, 2309.

92. Hosaka, S. et. al. (1981) "Impurity contamination of the SiO_2 layer on Si wafers during ion etching" J. Vac. Sci. Technol., 18, 1, 17.

93. Hughes, H. and Baxter, R.D. (1972) IEEE Trans. Nucl. Sci., 19, 6, 256.

94. Hunter, W.R. et. al. (1978) "One micrometer electron-beam lithography FET technology" Proc. IEEE Electron Devices Meeting, December 1978, p 54.

95. Ianno, N.J. and Verdeyen, J.T. (1981) "Comparison of the etching and plasma characteristics of discharges in CF_4 and NF_3" Electrochemical Society Spring Meeting 1981, Extended abstracts, p 166.

96. Iizuka, T. (1980) "Fully static 16 kbit bulk CMOS RAM" Proc. IEEE International Solid State Circuits Conference, 1980.

97. Ion-Tech Ltd., 2, Park Street, Teddington, Middx.

98. Irving, S.M. (1971) "A plasma oxidation process for removing photoresist films" Sol. St. Technol., June 1971, 47.

99. Irving, S.M. et. al. (1971) "Gas plasma vapor etching process" U.S. Patent 3,615,956, October 1971; Assignee, Signetics Corp.

100. Jacob, A. (1976) "The versatile technique of RF plasma etching. Part I: The etch profile" Sol. St. Technol., Sept. 1976, 70.

101. Kaufman, H.R. (1978) "Technology of ion beam sources used in sputtering" J. Vac. Sci. Technol., 15, 2, 272.

102. Kaufman, H.R. and Robinson, R.S. (1981) "Ion source design for industrial applications" NASA report CR-165334.

103. Koch, F.B. et. al. (1974) "Implantation of argon into SiO_2 films due to backsputter cleaning" J. Electrochem. Soc., Sol. St. Sci. and Technol., April 1974, 558.

104. Kumar, R. et. al. (1976) "Characterisation of plasma etching for semiconductor applications" Sol. St. Technol., October 1976, 54.

105. Kushner, R.A. et. al. (1974) "Mobilisation of sodium in SiO_2 films by ion bombardment" Phys. Rev. B, 10, 6, 2632.

106. Kynaston, D. (1970) "Away with sliced up specimens" New Scientist, February 5, 1970, 256.

107. Laegreid, N. and Wehner, G.K. (1961) "Sputtering yields of metals for Ar^+ and Ne^+ ions with energies from 50 to 600 eV" J. Appl. Phys., 32, 3, 365.

108. Lee, M.H. and Schwartz, G.C. (1980) "Reactive ion etching process" I.B.M. Tech. Discl. Bull., 22, 8A, 3347.

109. Lee, R.E. (1979) "Microfabrication by ion-beam etching" J. Vac. Sci. Technol., 16, 2, 164.

110. Lewis, G.W. et. al. (1980) "Dynamic study of ion etching in a high resolution S.E.M. J. Mater, Sci., 15, 681.

111. Maddox, R.L. (1980) "The new microelectronic processing technology; a review of the state-of-the-art" Microelectronics Jnl. 11, 1, 4.

112. Mader, L. and Hoepfner, J. (1976) "Ion beam etching of silicon dioxide on silicon" J. Electrochem. Soc.: Sol. St. Sci. and Technol., 123, 12, 1893.

113. Maniv, S. and Westwood, W.D. (1980) "Discharge characteristics for magnetron sputtering of Al in Ar and Ar/O_2 mixtures" J. Vac. Sci. and Technol., 17, 3, 743.

114. Matsui, S. et. al. (1980) "Fabrication of SiO_2 blazed holographic gratings by reactive ion etching" Japan. J. Appl. Phys. 19, 3, L126.

115. Mayer, T.M. et. al. (1981) "Investigation of plasma etching mechanisms using beams of reactive gas ions" J. Vac. Sci. and Technol., 18, 2, 349.

116. McCaughan, D.V. and Murphy, V.T. (1973) "Low energy ion bombardment of SiO_2 films on Si. Pt. II: Inert ambient annealing of degradation in MOS devices" J. Appl. Phys. 44, 7, 3182.

117. McCaughan, D.V. and Kushner, R.A. (1974) "Degradation of oxide films due to radiation effects in exposure to plasmas in sputter deposition and backsputtering" Proc. IEEE, 62, 9, 1236.

118. McCaughan, D.V. et. al. (1980) "Effects of bombardment by low energy neutral particles on SiO_2 films" J. Appl. Phys. 51, 1, 299.

119. McClure, G.W. (1963) "Low pressure glow discharge" Appl. Phys. Lett. 2, 12, 233.

120. McDaniel, E.W. (1964) "Collision phenomena in ionised gases" John Wiley and Sons.

121. McIlraith, A.H. (1966) "A charged particle oscillator" Nature, 212, 1422.

122. McIlraith, A.H. (1972) "A charged particle oscillator" J. Vac. Sci. Technol., 9, 1, 209.

123. McTaggart, F.K. (1967) "Plasma chemistry in electrical discharges" Elsevier.

124. Mead, C. and Conway, L. (1980) "Introduction to VLSI systems" Addison-Wesley.

125. Melliar-Smith, C.M. (1976) "Ion etching for pattern delineation" J. Vac. Sci. and Technol., 13, 5, 1008.

126. Meusemann, B. (1979) "Reactive sputter etching and reactive ion milling-selectivity, dimensional control, and reduction of MOS interface degradation" J. Vac. Sci. and Technol., 16, 6, 1886.

127. M.I.T.E. Chrome-on-glass resolution test pattern mask manufactured by Micro Image Technology (Engineering) Ltd., Derby.

128. Mogab, C.J. (1977) "The loading effect in plasma etching" J. Electrochem. Soc; Sol. St. Sci. and Technol., 124, 8, 1262.

129. Mogab, C.J. and Levinstein, H.J. (1980) "Anisotropic plasma etching of polysilicon" J. Vac. Sci. Technol., 17, 3, 721.

130. Moore, G. (1975) "Progress in digital integrated electronics" IEEE Technical Digest of the International Electron Devices Meeting, 1975, p 11.

131. Moore, R. et. al. (1981) "Electron beam writes next generation I.C. patterns" Electronics, November 3, 1981, 138.

132. Neureuther, A.R. et. al. (1979) "Modelling ion milling" J. Vac. Sci. and Technol., 16, 6, 1767.

133. New Scientist (1981) "Argon gun shoots solids into mass spectrometer" New Scientist, 16 July 1981, 149.

134. Poulsen, R.G. (1977) "Plasma etching in integrated circuit manufacture" J. Vac. Sci. Technol., 14, 1, 266.

135. Rai-Choudhury, P. (1971) "Sulphur hexafluoride as an etchant for silicon" J. Electrochem. Soc. 118 2, 266.

136. Revell. P.J. (1979,a) Third quarterly technical progress report to ACTP, Department of Industry, August 1979.

137. Revell, P.J. (1979,b) Second quarterly technical progress report to ACTP, Department of Industry, April 1979.

138. Revell, P.J. (1980) Final report to ACTP, Department of Industry, January 1980.

139. Revell, P.J. and Evans, A.C. (1982) To be published in Thin Solid Films. See this work, Chapter 12, number 3.

140. Robb, F. (1979) "High resolution polysilicon etching" Semiconductor International, Dec. 1979, 60.

141. Roberts, J.D. and Caserio, M.C. (1965) "Basic principles of organic chemistry" W.A. Benjamin.

142. Robinson, R.S. (1979) "Physical processes in directed ion beam sputtering" Ph.D. Thesis, Colorado State University. NASA Report CR-159567.

143. Rodionov, Y.A. et. al. (1980) "Compensation method for plasma etching (deposition) control monitor" Zb. Rad. Jurema, 25, 2, 117.

144. Rushton, G.J. and Fitch, R.K. (1971) "The performance of the twin wire electrostatic charged particle oscillator" Vacuum, 21, 10, 449.

145. Rushton, G.J. et. al. (1973), "Modes of operation of an electrostatic ion gun" J. Phys. D: Appl. Phys., 6, 1167.

146. Saddle-Field source: Trade Mark of Ion-Tech (UK) Ltd.

147. Sax, N.I. (1979) (Editor) "Dangerous properties of industrial materials" Fifth edition, Van Nostrand.

148. Schaible, P.M. et. al. (1978) "Reactive ion etching of aluminium and aluminium alloys in an R.F. plasma containing halogen species" J. Vac. Sci. Technol., 15, 2, 334.

149. Schwartz, G.C. et. al. (1976) "Reactive ion etching" Proc. Spring 1976 Meeting, Electrochemical Society, Washington D.C.

150. Schwartz, G.C. et. al. (1979) "Competitive mechanisms in reactive ion etching in a CF_4 plasma" J. Electrochem. Soc., Sol. St. Sci. and Technol., 126, 3, 464.

151. Schwartz, G.C. and Schaible, P.M. (1980) "Reactive ion etching in chlorinated plasmas" Sol. St. Technol., November 1980, 85.

152. Sigmund, P. (1969) "Theory of Sputtering, I: sputtering yield of amorphous and polycrystalline targets" Phys. Rev. 184, 2, 383.

153. Smolinsky, G. et. al. (1981) "Plasma etching of III-V compound semiconductor materials and their oxides" J. Vac. Sci. and Technol., 18, 1, 12.

154. Southern, A.L. et. al. (1963) "Sputtering experiments with 1 to 5 keV Ar^+ ions" J. Appl. Phys. 34, 1, 153.

155. Spencer, E.G. and Schmidt, P.H. (1971) "Ion beam techniques for device fabrication" J. Vac. Sci. and Technol., 8, 5, S52-S70.

156. Steinfeld, J.I. et. al. (1980) "Surface etching by laser generated free radicals" J. Electrochem. Soc., Electrochem. Sci. and Technol., 127, 2, 514.

157. Stinson, L.J. et. al. (1976) "SF_6 etching effects in silicon" J. Electrochem. Soc., Sol. St. Sci. and Technol., 123, 4, 551.

158. Stirling, C.J.M. (1965) "Radicals in organic chemistry" Oldbourne.

159. Suzuki, K. (1978) "Behaviour of ions and neutral radicals in microwave plasma etching" Proc. 1978 Meeting of the Institute of Electronic and Communications Engineers of Japan.

160. Texas Instruments Bubble Memories. Technical Data for device type TBM 0101.

161. Tombs, N.C. and Sewell, F.A. (1968) J. Electrochem. Soc; Sol. St. Sci. and Technol, 115, 1, 101.

162. Townsend, P.D. (1970) "Ion beams in optics - an introduction" Optics Technology, May 1970, 65.

163. Ukai, K. and Hanazawa, K. (1979) "End point determination of aluminium reactive ion etching by discharge impedance monitoring" J. Vac. Sci. Technol., 16, 2, 385.

164. Vasile, M.J. (1980) "Etching of SiO_2 and Si in a He-F_2 plasma" J. Appl. Phys. 51, 5, 2510.

165. Wang, D.N.K. and Maydan, D. (1981) "Dry etching technology for fine line devices" Sol. St. Technol., May 1981, 121.

166. Ward, R. (1981) "Electron-beam projector suits up for submicrometer race" Electronics, November 3, 1981, 144.

167. Weikel, T.D. and Yuen, H.H. (1972) "Vacuum pump explosion study" U.S. Naval Air Engineering Centre Document NAEC-GSED-60, August 1972.

168. Weisberg, L.R. (1978) "The new D.O.D. initiative in integrated circuits" IEEE Technical Digest of the International Electron Devices Meeting, 1978, p 684.

169. Wilson, I.H. (1973) "The topography of sputtered semiconductors" Radiation Effects, 18, 95.

170. Zaininger, K.H. and Heiman, F.P. (1970,a) "The C-V technique as an analytical tool. Part 1" Sol. St. Technol., May 1970, 49.

171. Zaininger, K.H. and Heiman, F.P. (1970,b) "The C-V technique as an analytical tool. Part 2" Sol. St. Technol., June 1970, 46.

12 PUBLICATIONS

This section lists, in chronological order, the publications by the author.

1. Revell, P.J. and Goldspink, G.F. "The use of Saddle-Field Ion Sources for Etching Semiconductor Materials". Paper presented at Microcircuit Engineering '80, September 30, October 1-2, 1980, Amsterdam. Proceedings p.543.
2. Goldspink, G.F. and Revell, P.J. "The use of Saddle-Field Ion Sources for Etching Semiconductor Materials". Microelectronics Journal, 11, 6, 13, 1980.
3. Revell, P.J. and Evans, A.C. "Ion Beam Etching using Saddle-Field Sources". Paper presented at the Seminar on Film Preparation and Etching by Plasma Technology, University of Sussex, 25-27 March, 1981. To be published in Thin Solid Films.
4. Revell, P.J. and Goldspink, G.F. "Reactive Ion Beam Etching of Silicon Compounds with a Saddle-Field Ion Source". Paper K-4 presented at the IEEE 16th Symposium on Electron, Ion and Photon Beam Technology, Dallas, 26-29 May, 1981. To be published in the Journal of Vacuum Science and Technology.

APPENDIX I

PREPARATION OF SPECIMENS FOR ETCHING

1. WAFERS

All were single crystal silicon, polished on one side only.

For the majority of etching experiments, 280 μm thick, 38 mm diameter wafers of n type, (1,1,1) orientation and 3-6 ohm-cm resistivity were used.

For the Radiation Damage Studies, 318 μm thick, 50 mm diameter, n type (1,1,1) orientation and 9-15 ohm-cm resistivity were used.

2. PRECLEAN

All wafers were cleaned initially as follows:

2.1 Wash in ultrasonically agitated isopropyl alcohol (IPA) for 5 min, blow dry with warm nitrogen.
2.2 Spin rinse with deionised water (D.I.W.) for 5 min, spin dry for 2 min.
2.3 Dip in 20:1 hydrofluoric acid (HF):D.I.W. for 1 min.
2.4 Rinse in D.I.W., spin rinse with D.I.W. for 5 min, spin dry for 2 min.
2.5 Immerse in boiling concentrated nitric acid (c.HNO_3) or 1:1 concentrated sulphuric acid (c.H_2SO_4:100 volume hydrogen peroxide (100 v H_2O_2) for 1 min.
2.6 Rinse in D.I.W., spin rinse with D.I.W. for 5 min, spin dry for 2 min.
2.7 Immerse in 20:1 HF:D.I.W. for $\frac{1}{2}$ min.
2.8 Rinse in D.I.W., spin rinse with D.I.W. for 5 min, spin dry for 2 min.

After cleaning, wafers were either coated with resist for Si etching experiments, deposited with nitride or oxidised by one of two methods.

3. FORMATION OF "THICK" OXIDE

(all SiO_2 etching experiments except for C-V measurements)

Using the specified times and conditions, the SiO_2 films were found to be approximately 1 μm thick.

3.1 Steam clean the furnace (1000°C) with wet oxygen for 2 hours.
3.2 Insert wafers, positioned vertically in quartz boat at end of furnace, allow to equilibrate for 10 min with dry oxygen flowing. Move boat to centre of furnace.

3.3 $4\frac{1}{2}$ hours oxidation with nitrogen, oxygen and water vapour.
3.4 20 min anneal in dry nitrogen.
3.5 Withdraw boat to end of furnace, remove after 5 min.

4. FORMATION OF OXIDE FOR RADIATION DAMAGE STUDIES

To produce SiO_2 films of approximately 1000 Å thickness. Follow steps 2.1 to 2.8 and 3.1, then:

4.1 Purge the furnace tube (1000°C) with N_2 for 5 min.
4.2 Insert wafers, positioned vertically in quartz boat at end of furnace, allow to equilibrate for 10 min with N_2 flowing.
4.3 Move boat to centre of furnace.
4.4 2 hours 10 min dry oxidation with equal flow of N_2 and O_2.
4.5 1 hour dry N_2 anneal.
4.6 Withdraw boat to end of furnace, remove after 5 min.

5. SILICON NITRIDE DEPOSITION

Follow steps 2.1 to 2.8.

Wafers were positioned horizontally on a quartz plate and placed at the centre of a furnace tube at 800°C. Silicon tetrachloride ($SiCl_4$) vapour, generated by bubbling dry N_2 through a liquid source of the compound was mixed with ammonia (NH_3) and passed into the furnace. Typical film thicknesses were of the order of 2000 Å, which were deposited in approximately 15 min.

6. ALUMINIUM FILMS

Gate electrode metallisation for the Radiation Damage Studies was carried out in a commercial MOS fabrication facility. Specific details of the process were not released.

Aluminium films for etch depth and topography studies were prepared either by electron beam evaporation (usual thickness of film 2000 Å) or by thermal evaporation from tungsten filaments (usual thickness 1.2 μm).

7. TUNGSTEN FILMS

Sputtered in an argon discharge from a pure (99.9999%) tungsten target onto heated substrates. Film thickness was usually ≃ 2000 Å

8. RESIST MATERIALS Using Kodak Microneg 747 (negative working resist)

Photolithography was carried out as follows:

8.1 Bake the slice for 10 min at 130 $\pm$ 5°C.

8.2 Coat the slice with resist and spin for 30 $\pm$ 1 seconds at 6000 r.p.m. The resulting film was 6000 Å thick.

8.3 Bake the slice for 10 min at 80 $\pm$ 5°C.

8.4 Align mask and expose to U.V. for 6.5 $\pm$ 1 seconds (1.5-3 seconds for Al and W films).

8.5 Spray develop the resist with proprietary developer for 30 seconds.

8.6 Spray rinse the slice with proprietary rinse solvent for 20 seconds.

8.7 Blow dry with warm N_2.

8.8 Bake the slice for 15 min at 130 $\pm$ 5°C.

Electron beam lithography was carried out at the E.B.M.F. facility of the S.E.R.C. Rutherford Laboratory. The details of resist application and development were as follows:

8.9 Wafer pre bake.

8.10 Coat the slice with PMMA and spin at 7000 r.p.m. The resulting film was $\simeq$ 9000 Å thick.

8.11 Post bake at 160°C in vacuum for 15 min.

8.12 Electron beam exposure.

8.13 Develop the resist with methyl isobutyl ketone (MIBK), 5 min.

8.14 Blow dry with warm N_2.

8.15 Final bake, 100°C maximum at atmospheric pressure.

9. MASKS

Two masks were used for U.V. photolithography:

(i) A pattern consisting of a series of parallel lines arranged in groups. The linewidth and spacing between the lines was approximately equal (4.5 μm).

(ii) A commercially available resolution test pattern (Micro Image Technology Ltd.) with positive and negative alternately arranged across the mask. The smallest features were 1.2 μm equal mark-space ratio bars and spaces.

Electron beam direct-writing was used to define a regular array of bars with widths ranging from 20 μm down to 0.5 μm. The beam energy was 20 keV and the exposure dose 1.92×10^{-5} $c.cm^{-2}$. As the wafers were of a size incompatible with the substrate clamps in the electron beam unit, some of the patterns were incorrectly exposed and loss of definition resulted.

APPENDIX II

Experimental Procedure for Ion Beam Etching using the B93 Source

1. EQUIPMENT

The vacuum system was a CVC model PSM66 with electro-pneumatic valves. The rotary pump was charged with Sargent-Welch "Duo-Seal" oil and the diffusion pump contained Convoil-20. During operation of the vacuum system the chevron baffle was usually maintained at $77^{o}K$ by pumping liquid nitrogen. The foreline was not fitted with a trap. The vacuum chamber was Pyrex glass, 18 inches (457 mm) diameter and 24 inches (610 mm) long. The top plate was machined Dural, 1" (25.4 mm) thick. The B93 was mounted centrally from the top plate and water, gas and electrical connections were made to the source through one feed through duct. The aluminium water-cooled target holder was fixed beneath the source and on the same axis. The distance between the cathode aperture and the target front face (C.A.T.T.) was fixed at 150 mm (except for certain, specified experiments). The beam shutter, which was added late in this study intercepted the beam at about 30 mm from the cathode aperture.

2. EVACUATION

When not in use the vacuum chamber was isolated in an evacuated condition. Venting of the chamber to atmospheric pressure was carried out with the admission of oxygen-free nitrogen from a cylinder. The top plate was only removed from the chamber long enough to change samples. Maintenance of the source was carried out whilst the chamber was evacuated with a second, blank top plate in position. Evacuation to a base pressure of at least 1.2×10^{-5} torr (CVC ionisation gauge) was carried out before each experiment.

3. SAMPLES

The target holder was constructed to hold one wafer and a milled recess ensured reproducible positioning. On samples to be used for topographical studies, a very light smear of thermally-conducting grease (R.S. components "heat-sink compound") was applied to the target holder, and the wafer was gently pressed into position using tweezers.

Samples intended to provide "absolute" etch rate data were positioned as described. A rectangle of stainless steel was screwed to the holder such that the

wafer was masked from the beam over an area of several square centimetres. This mask provided three straight edges along which step-height measurements were made.

4. ETCHING

With the beam shutter closed, gas was admitted to the source until the chamber pressure was approximately 5×10^{-4} torr and the high voltage supply was energised at zero current setting. The discharge current was increased to the predetermined level and the anode voltage was set at about 2 kV by adjusting the gas flow. Adjustments were made to the gas flow over a period of about 10 minutes to regulate the anode voltage drift. The anode voltage was set at the requisite level when stability of the source was indicated and the beam shutter was opened for the duration of etching. After this period the shutter was closed, the source was de-energised and the gas supply was turned off. Pumping was continued for at least 5 minutes (assuming halocarbon etching) to reduce the concentration of hazardous compounds and nitrogen was admitted until the chamber was at atmospheric pressure. The vacuum chamber was then evacuated to about 5×10^{-4} torr and subsequently vented as described. Following replacement of the sample with the next, the chamber was evacuated as before.

5. POST-ETCH TREATMENT

Grease was removed from wafers using a "cotton bud" soaked in I.P.A. (iso-propyl alcohol). Samples were often bifurcated at this stage and one half was sputter-coated with gold (200 Å thick) for S.E.M. examination of the resist layer. The other half was placed in a Nanotech P100 barrel reactor and exposed to an air plasma (60 W, 13.56 MHz for 5 minutes), for removal of the photoresist. This treatment was found to be necessary as resist films after exposure to a B93 beam were crosslinked and could not be readily removed using the normal stripping procedure (1:1 mixture of concentrated sulphuric acid and 100 volume hydrogen peroxide).

APPENDIX III

1. ATOMIC OR MOLECULAR DENSITY

$$n = \frac{6.02 \times 10^{23}}{MW/\rho} \quad cm^{-3}$$

Material	n	Units
Si	5×10^{22}	atoms cm^{-3}
SiO_2	2.3×10^{22}	molecules cm^{-3}
Si_3N_4	1.48×10^{22}	molecules cm^{-3}
Al_2O_3	2.2×10^{22}	molecules cm^{-3}
Al	6.03×10^{22}	atoms cm^{-3}
W	6.32×10^{22}	atoms cm^{-3}
Cu	8.47×10^{22}	atoms cm^{-3}

TABLE III-1

Formulae, Nomenclature and Physical Data for Gaseous Etchants used in R.I.B.E.

"Freon" Reference	Formula	I.U.P.A.C. Name Other Name(s)	Molecular Weight	Boiling Point °C
F14	CF_4	Tetrafluoromethane Carbon tetrafluoride (trivial)	88.01	- 128
F23	CHF_3	Trifluoromethane Fluoroform(trivial)	70	- 82
F116	C_2F_6	Hexafluoroethane Perfluoroethane	138.02	- 78
F218	C_3F_8	Octafluoropropane Perfluoropropane	188	- 37
-	SF_6	Sulphur hexafluoride	146.1	- 64

TABLE III-2

Hazards Associated with Compounds used in or Produced During the Gas Phase Etching of Silicon Compounds

Formula	Compound Name	T.L.V. p.p.m.	Notes	Reference
CF_4	Tetrafluoromethane	N.D.	Asphyxiant	1
CHF_3	Trifluoromethane	N.D.	"	1
C_2F_6	Hexafluoroethane	N.D.	"	1
C_3F_8	Octafluoropropane	N.D.	"	1
CCl_4	Carbon tetrachloride	10	Skin Contact	2,3,R
CO	Carbon monoxide	50	Inhalation	3
$COCl_2$	Carbonyl chloride	0.1	Inhalation	2,3
COF_2	Carbonyl fluoride	5	Inhalation	2,3,R
$(CN)_2$	Cyanogen	10	"	2
Cl_2	Chlorine	1	"	2,3
F_2	Fluorine	1	"	2
HF	Hydrogen fluoride (gas)	3	"	2
SiF_4	Silicon tetrafluoride	No Data	Toxicity "high"	3,S
SF_4	Sulphur tetrafluoride	0.1	Inhalation	2
SF_6	Sulphur hexafluoride	1000	"	2,3
SO_2F_2	Sulphuryl fluoride	5	"	2,3

References

1 Air Products Ltd, Data on handling and storage of special gases.

2 Health and Safety Executive, 1981.

3 Sax, 1979.

Notes

N.D. No data available.
T.L.V. is defined in the Glossary.
R Under Review: Reduction in T.L.V. has been proposed.
S Special precautions required in handling and use.

APPENDIX IV

Characteristics and Operating Conditions of the Three Saddle Field Sources used in this Study

Source type	B21	B93	B95
Anode potential (V_A); kV	5	3	3
Discharge current (I_D), mA	2	150	300 (1)
Total beam "current" (I_B), mA	0.1	4.2(2)	20 (3)
Beam area, cm^2	6.4	57 (2)	1000
C.A.T.T. distance, mm	75	72 (2)	400
Cathode aperture	Rectangular 10x1.5mm	32, 2.4mm diameter holes in 25mm diameter carbon disc	1225, 2.4mm diameter holes in 75x150mm carbon plate
Chamber pressure, torr	$5x10^{-4}$	$5x10^{-4}$	$1x10^{-3}$
Pump speed, $l.sec^{-1}$	150	400	3500
Cooling	Uncooled	Cathode body only	Anodes and cathode body

Notes
(1) Designed for operation with power supply delivering 1.5 A
(2) Experimentally determined, this study
(3) Beam "current" value based on earlier work with B93 source
Data for B21 and B95 sources from Ion-Tech Ltd